ETHANOL FLUSHING OF GASOLINE RESIDUALS - MICROSCALE AND FIELD SCALE EXPERIMENTS

by

Everton de Oliveira

A thesis
presented to the University of Waterloo
in fulfilment of the
thesis requirement for the degree of
Doctor of Philosophy
in
Earth Sciences

Waterloo, Ontario, Canada, 1997

The University of Waterloo requires the signature of all persons using or photocopying this thesis. Please sign below, and give address and date.

ABSTRACT

Gasoline residuals formed by either removal of the gasoline in free phase during cleanup processes or by seasonal variation of the water table are a very common and lasting source of contamination of soil and groundwater. One method to remove these residuals at or below the water table is to pass or flush alcohol through the residuals and to remove the gasoline in the alcohol phase.

The study of the gasoline-water-ethanol interactions showed a relatively large 2-phase region, with ethanol partitioning preferentially to the aqueous phase. The interfacial tension (IFT) is reduced as ethanol content increases and a miscible system, well suite to flushing, can always be obtained for ethanol concentrations above 88% wt.

Visualization experiments using glass micromodels showed that IFT differences are responsible for gasoline removal by a mechanism described as *blob ejection*, where the tip of the trapped blob or cluster of blobs that is in contact with ethanol has its IFT reduced, and the blob is ejected into the flowing ethanol rich fluid. This phenomenon facilitates further dissolution of partially ejected blobs into the flushing fluids.

Using sintered glass beads models, the horizontal direction was chosen for field trial of ethanol flushing. Pore scale instabilities were responsible for fingering development during the vertically downward flushing. Larger scale instabilities were responsible for fingering during vertically upward flushing. The model was completely cleaned up after 2-3 pore volumes of ethanol during lateral flushing.

During the field experiment, the density difference between water and ethanol caused the segregation of the fluids, with ethanol flowing upwards in the groundwater system. Although most of the injected ethanol missed the target region of residuals, 36% wt. of the emplaced gasoline was removed from the aquifer, and 45% wt. ethanol was recovered. Further laboratory experiments using a sintered glass beads model showed that the buoyancy effects can be used for the precise delivery of ethanol to the target regions by adjusting the level of the water table within the zone of residuals. By doing so, complete removal of the gasoline residuals was achieved in the laboratory after about 2 pore volumes of ethanol was injected.

ACKNOWLEDGEMENTS, EH

Working through a Ph.D. is more than an art or a tour de force. It is like learning how to play the piano while carrying it, and composing your own song. I had the fortune to have both good players and carriers to help me accomplish my task. I would like to acknowledge the support I received from these individuals and from the institution that sponsored me.

My two advisors. Dr. Jim Barker, a marvelous piano player. From him I could always seek advice not only for my research, but, more importantly, for my professional career as well. As good a diplomat as a politician, Jim was able to teach me how to play difficult songs on the piano, - while I carried it! The load felt lighter instead. I will definitely miss the enjoyable dinners at the Barker's, a certain pleasure, with Jim and Gayle's intelligence and wit. Dr. Ioannis Chatzis, another wonderful player. Always keeping me in tune, he would never allow me to play out of key. His bright and inquisitive mind drove me to the wonders of the microscale. Lots of coffee and beer flowed through our porous media conversations. Luckily enough, more than advisors, I found two good friends for life.

The members of my advisory committee, my music critics, who never completely nodded to my composition, style or performance. Their suggestions helped me develop my ear and the quality of my composition this much.

Jeff Barbaro, the man with an attitude. He helped me carry the load of my piano through inclement weather. More than a strong carrier, he shared with me the same musical taste, making the playing while carrying much more fun.

Leanne Murdie, the most stoic helper someone could ask for. Having her by my side during the field season (yes, Canadian winter!) gave me the special moral strength I needed when the piano seemed too heavy for me.

Klitia Bicalho de Sá, who added a bit of Brazilian rhythm to my playing.

Dominique Sorel, above all qualities, a Quebec driver, who drove us into the ditch. What a ride! Both author and piano survived the thrilling experience. The Québecois flavor was added to my music.

Dave Redman, an artisan who carefully helped me craft my composition.

Paul Johnson and all other technicians, with their big drums of backhoes, hammers and all sorts of percussion instruments.

All the friends I made along the way. Big carriers, small carriers, big singers, small singers, big players, small players. They are so many that I cannot do them justice. To name just a few, Mario & Kristin Schirmer for all the beer that is yet to come and for Mario's impressive soccer skills (for a German, I mean); Joe Pach, the pillowcase biter; Raymond Henry, for the long hours sharing the piano load when I first arrived; Chris Hanton-Fong, always efficient and polite, having her as an officemate was a pleasure; Carey "Scary" Austrins, the night shift fellow who spends all his money to keep his nasty habit of eating a full meal every two hours; Geraldo Torres, for sharing his "maromba" knowledge and friendliness; and many, so many others I feel I could write another thesis-like volume (no, I mentioned the evil T-word!!)

Braswat - Brazilian Association of Graduate Students of the University of Waterloo, whose members and organization helped me settle down and provided me with invaluable information about bureaucratic procedures and hints on how to survive in the Canadian jungle. Special thanks go to Nilson Guiguer, for his "auxilio luxuoso", and for Alexandre and Elaine Brolo, true friends.

Celso Kolesnikovas, a great partner, for keeping the band always on the road.

Capes - Fundação Coordenação de Aperfeiçoamento de Pessoal de Nível Superior, from Brazil, who awarded me the scholarship.

You, the reader, the only one who may ever read this, for making sure that the band plays on. Coming soon to a concert hall near you.

And last, to my lovely wife Adriana, that always believed in me - what a proof of true love!

With love,

to my beautiful and lovely wife, Adriana.

"When I'm sad she comes to me

with a thousand smiles

She gives to me free

It's all right, she says, it's all right

Take anything you want from me"

TABLE OF CONTENTS

LIST OF TABLES

LIST OF ILLUSTRATIONS

1. INTRODUCTION

Leaks of gasoline from underground storage tanks pose a serious threat to subsurface water supplies. Gasoline are complex blends of petroleum-derived chemicals which sometimes contain additives to improve fuel performance and minimize engine wear. There is no one chemical formula for gasoline as it contains over 200 different compounds. The hydrocarbons in the gasoline composition that constitutes the spill exhibit low aqueous solubilities and persist as a separate, immiscible phase. This liquid is known as LNAPL, light non-aqueous phase liquid.

Gasoline that leaks from an underground storage tank contains highly volatile aliphatics, somewhat volatile aromatics and a wide range of solubilities of compounds within each of the these broad groups. This can result in the following distinct phases as Figure 1-1 illustrates: liquid, dissolved and vapor.

Remediation strategies for removing LNAPL contamination from groundwater typically involve the application of pump-and-treat technologies. At most sites, pump-and-treat operations alone do not effectively remove the total contamination. Large residual concentrations of the contaminant are usually left behind in the formation, due to trapping of the LNAPL blobs or cluster of blobs by capillary forces. These trapped blobs can occupy 14% to 30% of the total pore volume (Wilson et al., 1990) and can serve as long term source of groundwater contamination. Continued waterflooding (by pump-and-treat or natural groundwater movement) reduces the LNAPL saturation by the slow process of dissolution, with complete contaminant removal often requiring years or decades (Mackay and Cherry, 1989).

Complete remediation of a gasoline spill involves the removal of liquid, dissolved and vapor phase hydrocarbons. Clean up usually begins with removal of free product. In an older spill, where a large contaminated plume has already developed, free product represents only about 5% of the total volume of contaminated groundwater. However, on a weight percent basis, free product may represent 95% of the total mass of contaminants. Experience with recovering free product in USA has shown that on average only 29% of the leaked product is recovered. The remainder either ends up as a residual phase or as a dissolved or vapor phase (Oliveira et al., 1991).

Other remedial approaches are presently being considered for removing LNAPL residuals in a more timely and cost-effective manner, for example in situ volatilization, steam/hot air injection and bioremediation (Nyer et al., 1996). In situ volatilization has been applied with reasonable success, but recovery of gasoline compounds typically tail off as it does with pump-and-treat. Steam or hot air may be injected to improve volatilization, but the tailing of the concentration still persists (Nyer, 1996).

Gasoline compounds are easily biodegradable under dissolved phase and adequate nutrient and electron acceptor conditions. Alternatively, bioremediation programs have been studied for remediation of gasoline residuals, but significant removal of the residuals has not been achieved yet.

Chemical floods (e.g., surfactants, alcohols) can also be used to remove gasoline residuals by reducing the interfacial tension between the fluid phases. The use of alcohol for enhanced oil recovery was considered in the 1960s (Holm and Csaszar, 1965; Taber and Meyer, 1965), but has never been applied commercially due to marginal benefits. However, in the environmental field, the objective of a remediation effort is to restore the contaminated

site to its original state; for this application alcohol flushing may offer an environmentally safe and economically attractive groundwater restoration alternative.

Boyd and Farley (1991) mention that in addition to LNAPL mobilization, alcohol floods can simultaneously remove sorbed contaminants by functioning as a cosolvent for hydrophobic material in the aqueous phase. Another advantage of alcohol flushing is that low molecular weight alcohols are less likely to sorb to mineral surfaces due to their low carbon number and high molecular polarity; thus, alcohol solutions are easily displaced from the aquifer by subsequent water flushes (Boyd and Farley, 1991). Finally, any alcohol that remains in the subsurface should be easily biodegraded by native microorganisms.

The use of ethanol in the present work has been suggested by its use as a fuel in Brazil and parts of USA and Canada. This use presents the advantage of abundant availability of ethanol close to points where gasoline spills often occur. This research addresses the potential use of ethanol as a flushing fluid to remove gasoline residuals near the water table.

The objectives of this work are:

- to study in detail the gasoline-water-ethanol interactions and fluid properties through the use of ternary diagrams, focusing on miscibility, variation of interfacial tension and variation of density;
- to study the process of gasoline residuals removal by ethanol flushing at the pore scale level through the use of network micromodels etched on glass;
- evaluation of the best direction of ethanol flushing (horizontal, vertical upward and vertical downward);
- to test the use of ethanol flushing technology to cleanup gasoline residuals at the field scale.

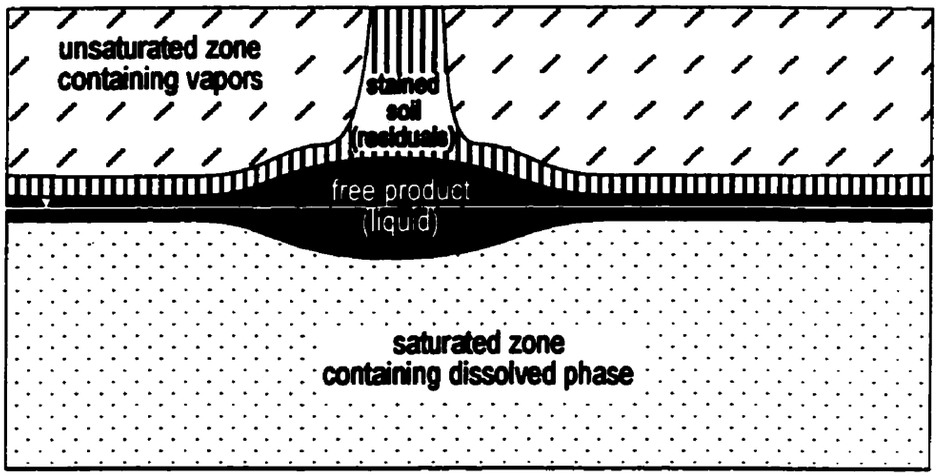

Figure 1-1 - Phase distribution of gasoline in a typical gasoline spill

2. GASOLINE-WATER-ETHANOL INTERACTIONS AND FLUID PROPERTIES

2.1 Objectives

The main objectives of this chapter are:

- To present a detailed analysis of the phase behavior of the pseudoternary diagram gasoline-water-ethanol, relating the results to the minimum content of ethanol necessary in the flushing fluid to attain miscible displacement for a complete removal of gasoline residuals in a flushing process.
- To determine the relationship between interfacial tension and ethanol content for aqueous and oleic phases. Reduction in IFT and increasing in flushing fluid velocities are the major factors to physically remove residuals in porous media. Since the fluid velocities are naturally limited by field conditions, reduction in IFT is the feasible choice. This determination allows an interpretation about the potential of mobilization of the residuals for the measured IFT reductions.
- To describe the density behavior of the ternary system gasoline-water-ethanol, considering non-additivity of volumes of water and ethanol, with eventual gaseous phase formation. The densities of displacing and displaced fluids are important in determining the stability of displacement of the flushing process. Varying compositions of aqueous and oleic phases present varying densities that are addressed in the present work to be used in displacement experiments to determine the best direction of flow for the ethanol flushing process. Furthermore, ethanol and water do

not have additive volumes and the final density of the mixtures containing ethanol and water are affected by the volume reduction.

2.2 Phase Behavior

2.2.1 Background

When ethanol is added to a 2-phase system of pure gasoline and pure water, it partitions in different proportions to the aqueous phase and to the oleic (gasoline) phase. The equilibrium system consists of a water-rich phase (named *aqueous phase*) with ethanol and dissolved gasoline and a gasoline-rich phase with ethanol and dissolved water (named *oleic phase*). The amount of gasoline dissolved in the aqueous phase and the amount of water dissolved in the oleic phase increase with the increasing amount of ethanol. If enough ethanol is added to the system, a single phase develops. *Ternary diagrams* are used to describe the behavior of three component systems when two of the three components are immiscible. The partition of ethanol into aqueous and oleic phases is well described with the use of a *pseudo*ternary diagram, which allows the grouping of multiple components as a single pseudocomponent (e.g., gasoline) (Stalkup, 1983). The construction and use of ternary diagrams is common in the chemical engineering literature and is described elsewhere (Treybal, 1987; Burns, 1984). Figure 2-1 presents an example of a typical ternary diagram with its important features.

Ternary diagrams for the benzene-water-ethanol ternary system are presented by Brandani et al. (1985), Ross and Patterson (1979) and Varteressian and Fenske (1936). Letcher et al. (1986) presented a pseudoternary diagram for gasoline-water-ethanol, but the compositions of the points of the binodal curve and tie lines were not presented.

Donaldson (1992) studied the phase behavior of the gasoline-water-methanol pseudoternary system, but the tie lines were not defined due to the lack of complete composition analysis of the aqueous and oleic phases.

In this work we present a detailed analysis of the pseudoternary diagram gasoline-water-ethanol, relating the results to the minimum content of ethanol necessary in the flushing fluid to attain miscible displacement for a complete removal of gasoline residuals in a flushing process.

2.2.2 Experimental Procedure

Ten different compositions of water and ethanol were prepared using de-ionized, de-aired, organic free distilled water and pure ethanol. Pure ethanol (ethyl alcohol class 3.2 UN 1170 PG II) was supplied by Commercial Alcohols Inc.. The composition of the mixtures prepared varied from 10% to 80% by volume ethanol in 10% intervals, including the compositions 75% and 88% by volume ethanol. The volumes were measured using 1 ml, 2 ml, 5 ml, 10 ml and 20 ml glass pipettes and inserted into 160 ml oven cleaned glass bottles, sealed with Teflon septa and aluminum caps. The bottles were agitated with a rotary shaker (Orbit shaker) at 300 rpm for 60 minutes. Similarly, following identical procedure, eight different mixtures of gasoline and ethanol were prepared. API-91-01 gasoline used in the experiment was supplied by the American Petroleum Institute. These 18 different compositions were used as stock solutions in the determination of the binodal curve of the ternary diagram.

The phase diagram (pseudoternary diagram) was obtained by the cloud-point technique (Desnoyers et al., 1893). Stock solutions prepared with water and ethanol were

added to pure gasoline and those prepared with gasoline and ethanol were added to pure water. The initial proportions for the mixtures (points on the 2-phase region of the diagram) were based on literature (Letcher et al., 1986) and the liquids were added with the help of glass pipettes to 160 ml oven cleaned glass bottles, which were sealed with Teflon septa and aluminum crimps immediately afterwards. Fine adjustment of the points of the binodal curve were achieved with the addition of stock solution through the insertion of a 25G5/8 needle of a 1 ml gas-tight Teflon plunger microliter Hamilton syringe. The mixtures were continuously agitated by hand during the addition of stock solution (2-3 hours average for each point) and left at rest to reach equilibrium for 24 hours to allow for phase separation. The transition from two-phase to one phase system (and vice-versa) is gradual and several times had a slightly milky appearance, in which the transition point is somewhat subjective. The final points of the binodal curve were named W90, W80, W70, W60, W50, W40, W30, W25, W20 and W12, according to the original water percent by volume of their stock solutions, and, similarly, G90, G80, G70, G60, G50, G40, G30, G20, according to the original gasoline percent by volume of their stock solutions. The refractive index and density of each of the final solutions was determined.

The refractive indexes were determined with a Carl Zeiss glass face refractometer. About 0.5 ml of the solution to be measured was removed from the 160 ml bottle using a 1 ml gas tight syringe and placed in excess on the refractometer glass plate and the refractive index determined and recorded. The refractometer face and gas tight syringe were cleaned with ethanol, then acetone, then air dried between each solution sampled.

The densities of the final solutions, pure water, pure ethanol and pure gasoline were determined by weighing solutions in two 25 ml glass specific gravity determination flasks (fixed volume) with their dry weight previously recorded using a Fisher Scientific Gramatic scale and. The flasks were rinsed with detergent, then rinsed with water, then ethanol, then acetone and then twice with the same solution that was having its density determined.

The final compositions in percent by volume were then transformed to percent by weight using the determined densities of pure water, pure ethanol and pure gasoline and plotted into a ternary diagram. Percent by mass is preferred to percent by volume because the volumes of ethanol and water are not additive, as it is studied in detail later.

To determine the tie lines, the composition of the initial points (corresponding to compositions falling within the 2-phase region of the diagram) were chosen based on the literature (Letcher et al., 1986). The volumes of gasoline, water and ethanol were measured using 1 ml, 2 ml, 5 ml, 10 ml and 20 ml glass pipettes and inserted into 160 ml oven cleaned glass bottles, sealed with Teflon septa and aluminum caps. After prepared, the solutions were agitated with a rotary shaker (Orbit shaker) at 300 rpm for 60 minutes and left at rest for 24 hours. Refractive indexes of each of the two separate phases thus obtained (corresponding to ends of the tie lines) were determined as described previously. The composition of each sample (in gasoline , water and ethanol) was interpolated from the refractive indexes of points of the binodal curve.

Following the same procedure, extra samples were prepared later to be used in the tie line determination. The composition of the separate phases of these samples were

determined with UV analyses (UV analyses methods for oleic phase and aqueous phase are presented in Appendix I).

All experiments were run at room temperature (21 ± 0.5 °C)

2.2.3 Results and Discussion

The densities of the pure compounds water, gasoline and ethanol were measured and the results obtained are presented on Table 2-1. The composition of the points belonging to the binodal curve were initially determined in percent by volume. These measured compositions were transformed into percent by weight using the determined values of the densities of the pure components. All determined compositions and calculated compositions for the solubility points are summarized in Table II-1, in Appendix II.

Table 2-1- Densities of Gasoline, Water and Ethanol at 21°C.

Sample	Density (g/ml)
Pure Gasoline	0.747
Pure Water	0.996
Pure Ethanol	0.784

Refractive indexes correlated to the binodal curve points are presented in Table II-2, in Appendix II. Figure 2-2 illustrates the ternary diagram with the determined binodal curve points (and binodal curve) matched with the plot of their respective refractive indexes versus water percent (in weight).

The pseudoternary diagram obtained (Figure 2-2) is characterized by a relatively large 2-phase region. The proximity of the water rich portion of the binodal curve (left

hand side of the curve) to the water-ethanol side of the diagram indicates low solubility of gasoline at low ethanol content (less than 50 wt%). Above 50 wt% ethanol the solubility of gasoline is increasingly sharpened as suggested by the progressive deviation of the curve from the ethanol-water side of the diagram. It is important to point out that low solubilities of gasoline in water in this context are orders of magnitude higher than the original solubility of gasoline in water (gasoline being considered here as a single pseudocomponent). However, the study of the increase in solubility for low concentrations of gasoline in water, considering exclusively the dissolved phase (i.e., aqueous phase), is out of the scope of this work. The reader is referred to Donaldson (1992) and Cline et al. (1991).

The refractive indexes display a steeper change for points of the gasoline-rich portion of the binodal curve. The behavior of this diagram reflects the minor differences for refractive indexes of water and ethanol but the more significative difference for gasoline ($R.I._{Water}$ = 1.3310; $R.I._{Ethanol}$ = 1.3579; $R.I._{Gasoline}$ = 1.4156). Moving along the binodal curve, starting from the water end, the values of the refractive indexes increase gradually from the value of pure water - the lowest - towards values of maximum ethanol content (refractive index of about 1.3630, not very far from that of pure ethanol, 1.3579), as ethanol partitions to the aqueous phase and very little gasoline is incorporated to this phase. From this point on, the gasoline content increases rapidly and the values of the refractive indexes reflect this change, with the graph exhibiting a steeper change corresponding to the bigger difference between the refractive index of pure gasoline and that of pure ethanol or ethanol water mixtures.

Figure 2-3 presents the tie lines for the ternary system water-gasoline-ethanol. Any two separated phases in equilibrium formed by liquid-liquid extraction of the prepared mixtures have their compositions falling on the binodal curve of the ternary diagram. A straight line joining the two points representing the compositions of the separate phases is called tie line, and this line intercepts the point representing the composition of the original mixture. Any other point on the same tie line would produce separate phases with the same compositions of the one chosen, the difference would be that the volume of each separate phase would change. Twelve mixtures with compositions falling within the single phase region of the diagram were chosen and prepared and their positions are presented in the Figure 2-3, along with their respective resulting tie lines. The compositions of the points forming the ends of the tie lines (numbered 1 to 12) were based on the interpolation of the values of the refractive indexes of the separate phases with that of the binodal curve points (as per Figure 2-2). The initial compositions (before phase separation) and the measured refractive indexes of the tie line ends and their refractive-index-based compositions are presented in Table II-3 and Table II-4, respectively, in the Appendix II. Due to errors in determining the refractive indexes, not all the tie lines in Figure 2-3 intercept the three points. During the determination of the refractive indexes, the liquid can volatilize from the open plate of the open plate. The process of pouring the liquid with a syringe, adjusting the equipment and reading the value takes about 10 to 15 seconds, and volatilization occurs during this time. Preferential volatilization of gasoline compounds, followed by ethanol (both more volatile than water), tends to shift the refractive indexes to lower values, since water has a relatively lower refractive index.

The tie lines have negative slopes, characterizing the ternary diagram for ethanol-water-gasoline as a plait-point-to-the-right type. This feature of the diagram is characteristic of systems where the cosolvent (ethanol) partitions preferentially to the aqueous phase (Larson et al., 1982). Several attempts were done to determine the plait point, but its actual position could not be exactly determined.

Another independent experiment, with a new set of mixtures was prepared to determine the tie lines by a different method, with the resulting composition of the solutions corresponding to the ends of the tie lines analyzed by a UV method. The results obtained with this method are presented in Figure 2-4 and the initial proportions (before phase separation) and the compositions for the end-points of the tie lines are presented in Table II-5 and Table II-6, respectively, in Appendix II. The comparison of the tie lines obtained by UV analyses with those obtained by refractive indexes interpolation shows good agreement, with the binodal curve showing a slight displacement from the water-ethanol side of the diagram (Figure 2-4) compared to the results obtained by the cloud point method (Figure 2-3). The accuracy of both methods is similar, but the handling to prepare the samples and time required in the UV method are much less.

Figure 2-3 shows (and Figure 2-4 confirms) that the "top" of the binodal curve corresponds to about 70% (69.6%) by weight ethanol, which implies that 70% by weight ethanol content, any composition falls within the single phase region of the diagram. However, this composition is not sufficient to maintain miscible displacement of the residuals, a necessary condition to avoid trapment of oleic phase. Actually, the original composition of the residual fluids in the porous medium (water and gasoline) mixes with

the flushing fluid, generating a fluid of different composition, with a lower ethanol content.

Figure 2-5 clarifies this point, exhibiting a situation whether the desired miscibility (a and b) is attained or (c and d) is not attained. The dispersive mixing within each phase is neglected in these illustrations. The definition and theory of developed miscibility is presented by Clark et al. (1958) and Benham et al. (1960).

The situation presented in Figure 2-5 shows de displacement of a continuous gasoline phase (Figure 2-5 a and c) formed from displaced gasoline residuals.Presuming that the phases in contact maintain equilibrium with each other, the gasoline and water at the rear of the continuous gasoline phase each are displaced miscibly by the respective oleic phase and aqueous phase of compositions lying at the ends of a tie line infinitesimally above the base of the diagram. These phases in turn are displaced miscibly by phases of compositions lying at the ends of a slightly higher tie line, and so on. The progression continues until the limiting tie line (the plait point) is reached; the fluid of this composition is displaced miscibly by pure injected flushing fluid (Figure 2-5 a and b). In the circumstances of the Figure 2-5 c and d, the miscibility is not attained because the ongoing contacting of the aqueous and oleic phase with more and more of the injected solution produces a progression of tie lines that terminates at the one tie line which, when extended, passes through the injected composition on the diagram. The miscible region, as opposed to the single phase region, is that portion of the ternary diagram through which pass neither tie lines nor their extensions (Larson et al., 1982). This region is delimited by the limiting tie line at the plait point, i.e., the tangent of the solubility (or binodal) curve, at the composition where the aqueous and oleic phase

become identical (plait point). In Figure 2-5, the graphic determination of this tangent was approximate, since the plait point composition could not be determined exactly in the laboratory. The minimum percent of ethanol required in the flushing solution thus determined corresponds to approximately 88% by weight ethanol and 12% by weight water (Figure 2-5).

2.3 Interfacial Tension Variation with Composition

2.3.1 Background

When two immiscible fluids are in contact there is a free interfacial energy between them, which arises from the difference between the inward attraction of the molecules in the interior of each phase and those at the surface of contact. Since a surface attempts to minimize free energy, it contracts if it can do so, the free interfacial energy manifests itself as interfacial tension (IFT). Thus interfacial tension, σ_{ik}, which is a parameter for each pair of substances i and k, is defined as the amount of work that must be performed in order to separate a unit area of substance i from substance k (Bear, 1979). From a mechanical standpoint, the system behaves as if it consisted of two homogeneous fluids separated by a uniformly stretched membrane of infinitesimal thickness (Dullien, 1979). In miscible displacement, on the other hand, even if the two fluids are initially separated by an abrupt interface, a transition zone is immediately created due to hydrodynamic dispersion, and the IFT concept does not apply. Across this zone, the composition of the fluid varies from that of one pure fluid to that of the other pure fluid (Bear, 1979). An illustrative example of the IFT is a soap bubble, Figure 2-6

(Dullien, 1979). It can be demonstrated that the difference in pressure at the interior of the bubble to its exterior is given by Laplace's equation:

$$\Delta P = \frac{2\sigma_{ik}}{r} \qquad \text{(Equation 2-1)}$$

where:

$$\Delta P = P_i - P_o \qquad \text{(Equation 2-2)}$$

P_i = pressure at the interior of the bubble [F/L^2];

P_o = pressure at the exterior of the bubble [F/L^2];

σ_{ik} = interfacial tension [F/L];

r = radius of the bubble [L].

The partition of ethanol to the aqueous and oleic phases allows water to dissolve into the oleic phase and gasoline to dissolve into the aqueous phase. The changes in composition of the two phases that coexist in equilibrium result in changes to the IFT between the two phases. The maximum value of IFT corresponds to that of the original two-phase system composed of pure gasoline and pure water, and it decreases as more ethanol is added to the system. As the compositions of the two phases move towards the plait-point in the ternary diagram with the addition of more ethanol, the length of the tie lines decreases (as it is seen in Figure 2-3 and Figure 2-4), with the phases progressively having composition more "similar" to each other. At the plait-point the length of the tie line is zero, and the compositions of both gasoline and aqueous phases are identical, corresponding to IFT equals to zero. The surface tensions of the conjugate phases

approach each other and become equal at the plait point and, consequently, the IFT falls to zero at the same point.

Ross and Paterson (1979) present the surface and IFTs of conjugate solutions for two ternary systems, benzene-water-ethanol and *n*-hexane-water-ethanol. Lee and Parrish (1989) present IFTs of conjugate solutions for the ternary systems benzene-water-ethanol and surrogate gasoline (70/30 wt% isooctane/toluene)-water-ethanol.

Reduction in IFT and increasing in flushing fluid velocities are the major factors to physically remove residuals in porous media. Since the fluid velocities are naturally limited by field conditions, reduction in IFT (and eventually its complete elimination) is the viable choice. This work presents the behavior of the IFT relative to ethanol content with an interpretation about the potential of mobilization of the residuals for the measured IFT reductions.

2.3.2 Experimental Procedure for Determination of IFT Variation with Composition

IFTs of separate phases for the tie lines presented in Figure 2-4 were determined by the Drop Weight Method (Adamson, 1967; Padday, 1969).As illustrated in the Figure 2-7a (after Adamson, 1967), the procedure consists of forming drops of the aqueous phase (more dense) at the end of a glass tube, which is submerged into the corresponding oleic phase (less dense), allowing them to fall until enough have been collected so that the volume per drop can be determined accurately by measuring the change in the head in the tube of known cross section. Figure 2-7b (after Adamson, 1967) illustrates the fact that part of the drop remains attached to the tip of the tube and for this reason a

correction factor must be used to account for this non-ideality. The correction factor is related to (V/r^3) and is tabulated for several values of (V/r^3) (Padday, 1969). The IFT is calculated by:

$$\sigma = (\frac{V \cdot \Delta\rho \cdot g}{r}) \cdot F \qquad \text{(Equation 2-3)}$$

where:

σ = interfacial tension [F/L];

V = volume of drop [L^3];

$\Delta\rho$ = density difference between the two phases [M/L^3];

g = acceleration due to gravity [L/T^2];

F = correction factor;

r = external radius of the tip of the tube [L].

Densities were determined following procedure described previously (section 2.3.2).

2.3.3 Results and Discussion

Table 2-2 presents the interfacial tensions measured by the drop weight method. Tie lines identified here as L_0 to L_8 were previously presented in Figure 2-4. L_0 represents the water-gasoline base of the diagram. Consequently, 0.7469 g/ml and 0.9989 g/ml correspond to the densities of pure gasoline and pure water, respectively. Tie line L_9 in the diagram did not produce enough oleic phase to have IFT determined and is not presented in this table. The radius of the tip of the glass tube is 0.1754 cm. X_e is the mole fraction of ethanol present in the aqueous phase composition of the tie line.

Table 2-2 - Interfacial tension variation for pseudoternary system gasoline-water-ethanol.

Tie Line ID	Volume of the Drop (ml)	Density of the Oil Phase (g/ml)	Density of the Water Phase (g/ml)	F	Interfacial Tension (mN/m)	Length of the Tie line (cm)	(1-L/Lo)	X_e Water Phase
L_o	0.0650	0.7469	0.9965	0.2379	21.872	23.00	0.00	0.0000
L_1	0.0570	0.7559	0.9970	0.2405	18.486	22.10	0.04	0.1362
L_2	0.0367	0.7446	0.9812	0.2488	12.084	20.85	0.09	0.3127
L_3	0.0262	0.7432	0.9621	0.2547	8.169	20.10	0.13	0.4317
L_4	0.0210	0.7439	0.9450	0.2581	6.095	19.80	0.14	0.4983
L_5	0.0167	0.7433	0.9304	0.2611	4.564	19.30	0.16	0.5803
L_6	0.0120	0.7432	0.9031	0.2641	2.834	18.30	0.20	0.6098
L_7	0.0098	0.7435	0.9750	0.2650	1.900	18.10	0.21	0.6202
L_8	0.0064	0.7437	0.8470	0.2632	0.973	15.80	0.31	0.5517

Figure 2-8 shows a plot of values of IFT against the variable $(1\text{-}L/L_o)$, where L is the length of a tie line and L_o is the maximum length of the tie lines (which corresponds to the side of the ternary diagram). A similar plot is presented in Figure 2-9, but the variation of IFT is presented as a function of mole fraction of ethanol in the aqueous phase.

The curve on Figure 2-8 exhibits an exponential behavior, with a steep decrease in IFT values for $0 \leq (1\text{-}L/L_o) \leq 0.2$, when the IFT values decreases from 22 mN/m to about 7 mN/m, a three-fold decrease. After this point, the decrease is more gentle, and at $(1\text{-}L/L_o) = 0.5$ the IFT is on the order 10^{-1} mN/m. It is important to point out that an IFT close to zero still corresponds to the existence of two separate phases. Only at the plait-point is the IFT zero ($1\text{-}L/L_o$ is equal to one), characterizing a single phase situation.

As mentioned before, the maximum content of ethanol is 70% by weight, corresponding to a mole fraction of 0.58. The plait point is located at the right-hand side of the solubility curve, and the mole fraction of ethanol decreases after reaching a maximum at the top of the solubility curve. Up to the maximum ethanol content in the aqueous phase, the IFT shows an approximate linear behavior (see Figure 2-8). Lower values of interfacial tension for compositions close to the plait point could not be measured in the experiments.

Reduction of interfacial tension caused by ethanol partition between aqueous and oleic phase is important in determining the potential for removal of gasoline residuals from the pores. This potential is well represented by the capillary number, a relationship between capillary to viscous forces, which correlates to the residual saturation of organic liquid (non-wetting phase). Chatzis and Morrow (1981, 1984) performed a large number of experiments using sandstone cores to establish the correlation between capillary number, $N_c^{'}$, and residual saturation of organic liquid. Several capillary number definition appear in the literature, two of which are given below (Chatzis and Morrow, 1981):

$$N_C^1 = \frac{k \nabla P_w}{\sigma} \qquad \text{(Equation 2-4)}$$

$$N_C^2 = \frac{q_w \mu_w}{\sigma} \qquad \text{(Equation 2-5)}$$

where:

k = absolute permeability of the medium [L^2];

∇P_w = water phase pressure gradient of the water

phase [F/L^3];

q_w = specific discharge [L/T];

μ_w = viscosity of water [FT/L^2];

σ = interfacial tension [F/L]

Superscripts (1,2) refers to the version of the dimensionless number. Version 1 of the capillary number assumes that the hydrostatic forces are negligible, version 2 inherently accounts for relative permeability and the gravitational (hydrostatic) portion of the driving force - $\nabla(\rho wgz)$ in the expression of q_w:

$$q_w \equiv \frac{k_{rw}\, k}{\mu_w} \nabla(P_w + \rho_w g z) \qquad \text{(Equation 2-6)}$$

$$v = \frac{q_w}{\theta} \qquad \text{(Equation 2-7)}$$

where:

ρ_w = density of water [M/L^3]

k_{rw} = relative permeability for the water phase;

v = average linear velocity;

θ = porosity;

z = elevation [L].

The residual saturation decreases with increasing capillary numbers. From equations 2-4 and 2-5, capillary number increases with increasing flushing fluid velocity (v, related to the specific discharge) and decreasing IFT. Increasing in fluid velocity is

limited by field conditions, and reduction of IFT is the only feasible alternative to increase the capillary number.

Wilson and Conrad (1984) defined a related capillary number for groundwater situations:

$$N_C^3 = \frac{K_w J_w \mu_w}{\sigma} \qquad \text{(Equation 2-8)}$$

where:

K_w = water-saturated hydraulic conductivity [L/T], $\frac{k \rho_w g}{\mu}$;

J_w = hydraulic gradient in the water phase, $\nabla\left(\frac{P_w}{\rho_w g} + z\right)$;

This definition of the capillary number does not contain the relative permeability built into (2-5), but does contain the gravity term neglected in (2-4). When hydrostatics are neglected, (2-8) reduces to (2-4) (Wilson and Conrad, 1984).

Figure 2-10 shows a typical S_o/S_{or}^* vs. $N_C^{'}$ correlation, where S_{or}^* is the residual saturation of the organic liquid originally in place; S_{or} is the saturation of organic liquid after displacement by water or chemical flood. Chatzis and Morrow (1984) showed that trapped residual phase starts to mobilize for capillary numbers of $N_C^{'} = 2 \times 10^{-5}$ for sandstones (critical capillary number) and that at $N_C^{'} = 3 \times 10^{-3}$ complete mobilization is achieved. This correlation holds for a wide variety of water-wet sandstones and organic fluids. For unconsolidated sands, these values increase about two orders of magnitude (Chatzis, pers. comm.).

Substituting the values of K_w, J_w, μ_w and σ for typical values of Borden sand aquifer and measured gasoline-water IFT, the critical capillary number, $N_c^{'}$, can be calculated as:

$$K_w = 0.5 \times 10^{-4} \text{ m/s}^{(1)};$$

$$J_w = 0.0043^{(1)};$$

$$\mu_w = 1.124 \times 10^{-3} \text{ N.s/m}^{2\ (2)};$$

$$\sigma = 21.87 \times 10^{-3} \text{ N/m}$$

(1) Mackay et al. (1986) (2) Freeze and Cherry (1979)

$$N_c^{'} \approx 1.1 \times 10^{-8}$$

The value of the capillary number must be increased by 5 orders of magnitude to reach the critical capillary number for mobilization of an oleic phase for unconsolidated Borden sand in order to attain complete removal, by mobilization, of the residuals. As Figure 2-8 (and values from Table 2-2) shows, these capillary numbers are not attained up to the values of $(1\text{-}L/L_0) = 0.31$ measured in the laboratory (IFT = 0.9×10^{-3} N/m). From Equation 2-7 it is necessary that the IFT becomes $\sigma = 2 \times 10^{-7}$ N/m in order to have the residuals completely removed based on changes of IFT alone. Such low values of IFT cannot be measured in the laboratory.

However, the position of the tie lines close to the plait point present an overall alignment to the tangent to the plait point, and the rate of decrease in the tie line sizes corresponds to a sharp decrease in IFT (as suggested by Figure 2-5). These factors leads to the conclusion that the values of IFT that are necessary for the complete removal of

residuals may be attained before the plait point composition is reached. The gasoline residuals can be mobilized before dissolving into the mainstream ethanol flood.

2.4 Density Behavior of the Ternary Mixture Gasoline-Water-Ethanol

2.4.1 Background

The densities of displacing and displaced fluids are important in determining the stability of displacement of the flushing process. Varying compositions of aqueous and oleic phases present varying densities that are addressed in the present work to be used in displacement experiments to determine the best direction of flow for the ethanol flushing process. Furthermore, ethanol and water do not have additive volumes and the final density of the mixtures containing ethanol and water are affected by the volume reduction. This section focus on the density behavior of the fluids involved in this work, taking into consideration the non-additive volumes of ethanol and water.

The density for the ternary system gasoline-water-ethanol will be treated here in two separate steps because of the non-linear behavior of water and ethanol mixtures. The mixture of ethanol and water forms a single phase in which the components are completely miscible or soluble in each other. According to Nielsen (1978), the final one-phase binary mixture should be predicted based on simple mixture rules. An equation of the general form,

$$\rho = \rho_W X_W + \rho_E X_E + I X_W X_E \qquad \text{(Equation 2-9)}$$

where:

ρ = density of the mixture [M/L^3];

ρ_i = density of the component *i* [M/L^3];

X_i = mole fraction of the component *i*;

I = molecular interaction term.

can be used.

The molecular interaction term is related to the degree and type of mixing which exists in a specific system and must be determined empirically from the experimental data (Nielsen, 1978 in Donaldson, 1992).

Assuming water-ethanol (after equilibrium) and gasoline as a single pseudocomponent, the mixture of gasoline and water-ethanol behaves as a linear combination of the properties of the pseudocomponents making up the mixture. The equation representing the density of the final mixture is the simplest mixture rule (Nielsen, 1978):

$$\rho = \rho_1 X_1^M + \rho_2 X_2^M \qquad \text{(Equation 2-10)}$$

where:

ρ = density of the mixture (M/L^3);

ρ_i = density of the pseudocomponent *i* (M/L^3);

X_i^M = mass fraction of the pseudocomponent *i*.

In this case, mass fraction is preferred to mole fraction, since the equation deals with pseudocomponents (i.e., gasoline and ethanol+water) instead of single components.

2.4.2 Experimental Procedure for Determination of Solution Density

Eleven different compositions of water and ethanol were prepared using de-ionized, de-aired, organic free distilled water and pure ethanol. The compositions varied from 10% to 90% by volume ethanol in 10% intervals, including the compositions 45% and 55% by volume ethanol along with pure water and pure ethanol. The components were measured in the appropriate ratios using 1 ml, 2 ml, 5 ml, 10 ml and 20 ml glass pipettes and inserted into 125 ml oven cleaned glass bottles, sealed with Teflon septa and aluminum caps. The solutions were then agitated with a rotary shaker (Orbit shaker) at 300 rpm for 60 minutes. The densities of the final solutions were determined by weighing precise volumes with a Sartorius research scientific balance (±0.0005g) using 25.000 ml glass specific gravity determination bottle, Gay-Lussac type (ASTM D-369, D-854) with their dry weight previously recorded. The flasks were rinsed with water, then ethanol, then acetone and then twice with the same solution that was to be assessed. Rinse solutions were discarded. The volume changes were calculated based on the density changes (measured densities compared to calculated densities where additive volumes are assumed).

2.4.3 Results and Discussion

The results of the volume changes and density measurements for water and ethanol mixtures are summarized in Table 2-3. A positive value of the variation in density corresponds to the actual density of the final solution being greater than the density calculated on the basis of additive volumes of ethanol and water. Similarly, a

negative variation in the volume of the final solution means that the final volume of is less than the sum of the volume of both water and ethanol.

Table 2-3 - Measured and predicted densities and volumes and volume changes for water and ethanol mixtures.

Mole Fraction Ethanol (X_e)	Measured Density (g/ml)	Predicted Density [1] (g/ml)	Density Changes (%)	Measured Volume Change (%)	Predicted Volume[1] Change (%)
0.000	0.996	0.996	0.000	0.000	0.000
0.033	0.984	0.985	0.714	-0.719	-1.001
0.071	0.971	0.972	1.631	-1.658	-1.895
0.117	0.956	0.958	2.506	-2.571	-2.643
0.170	0.939	0.941	3.100	-3.199	-3.199
0.201	0.931	0.932	3.277	-3.388	-3.388
0.235	0.921	0.922	3.394	-3.514	-3.506
0.237	0.911	0.911	3.395	-3.515	-3.544
0.316	0.900	0.900	3.291	-3.403	-3.492
0.418	0.877	0.874	2.987	-3.079	-3.083
0.552	0.851	0.845	2.486	-2.550	-2.228
0.735	0.820	0.814	1.622	-1.648	-1.004
1.00	0.784	0.784	0.000	0.000	0.000

[1] Predicted densities and volumes refer to calculated densities based on Nielsen (1978)

Substituting the values of the densities of pure water and pure ethanol in Equation 2-9:

$$\rho_{mix} = 0.9989 X_W + 0.7845 X_E + I X_W X_E \qquad \text{(Equation 2-11)}$$

The molecular interaction term may be calculated using the value of the measured density of the mixture for a given ethanol mole fraction (X_E = 0.20 gave the best fit by visual trial and error). The calculated value is I = -0.138, and the Equation 2-11 becomes:

$$\rho_{mix} = 0.9989 X_W + 0.7845 X_E - 0.138 X_W X_E \qquad \text{(Equation 2-12)}$$

Equation 2-11 provides a good prediction for the values of density measured as illustrated by Figure 2-11, where a plot of the values of density as a function of mole

fraction of ethanol is shown. In this figure are plotted the points representing the measured values of density (cross points), the density calculated assuming additive volumes (dashed line) and the predicted density based on Nielsen (1978).

Figure 2-12 presents the changes (in percent) of density as a function of the mole fraction ethanol. The maximum density change occurs at an ethanol mole fraction of 0.235 (or initial volume fraction ethanol of 0.55) and corresponds to 3.4%, a positive variation in density that corresponds to a negative variation in the volume of the final solution (final volume of the mixture is less than the sum of both water and ethanol separated). Similar to Figure 2-12, Figure 2-13 graphically exhibits the volume changes for ethanol and water mixtures. Both figures Figure 2-12 and Figure 2-13 show a good agreement between the measured values of density and the predicted values for mole fraction ethanol between 0 and 0.45, with a small variable discrepancy for mole fractions of ethanol between 0.45 and 1.0.

Corrections for density changes due to non-additive volumes of ethanol and water were incorporated, through the use of Equation 2-12, in the calculation of final densities of the single phase solutions in the ternary diagram (Equation 2-9). Selected ternary compositions (varying 2% by weight on the three components - gasoline, water and ethanol) were used to produce a density field on the ternary diagram and isodensity contours were plotted in Figure 2-14. The region in the diagram where the changes in volume could have been larger falls predominantly within the two-phase region, i.e., below the solubility curve. The maximum volume change (-3.4%) occurs at the water-ethanol side of the diagram (pure water and pure ethanol present only). As the compositions move towards the inner part of the diagram and more gasoline is

incorporated to the system, the volume changes are diminished and are not perceptible graphically as shown in the Figure 2-14, where the isodensity contours seem to be plotted as straight lines. Actually, the lines are minimally (and imperceptibly) curved inwards, towards the water apex of the diagram (density increases due to negative volume changes).

The shading in the single phase region in Figure 2-14 varies in intensity, where the higher density value (pure water) corresponds to the darker shade (black), grading towards the lower density value (pure gasoline) corresponding to the lighter shade (white). The distance between two isodensity contours corresponds to 10% by weight on the water-ethanol side of the diagram and varying weight percent on the gasoline-ethanol side. These distances were chosen merely for graphical reasons because they are regularly spaced. The figure indicates that, as expected, along the solubility curve the oleic phase is less dense than the aqueous phase for all circumstances. Figure 2-14 also indicates that an injected ethanol-water mixture with the minimum ethanol content for miscible displacement (88% by weight or more ethanol content) will have higher density than a displaced oleic phase developed by its injection, and lower density than water, the original fluid contained in the pores. The results of this diagram have important consequences to determine the best direction of flow for the ethanol flushing process, as it is shown in Chapter 3.

The changes in volume due to molecular interactions between water and ethanol creates a local region of low pressure, with the consequent potential formation of a gaseous phase. Degassing of the water due to changes in aqueous phase internal structure, resulting from the mixing with ethanol, would account for the gaseous phase formation.

The gas so formed would be expected to contain BTEX. Donaldson (1992) analyzed a similar phenomenon for methanol and water, a system that also presents non-additive volumes.

The fraction of each constituent which would be present in the gas and aqueous phase can be approximated using Henry's law which describes the partitioning of solutes between gas and aqueous phases:

$$H_{cc} = \frac{C_{g,i}}{C_{w,i}} \qquad \text{(Equation 2-13)}$$

where:

H_{cc} = dimensionless Henry's constant [mole.m^{-3} / mole.m^{-3}];

$C_{g,i}$ = concentration of component *i* in the gaseous phase [mole.m^{-3}];

$C_{w,i}$ = concentration of component *i* in the aqueous phase [mole.m^{-3}].

Assuming that there are no other processes involved in the partitioning of organic constituents (e. g., sorption), a mass balance expression relating the mass of each constituent in the aqueous ($M_{w,i}$) and gaseous phase ($M_{g,i}$) to the total system ($M_{T,i}$) is:

$$M_{T,i} = M_{g,i} + M_{w,i} = C_{g,i}V_g + C_{w,i}V_w \qquad \text{(Equation 2-14)}$$

where:

V_g = volume of the gaseous phase [m^3];

Substituting $C_{w,i}$ from Equation 2-13 into Equation 2-14, the fraction of mass of each constituent transferred to the gaseous phase after partitioning may be represented by:

$$\frac{M_{g,i}}{M_{T,i}} = \frac{1}{\frac{V_w}{H_{CC}V_g} + 1} \qquad \text{(Equation 2-15)}$$

Henry's constant for benzene, toluene and o-xylene were from Lyman et al. (1990). Henry's constants for ethyl-benzene, p-xylene and m-xylene were approximated by:

$$H_{pc} = \frac{P_{vp,i}}{S_{w,i}} \qquad \text{(Equation 2-16)}$$

where:

H_{pc} = Henry's constant [atm mole m^{-3}];

$P_{vp,i}$ = vapor pressure of component *i* [atm];

$S_{w,i}$ = solubility of component *i* in water [mole m^{-3}].

This version of Henry's law is related to the dimensionless version (H_{CC}) by the gas law. Values for component vapor pressure and solubility were taken from Lyman et al. (1990). Table 2-4 presents the values of H_{CC} for BTEX compounds (benzene, toluene, ethylbenzene, ortho-xylene, meta-xylene and para-xylene) and their respective mass fractions (in percent).

Table 2-4 - Mass fraction (maximum) of BTEX compounds that partition to the the gaseous phase formed by volume changes due to mixing of water and ethanol.

Compound	Hcc	Mg/MT (%)
Benzene	0.24	0.071
Toluene	0.28	0.083
Ethylbenzene	0.37	0.109
O-xylene	0.22	0.065
M-xylene	0.26	0.077
P-xylene	0.19	0.056

Based on the calculations, 0.5% of the BTEX dissolved in the water may be transferred to the gaseous phase created by volume changes due to water and ethanol mixing. Experiments for volume changes calculation have shown gaseous phase formation without the presence of volatiles such as gasoline compounds. As ethanol is completely soluble in water, the Henry's constant determined using Equation 2-16 would be infinitely small, indicating that ethanol would remain almost entirely in the aqueous phase. The gaseous phase formed likely consists of gases dissolved in water (e.g., N_2, O_2, CO_2) prior to mixing.

2.5 Conclusions

The pseudoternary system gasoline-ethanol-water present a relatively large 2-phase region in the pseudo ternary diagram. Tie lines have a negative slope, characterizing the system as plait-point-to-the-right type, indicating that ethanol partitions preferentially to the aqueous phase.

For a flushing fluid composed of ethanol and water, the minimum ethanol content necessary to flush the gasoline residuals with complete miscibility is 88 wt% ethanol and 12 wt% water. This determination, based on the tangent of the binodal curve at the plait point, was approximate because the plait point could not be determined exactly in the laboratory. Considering the percent of water present in commercial alcohols such as ethanol (about 5% by volume), none or little water should be added to commercial ethanol to be used for gasoline residuals cleanup. The presence of methanol in very low

percentages in denatured commercial ethanol is not expected to significantly alter the behavior of the ternary diagram, the major problem being that methanol is a regulated compound as opposed to ethanol

The IFT increased exponentially with increasing ethanol content, with a 20-fold decrease from 21.9 to 1.0 mN/m for 0 to 0.65 mole fraction of ethanol in the water phase, respectively. Low IFT values (lower than 10^{-3} N/m) were difficult to measure in the laboratory and values of IFT for tie lines close to the plait point could not be measured. However, the rapid decrease in size of the tie lines close to the plait point suggests, for small increases in ethanol content, an exponential decrease in IFT values, as shown in the diagram.

Although ethanol and water mixture have non-additive volumes, this does not have a major effect on the final densities of the pseudoternary system gasoline-ethanol-water. Isodensities plotted on the pseudoternary diagram show that the mixtures of gasoline, water and ethanol that fall within the single phase region of the diagram are always denser than the gasoline phase that originated it. This have a major role on the stability of displacement.

The change in volume during mixing of water and ethanol may lead to the formation of a gas phase. The maximum volume change (and consequently volume of gas formed) is 3.4% and occurs for mixtures with 0.55 volume fraction of ethanol relative to water. For this volume of gas formed, the maximum BTEX transferred from dissolved phase to the gas phase is 0.5% of the total mass of BTEX dissolved in water. Thus, this gas phase does not represent a significant pool of BTEX in the porous media.

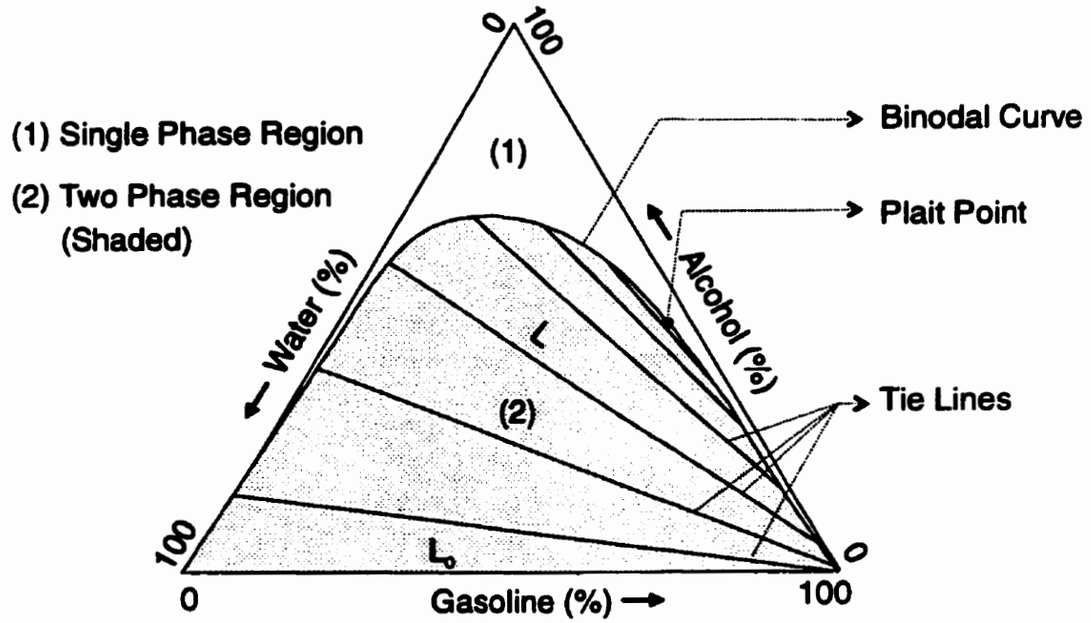

Figure 2-1- Typical Ternary Diagram

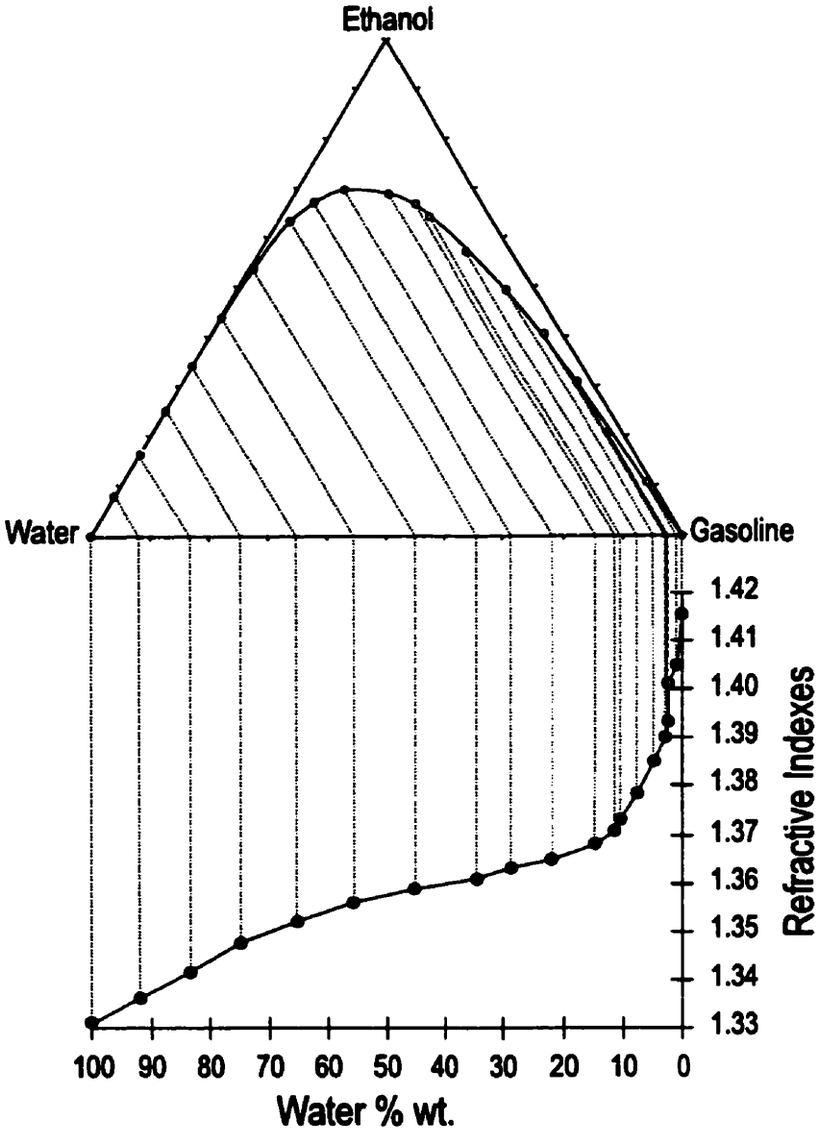

Figure 2-2 - Ternary Diagram and Refractive Indexes.

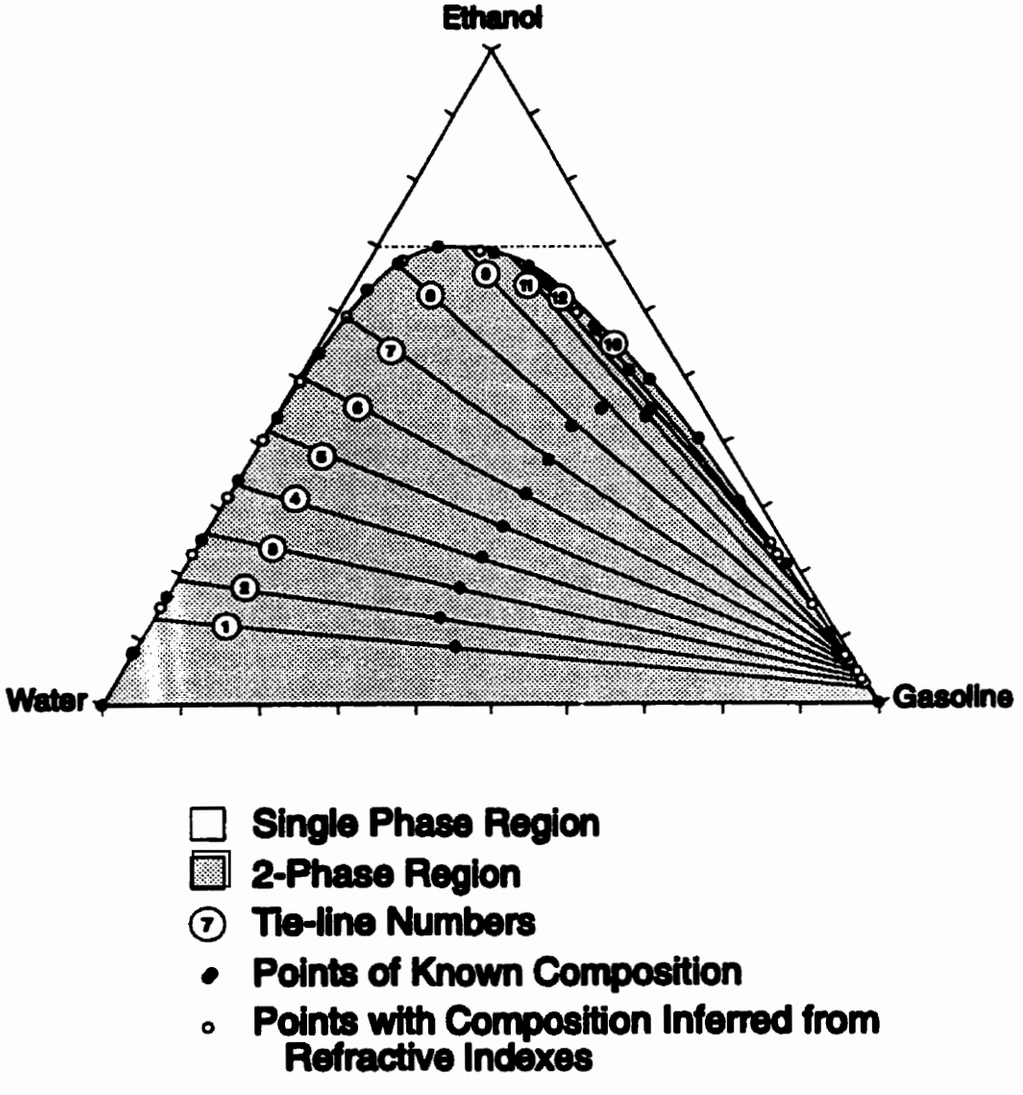

Figure 2-3 -Ternary Diagram for Gasoline-Ethanol-Water.

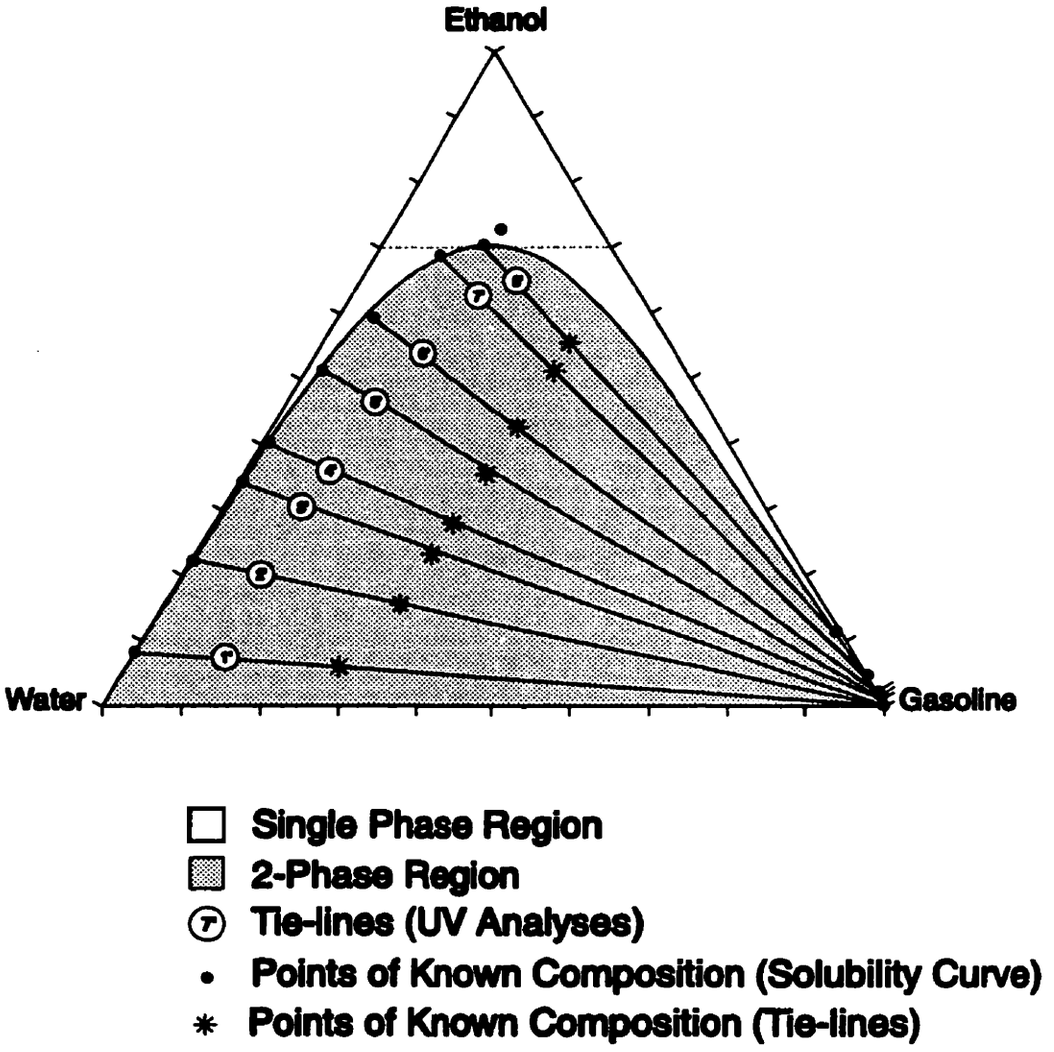

Figure 2-4 - Ternary Diagram for Gasoline-Ethanol-Water (Obtained by UV Analyses).

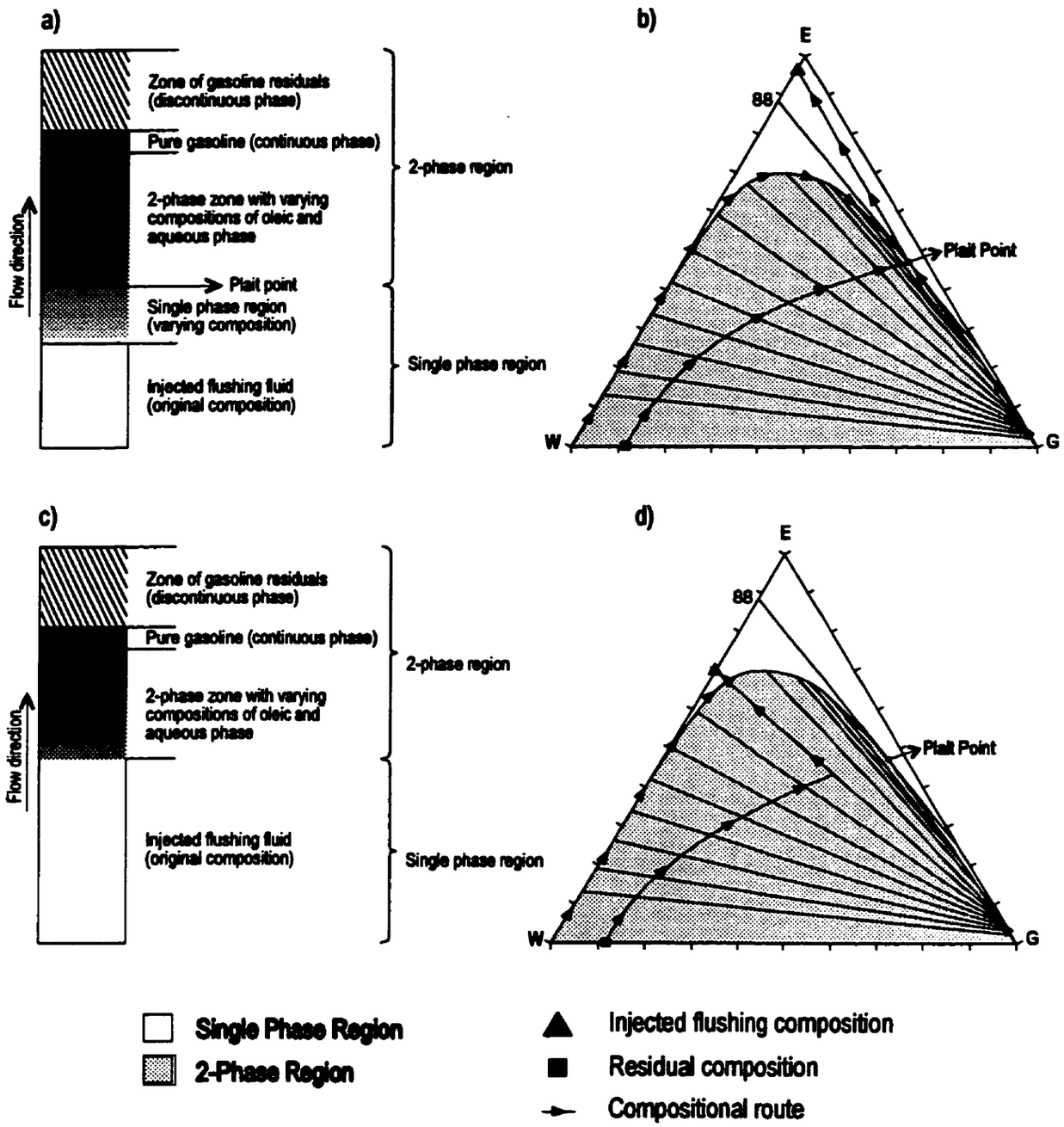

Figure 2-5 - Minimum percent of ethanol controlling whether developed miscibility is (a,b) not attained or (c,d) attained (adapted from Larson et al., 1982)

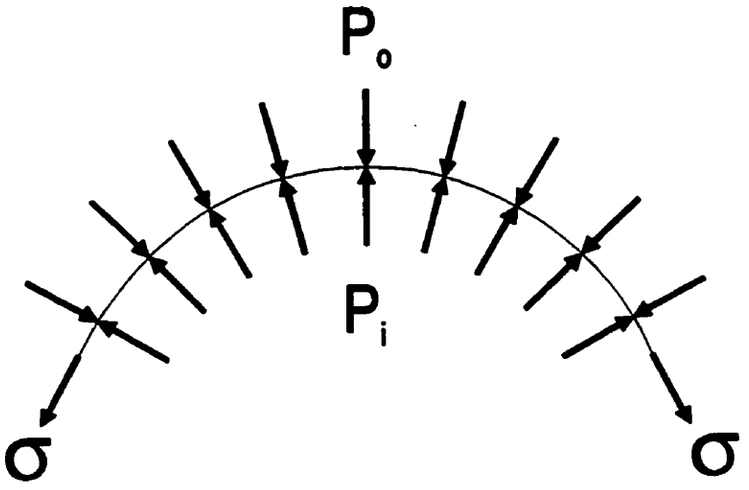

Figure 2-6 - Soap Bubble (Dullien, 1979)

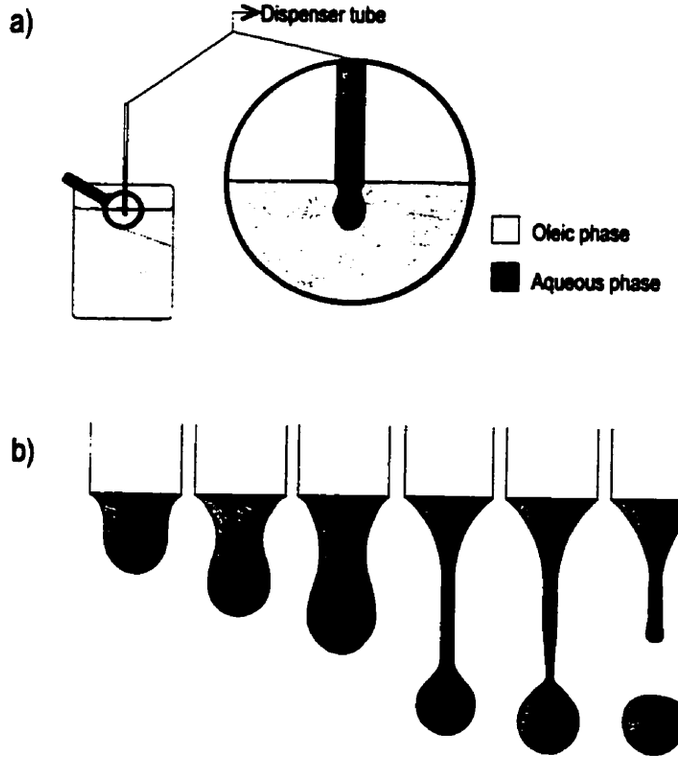

Figure 2-7 - Drop Weight Method (after Adamson, 1967)

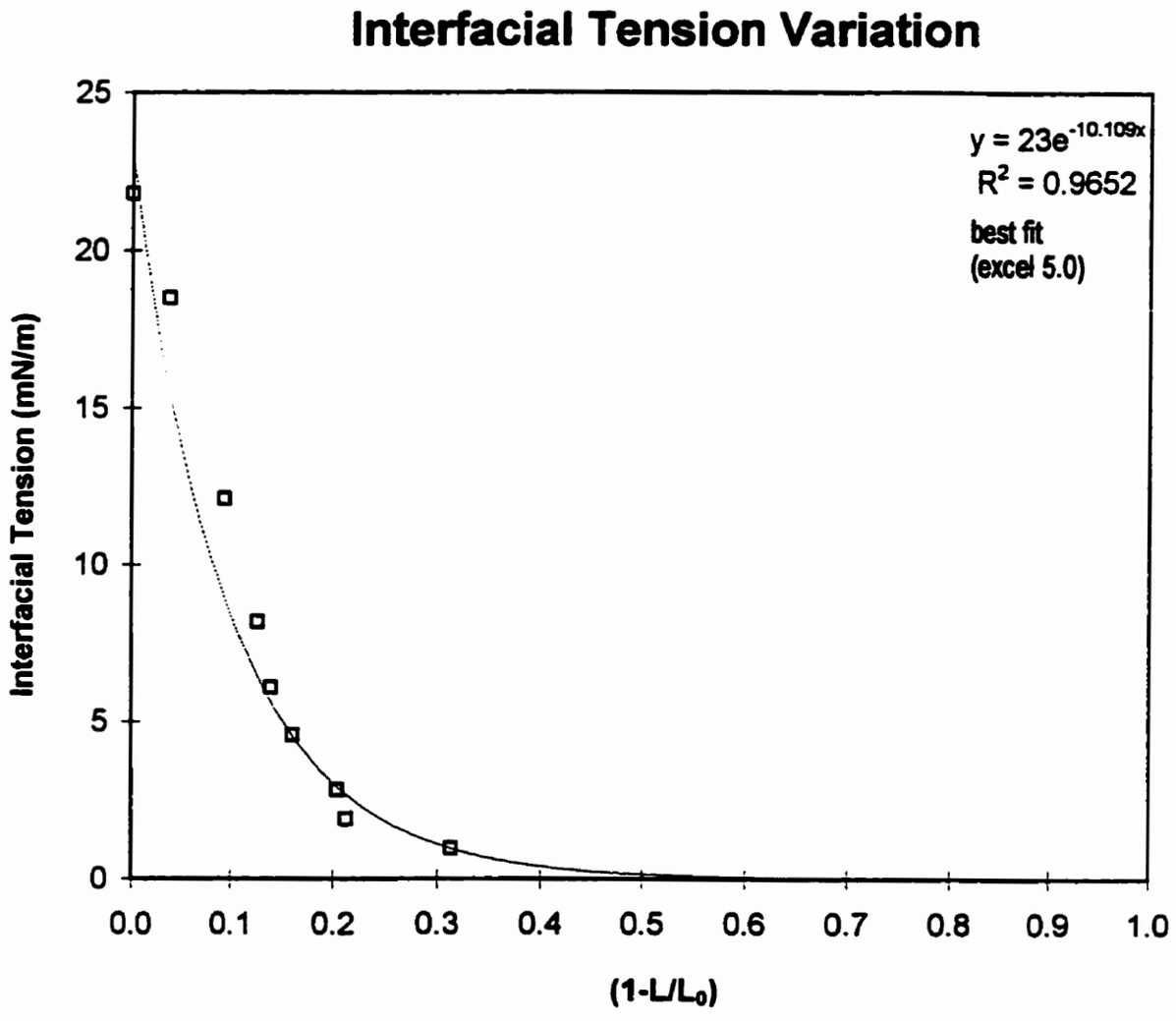

Figure 2-8 - Variation of Interfacial Tension as a Function of the Tie line Length in the Pseudoternary System Gasoline-Water-Ethanol

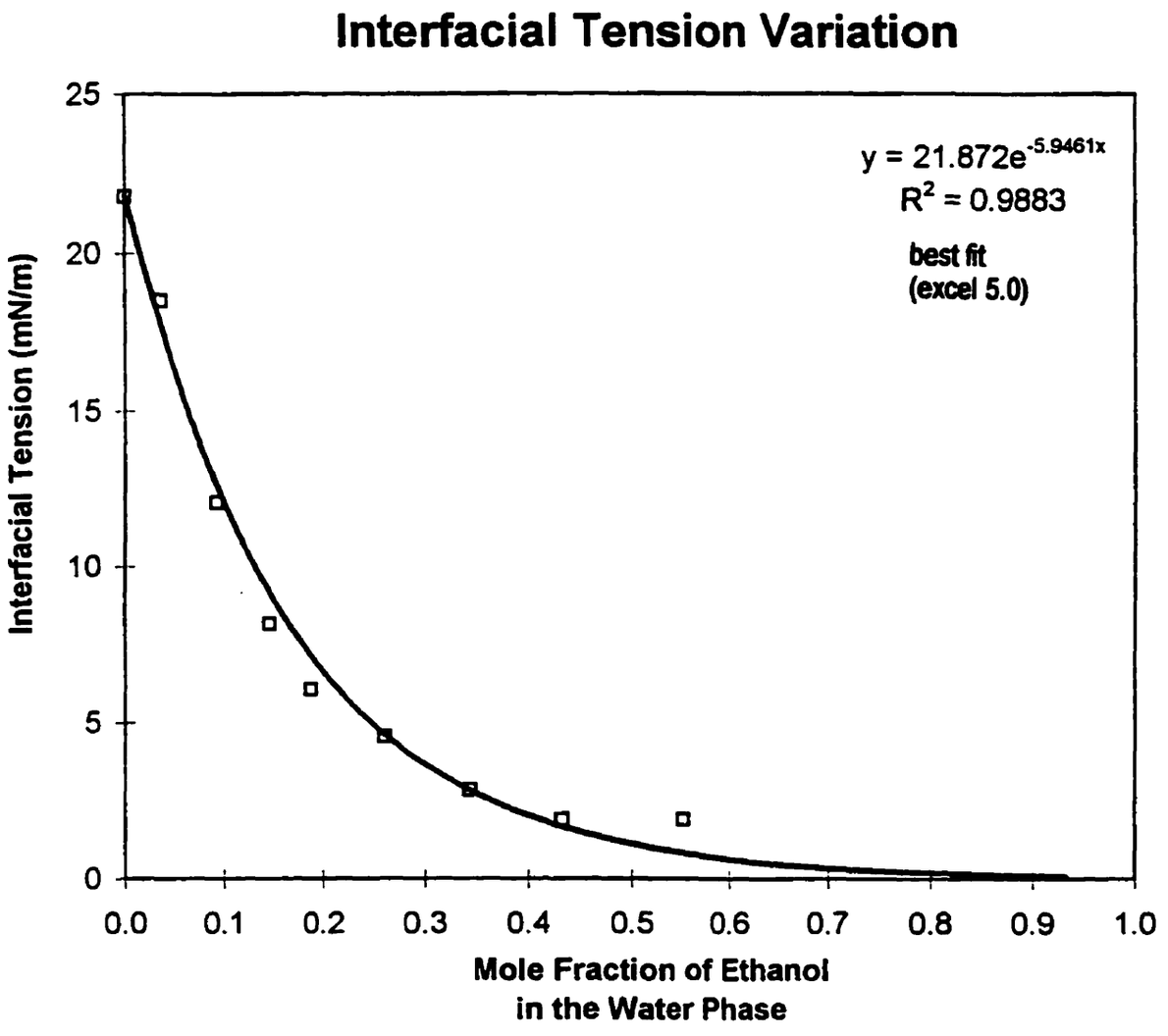

Figure 2-9 - Variation of Interfacial Tension as a Function of the Mole Fraction of Ethanol in the Aqueous phase in the Pseudoternary System Gasoline-Water-Ethanol

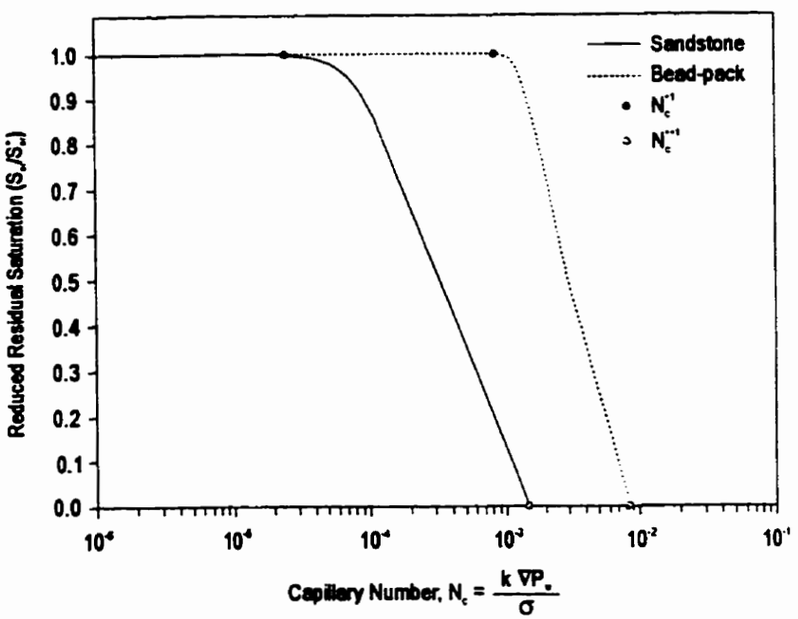

Figure 2-10 - Capillary number correlation for the mobilization of residual oil in water-wet sandstone (after Chatzis and Morrow, 1981).

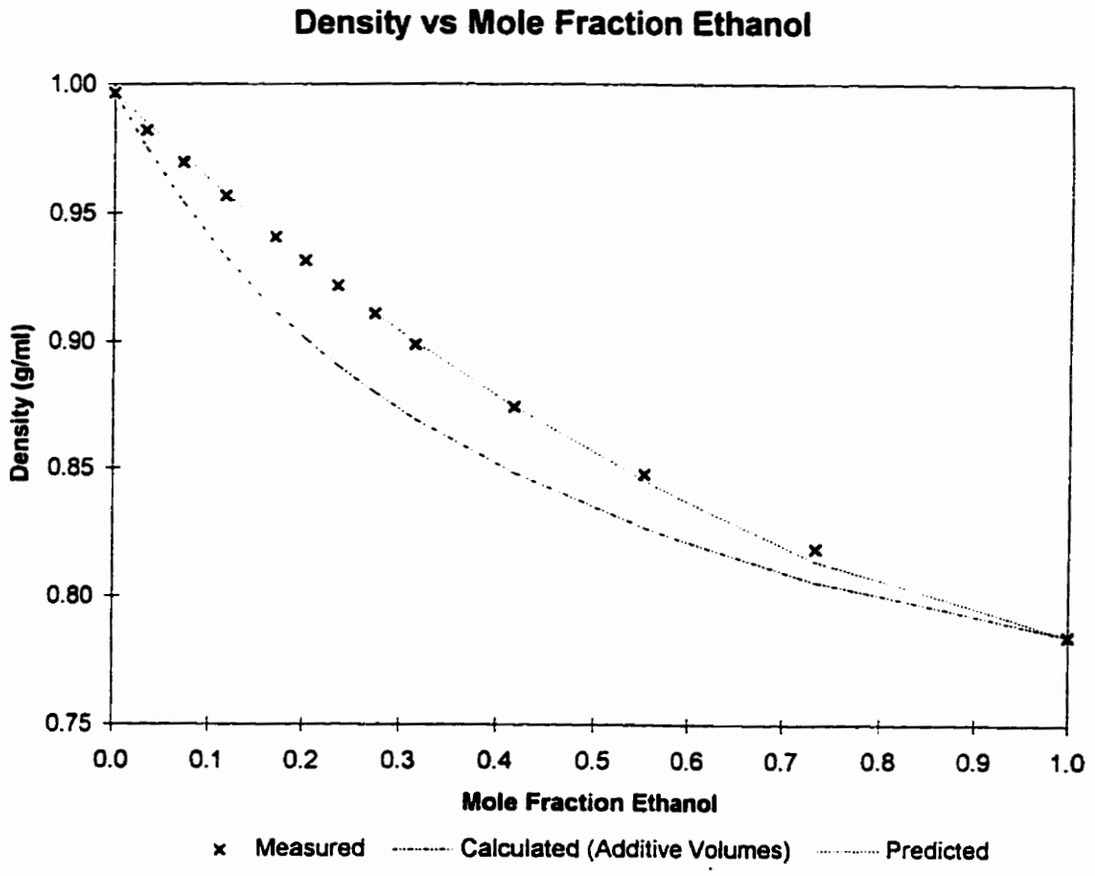

Figure 2-11 - Densities of Ethanol and Water Mixtures (20°C)

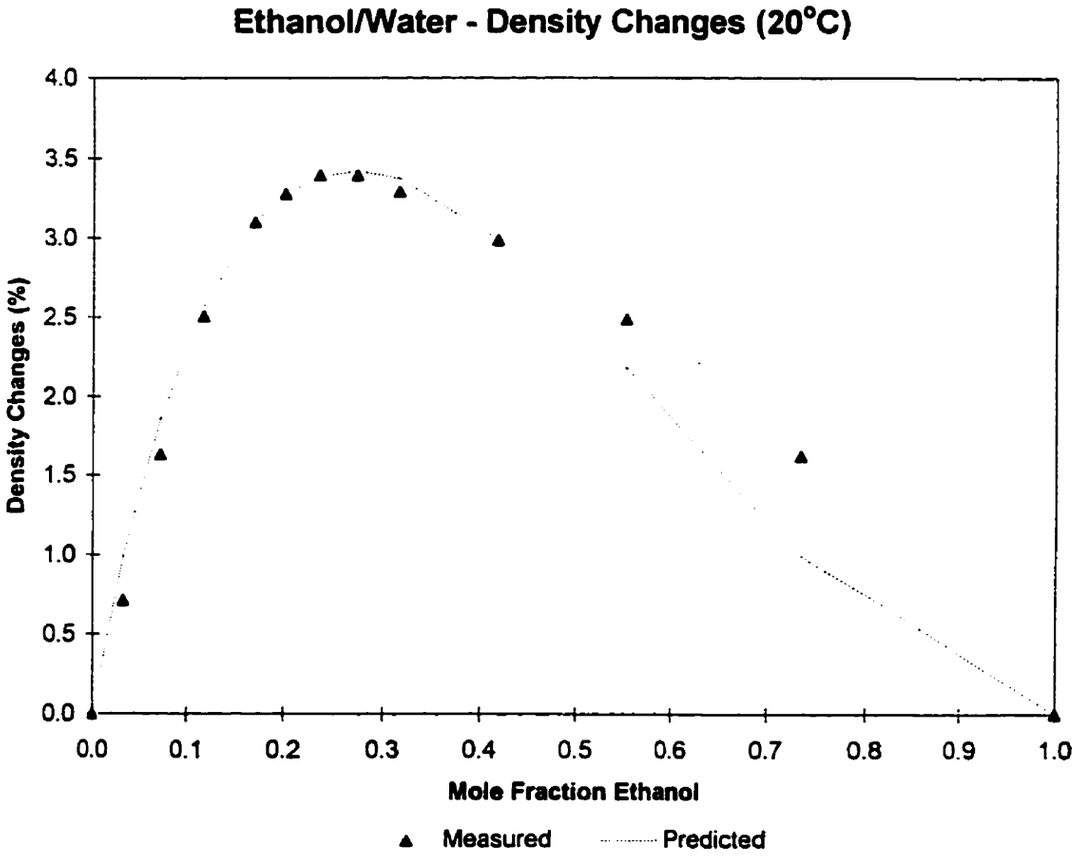

Figure 2-12 - Density Changes for Ethanol and Water Mixtures (20°C)

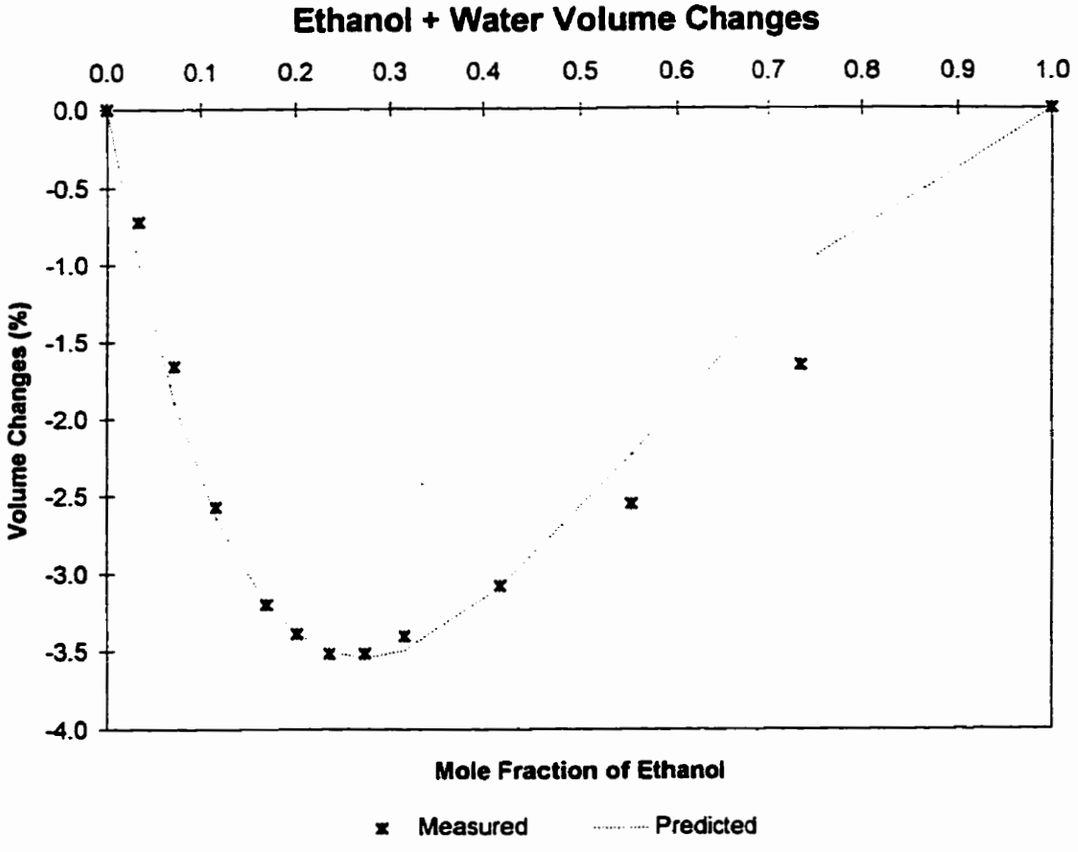

Figure 2-13 - Volume Changes for Ethanol and Water Mixtures (20°C)

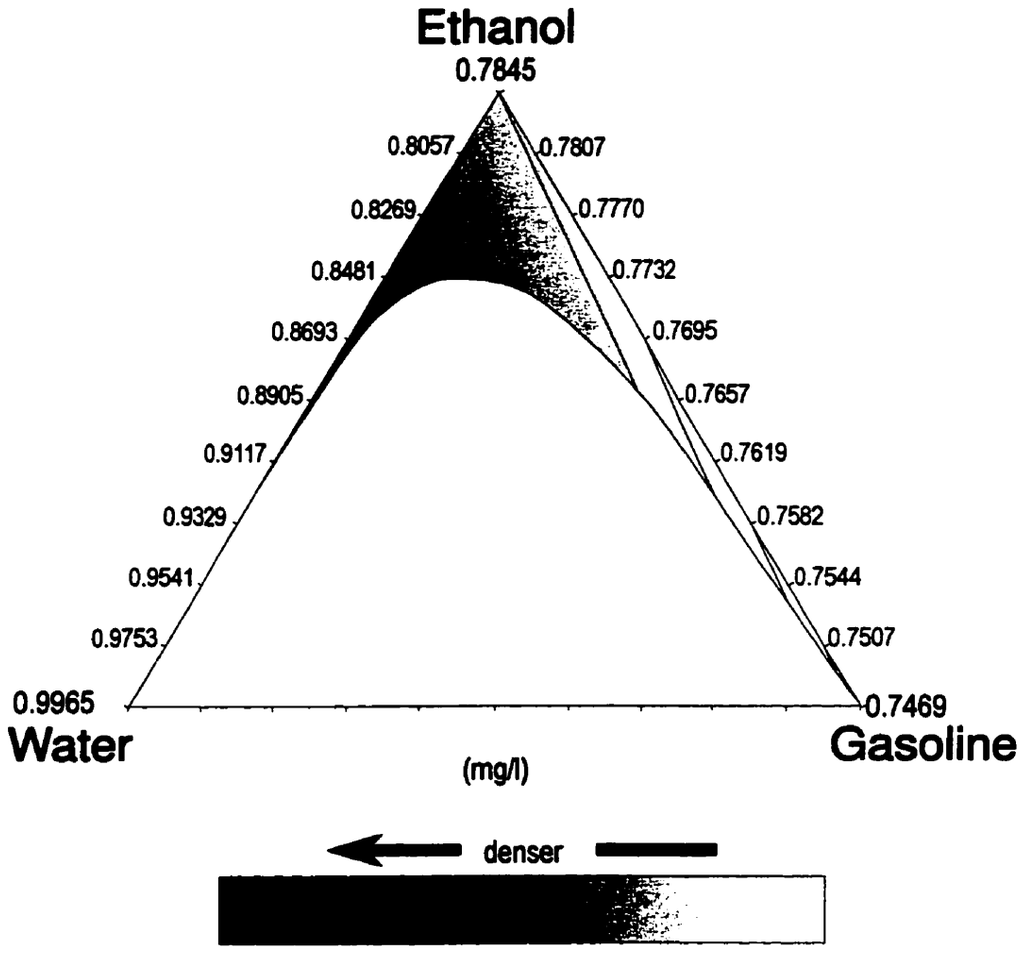

Figure 2-14 - Density distribution for the pseudoternary system gasoline-water-ethanol

3. PORE AND MICRO SCALE STUDY OF ETHANOL FLUSHING OF GASOLINE RESIDUALS

3.1 Objectives

The main objectives of this chapter are:

- Study the process of gasoline residuals removal by ethanol flushing at the pore scale level through the use of network micromodels etched on glass.
- Evaluation of the influence of the directions of ethanol flushing (horizontal, vertical upward and vertical downward flow).
- Provide guidance for design and implementation of the field experiment.

3.2 Pore scale study of ethanol flushing using micromodels

3.2.1 Background

Micromodels are physical model prototypes of a pore space network, created by etching a network pattern onto two glass plates which are then fused together. The pores have a complex three-dimensional structure, although the network is two-dimensional (Wilson et al., 1990). The details of the fabrication of micromodels can be found in the works of Chatzis et al. (1983), McKellar and Wardlaw (1982) and Wilson et al. (1990). The pore throats in the micromodel have elliptical cross-section with pointed ends, "eye shaped" (Figure 3-1), with the major axis in the plane of the plate, while the pore bodies are spheroids. The transparent nature of the micromodel allows the pore-scale of the water film along the edges to be visually observed and video-recorded. As pointed out by

Chatzis and Dullien (1977) and Dullien (1979), two-dimensional networks do not allow the existence of bicontinua, only three-dimensional models do. In a three-dimensional model, the pore edges may interconnect and form a continuum throughout the porous medium (Chatzis, 1980). In a two-dimensional model, however, most of the edges form loops, and a wetting liquid can form film loops in these edges. Because of the roughness of the solid wall and the angular cross section of the pores, pinch-off of the wetting phase can result in continuous networks in some areas of the model (Lenormand and Zarcone, 1983). Therefore, the topological properties of a 3D network of real porous space are to some extent represented also by a 2D micromodel. Two-dimensional (2D) etched pore network (micromodels) have been used to study mechanisms of oil or gas entrapment in the course of water flooding experiments (Chatzis et al. 1983). Use of etched glass micromodels also permits direct observation of processes that accompany residual oil mobilization.

Processes of gasoline (oil) entrapment have been described in the literature (Moore and Slobod, 1956; Mohanty et al., 1980, Chatzis et al., 1983; Wardlaw, 1982; Wilson and Conrad, 1984; to name a few examples). The study of this phenomenon is facilitated by the so called pore-doublet model (Figure 3-2), in which the dynamic displacement mechanisms were detailed in the study of Chatzis and Dullien (1983).

On the onset of a gasoline spill, as the gasoline moves downward, it eventually reaches the capillary fringe, depresses it and reaches the water table. Assuming the aquifer is strongly water-wet, gasoline (the non-wetting phase) displaces water (the wetting phase) from the pores during this process (drainage process). For typical groundwater velocities, capillary forces dominate over viscous forces, and trapping

behavior is controlled by the pore structure at the pore level. Chatzis and Dullien (1983) presented an analysis of immiscible displacement in which it was verified experimentally that the advancement of the fluid-fluid interfaces from one pore to the next occur in a hierarchic manner - one pore at a time. During drainage, the non-wetting fluid proceeds through the largest pore throat to the next pore, trapping the wetting fluid entirely in the small throat of the pore-doublet model (Figure 3-3).

Eventually, as the spill ceases, the continuous phase of gasoline standing on the top of the water table and/or capillary fringe (named free-phase gasoline) is subsequently displaced by water, due to water table seasonal variation and natural groundwater flow. During this process, the advancement of the water-gasoline interface is an imbibition process. Water advancement occurs through the smaller pore throat first, with the non-wetting phase remaining stationary in the largest pore in a doublet cofiguration until the interface reaches the downstream node. If capillary stability exists in the downstream mode of the doublet, then complete recovery of the non-wetting phase from the larger pore throat occurs (Figure 3-4). If the downstream mode has a geometry that leads to capillary instability, trapping of the gasoline in the large pore throat occurs, as shown in Figure 3-5 (Chatzis et al., 1983). Trapping of either wetting or non-wetting phase in a pore doublet model is called "by-pass".

Along with the by-passing mechanism, "snap-off" is another major mechanism for the trapping of the non-wetting phase. This mechanism occurs due to instabilities of interfaces when interfaces compete for advancement in a pore body and pore throat, as shown in Figure 3-6. The mechanism strongly depends on wettability and aspect ratio - the ratio of pore-body diameter to pore-throat diameter (Wardlaw, 1982). Figure 3-6

(after Chatzis et al., 1983) shows the effect of pore aspect ratio on non-wetting phase trapping in a tube of non-uniform cross-sectional area.

Micromodels have been used for different purposes and are invaluable tools to study the basic physics of pore level flow. Wilson et al. (1990) explore the use of micromodels to study the effects of heterogeneities on the movement and capillary trapping of NAPLs. Wan and Wilson (1994a,b; 1993; 1992) studied the visualization of colloid transport. Wan et al. (1994) used micromodels to study the transport and colonization of microorganisms in pore spaces. Donaldson (1992) studied the pore scale behavior of M-85 (85% methanol and 15% gasoline). Dong (1995) used micromodels to study flow of the wetting phase along the edges of the pores.

3.2.2 Experimental Procedure

The water-wet micromodel used in this experiment has a square array type of pore geometry with pore body sizes and pore throat sizes randomly distributed (micromodel SQ1, as described by Kantzas et al., 1988). Typical pore throat sizes calculated from capillary interface positions during drainage of water by air correspond to equivalent capillary tube diameters in the range of 120 μm to 150 μm. The maximum body size varies between 200 μm to 1500 μm in top view (Kantzas et al., 1988). The pore volume of the micromodel was measured by the difference in mass of the model saturated with water and its dry weight, corresponding to 0.187 ± 0.005 ml. The measurements were determined using a Fisher Scientific Gram-atic balance accurate to ± 0.0001 grams.

Prior to the experiments, the micromodel was initially cleaned by injecting several pore volumes of ethanol, followed by several pore volumes of acetone and finally air. The dry micromodel was then rinsed thoroughly with distilled water. The model was then flushed with air for several minutes until completely dry, then the model was flushed with CO_2 to fully displace the air, making it ready for water saturation. Distilled, de-aired water was then injected continuously until no gaseous phase was present. Figure 3-7 shows a top view of the setup of the injection of fluids into the micromodel. The micromodel was maintained in a horizontal position during the whole procedure and the displacement process was video recorded.

The micromodel was connected to a syringe pump (Sage Instruments model 351 and model 355) through 1/8" O.D. Teflon tubing, with brass fittings and teflon ferrule and o-ring at one end and connected with the help of larger diameter Tygon fuel tubing to the syringe at the other. Identical brass fitting and teflon tubing connected the exit end of the micromodel to the disposal vial.

Flushing of gasoline residuals from the saturated zone of the aquifer was simulated in micromodel displacement experiments. Gasoline used in this work was provided by API and its approximate composition is presented on Appendix IV. Entrapment of gasoline residuals in this zone occurs due to free-phase product reaching the top portion of the water table by depressing the capillary fringe (drainage process), followed by later displacement of this continuous phase by changes in the water table and natural flow of groundwater (imbibition process). Gasoline residuals in the micromodel were obtained by injecting gasoline into the water saturated model (S_w = 100%) at a constant rate (~ 10 µl/min) until it broke through at the exit end. Gasoline injection was

maintained for a few minutes after that no more water came out of the model and maximum gasoline saturation was established (S_o). The same injection procedure was repeated for water, at the same rate, to displace the gasoline and establish residual oil saturation (S_{or}). Ethanol injection followed at the same rate. The gasoline used was dyed red using Oil Red O (an oil soluble dye) for flow visualization and interfacial tensions were determined for dyed gasoline.

Several experiments were carried out to observe the behavior of the gasoline residuals when ethanol is injected. Since the physics of the displacement was the main objective of this experiment, complete removal of all residuals was not achieved in every attempt. Attention was focused on a few details of each run.

Visualization was helped with the use of a Bausch & Lomb StereoZoom©7 microscope with a video recorder camera attached to it. The video camera was connected to a VCR and a television monitor in order to record the observed phenomena. The phenomena were visualized through transmitted light, with the model being illuminated from below.

3.2.3 Results and Discussion

3.2.3.1 Emplacement of residuals

Injection of water in the dry, air filled micromodel tends to trap gaseous phase by imbibition mechanisms as described before. The utilization of CO_2 eliminated this problem, because after several pore volumes of water have been flushed through the model, the trapped CO_2 dissolves in water and 100% water saturation is achieved. Injection of gasoline displaced water leaving trapped wetting phase behind in small pores

and in the corners of pores invaded by gasoline. Several pore volumes of gasoline were injected until water production at the exit end had ceased. Following model saturation with gasoline, water was injected (waterflooding) to establish gasoline residual distribution in the model. The water injection terminated after water broke through the model.

Waterflooding the model after gasoline injection was carried out at a rate of 5 to 20 μl/min. For this flow rate, the average linear velocity was calculated to be in the range of 0.69 cm/min to 2.76 cm/min (100 to 400 times the typical groundwater velocity for Borden aquifer). The micromodel used is composed of 41 capillaries parallel to the main direction of flow, each of them with a variable cross section of 120 μm to 150 μm. For the flow velocity calculations the value of 120 μm was used. This range of velocity, although apparently high, corresponds to capillary number conditions in the range $5.26 \times 10^{-7} \leq N_c' \leq 2.10 \times 10^{-6}$. This range is one order of magnitude less than the critical capillary number ($N_c'^{*} \approx 2 \times 10^{-5}$) at which oil mobilization starts for sandstone aquifers (see Figure 2-11, Chapter 2). For unconsolidated materials, where the aspect ratio (the ratio between the diameter of the pore to the diameter of the throat) is small compared to sandstones and the blobs of residuals tend to occupy single pores, the N_c' is higher (order of magnitude of 10^{-3}, Morrow and Chatzis, 1982; Morrow et al., 1988). Thus, this range of velocities for fluid injection was not high enough to displace the residuals by simply overcoming the capillary forces. Rather, interfacial tension reduction from ethanol partition to the oleic phase will be required to remove residuals.

Chatzis et al. (1988) described the emplacement of oleic phase residuals at the microscopic scale. The authors observed that, under the water wet conditions prevailing in aquifers, the trapping of oleic phase occurs in the relatively large pores and that it is first mobilized from pores with relatively large pore throats. Regions of low permeability with residual oil will be formed where the trapped blobs are surrounded by water flowing through higher permeability channels around them. These blobs may be of different sizes and shapes, varying from singlet blobs (blob occupying a single pore) to multiple pore-body elongated or branched blobs. The magnitude and the structure of oil residual saturation was studied in detail experimentally by Chatzis et al. (1982, 1984). The authors performed experiments in random packs of equal sized spheres, heterogeneous packs with heterogeneities of different scales, two-dimensional capillary networks and Berea sandstone. Residual blobs occupy a single pore (singlet) up to clusters of 20 pores multiply connected. The amount of residual non-wetting phase trapping and the size distribution of trapped blobs depend to a very large extent on the aspect ratio and on the manner different size pores are distributed relative to each other. Pore systems with large aspect ratio cause very high residual oil saturations. Large pores and clusters of large pores surrounded by smaller pores are potential sites for trapping non-wetting phase during waterflooding (Chatzis et al., 1982).

For large and branched blobs, a large portion of the blob surface can be in contact with only a film of water along the pore walls or pore edges in non-circular geometries. In such cases, the interface (NAPL-water) transfer rate may be limited by advection or diffusion through these films of water to flowing groundwater (Wilson, 1994). Observations in micromodels indicate that the flowing water tends to move preferentially

around the blobs, through completely water filled pores with much less water movement through the water films or in pore wedges, to help advect organic compounds away (Wilson et al., 1990; Conrad et al., 1992). Wilson (1994) also mention that it is possible that the majority of organic constituents may enter the water through the ends or "tips" of the branched blobs, since it is likely that these "tips" are the only part of the blobs exposed to flowing groundwater. The author suggested that this observation required additional experimental confirmation. Results of the mobilization/dissolution of gasoline blobs in this work show strong evidence that this is, in fact, the case.

Blob ejection mechanism

During the injection of ethanol to flush the gasoline residuals in the micromodel, an interesting phenomenon occurred. A small blob (an approximately spherical drop) detached itself from a larger blob and flowed horizontally against the ethanol flow. This phenomenon is referred to as the *blob ejection* mechanism. Figure 3-8 shows a stepwise sequence of photographs showing a blob moving against the ethanol rich flow. A balance of forces acting on the blob is presented on Appendix IV.

The blob that moves against the ethanol flow belonged to a larger gasoline body being ejected from a pore where it is trapped. The blob ejection phenomenon was video-recorded and a sequence of photographs is presented on Figure 3-9.

The sequence of photographs shows the blob being ejected to the mainstream. For these experiments, it was assumed that ethanol diffuses through the pore throat and momentarily reduces the IFT for the portion of the blob surface most exposed to ethanol rich fluid. For very short length of pore throats, advection might be the main phenomenon that transport ethanol to the gasoline blob. The lower IFT causes capillary

instability and drives the trapped gasoline blob out of the pore towards the main ethanol-rich flow. Figure 3-10 presents, in a schematic illustration, a simple description of the phenomenon. Figure 3-10a exhibits the initial idealized setup. A spherical blob is trapped into a spherical pore body and almost completely fills the pore space. A film of water of negligible thickness separates the gasoline blob from the pore wall. This pore is connected by a pore throat to another spherical pore where the preferential flow occurs. Initially, water is the only flowing fluid. The gasoline blob is acting as a pore constriction, and only film flow of water can take place in the pore occupied by the blob. In Figure 3-10a the main parameters influencing the blob ejection mechanism are presented. R_1 and r_2 are the radius of the pore body and pore throat, respectively; x corresponds to the length of the pore throat and σ_1 is the interfacial tension between pure gasoline and pure water. The pore throat, initially filled with water, is an open channel where ethanol can subsequently diffuse through (or flow through as a film flow) to contact the gasoline blob (Figure 3-10b). As this occurs σ_2 is reduced.

Figure 3-10b shows when ethanol has reached the gasoline blob, decreasing the interfacial tension at a small area of the blob closest to the pore throat. Mass transfer is very intense at this point locally decreasing the IFT, and the blob starts to stick out of the pore. In the figure, σ_2 represents the minimum IFT necessary to start the blob ejection. Figure 3-10c shows the blob ejection phenomenon in a later stage. By differences in IFT, the trapped blob is pushed toward the main stream of ethanol flow. The volume of gasoline (or oleic phase) pushed through the pore throat is compensated by a reduction in

the overall size of the trapped blob (as shown in the figure) and less significantly, by swelling due to ethanol partitioning to the oleic phase.

From Figure 3-10b, the capillary pressure P_{C_1} for the blob, corresponding to the part located within the pore space and not connected to the throat where ethanol diffuses through, must overcome capillary pressure P_{C_2}. Thus, for Figure 3-10b:

$$P_{C_1} \rangle P_{C_2} \qquad \text{(Equation 3-1)}$$

or

$$\frac{2\sigma_1}{R_1} \rangle \frac{2\sigma_2}{r_2} \qquad \text{(Equation 3-2)}$$

Therefore,

$$\sigma_1 \rangle \sigma_2 \frac{R_1}{r_2} \qquad \text{(Equation 3-3)}$$

From Equation 3-2, the interfacial tension in the pore space must exceed the interfacial tension at pore throat by a factor of R_1/r_2, which corresponds to the aspect ratio of a given medium. For unconsolidated sand, typical aspect ratios are between 1.5 to 3 (Chatzis, pers. comm.), and consequently the interfacial tension reduction that has to be achieved for blob ejection corresponds to 0.33 to 0.66 of the IFT of the blob within the pore where it is trapped. These calculated reduction of IFT are much higher than those predicted from capillary number experiments (based on interfacial tension reduction alone) presented by Chatzis et al. (1983). The model observations are that mobilization of gasoline residuals with ethanol flushing starts at lower values than the critical capillary number for mobilization conditions.

The correspondence between R_1/r_2 (radius of the blob within the pore body over the radius of the blob within the pore throat) and the aspect ratio is true when the water film has negligible thickness and the radius of the blob corresponds to the radius of the pore (throat or body). For most cases, the aspect ratio represents a good description for the ratio of the blob itself. But after ejection starts, the volume of the blob may vary and so may its radius. For this reason, it is more appropriate to refer to the relationship R_1/r_2 as *capillary ratio*, bearing in mind that it corresponds to the aspect ratio for most cases.

The phenomenon of ejection is neither continuous nor a single pulse. When an ejection pulse takes place, the capillary ratio R_1/r_2 changes. A detailed sequence of the ejection of a single blob with variations in the *capillary ratio* is schematically presented in Figure 3-11. The pulses of the ejection mechanism could be due to shear forces chopping the blob at the throat of the pore, by mechanisms similar to snap-off of continuous phase of non-wetting fluids, as mentioned earlier in this chapter, or by swelling of the tip of the ejected portion by ethanol that is incorporated. The mass removal by this chop off, not assessed in this work, could provide an evaluation of mass removal by blob ejection.

A trapped blob usually assumes an irregular shape from adapting itself to the pore space that confines it. At pore throat openings, its surface is more convex as a consequence of higher IFT, as shown in Figure 3-11a. When the blob is reached by ethanol from one pore throat, a first ejection pulse takes place. After this very brief pulse, when the blob size decreases by ejecting mass through the pore throat, the more convex points disappear and the radius of the blob (R_1') becomes approximately the radius of the pore body (R). Momentarily the *capillary ratio* increases (from R_1/r_2 to R_1'/r_2) and the

ejection tends to slow down (Figure 3-11b). But the IFT in the pore throat (σ_2) decreases because the portion of the blob that is being ejected advances and reaches an ethanol-richer solution, and ejection continues (Figure 3-11c). If the rear of the blob is reached by relatively high ethanol content aqueous phase, the IFT difference decreases and ejection slows down again. In the process, IFT decreases over the entire blob and the blob is mobilized when IFT is very low. If relatively low ethanol content aqueous phase reaches the rear of the blob, it may be completely ejected (mobilized).

As the blob becomes is ejected, more ethanol is incorporated to film of water in between the trapped blob and the pore wall. The ethanol content may eventually turn the composition of fluid to locally reach composition of single phase, and the trapped blob at the portion clings to the pore wall, a phenomenon called wettability change. When this occurs, the removal of the blob is slowed and the main removal of gasoline mass occurs by dissolution. The total mass that is removed by blob ejection alone could not be properly assessed in this work, and a visual estimate from the video recording suggests that approximately 40% of the mass is removed by ejection, and the remaining mass is removed by either an overall decrease of the IFT of the blob (mobilization) or dissolution. The *blob ejection* mechanism facilitates the flow of ethanol around the partially ejected blob, creating regions of higher permeability by removing mass of the blob, favoring later removal of the blob by the other mentioned mechanisms.

Based on the same principles of the single blob ejection, a cluster of blobs may be mobilized by ejection in a similar but stepwise manner. An *idealized* removal of a branched blob constituting a cluster of seven interconnected pore bodies is showed in Figure 3-12. All pore bodies are identical in dimensions and shapes and so are the pore

throats. For simplification, the variation in *capillary ratio* due to mass ejection is not represented in the figure, assuming that the mass of the cluster is much larger than the portion of mass ejected. Film flow is considered negligible. Figure 3-12a shows the preferential pathways for ethanol, with higher ethanol content at flow paths of higher fluid velocity. Ethanol diffuses through the pore throats to reach positions 1, 2 and 3 (Figure 3-12a). Diffusion at position 3 is favored by its proximity to the higher ethanol content flow, and ejection is expected to start at this point (Figure 3-12b). As part of the blob is ejected into the pore at position 3, ethanol rich flow at position 2 may develop and more of the blob is removed by ejection, further mobilization and dissolution, up to a point where ethanol flows freely through the developed now open path (Figure 3-12c). Next, position 1 is reached earlier by higher content ethanol. Ejection is favored and the pore is cleaned up following a similar process. Figure 3-12d shows a situation similar to the initial. Mass removal proceeds until all residuals are removed from the pores.

Assuming that the major factor that controls the onset of the mobilization by ejection is the diffusion of ethanol in water through a pore throat, a very simplistic calculation was done to give an idea of order of magnitude of the times involved in this process. The beginning of the ejection process depends on the length of the pore throat, the *capillary ratio* (which determines the necessary concentration of ethanol to reduce the interfacial tension) and the diffusion coefficient of ethanol in water. Figure 3-13 shows different start times for blob ejection for different *capillary ratios* and length of the pore throats. The solution for time required for the start of blob ejection was based on the one-dimensional solution of Fick's Second Law (Crank, 1956), assuming a constant diffusion coefficient (D) for ethanol equals to 8×10^{-10} m^2/s, and ethanol concentrations related to

capillary ratios determined from Figure 2-10 (Chapter 2). In this simplistic approach, it is assumed that the diffusion of ethanol through the pore throat does not change when ethanol reaches the water-gasoline interface of the blob, and the diffusion progresses infinitely. The estimated time is a characteristic time.

As showed in the Figure 3-13, the necessary characteristic time for the start of the blob ejection is of the order of a few seconds to thousands of seconds (few hours). These times are relatively short, even for high *capillary ratios* or long pore throats. For typical groundwater velocities, or even for relatively higher fluid velocities through forced gradients during cleanup processes, the injected fluid moves only a short distance during the time necessary for ejection (few centimeters or tens of centimeters for typical groundwater velocities). This suggests the importance of blob ejection for field applications, because the mobilization of the residuals is possible for the typically low velocities in the aquifers, and a high hydraulic gradient is not necessary for cleanup.

Wilson (1994) suggests that it is possible that the majority of the trapped organic constituents may enter the mainstream (aqueous phase) through the ends or 'tips' of the blobs or clusters of blobs, since it is likely that these tips are the only part of the blobs that are exposed to flowing fluids. The observed ejection phenomenon confirms this hypothesis. A major mass removal occurs with blob ejection when compared to dissolution of the blob by fluids flowing around it. As a consequence, pathways of relatively higher permeability are cleaned up earlier because they allow more injected fluid to flow beside a trapped blob, maintaining a high ethanol gradient necessary to eject the blob. In this sense, film flow of water through very narrow pathways, and mass removal may be considered negligible when compared to ejection mechanism.

IFT differences are the basic condition for ejection. A blob that is uniformly reached by ethanol from different sides may distribute the IFT changes more evenly along its surface and not have the necessary IFT difference to be ejected. When this situation happens, the blob is removed after its overall IFT is reduced and flow conditions reach the critical capillary number for that specific blob.

3.2.3.2 Gas phase formation

The gas phase formation was analyzed quantitatively and qualitatively in Chapter 2. As predicted, a few bubbles did form in the micromodel experiment, but did not have a noticeable influence in the overall flow pattern. Not enough gas formed to develop a continuous phase. Only two or three pores were blocked by the presence of a gas bubble formed after ethanol injection.

3.3 Study of the Effects of Flow Direction on the Ethanol Flushing Using Sintered Glass Bead Models

3.3.1 Background

For flushing of residuals, when a fluid displaces another (e.g. ethanol displacing water), the maximum sweep efficiency is achieved when the interface between the two fluids (displacing and displaced) moves as a plug front. This is described as a *stable displacement*. Sintered glass bead models have been used to study the stability of displacement for oil (DNAPL) and water by Deng (1996). Sintered bead packs have been used for visualization by Chatzis and co-workers in several studies. Sintered glass plates are made of lightly sintered glass beads (about six layers) between two rectangular glass

plates separated by a distance of about 3 to 6 mm. A description of model construction may be found in Morrow et al. (1988).

Although ethanol and water are miscible fluids, the basic principles of stability of displacement of immiscible fluids are useful to understand the behavior for ethanol flushing encountered in the sintered glass bead experiments. Kueper and Frind (1988) presented an overview of immiscible fingering in porous media where stability of displacement is analyzed under the interpretation of the equation (Hill, 1952):

$$v = \frac{g(\rho_2 - \rho_1)\cos\alpha}{\frac{\mu_2}{k_2} - \frac{\mu_1}{k_1}} \qquad \text{(Equation 3-4)}$$

where:

v = velocity of displacement [L/T];

ρ_i = density of fluid i [M/L^3];

μ_i = dynamic viscosity of fluid i [M/LT];

k_i = relative permeability of fluid *i* [L^2];

α = dip angle.

Equation 3-4 considers the displacement of fluid 2 by fluid 1 in a direction which makes an angle α with the vertical (the dip angle). The fluid moves at a constant velocity v. Equation 3-4 implies that there exists a critical velocity v_c beyond which a finger will develop from a microscopic perturbation. The equation is similarly developed for either nonwetting fluid displacing a wetting fluid or vice-versa. Both gravitational and viscous forces can have either a stabilizing of a destabilizing influence on the displacement depending on the direction and velocity of displacement. Table 3-1 lists eight possible

combinations of fluid properties and displacement configurations along with the required critical velocities for a stable displacement (Kueper and Frind, 1988).

Table 3-1 - Relationships between fluid properties and displacement configurations (Kueper and Frind, 1988).

Fluid Properties	Downward Displacement	Upward Displacement
$\rho_1 > \rho_2, \mu_1 < \mu_2$	always unstable	stable if $v < v_c$
$\rho_1 > \rho_2, \mu_1 > \mu_2$	stable if $v > v_c$	always stable
$\rho_1 < \rho_2, \mu_1 < \mu_2$	stable if $v < v_c$	always unstable
$\rho_1 < \rho_2, \mu_1 > \mu_2$	always stable	stable if $v > v_c$

For fluids with similar viscosities, like water and ethanol, the influence of the densities on the stability in downward displacement of water by ethanol is physically intuitive, since the less dense one tends to remain at the top of the denser one.

The viscosity of ethanol is slightly higher than that of water and the relative permeabilities for both fluids in miscible displacement are equal. Based on Equation 3-4, stability of displacement for ethanol flushing is expected to be achieved by having a vertical downward direction of injection. And upward movement is always unstable, as well as lateral movement. Accordingly, downward ethanol flushing should be used to achieve maximum sweep efficiency.

Boyd and Farley (1991) presented a study of alcohol flushing (isopropyl alcohol) of TCE (trichloroethylene) in glass bead columns (one-dimensional). The analysis of flow stability was based on the gravitational instability expressed in terms of density difference between the injected and resident fluids ($\Delta\rho$) and the column orientation as

$\Delta\rho \cdot g \cdot \sin\beta$ (β is the angle between the column and the horizontal). When the term $\Delta\rho \cdot g \cdot \sin\beta > 0$, the positioning of the fluids relative to each other is stable. When $\Delta\rho \cdot g \cdot \sin\beta < 0$, the positioning of the fluids is unstable and gravitational fingering is likely to occur. This effect, however, can be mitigated by increased capillary and viscous forces, as the authors mentioned.

3.3.2 Experimental Procedure

The sintered glass bead models consisted of 350 to 500 μm glass beads packed between two glass plates. Minimum porosity associated with close random packing of glass beads range from 0.359 to 0.375 (Haughey and Beveridge, 1969) while the porosity of sintered glass bead models is 0.27 to 0.28.

Two different models were used in the experiments, one for vertical and another for horizontal flushing. The dimensions of the models were 18 x 31 cm and 23 x 35 cm, length x height, respectively. The thickness of the glass plates was 2 mm and the thickness of the bead layer was 2 mm. The sides of the model were sealed with epoxy resin. The ports for injection and extraction of fluids were located outside the glass bead zone, that is, the layer of beads did not reach the extremities of the model. For vertical flow these ports act as horizontal wells or fully penetrating wells in horizontal flow experiments. The average distance separating the end of the bead layer to the end of the model (edge gap) is about 2 mm. Figure 3-14 schematically shows the sintered glass bead model used in the experiments, with detail of the open port and the space void of glass beads between the two glass plates.

Each visualization experiment was recorded using a video camera (Panasonic VHS) fitted with a magnifying lens which allowed extreme close-up viewing. The format of video signals from the VCR complies with the National Television System Committee (NTSC) standards that are used in North America. The frames were photographed directly from a TV screen (camera Nikon FM2 with a 75-300mm Sigma zoom lens).

Preparation of the glass bead models followed the basic cleaning procedures utilized for the micromodels (see Section 3.3.2). The cleaning process was done with the model placed horizontally on the bench. After cleaned, the models were flushed for about 15 minutes with CO_2 to fully displace the air. Initial waterflood was done by injecting several pore volumes of distilled, deaired water until no gas phase was detected. This process was done at constant head during the injection at very low rate (0.1 ml/min) with the model kept in vertical position and water injected from bottom to top to minimize trapping of the non-wetting phase.

The establishment of gasoline residuals within the saturated zone for vertical flushing tried to mimic a field situation, where a layer of gasoline standing at the top of the capillary fringe is brought downward and upward by water table fluctuations. After the model was fully saturated with water (flow upward), the flow direction was reversed (from top to bottom now) and water was replaced by gasoline as the injecting fluid. Constant head was maintained again and the flow rate was reduced to about 0.05 ml/min. After gasoline broke through at the bottom port and no more water was produced, approximately one more pore volume of gasoline was put through the system. Flow was then reversed and water was injected from bottom to top again until it broke through at

the top port. Approximately two pore volumes of water flowed after gasoline stopped being produced at the top exit end.

Immediately after the residual saturation was reached, the syringe pump was attached to the injection end port to start the ethanol flushing experiment. Injection rates of ethanol were maintained at about 0.1 ml/min with the model in vertical position throughout the experiments. Figure 3-15 shows the setup used for the experiments.

Lateral flushing experiments needed a different approach in order to place the residuals. This model was prepared with ports located in different positions. Two extra ports were located at the bottom of the model, at 7 cm from the edges (the lateral dimension being 35 cm). At the center of the model, 10 cm from the bottom, another port was placed. Two more ports were placed at the top portion of the edge gaps. This model did not have edge gaps, and injection and extraction were done through four ports at each of the sides of the model.

Initial preparation and waterflood procedure was done as described for vertical flushing. After the model was waterflooded, the model was turned to a 90° angle for the horizontal experiment. The water table was lowered through the two lower ports and gasoline was released at the water table using the new central port. Although different in conception from the previous residual installation for vertical flushing, it intended to be closer to the gasoline release at the field experiment, described in the next chapter. When gasoline was introduced to the system for vertical flushing, the position of the water table was not an issue, because there is no formation of a capillary fringe. When the water table is brought down for gasoline release 'at the water table', gasoline is of course released at the top of the capillary fringe, which happened to be almost as high as the

height of the model (20 cm for the height of the capillary fringe and 25 cm for the model). To maintain the top of the capillary fringe at the level of the center port, the position of the water table was actually lowered below the lower boundary of the model during the gasoline release.

The injected gasoline thus spread laterally following the irregularities of the capillary fringe. Then the water table was lowered while gasoline was still being released, until gasoline broke through at the bottom ports. The level of the water table was then controlled so that no more gasoline could be produced at the bottom ports. When gasoline reached the higher portions of the model and broke through at the top ports of the lateral edges, the gasoline injection ceased to give place to the imbibition process. The water table was slowly raised (1 cm/hour) until no more gasoline production was noticed at the top ports. The final residual distribution obtained with this method is not as even as the vertical one. Injection rates of 0.1 ml/min were maintained for lateral flushing.

3.3.3 Results and Discussion

3.3.3.1 Vertical Downward Flushing

Although in low saturation, gasoline is present in the system and as it is removed from the pores, it affects the original characteristics of the fluids ethanol and water. The presence of gasoline in residual saturation (about 12% of the pore volume in the zone of the spill) was expected to have a small interference in the stability of the displacement, because the gasoline-ethanol-water mixture is less dense than water. Figure 3-16 presents

a series of photographs taken from the downward flushing experiment where fingering development is clear.

As Figure 3-16b shows, ethanol flow progresses downward at the top center of the model, with removed gasoline residuals forming an "halo" around the area of purer ethanol. Later on, the pattern of the fingers changed, and developed laterally, moving away from the vertical line linking both injection and extraction ports, forming two fingers and finally breaking through at different positions (and different times) at the bottom edge gap.

One point that has to be considered here is the stability of the fluid distribution after the ethanol flow pattern has developed. When the finger moves laterally, a relatively large area of the porous medium immediately above the finger remains saturated with water and trapped gasoline residuals. Based on the stability of displacement principles, it could be expected that this water would displace the ethanol and finger downward through it. The progress of flow in the experiment shows that this actually does not happen. The explanation comes from the distribution of the halo of gasoline around the ethanol path. The variation of composition of this halo, from a point closer to the ethanol to a point closer to the water, follows the solubility curve of the pseudo-ternary diagram for ethanol-water-gasoline. As the water content in the overall composition increases, phase separation occurs and oleic phase is extracted from solution, reducing the permeability around the ethanol path. This is a dynamic process, the halo moves laterally, outward from higher ethanol composition, and the outer zone of reduced permeability accompany the movement of the finger. This halo corresponds to an incipient oil bank, in which gasoline (oleic phase) has continuity, although short-lived.

The water/ethanol permeability reduction caused in the edges of the beads is effective in limiting the water from flowing downward through the ethanol finger.

The analysis of the phase behavior for the ternary system ethanol-water-gasoline presents the cause of the pore scale instability that leads to fingering displacement. As described in the micromodel experiments, ethanol tends to follow the relatively large permeability paths, following the preferential flowpath of water through the porous medium. When the flow is downward, the ethanol front would move as a plug front and all pores at the same elevation would tend to be reached at approximately the same time. This situation holds true for pure ethanol displacing pure water in a clean, homogeneous porous medium. However, when a gasoline blob is removed by blob ejection from the pore where it is trapped, the mainstream fluid at that given location will have different density from that of pure ethanol (or ethanol/water mixture). Momentarily, the gasoline that is ejected and incorporated into the mainstream (oleic phase) will cause a lower density than that of the fluid that follows immediately after it (aqueous phase), coming from above in downward flow. Figure 3-17, based on Figure 2-15 (Chapter 2) illustrates this situation. The fingering formation caused by the mobilization of gasoline blobs reduces sweep efficiency and compromises the use of this flow direction for ethanol flushing.

Figure 3-17 shows a hypothetical sequence of fluid compositions (A to D, from top to bottom) existing in a flowpath of injected fluid immediately after a gasoline blob is incorporated to the flow stream. Possible compositions are presented on the ternary diagram with isodensities. Fluid A corresponds to the composition closer to the injected composition (pure ethanol), within the single phase region of the diagram. Fluid B is the

aqueous phase of the phase separation, corresponding to the region where the gasoline (oleic phase is being dissolved by ethanol). Fluid C corresponds to the oleic phase, formed from the gasoline removed from the pores. Immediately below is fluid D, corresponding to a composition richer in water, extracted or not, located on the solubility curve. The relative positions of the compositions on the ternary diagram shows the density relationship between them. Fluid C presents the lowest density of all the fluids, and is being displaced downward by a more dense fluid. The type of displacement is characterized as unstable and fingering of B into C is expected.

As ethanol locally fingers through fluid C and flows further downward, a similar phenomenon happens a little further downward, and so on, and the injected fluid follows this preferred pathway, developing into a macroscopic finger. Therefore, as the oleic phase (fluid C) is displaced by the more dense injected fluid placed above it, fluid C moves to a region of lower ethanol content and consequently higher water content. Phase extraction occurs and this results in the development of the mentioned halo of oleic phase.

Based on these results, it can be argued that on a larger scale of a field situation, where the gasoline residuals are not homogeneously distributed, regions of lower residual saturation would correspond to preferred flowpaths for ethanol. These results also suggest that ethanol will break through residual zones where residual saturation is lower, creating a preferential pathway (finger), deteriorating the sweep efficiency of the downward ethanol flushing. The complete removal of residuals (visually determined) occurred after about 3 to 4 pore volumes of ethanol were injected.

3.3.3.2 Vertical Upward Flushing

Studies of dissolution of gasoline residuals in one-dimensional columns have been made using upward flow. In these experiments, water is the dissolving injected fluid used throughout the whole experiment and therefore stability of displacement is not an issue. For dissolution experiments the upward direction of flow agrees with gravity (buoyancy) forces on the trapped blobs (e.g., Bicalho, 1996). Although upward flow of ethanol displacing water initially is characterized as unstable displacement, the results may be compared to the results of downward flow. Figure 3-18 shows a sequence of photographs taken from the upward displacement experiment.

From Figure 3-18a, contrary to what happened in the downward flushing experiment, the injected ethanol was not initially confined to the region immediately around the injection port. It spreaded laterally through the edge gap, showed by a blue halo that formed at the base of the model and covered its complete lateral extent. The ethanol, at its very early stage, approximated a plug-type front. However, fingers formed immediately after ethanol started moving up. Again, the injected ethanol follows the pathways of higher relative permeability. Water is placed above ethanol and gravitational instabilities take place. Even after the mixture of both fluids is completed, the final density will still be lower than that of the pure water and unstable displacement still takes place. The sequence in Figure 3-18 (b, and c) shows that the fingers tend to move straight upward, with injected ethanol following ethanol filled pore pathways. Ethanol preferentially flows through the ethanol filled pores (fingers) and gasoline blobs start to be mobilized and removed from the lower permeability halos of extracted oleic phase. This removal is minimally favored by gravity, since the pores to where the blobs are

removed to are filled with high ethanol content, a denser fluid than the ejected blobs in which the gasoline is completely miscible. Figure 3-18b and Figure 3-18c show a progressive enlargement of the width of the fingers, corresponding to more incorporation of the residual gasoline to the ethanol mainstream.

The formation of the halo in this experiment shows that the recovery of gasoline from the development of an oil bank is not a major factor in the cleanup process. Pure gasoline or high gasoline content oleic phase is produced at the exit end until ethanol breaks through. As showed in Figure 3-18c, the ends of fingers are very narrow when ethanol breakthrough happens. Most of the product in residual phase is removed from the pores by later mobilization (ejection) and does not form a gasoline bank. This agrees with the behavior of gasoline removal described in the micromodel experiments.

Besides the major flow instability, originated by the difference in density between ethanol and water, another instability, local and short-lived, adds up to the overall source of displacement instabilities. The oleic phase removed from a pore also has a lower density than water that originates an instability. Figure 3-19 illustrates this situation, providing a good comparison to the instabilities originated in the downward flushing.

Although vertical flushing of gasoline residuals by ethanol presents low sweep efficiency (evaluated visually from the recorded experiments), upward injection may be slightly more advantageous due to the action of buoyancy forces on the gasoline blobs. The complete removal of residuals (visually determined) also occurred after about 3 to 4 pore volumes of ethanol were injected.

Both methods presented similar problems. The major drawback of vertical flushing is the practical difficulties in installing and controlling a reliable system of

ethanol injection and extraction in a real situation. A higher sweep efficiency could be achieved by using horizontal wells, which help in distributing the injected fluid but do not eliminate the fingering problem.

3.3.3.3 Lateral Flushing

A usual zone with gasoline residuals resulting from a spill is longer horizontally than vertically. In a real situation, any attempt of cleanup that involves lateral (horizontal) movement of injected fluids has a natural advantage over a vertical one because vertical flushing requires more sophisticated solutions to be operated than horizontal flushing, that agrees with the natural lateral flow of the groundwater.

The results of experiments designed to evaluate the lateral flushing are summarized on the sequence of photographs presented on Figure 3-20. The colors of the photographs do not correspond to the colors of the dyes used because the experiment was backlit with a fluorescent light, which had an effect on the photographic film. The port-holder seen at the top right of the figure was only used to support the model and no port was attached to it (no injection or extraction through this point).

Figure 3-20a shows ethanol (bluer, flowing from left to right) with a tendency of flowing preferentially above and under the region where gasoline was injected. The distribution of residuals was more concentrated at the top right of the model and around the injection port, as seen by the deeper brown regions in the model. Consequently, at these regions the relative permeability for ethanol is lower.

In Figure 3-20b small fingers started to form after about a third of the residual zone (with lower residual content) had been flushed. Compared to vertical flushings, a

major finger did not develop from the beginning of the injection. The fingers did not show a preferential direction of flow either downward or upward. Figure 3-20c shows the progression of these fingers. The approach of a higher residual saturation region has already defined two incipient preferential paths for the fingers, with the residuals at the center of the model (horizontally) being left behind. Figure 3-20d shows the further development of the two finger, with the halos of mobilized and displaced gasoline residuals getting darker with increased gasoline removal. It may be noticed by comparing Figure 3-20c and Figure 3-20d that the finger at the top follows a region of lower residual saturation (clearer), initially moving slightly upward and downward closer to the region of higher residuals at the top right. A similar situation is shown by the finger of the bottom, that also follows the region of lower residual saturation. The finger at the top portion or the model is narrower and moves faster. The determination of the ethanol pathways by the regions of lower conductivity is clearly demonstrated in Figure 3-20e, when the finger of the top moves downward at the border of the darker region of the model. The region of the top of the model shows more removal compared to the region of the bottom. The change in direction of the finger of the top is partially responsible for slowing down the fluid velocities at the bottom by creating a preferential region of ethanol flow. The zones of higher residual saturation (originally in place and accumulated later by displacement) are removed by mobilization (ejection) from the flowing high ethanol content fluid within the finger. Figure 3-20f shows the state of the experiment after ethanol breakthrough. The removal of gasoline residuals continued by ejection as shown in Figure 3-20g and Figure 3-20h. The complete removal of residuals (visually determined) occurred after about 2 to 3 pore volumes of ethanol were injected.

The overall behavior of horizontal flushing shows ethanol preferentially flowing above and below the high saturation regions, with fingers developing and flowing continually through regions of lower residual saturation. The consistent formation of this pattern may be expected in a real site, where the top and bottom of the contaminated zone are regions of higher permeability in a homogeneous aquifer. Ethanol flowing around the contaminated zone would favor mobilization by ejection of the residuals and any ethanol fingering through the zone of residuals would increase the efficiency of removal.

3.4 Conclusions

Small interfacial tension (IFT) differences caused by mass transfer of ethanol and water to gasoline and vice-versa are responsible for small blob of gasoline to move upgradient, against the fluid flow, even for average linear velocities up to 2 orders of magnitude higher than typical groundwater velocities.

IFT differences are responsible for gasoline removal by a mechanism described as *blob ejection*. The portion of a trapped blob that is in contact with ethanol has its IFT differentially reduced, and the trapped blob is ejected into flowing ethanol rich fluid.

The extent of reduction in IFT necessary to start the ejection depends on the aspect ratio for a given porous medium but is much lower than that predicted by capillary number experiments for blob mobilization.

The removal of the trapped residuals starts at the tips of the blobs or cluster of blobs that are exposed to flowing fluids. For conditions of high ethanol concentration

gradients near the blob, gasoline mass removal by dissolution of fluid flowing around the blob may be considered minimal when compared to mass removed by ejection.

Assuming that diffusion is the main mechanism for ethanol transport through the pore throat between the flowing region and the trapped blob, it determines the characteristic time necessary for the start of the ejection. A simplistic approach shows that the for typical groundwater velocities the ethanol-rich fluid moves only a few centimeters to a few tens of centimeters before blob ejection starts.

The total mass that is removed by blob ejection alone could not be properly assessed in this work, and a visual estimate from the video recording suggests that approximately 40% of the mass is removed by ejection. The remaining residual mass is removed by either an overall decrease of the IFT of the blob (mobilization) or dissolution. The *blob ejection* mechanism facilitates the flow of ethanol around the partially ejected blob, creating regions of higher permeability by removing mass of the blob, favoring later removal of the blob by the other mentioned mechanisms.

During the experiment of ethanol flushing in the downward direction, the low residual gasoline saturation in the contaminated zone (e.g. about 12% P.V.) does not generate an oil bank upon ethanol injection and pore scale instabilities lead to expected fingering of ethanol, reducing the sweep efficiency of ethanol flushing.

Similar problems were observed in the upward direction of ethanol flushing. The formation of fingers observed in the upward flushing experiment corresponded to the theoretical prediction of instabilities (Kueper and Frind, 1988). The presence of gasoline residuals, although not sufficient to develop an oil bank, lead to the pore scale instabilities that developed into fingering.

Lateral flushing experiment shows ethanol preferentially flowing through regions of lower gasoline residual saturation and higher relative permeability. This pattern may be expected even in a relatively homogeneous aquifer where the top and the bottom of the contaminated region have relatively higher permeability to aqueous fluids.

A typical zone of gasoline residuals originated from a spill will be much more extensive horizontally than vertically and so horizontal flushing presents practical advantages over vertical flushing, i.e., easier to operate injection/extraction system. Since the laboratory experiment showed favorable results for lateral flushing, the relative operational advantage of this direction of flow was decisive to the choice of horizontal flushing for application of ethanol to displace gasoline residuals in the field experiment.

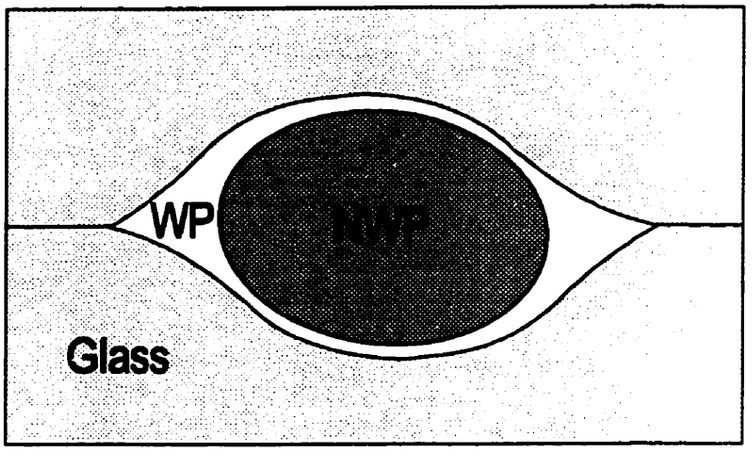

NWP = Non-wetting phase
WP = Wetting phase

Figure 3-1 - Schematic cross-section of a typical micromodel pore.

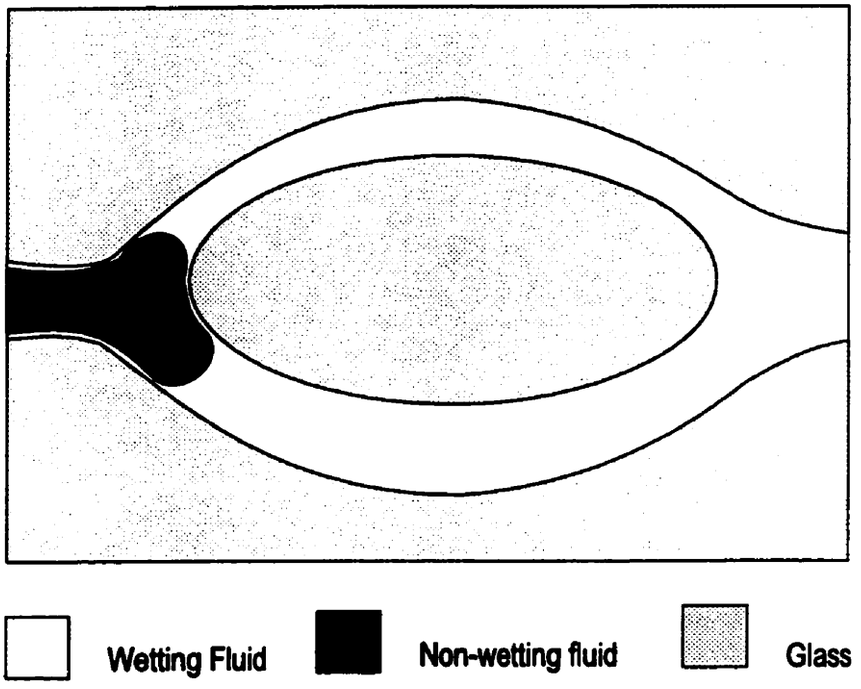

Figure 3-2 - Pore Doublet.

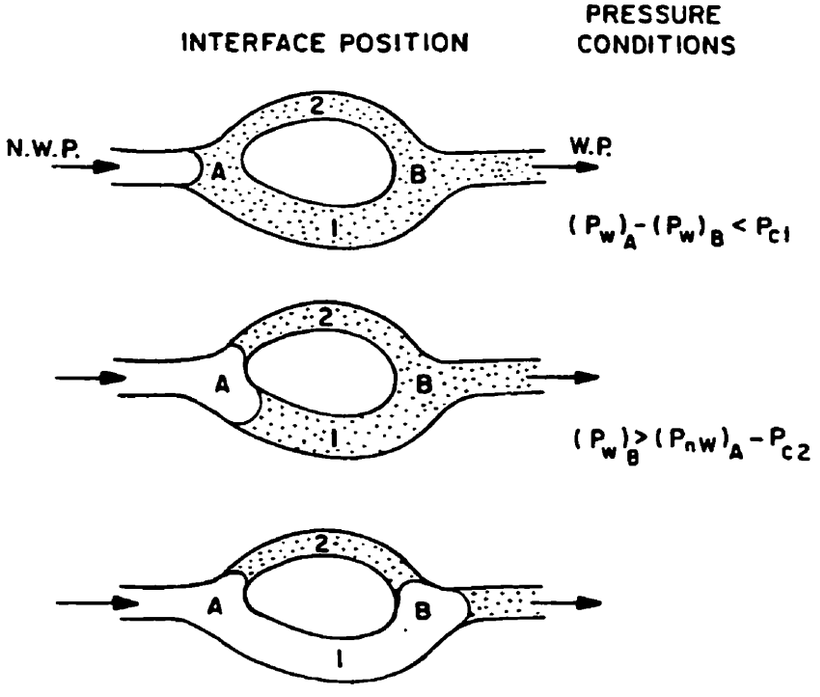

Figure 3-3 - Trapping of wetting phase during drainage process

(Chatzis and Dullien, 1983)

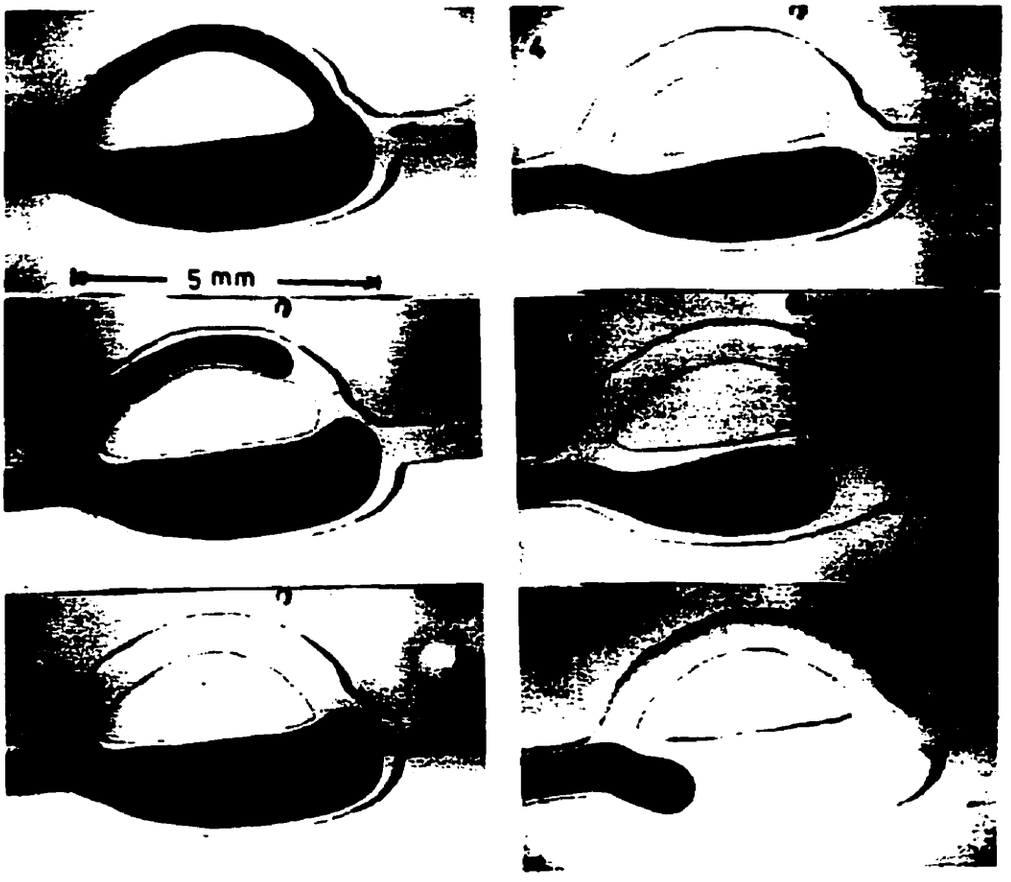

Figure 3-4 - Imbibition process - no trapment of the non-wetting phase occurs

(Chatzis.and Dullien, 1983)

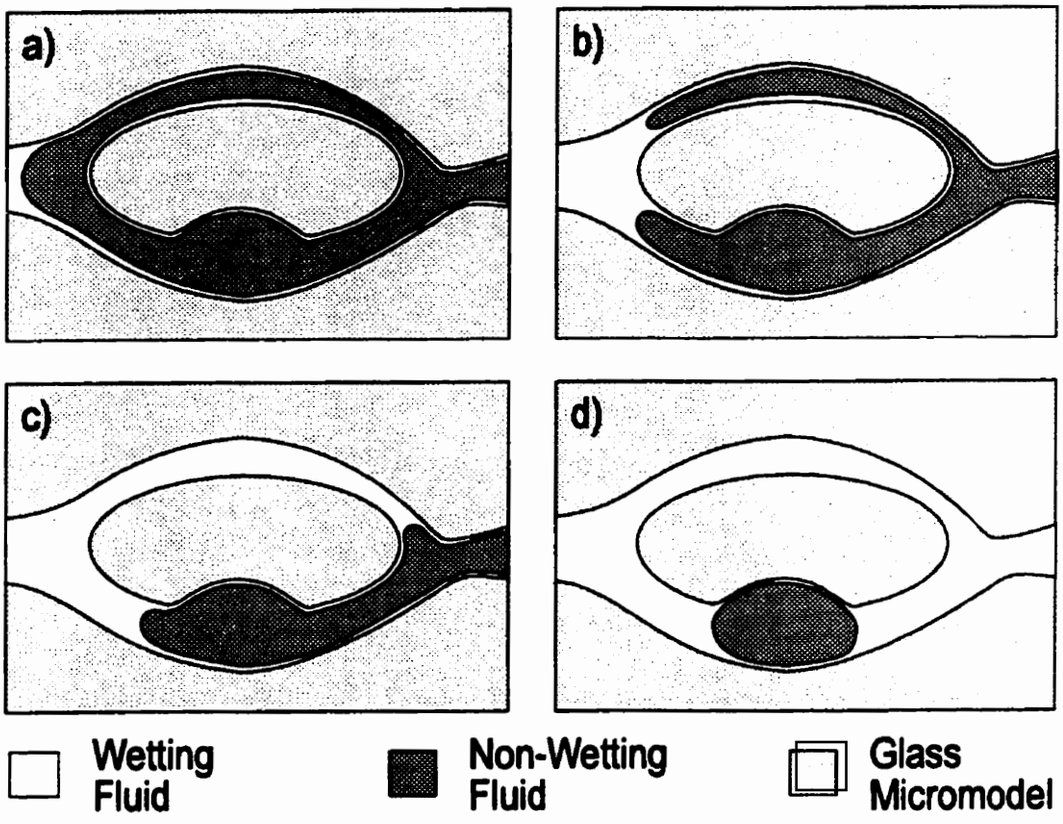

Figure 3-5 - Imbibition process - trapment of the non-wetting phase occur.

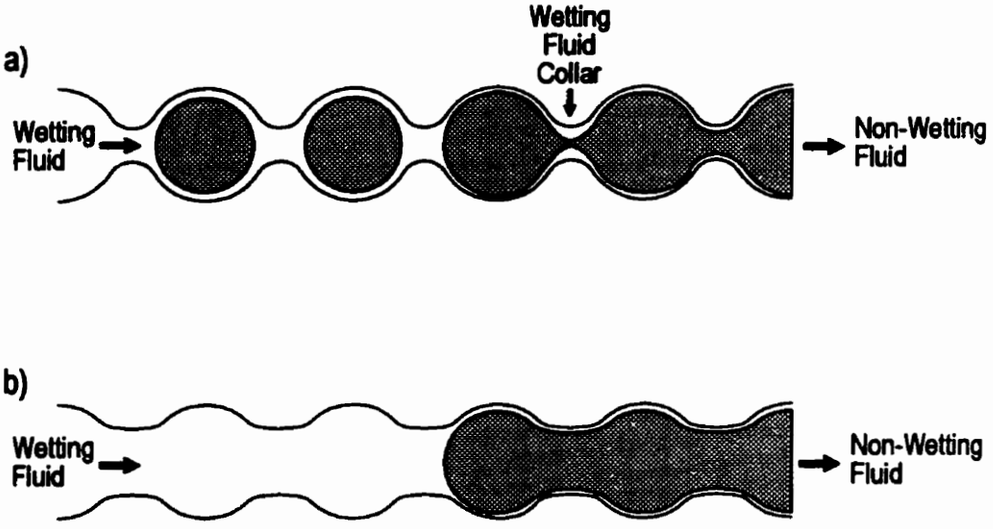

Figure 3-6 - Snap-off mechanism (Chatzis et al., 1983).

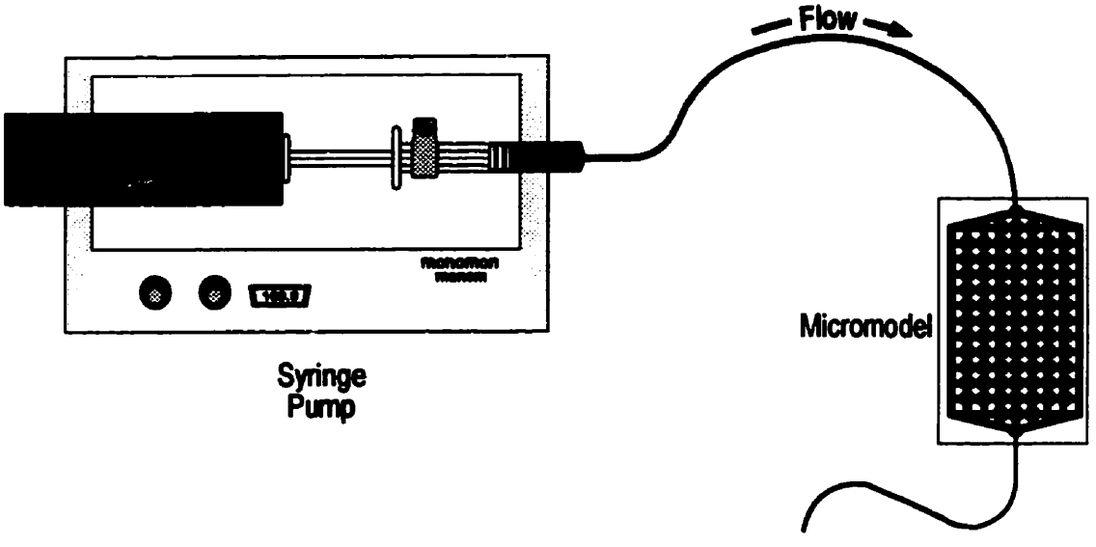

Figure 3-7 - Top view of injection setup for the micromodels.

a) blob detaches itself from original trapped blob

b) blob moves towards ethanol rich flow

c) blob moves against ethanol flow direction

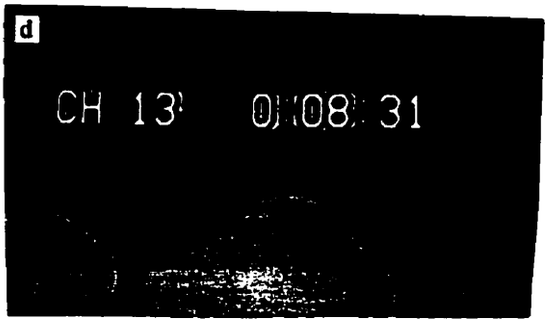

d) blob momentarily stops at the pore throat due to higher velocity of flow

e) blob is carried away by ethanol rich flow

Figure 3-8 - Stepwise sequence of photographs showing an ejected blob of gasoline moving against the ethanol rich flow

a) trapped gasoline blob starts to protrude towards the ethanol rich flow

b) the tip of the blob protrudes further

Figure 3-9 - Sequence of photographs of the blob ejection phenomenon

c) the tip of the blob reaches the adjacent pore body and shows swelling as it incorporates oncoming ethanol

d) the tip of the blob has low IFT and is carried along the ethanol rich flow

Figure 3-9 - Sequence of photographs of the blob ejection phenomenon (contd.)

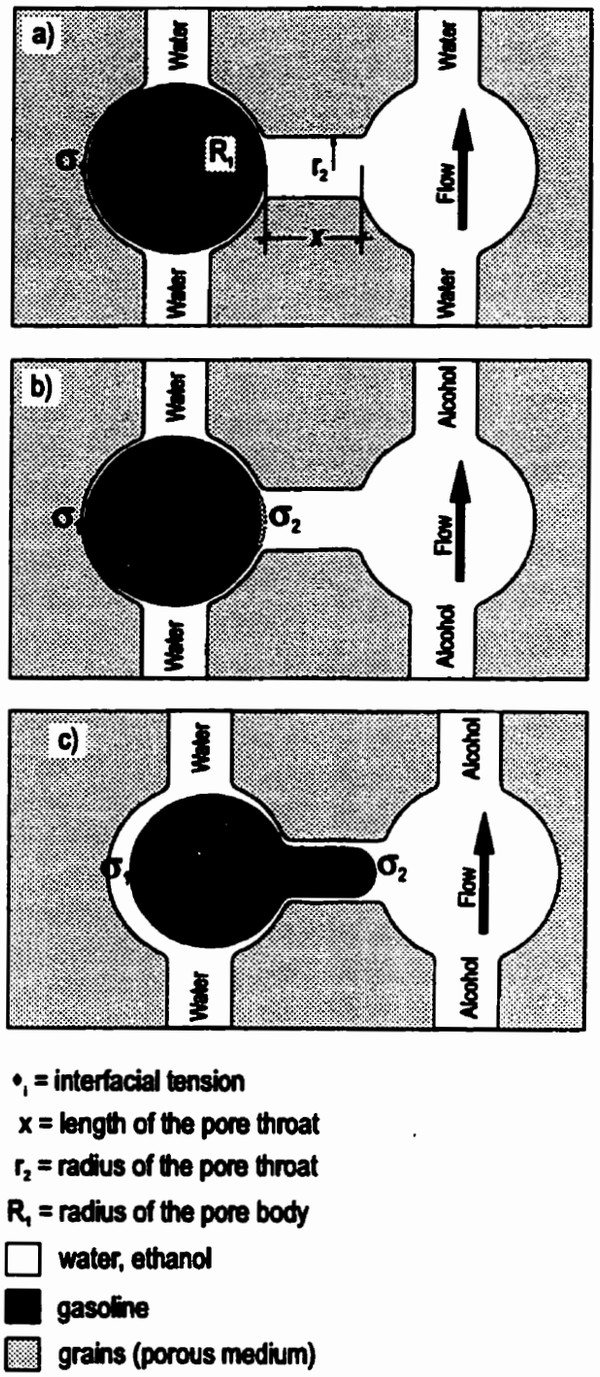

σ_1 = interfacial tension

x = length of the pore throat

r_2 = radius of the pore throat

R_1 = radius of the pore body

water, ethanol

gasoline

grains (porous medium)

Figure 3-10 - Blob ejection schematic representation ($\sigma_2 << \sigma_1$)

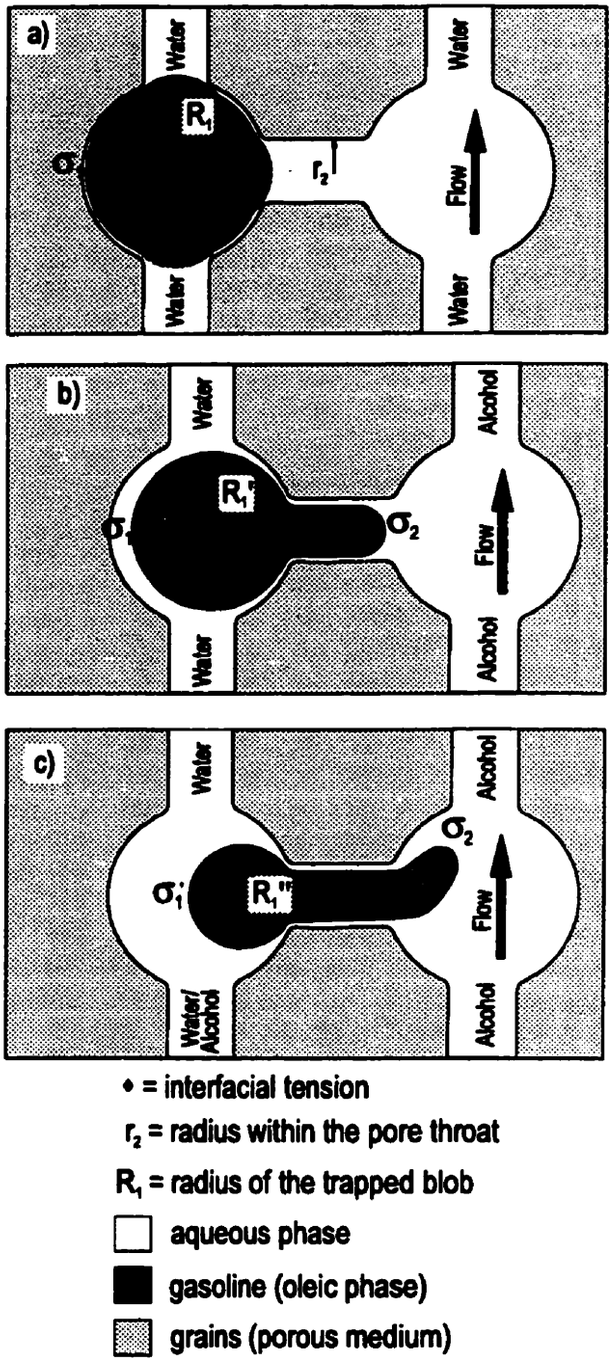

Figure 3-11 - Capillary ratio at different ejection steps

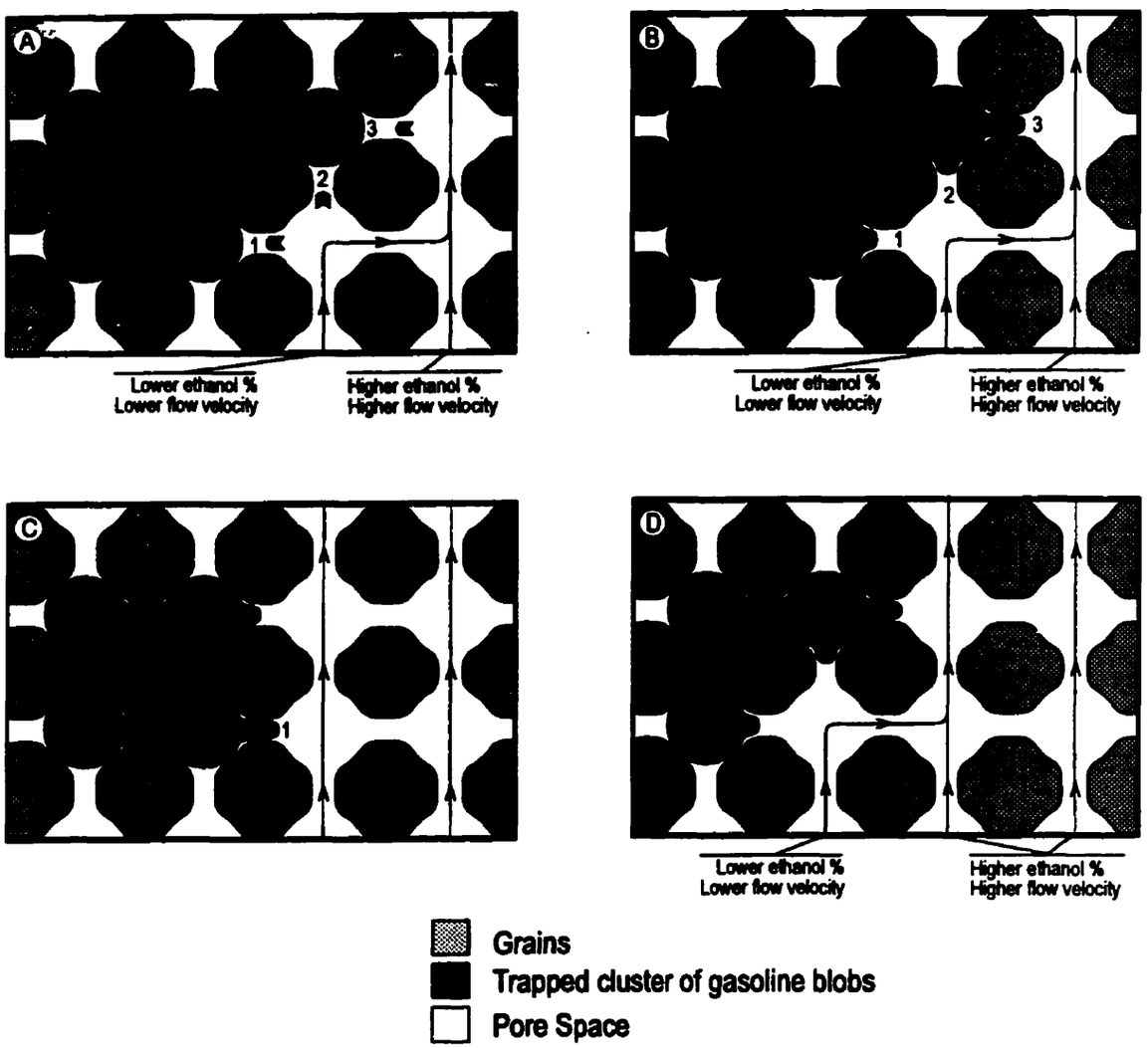

Figure 3-12 - Stepwise mobilization of a cluster of interconnected gasoline blobs by ejection

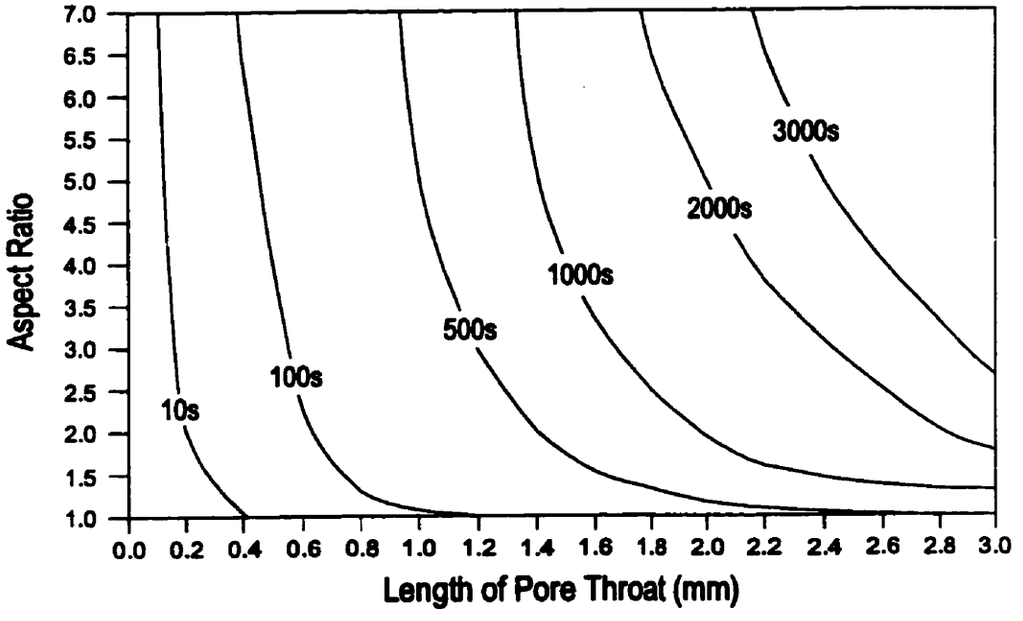

Figure 3-13 - Relationship of time required for blob ejection for different *capillary ratio* and length of pore throats

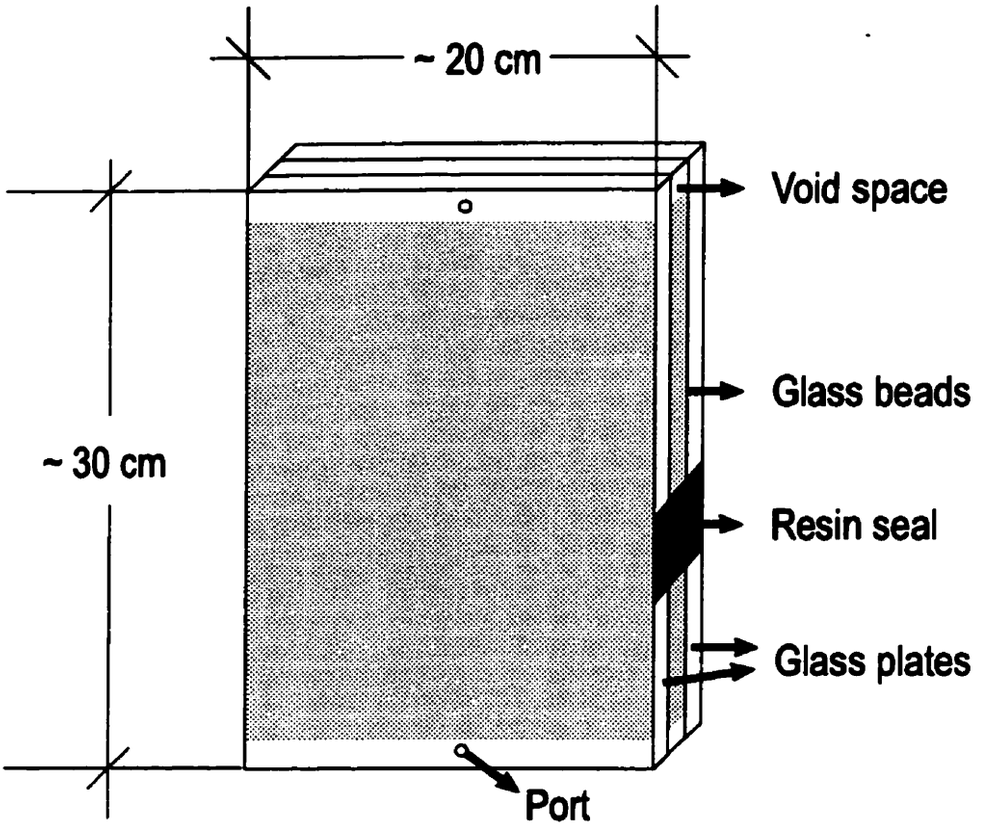

Figure 3-14 - Schematic representation of the sintered glass bead packed porous medium model used in the experiments.

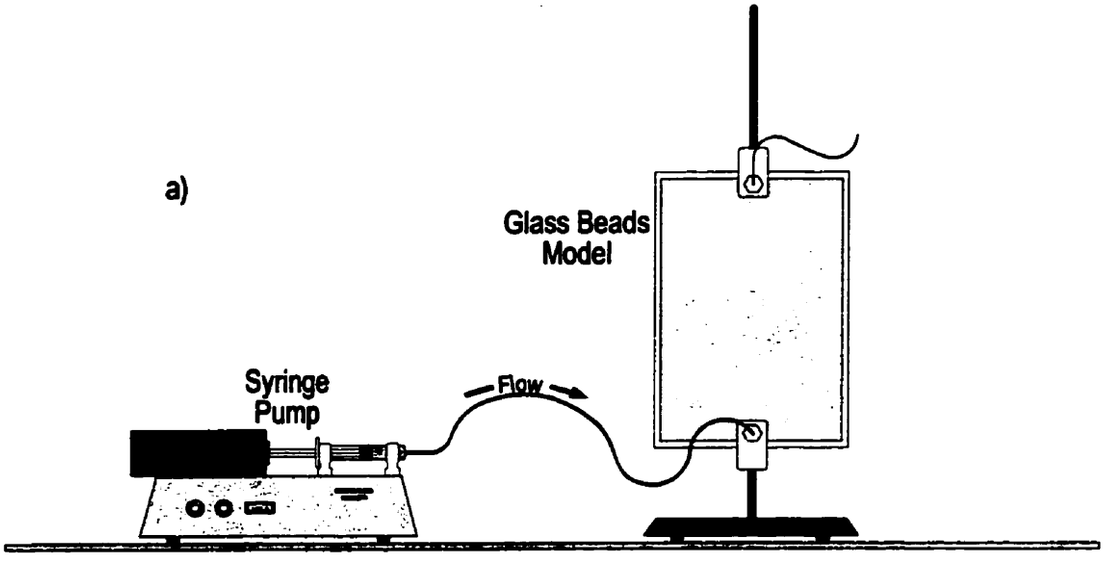

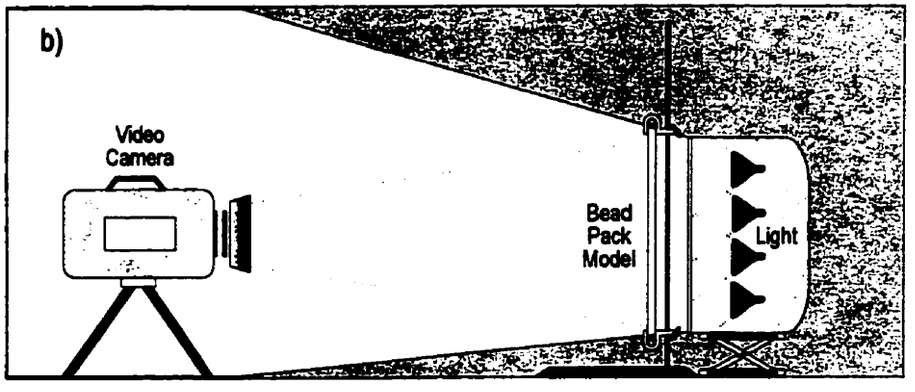

Figure 3-15 - Sintered glass bead experiment setup.

a) side view of ethanol injection wit model positioned vertically

b) side vew of video-recording setup

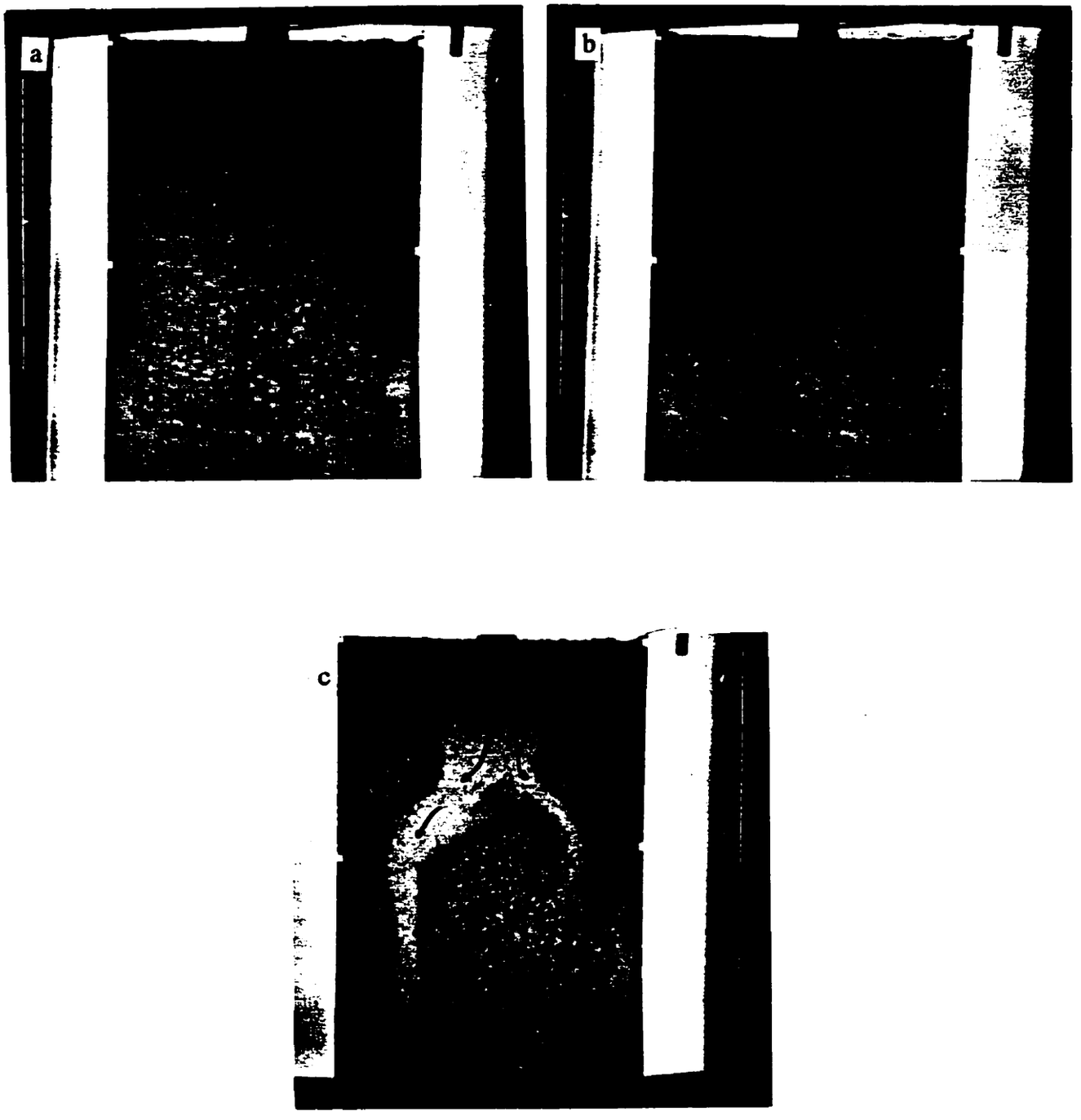

Figure 3-16 - Photographs of the downward ethanol flushing of gasoline residuals

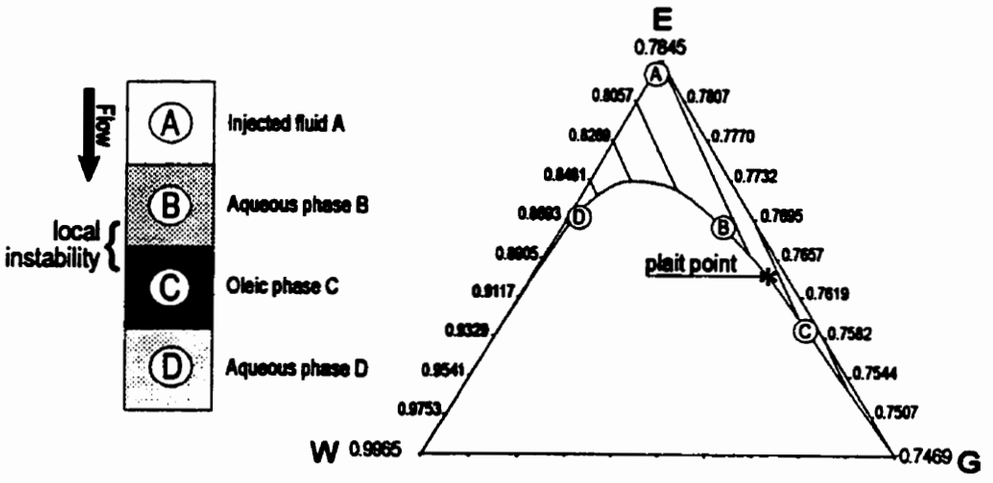

Figure 3-17 - Local instabilities originating finger development in downward ethanol flushing.

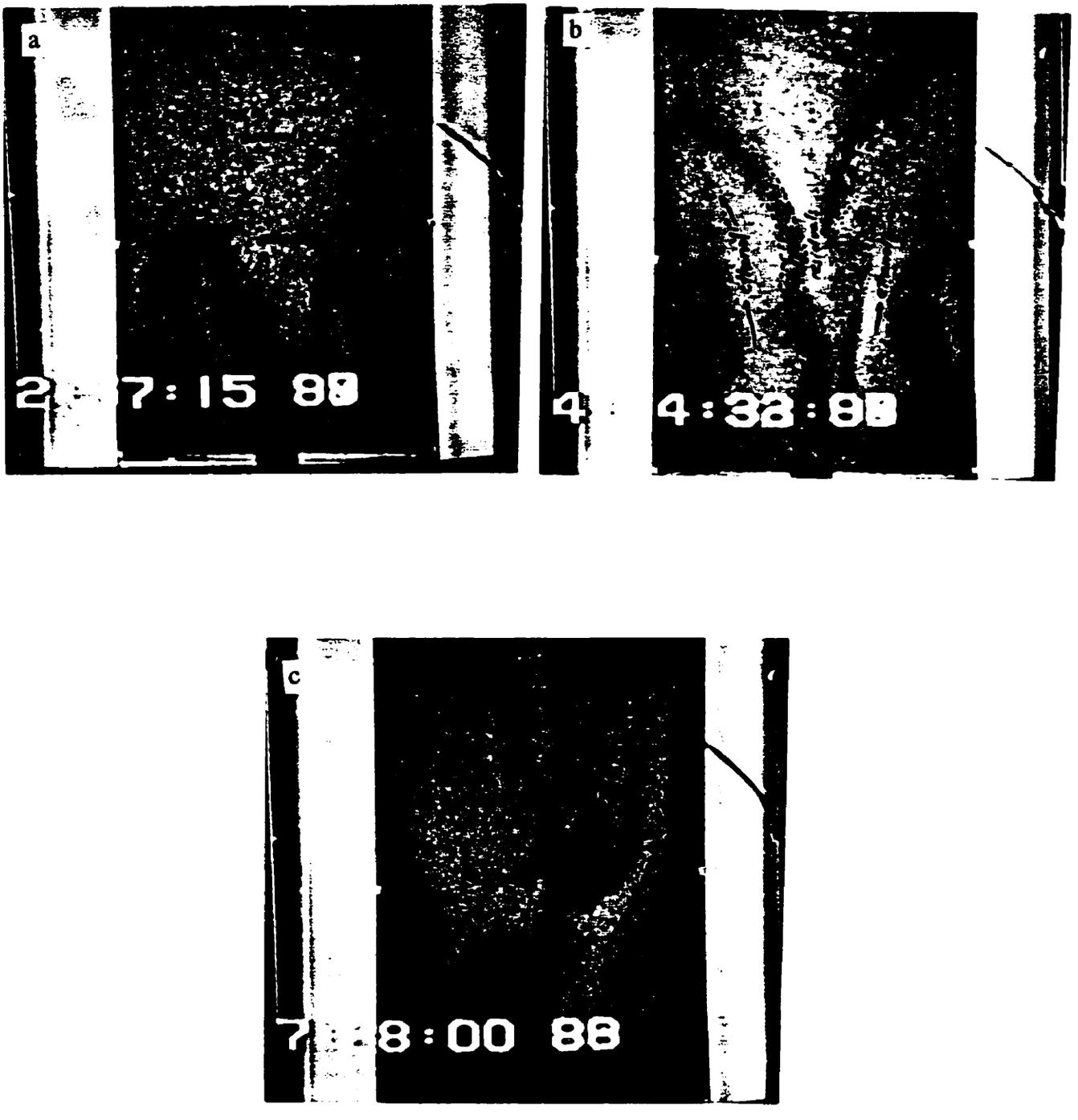

Figure 3-18 - Photographs of the upward ethanol flushing of gasoline residuals

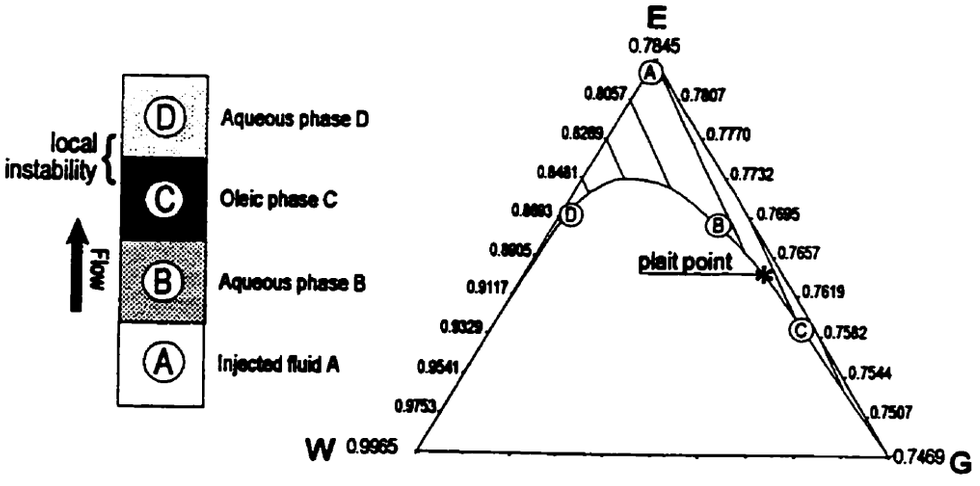

Figure 3-19 - Instabilities in a vertical upward displacement

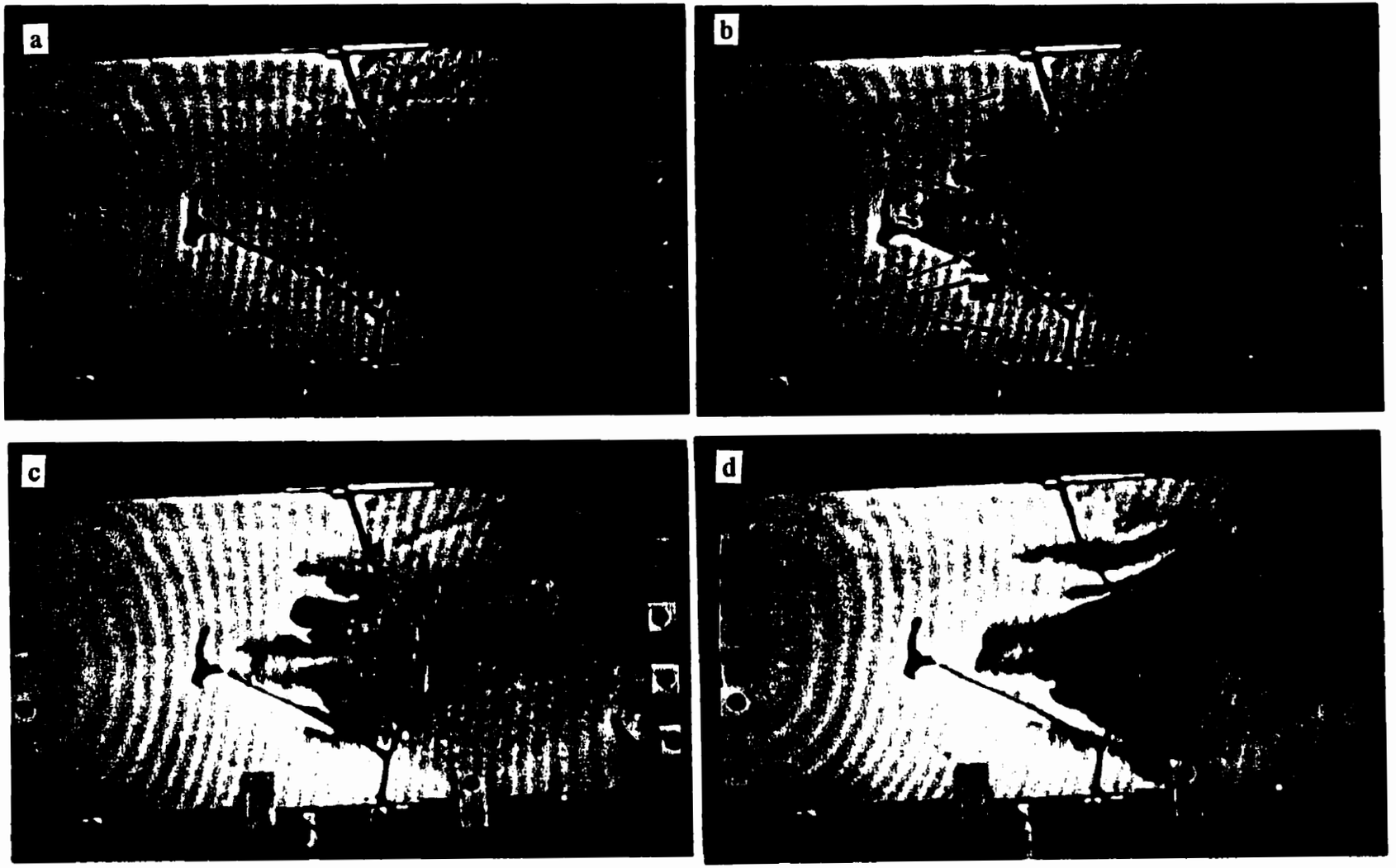

Figure 3-20 - Photographs of the horizontal ethanol flushing of gasoline residuals

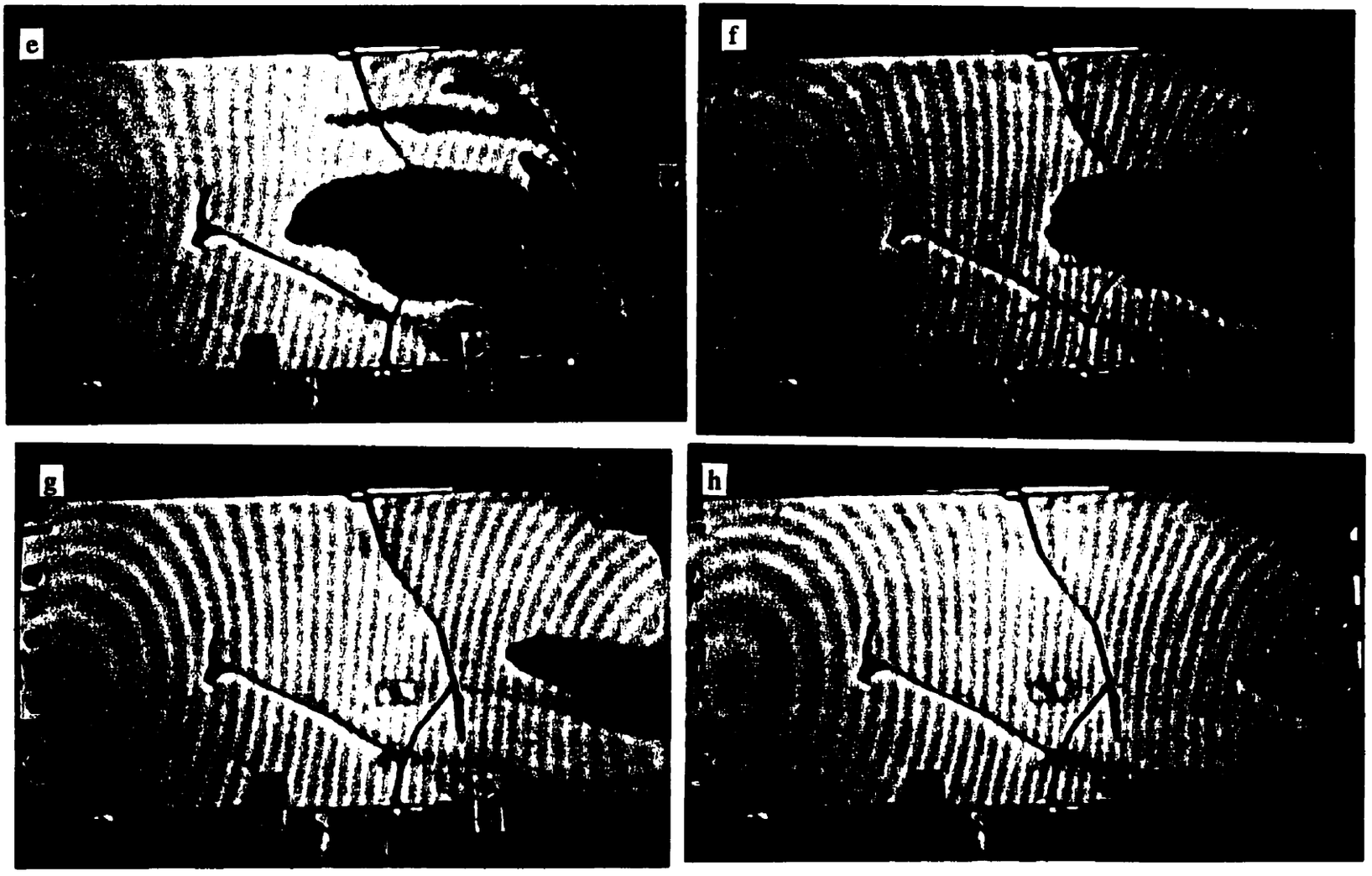

Figure 3-20 - Photographs of the horizontal ethanol flushing of gasoline residuals (contd.)

4. FIELD SCALE EXPERIMENT OF ETHANOL FLUSHING OF GASOLINE RESIDUALS

4.1 Objectives

The objective of the research described in this chapter is:

- To test the use of ethanol flushing technology to cleanup gasoline residuals at the field scale.

4.2 Background

The use of alcohols was considered for enhanced oil recovery in the early 1960s (Gatlin and Slobod, 1960; Taber et al., 1961; Holm and Csaszar, 1962; Taber and Meyer, 1964). In these early experiments, slugs of various alcohols were found to be capable of completely removing residual oil in long cores, but the method has never been applied commercially due to marginal profits. However, in the environmental field, alcohol flushing may offer an environmentally safe and economically attractive groundwater restoration alternative.

Boyd and Farley (1991) presented a series of one-dimensional experiments of isopropyl alcohol (IPA) displacing trichloroethylene (TCE). The results indicated that the displacement of TCE (an immiscible fluid denser than water) by IPA was most stable in the downflow direction and that the displacement of IPA by water was most stable in the upflow direction. The authors mention the likelihood of fluid segregation in horizontal flushing due to density differences. Brandes and Farley (1993) presented laboratory columns results showing that residual TCE and PCE (tetrachloroethylene) globules can

be removed from glass bead packings at low upflow gradients using alcohols that partition preferentially to the DNAPL (dense non-aqueous phase liquids). The displacement of DNAPLs had to consider the possibility of moving the contaminant even further downward, and the upward direction of flushing was always the choice, although it presented an unfavorable mobility ratio. These experiments did not addressed the displacement of LNAPLs (light non-aqueous phase liquids), such as gasoline.

4.3 Site Description and Characterization

The experiment was conducted in an unconfined sand aquifer at the Canadian Forces Base Borden, Ontario, Canada (see Figure 4-1). The abandoned sand quarry or sand pit, forming a broad local depression, was used as the location for the test. This site has been used for several other field experiments and is extremely well characterized. A thorough review of the site was presented by Devlin (1994).

The unconfined Borden aquifer is a shallow sand aquifer which ranges in thickness from approximately 20 m to about 9.5 m (MacFarlane et al., 1983). An underlying clayey silt layer acts as an aquitard. Within the sand pit, where considerable overlying aquifer material has been removed, the thickness of the sand layer is on the order of 9 m. This shallow aquifer is of glaciofluvial origin and is locally heterogeneous with complex distributions of beds and lenses of fine to coarse grained sand, and lenses of peat. MacFarlane et al. (1983) reported hydraulic conductivities for the aquifer between 5.0×10^{-7} and 1.0×10^{-3} m/s on the basis of 7 grain size analyses and 5 permeameter tests. Larger scale aquifer testing indicated an overall hydraulic conductivity of 1.0×10^{-5} to 5.0×10^{-5} m/s. A series of 26 slug tests (Hvorslev, 1951) were

performed in the sand pit by Mackay et al. (1986) and a mean hydraulic conductivity of 7.0×10^{-5} m/s was determined. Sudicky (1986) presented a detailed assessment of spatial variability of hydraulic conductivity using falling head permeameters for several cores, with a geometric mean value of 9.7×10^{-5} m/s. Borden sand presents an average total porosity of 0.33 (Mackay et al., 1986).

The local stratigraphy of the experimental site is a stratified, fine to medium sand from the surface to about 2.28 m deep, a brown sandy peat layer from 2.28 m to 2.30 m, gray fine to medium sand from 2.30 m to 2.40 m, a brown sandy peat with large wood fragments from 2.40 to 2.60 m and gray sand from 2.60 m to the bottom of the cell.

4.4 Experimental Procedure for the Field Experiment

4.4.1 Cell Description and Instrumentation

A plan view and a cross section of the installed cell showing the setup of the equipment is presented schematically in Figure 4-2a and b, respectively. A region of sand is contained by interlocked iron sealable sheet piles forming a square pattern measuring 2 m × 2 m and extending 3.1 m deep. Sixteen 350 cm long (11½') sheet-piles were driven into the ground using a vibrating hammer attached to a backhoe with extended reach. The top 40 cm of the sheet piling was left exposed above the ground. The sealable joints (see detail in 4-2a) were grouted with a bentonite slurry.

Fourteen drive-point wells (Broholm et al., 1994) for ethanol injection were built in a 2.54 mm (1") OD stainless steel drive point, with a 20 cm long stainless steel screened area threaded to 19.05 mm (¾") OD SCH 40 black steel pipe. Polyethylene

tubing of 12.7 mm (½") in diameter was connected to a male nipple on the internal end of the drive point. The external ends of the polyethylene tubes extending out of the black steel pipes were connected to 3.175 mm (1/8") OD Teflon® tubing using 12.7 mm - 3.175 mm (½"-1/8") brass Tubefit reductions. The drive-point wells were driven into the ground using a Cobra electric vibrating hammer. The depths of the injection wells were 1.15 m for wells numbers 2, 5, 8, 11 and 13; 1.35 m for wells numbers 3, 6, 9 and 12; and 1.55 m for wells numbers 1, 4, 7, 10 and 14.

Fourteen extraction wells were built of 6.35 mm (¼") OD, 3.175 mm (1/8") ID stainless steel pipe with a 15 cm long screened area at the bottom. The area where the screen was welded to the perforated pipe was machined down 0.5 mm on the lathe to maintain constant OD throughout. The bottom was fitted with a stainless steel, cone-shaped end point sealed with silicone. The external end of the extraction wells was connected to 3.175 mm (1/8") OD Teflon® tubing using 12.7 mm - 3.175 mm (½"-1/8") Tubefit reductions and brass compression fittings with Teflon® ferrules. The extraction wells were hammered into the ground using a brass ring sliding around the well. The depths of the extraction wells were 1.05 m for wells numbers 2, 5, 8, 11 and 13; 1.25 m for wells numbers 3, 6, 9 and 12; and 1.45 m for wells numbers 1, 4, 7, 10 and 14.

Five multilevel piezometers were built of 2.54 mm (1") OD SCH 40 stainless steel center pipe, 3.1 m in length. 9 ports made of 3.175 mm (1/8") OD, 1.59 mm (1/16") ID stainless steel tubing were soldered to the center tube at 30 cm intervals, with tubings placed inside the center tube. The bottom port was placed 10 cm from the base of the center tube. At each port 0.25 - 0.50 mm of the center tube wall was removed with a 6.35 mm (¼") round milling bit and a stainless steel screen soldered into the milling port.

The bottom was fitted with a stainless steel end point sealed with silicone. The depth of the ports were 30, 60, 90, 120, 150, 180, 210, 240 and 270 cm. The multilevels were jetted into the ground using a standard EW casing. Tubings placed internally and a center tube with a smooth surface were designed to minimize the creation of preferential pathways for an eventual upward migration of gasoline.

Variation of the water saturation within the cell was monitored using TDR and CPN methods. Three TDR/CPN access tubes were installed. The details of construction and installation, as well as interpretation of results for the geophysical tools used in this field experiment are presented on Chapter 5. A few interpretation of the results are presented in this chapter as necessary be.

The dewatering well at the center of the cell was built in a 19.05 mm (¾") SCH 40 PVC 8-slot 1.2 m well screen pipe, flush-threaded to a 19.05 mm (¾") SCH 40 PVC riser pipe. The well was installed by water jetting using a standard EW casing. The gasoline injection well was of the same structure as the ethanol drive-point injection wells with the position of the screen extending from 1.15 m to 1.35 m.

A 5 cm thick layer of bentonite paste was used at the top of the sand to seal the test cell. Two vents built in slotted 12.7 mm (½") OD SCH 40 PVC pipe were placed horizontally at the depth of 20 cm and connected to a 12.7 mm (½") OD SCH 40 PVC riser pipe by a PVC elbow. The exit end of the vent was fitted with a 12.7 mm (½") ID PVC end cap. Caps were removed during dewatering of the cell for gasoline injection, and further recovery of the water table. The bentonite layer was rewetted occasionally to maintain its properties, but eventually it developed deep cracks that reached the top of the sand.

The cell was finally covered with a wooden deck laid at the edges of the sheet piles to facilitate access to the instrumentation. A greenhouse was built to protect the experiment. Inside the greenhouse, a room was built with lumber and covered with clear plastic around the cell test to help maintain optimal temperatures.

4.4.2 Estimation of gasoline residual saturation for Borden sand

A column experiment was designed to estimate the gasoline residual saturation after water table fluctuation. Undisturbed Borden sand was collected from the unsaturated zone at the sand pit in a 1 m long 30.48 mm (12") OD PVC tube that was driven into the ground using a vibrating hammer. The column was transported to the laboratory and had the bottom end covered with 1 fine screen (200×200 mesh) and 2 coarse screens (20×20 mesh) and fitted with a 30.48 mm (12") PVC end cap filled with coarse sand (filter sand #1 dry). The top end was sealed with a plexiglass plate. One-quarter inch Swagelok compression fittings were used as inlet/outlet ends and were connected to 6.35 mm (¼") polyethylene tubes. Twenty 1.59 mm (1/16") stainless steel, fully penetrating TDR rods were inserted perpendicularly the column wall at 5 cm intervals along the length of column. Figure 4-3 shows the column setup.

The column was flushed with CO_2 for 24 hours prior to saturation and flushing bottom to top with de-ionized, de-aired water. The column was monitored with TDR measurements during the saturation with water until no variations were noticed. A few more pore volumes were run through (7 pore-volumes in total) to assure uniform saturation. Falling head tests (Freeze and Cherry, 1979) were carried out to determine the hydraulic conductivity.

Water was allowed to pond at the top of the sand to avoid the presence of a capillary fringe and regular unleaded gasoline dyed with oil red-O dye was injected on the top of the ponded water. Gasoline was continuously added as the water table was lowered (3.4 cm/hour) until gasoline broke through at the bottom exit. The water table was then raised at a rate of 5 cm/hour back to its original position at the top of the column and 0.5 pore-volumes of water ran upward through the column after this position was reached until no more gasoline was produced. TDR measurements were made right after this. Then the column was left to rest for 3 weeks to check for possible upward movement of the residuals. The final distribution of the gasoline residuals were then again analyzed by TDR measurements. Cores were removed from the column and 4 subsamples (1.0 cm^3 each) were taken at each 5 cm intervals along the depth of the column. The core samples were pushed into 18 ml glass bottles, the bottles were filled with de-ionized, de-aired, organic-free water, crimped with Teflon® septum and kept refrigerated. The samples were analyzed for BTEX using solvent extraction in gas chromatography analysis within 3 days of the sampling date.

4.4.3 Emplacement of the Gasoline Residuals

The emplacement of gasoline residuals in the field experiment was designed in order to simulate the entrapment of the gasoline in the saturated zone by seasonal variations of the water table. The cell was partially dewatered and gasoline released at the top of the capillary fringe, spreading laterally. The water table was restored to its original position. The upward movement of the water displaces the free-phase gasoline, imbibing through it, leaving disconnected gasoline droplets or clusters of droplets trapped in the

saturated zone.

The position of the top of the capillary fringe within the test cell before the gasoline spill was determined by TDR and CPN measurements of water content. The measurement and interpretation of the positioning of the capillary fringe using these methods is relatively slow. A simple laboratory experiment was carried out to anticipate the elevation of the capillary fringe and estimate the desired depth to the water table for dewatering purposes. A 1 m long 2.54 cm (1") diameter glass tube was filled with dry Borden sand previously homogenized, with the bottom end filled with a nylon screen. The column was then inserted into an Erlenmeyer filled with deionized, de-aired water. The system was allowed to equilibrate during one week and the height of the capillary fringe measured.

The cell was dewatered from the center well using a Simer pump at a rate of 950 ml/min. The initial position of the water table was 0.82 m below ground surface (bgs) and was pumped intermittently during approximately 10 hours until the water table was at 1.54 m bgs. The water table was maintained at this depth and TDR measurements were taken before the gasoline injection.

The gasoline was released to the cell by gravity from an elevated container controlled by a Cole-Parmer 150 mm variable area flowmeter with a glass floater. The flow rate was maintained at approximately 200 ml/min., and the 70 liters were spilled in 6 hours. The water extraction pump was turned off and the water table was allowed to recover naturally to its original position. The monitoring of the gasoline residual distribution was done with TDR and CPN measurements.

4.4.4 Ethanol flushing in Field Experiment

Ethanol was injected continuously at a rate of about 2.0 ml/min. in each injection well. Extraction was at the same rate. The peristaltic pumps used were four variable speed Masterflex L/S drives with Ismatec 8-channel minicartridge pump heads using Ismatec 3-stop Viton tubing fitted to the 3.175 mm (1/8") Teflon® tubings. Flow rates were adjusted using a manifold system of two 3.175 mm (1/8") brass needle valves fitted to a 3.175 mm (1/8") brass tee. 3.175 mm (1/8") Teflon® tubings were fitted to the tee and valves using a 3.175 mm (1/8") brass compression fitting with Teflon® ferrules. The same manifold system was used to collect fluid samples from the extraction wells.

The monitoring of the gasoline distribution and groundwater chemistry was done using fluid sampling for chemical analyses and TDR and CPN measurements. Fluid samples were collected in 22 ml glass bottles with aluminum crimp and Teflon® lined septa using a sampling head previously used and described by Mackay et al. (1986). This apparatus collected groundwater directly into the sample bottles, contacting only Teflon®, stainless steel or glass. Between 60 ml and 70 ml were drawn through the bottles to ensure a thorough flushing of all tubing prior to disconnecting the bottles from the system and capping them. Sixty ml plastic syringes were used to create vacuum and extract the fluids from the multilevels. No preservatives were added, the bottles were removed from the apparatus, capped and stored on ice to deliver to the Organics Laboratory of the Department of Earth Sciences of the University of Waterloo and analyzed by a UV method (Appendix I).

Monitoring using TDR and CPN (methods described previously) was done at the

same times as the chemical samplings. The depths of interest are the same described in the methods.

4.4.5 Core sampling and analysis

Five soil cores were taken after the ethanol flushing experiment was terminated. A 2.3 m long, 5.08 cm (2") diameter thin walled aluminum tube with a core-holder at the bottom end was driven to the soil using a Cobra electric vibrating hammer and removed with the help of a jack. Immediately after removal, 10 cm of the bottom was cut off using a pipe cutter and discarded (portion occupied by the core-holder). The bottom was sealed using a 2 layers of wrapping plastic and a PVC end cap. The aluminum tube was subsampled at different intervals, starting from the depth of 60 cm and going down to 180. The aluminum tube was cut at the desired depth and a subsample was taken using a 60 ml plastic syringe with the outlet end cut off. The syringe tube was driven to the sand material while the piston was maintained at the top of the soil to create a vacuum and to prevent fluid loss. The subsample was put in a pre-weighed, oven cleaned 150 ml glass bottle with 40 ml of ethanol in it. The bottle was sealed with a Teflon® lined lid and kept refrigerated to be analyzed by the UV method (Appendix I). After chemical analyses, the samples were oven dry at 105°C and the dry sand weighed using an AND electronic balance model FX3000 (±0.005g).

4.5 Results and Discussion

4.5.1 Results for Gasoline Residual Saturation for Borden Sand

Falling head tests (Freeze and Cherry, 1979) determined the hydraulic

conductivity of the sand material to be 8.6×10^{-5} m/s, which is within the range of hydraulic conductivities measured for Borden aquifer found in the literature.

Figure 4-4 presents the evolution of the gasoline saturation profile as determined by TDR measurements during the lowering of the water table, for times 0.25, 4.25, 6.08 and 8.5 hours after gasoline injection started. The gasoline moved downward leaving a minimum of 12% saturation of irreducible water behind. Gasoline addition was stopped after gasoline broke through at the exit end. Figure 4-5 shows the saturation profile of gasoline immediately after the water table was raised and 24 days after measured by TDR.

The gasoline residuals, after water table fluctuation, were approximately constant around 12% of the pore volume throughout the whole depth of the column, decreasing only at the bottom portion where the pre-water-table-raising maximum saturation of gasoline was lower, as showed in Figure 4-4. This consistency is in spite of the variable initial gasoline saturation along the depth profile before the imbibition process took place.

Another method used to determined the distribution of the gasoline residual saturation along the column was chemical analyses of core samples. BTEX analyses were used to estimate the volume of pure gasoline present in the subcores using mole fractions of BTEX compounds in gasoline obtained from the literature (Poulsen et al., 1991). Appendix V shows the BTEX results for the soil samples and calculated saturations, as well as the TDR measurements taken during the experiment.

The results obtained for each compound-based calculation were averaged to give an approximate estimate of the final gasoline saturation for each sample based on the gas

chromatography analyses. The average saturation obtained for each of the four samples taken at each depth were finally averaged to produce the final saturation presented in Figure 4-6. The mole fraction-based gasoline saturation for each subcore varied according to the BTEX compound considered as a base for calculation. This must have resulted from differences in the composition of the gasoline used in the experiment from that in the literature. In spite of this, the averaged gasoline saturation values obtained agreed to the values obtained with TDR measurements.

Error bars in Figure 4-6 represent the maximum and minimum values of gasoline saturation based on individual BTEX compounds. They reflect the discrepancies caused by the use of the mole fractions obtained from the literature as well as intrinsic differences resulting from the sampling method. Since the distribution of the gasoline phase is not homogeneous, small discrete samples may vary widely in gasoline concentration depending on the position it is taken from. TDR measurements, on the other hand, integrate the saturations between the position of the two rods and give the average saturation for that portion of the column being analyzed and so are considered more representative.

About 45 cm thick layer of gasoline residuals below the water table was aimed for in the field experiment. To accomplish this, the cell of 2 × 2 m at Borden, with porosity of 0.33, about 70 liters of gasoline were added based on the assumption that the gasoline residual saturation in the field experiment was expected to be 12% P.V., the same value as in the column experiment

4.5.2 Emplacement of the Gasoline Residuals

TDR-CPN measurements in the field produced the results shown in Figure 4-7. The water table was measured to be 124 cm bgs and from these results shown in this figure, the capillary fringe was estimated to be about 99 cm bgs. Also shown in this figure is the illustration of the results obtained in a column experiment with Borden sand, by matching the observed water table level in the field to that in the column experiment. The height of the capillary fringe of 25 cm (124 - 99 cm bgs) in the field experiment is consistent with the value of 20 cm (124 - 104 cm) in the column experiment. Considering the similarities in both cases, the height of 25 cm thick capillary fringe in the field was selected as appropriate number.

Based on the installed position of injection/extraction wells, the desired position of the zone with gasoline residuals was estimated to be located between 130 cm and 85 cm below ground surface. To accomplish this, the water table was lowered to 154 cm bgs by pumping out water. Once this was accomplished, the water table was maintained and a set of TDR-CPN measurements was taken, as shown in Figure 4-8. From this figure, it appears that the top of capillary fringe is a bit higher than the expected value. This figure also shows good agreement of water saturation profiles measured by TDR and CPN respectively. The position of the well screen in the figure represents the depth interval where gasoline was released.

The actual position of the top of the capillary fringe, 10 cm higher than expected. caused the planned top of the residuals to be moved to 0.75 cm bgs, 10 cm higher than the position of the higher extraction wells (0.85 cm).

Figure 4-9 shows the water saturation profile as measured by TDR and CPN thirteen days after the emplacement of the residuals. The shaded region in the Figure 4-9 corresponds to the position of the zone of residuals as predicted by the determinations of the elevation of the capillary fringe from the previous section and the residual saturation of gasoline determined in column experiment.

TDR readings in Figure 4-9 indicate a decrease of about 10% P.V. in water saturation, in agreement with expected gasoline residual saturation (12% P.V.), at a slightly deeper position (5 cm) than the bottom of the expected region, which may reflect a depression of the capillary fringe caused by the gasoline injection near the TDR & CPN access tube C2U7 used in this set of measurements, as showed in Figure 4-2. Water saturation as measured by TDR starts to increase again at a depth of 85 cm. Although the position of the top of the capillary fringe before the gasoline emplacement ended up being 10 cm higher than predicted, as seen in the previous paragraphs, the bottom of the residual zone was only 5 cm higher (as opposed to 10 cm) than predicted. The top of the gasoline residuals, however, was at the desired position, resulting in a final thickness of residual zone being 5 cm thinner than originally planned. At positions higher than the top of the residual layer, the TDR-measured water saturation does not reach 100 %, as shown at the depths 1.25 to 1.60 m. This may either reflect the measurement of the natural decrease for water saturations at regions above the top of the capillary fringe, or the presence of gasoline residuals at lower residual saturation up to shallower depths. The TDR measurements for access tube C2U9 (not showed in Figure 4-9, see Appendix VI) present a similar result. The results of access tube C2U6 are too variable over depth to be considered reliable (see Appendix VI). Several attempts were made to fix this problem

with no success.

For the hydrogen content ratio of gasoline to water (0.91:1), a good contrast for a 12% gasoline saturation is not expected using the CPN probe. Figure 4-9 showed it differently, however, with a similar decrease in water saturation for CPN and TDR measurements. One hundred percent of the pore volume gasoline saturation would have to be present to generate such results and no explanation was found. The increase in water saturation at shallower depths noticed by TDR measurements is not repeated by CPN measurements, and may be caused by different regions of the porous medium that are integrated in the measurements of each tool.

According to the results obtained by the TDR measurements, the planned emplacement of the residuals was successful, though an homogeneous distribution of residuals, everywhere in the cell is less likely. The irregular nature of the top of the capillary fringe tended to produce small localized pools of gasoline, making it difficult to produce an even thickness of spilled gasoline.

The complete sequence of TDR and CPN measurements, from the beginning of the experiment before dewatering the cell to the end, after ethanol flushing, is presented in Appendix VI.

4.5.3 Ethanol flushing

The ethanol flushing process involved the initial injection of ethanol and later injection of water. A sequence of figures is presented showing an interpretation for the distribution of ethanol and gasoline saturations in cross-sections of the cell test as measured in the fluid samples. The ethanol and gasoline saturations are compared to the

water saturation profiles as measured by TDR and CPN at the three access tubes (a detailed analysis of TDR and CPN measurements is presented on Appendix X. The behavior of ethanol injection and gasoline residuals displacement is analyzed in more detail through diagrams showing the variation of ethanol and gasoline saturation in time at every multilevel sampling port and all extraction wells. On each of these diagrams the composition of the samples is plotted on a ternary diagram to present to the evolution of the phase composition during the flushing process.

The field set up is shown in Figure 4-10. The ethanol injection started in October 24, 1995, and the pumps were halted about two days later after the injection of 90 liters of ethanol. The peristaltic pumps were not working properly and a better insulation system had to be built in order to maintain a temperature of about 20°C for the equipment (e.g., vyton tube response in peristaltic pumps is strongly affected by changes in temperature). The injection of ethanol restarted on November 07, 1995, and ran continuously until December 19, 1995, when the water injection was started. The injection and extraction systems were halted again on January 08, 1996, when the injection and extraction wells were moved to a higher position to improve ethanol extraction, and restarted on January 11, 1996 until the end of the experiment, on January 25, 1996. The depth of the extraction wells became 1.05 m for wells numbers 2, 5, 8, 11 and 13; 0.65 m for wells numbers 3, 6, 9 and 12; and 0.85 m for wells numbers 1, 4, 7, 10 and 14. The depths of the injection wells became 1.15 m for wells numbers 2, 5, 8, 11 and 13; 0.75 m for wells numbers 3, 6, 9 and 12; and 0.95 m for wells numbers 1, 4, 7, 10 and 14.

The complete evolution of the flushing experiment is presented on Figure 4-11, as

a series of snap-shots from the experiment based on the data collected on different dates. The sets are identified by their dates, starting on November 21, 1995 and finishing on January 25, 1996. Each set is composed by two cross sections of the cell test and three profiles. Figure 4-10 presents the basic features of the schematic cell used in Figure 4-11. In every cross section, flow of fluids goes from right to left. The bottom of the cell was truncated at the depth of 2.15 m below ground surface for graphical reasons, no ethanol or gasoline was detected at those lower levels. The ethanol and gasoline saturations are based on the UV analyses of the fluid samples. Concentrations of gasoline and ethanol are presented on a weight percent basis, with a linear scale used to define intervals for the ethanol saturation. The zone of the emplaced gasoline residuals is represented by a dashed region. The depth of the reach of injection and extraction well screens is represented as a rectangle at the lateral limits of the cell test (the sheet piles). The cross sections have a vertical exaggeration of 1.26:1. By the side of the two cross sections are represented the apparent water saturation profiles as determined by TDR and CPN in the three access tubes. The depths of the TDR/CPN diagrams and the cross sections are on the same scale. The TDR/CPN profiles are discussed in the next section.

The concentrations used to build the cross sections were those of multilevels A, C and D, and extraction wells 3, 4 and 5. The behavior of the concentrations at different monitoring points were highly dependent on depths only, with negligible variation of concentrations for points located at the same depth, justifying the use of single points as representative of the whole cell. This behavior is explained later in this chapter, when the breakthrough curves of each sampling point are presented and discussed. The distribution of concentrations near the injection wells was inferred by TDR measurements because of

the lack of sampling points in that region. It is important to note that in Figures 4-11 and 4-12 the gasoline saturation determined in the UV analyses represents only the dissolved gasoline. The gasoline residuals left in place are not represented by gasoline saturation distribution on the cross sections.

The first set of results shown on Figure 4-11 corresponds to November 21, 1995. The ethanol saturation cross section shows the main feature observed in the field experiment: ethanol overrides the zone of gasoline residuals, moving upwards to the higher portion of the saturated zone. Although expected at a much smaller extent, this behavior was not observed in the laboratory experiments.

The upward movement of the ethanol could have represented upward movement of the initial 90 liters of ethanol when the pumps stopped from October 27 to November 07,1995. The next sets, for November 23 and 25, suggests that this is not the case. During active pumping the ethanol does show a preferential upward flow, with only low ethanol saturation reaching the zone of residuals.

The distribution of the gasoline saturation suggests that part of the residuals formed a "halo" of oleic phase described in Chapter 3 (top center of the cross section). The presence of the halo is inferred by the higher mobile gasoline saturations, since the fluid samples presented only aqueous phase. The relatively higher gasoline saturation at the center of the zone of residuals could correspond to a higher original gasoline residual saturation at that point.

The November 23 set of results shows a region of dissolved gasoline saturation greater than 0.135% gasoline. Its position suggests that it was not mobilized from lower levels of the zone of the emplaced residuals. The explanation for this is as follows: as

suggested by the sintered glass beads experiments, the gasoline that is incorporated to the main flow of ethanol, after being dissolved, either remains in the dissolved phase or is immediately extracted, forming the halo around the path of higher content ethanol. This halo forms close to the point where the residual was emplaced. The interpretation is that this higher concentration region corresponds to dissolved gasoline coming from residuals emplaced near that position. One reason for the emplacement of the residuals at this place is that gasoline was injected at this location to begin with, and it moved upward during the water table rise using the monitoring well wall as a preferential path, which is suggested by the proximity of the higher concentration region and the monitoring well.

The sets for November 25, November 27 and November 29 show a continuation of the process with more ethanol at the higher portion of the saturated zoned and, as the amount of ethanol increases, higher contents of ethanol move lower towards the zone of residuals, increasing the amount of gasoline in the aqueous phase. The next set, December 01, shows the higher gasoline region above the 100 cm depth becoming a larger region of lower gasoline saturation, as this region is almost completely filled with high ethanol saturation. The decrease in the localized high gasoline saturation suggests the dissolution of the region of residuals present in the previous sets.

From December 04 to 19, high concentration ethanol continued to accumulate at the higher portions of the cell and gradually these higher ethanol concentrations move downward into the zone of gasoline residuals.

The measurements presented on the set of December 19 were taken before the water injection started on that same day. The injected water tended to underride the ethanol and slowly displaced the ethanol that remained at and above the level of the

injection well screens. This is showed in sets December 22 to January 15.

On the upper right portion of the cell, where the ethanol saturation was above 90% by weight (single phase composition expected), there is a region with persistent measurable gasoline. This persistence of the gasoline saturation suggests that the fluids flow at very low velocity in this region.

Since ethanol moves upwards in miscible displacement in a groundwater system, because the position of injection and extraction well screens are located much deeper in the cell, if the drawdown at the extraction well is not sufficient to bring the water-ethanol level below the level of the well screen, ethanol at depths of 30 cm to 60 cm cannot be extracted. For this reason, the extraction system was unable to efficiently extract the ethanol from the aquifer, and on January 09 the wells were raised. Figure 4-11, set of January 15, shows the first snap-shot after the wells were raised. As seen from this figure, ethanol production from the top portion of the cell was enhanced.

Variation of concentration with depth

The ethanol and gasoline saturation in fluid samples from multilevel ports and extraction wells were plotted as breakthrough curves (concentration versus time) as shown in Figures 4-13 and 4-14. The complete set of this type of results is presented on the Appendix VIII. The ports of different multilevels located at the same depth have similar shaped breakthrough curves and results of the Figure 4-12 are general., from multilevel D, illustrates the breakthrough curves for the multilevel ports. Only the two shallower ports (60 cm and 90 cm bgs) showed ethanol content above 88% by weight (see Chapter 2). The ports located at 120 cm bgs presented maximum ethanol content between 60 and 70% by weight. The compositions for the samples are showed in ternary

diagrams in the same figure. The points fall to the aqueous phase side of the ternary diagram, as expected. The absence of samples with oleic phase indicates either the low mobility of this phase or the absence of the development of a mobile oleic bank. The breakthrough curves also confirm that the zone of gasoline residuals was only partially reached by high ethanol content, above 88% by weight, necessary for removal of residuals by mobilization helped by the blob ejection mechanism.

Similarly to multilevel ports, the depths of the extraction wells determined the behavior of their respective breakthrough curves. Figure 4-13 presents the breakthrough curves for the extraction wells 4 (deeper), 5 (shallower) and 6 (intermediate) as an example of the behavior of the ethanol and gasoline production. Differences for arrival times at well screens located at the same depth were negligible (refer to Appendix VIII to see the complete set of figures) and this suggested that the formation of zones of preferential flow for ethanol (fingers) did not develop to a great extent. The absence of fingers might be related to the fact that ethanol did not flow mainly through the zone of gasoline residuals, but rather above it, moving gradually downward and reaching the residuals from above.

The experiment showed that gravity plays a key role in controlling the ethanol flow. Ethanol flows to the higher portions of the saturated zone, moving upwards in the system. This importance of ethanol flow behavior is addressed in more detailed manner in Chapter 5 using model experiments.

4.5.4 Mass Balance for Gasoline and Ethanol Recovery

The breakthrough curves of the extraction wells were integrated over time, and

the average pumping rate of 3 ml/min. at each extraction well was used to determine the total mass of gasoline and ethanol removed from the system, and the results are presented on Table 4-1.

Table 4-1 - Volumes of ethanol and gasoline produced at the extraction wells during the ethanol flushing field experiment.

Extraction Well #	Volume of Ethanol (l)	Volume of Gasoline (l)
1	20.13	0.32
2	130.66	2.99
3	74.12	0.50
4	34.56	0.38
5	133.41	2.05
6	75.52	1.34
7	20.04	0.17
8	139.29	4.40
9	79.14	2.33
10	23.76	0.62
11	133.48	5.16
12	81.40	1.79
13	120.84	3.15
14(*)	2.44	0.03
Total	1,068.79	25.23

(*) Well presented lower flux rate during the whole experiment

Only 36% of the injected gasoline was recovered (25 l out of 70 l injected) and only 45% of the injected ethanol was recovered (1070 l out of 2400 injected). The low recovery of gasoline is due to the fact that ethanol overrode the zone of emplaced gasoline residuals, with a consequent low sweep efficiency of this target zone.

Five cores were taken to evaluate the residuals left in place. Core locations are presented in Figure 4-14. The cores underwent compaction during their extraction, and a compaction factor was applied to the cores to correct for the depth of interest(see Appendix IX). A total of 39 5 cm long discrete subsamples were taken from the core sample, and the results are presented on Appendix IX. The compaction of the soil within

the core barrel somehow shortened the total depth of the core, which adds to the fact that ethanol was found at much deeper levels than expected from the final concentration distribution of ethanol on the water samples (see Figure 4-11, last set, January 25, 1996). The deeper core samples showed values of ethanol as high as 64% by weight ethanol (depth 117 cm below ground surface). This suggests much of the missing mass could have been below the cored interval. Unfortunately, no fluid sampling was done to confirm this hypothesis and deeper cores were not possible to be taken at the site.

The ethanol and gasoline saturation profiles for each core are presented in Figure 4-15. The profiles show ethanol saturation near 100% at the higher portions of the cell, and decreasing to about 40-50% by weight at the lower depths cored. All the cores showed similar profiles so the values were depth averaged and summed to give an evaluation of the total mass of ethanol within the cell. Based on this calculation, the volume of ethanol remaining in the cell was 890 liters, corresponding to 37% of the volume of ethanol injected into the cell test. This result and the mass recovered in the extraction wells account for 82% of the total ethanol injected, which is a good approximation considering the amount disconsidered by the core sampling.

The core analyses showed a relatively low gasoline saturation at most depths. The results indicate that the mass of gasoline left in place accounted for in the core analyses corresponded to gasoline in dissolved phase. This result is illustrated in Figure 4-16, that shows that very few core samples presented gasoline in residual phase (falling within the 2-phase region of the ternary diagram). Since most of the mass of gasoline left in place remained in residual phase, the core sampling did not give an accurate estimate of the mass balance. The same method of depth averaging used for ethanol was applied to

evaluate the volume of mass of gasoline remaining in the cell after the ethanol flushing. A total of 8 liters of gasoline remained, corresponding to 12% of the total 70 liters of gasoline initially emplaced.

The spatial distribution of the core sampling was adequate for ethanol, but gave a very poor representation of the gasoline residuals left in place.

4.6 Conclusions

The density difference between ethanol and water provoked the segregation of the ethanol from the water with ethanol flowing to the higher portions of the saturated zone, moving upwards in the groundwater system.

The core sampling method used in this field experiment offered a reasonable approach to determine the remaining ethanol. In more general terms, the spatial distribution of the core sampling was suitable for dissolved species, either gasoline or ethanol, but not for residual gasoline.

The field behavior of ethanol flushing was not well predicted from laboratory studies. The design used in this field experiment was not a successful remediation at pilot scale, but a better design can now be made and is presented on Chapter 5.

Most of the ethanol injected missed the target region of residuals, with a consequent poor recovery of the gasoline residuals. Only 36% by weight of the emplaced gasoline was removed from the aquifer (25 liters out of 70 liters), and only 45% by weight of the injected ethanol (1,068 liters out of 2,400 liters injected) was recovered.

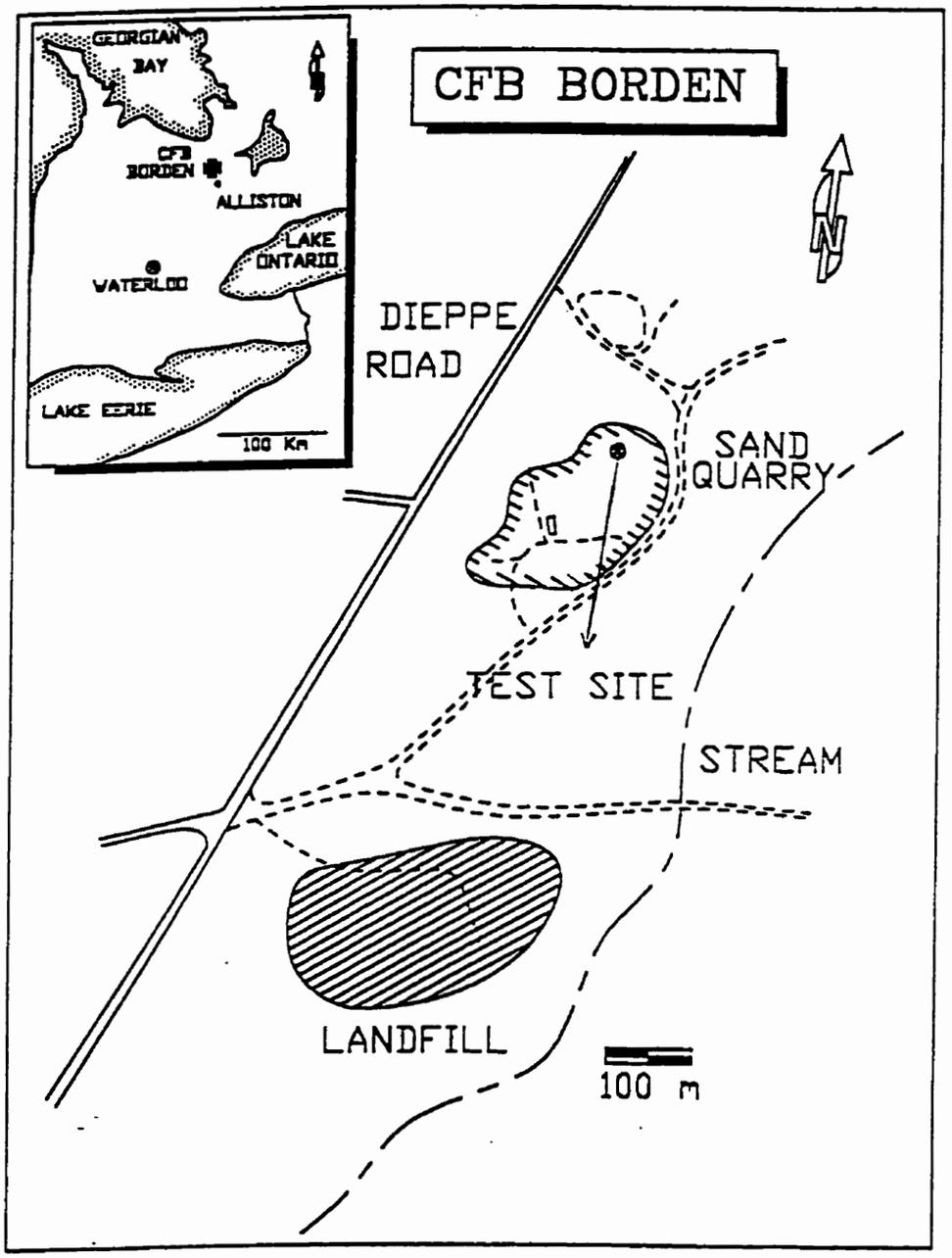

Figure 4-1 - Location of the site of the field experiment.

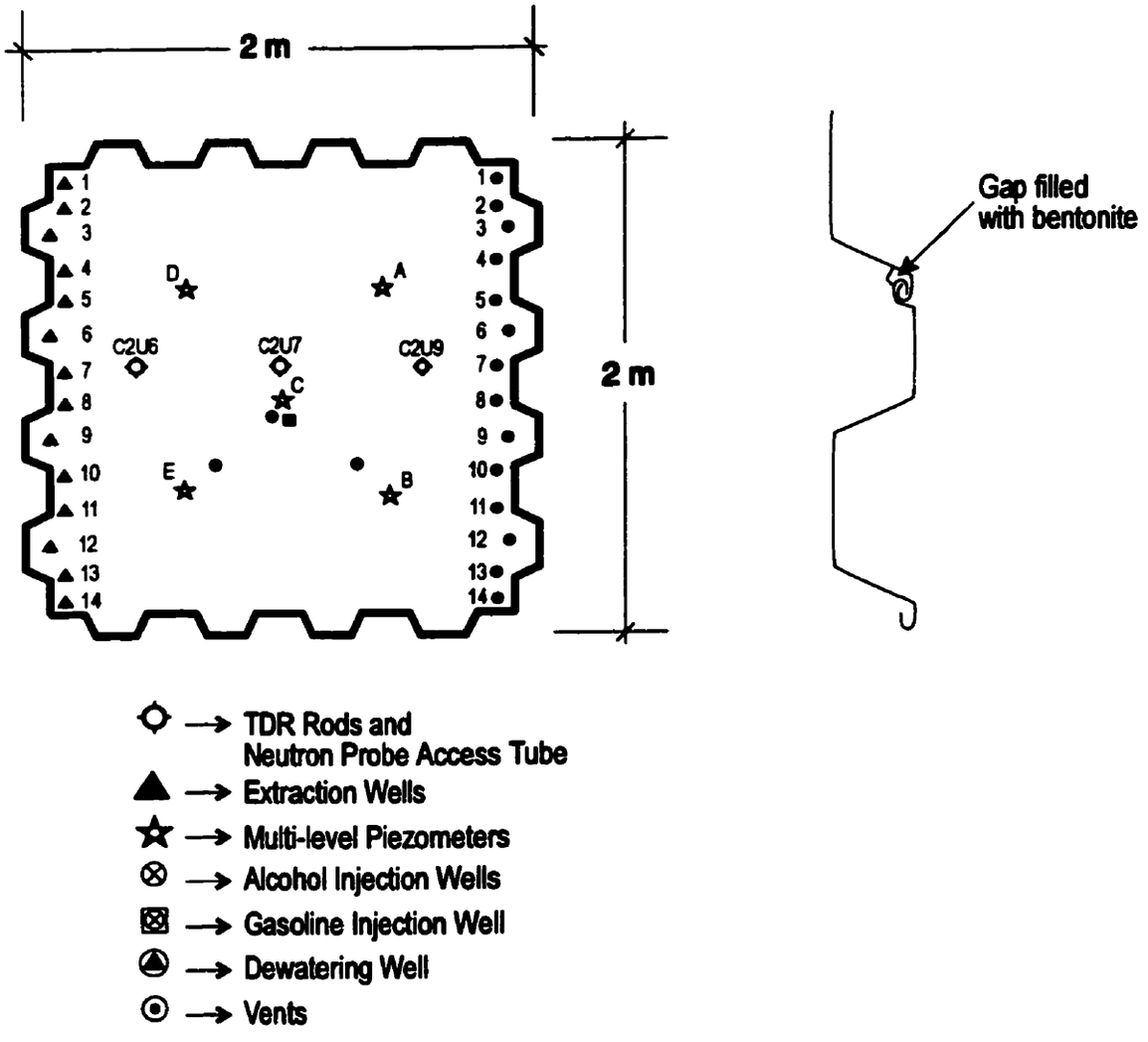

Figure 4-2 - Cell and instrumentation (a) plan view.

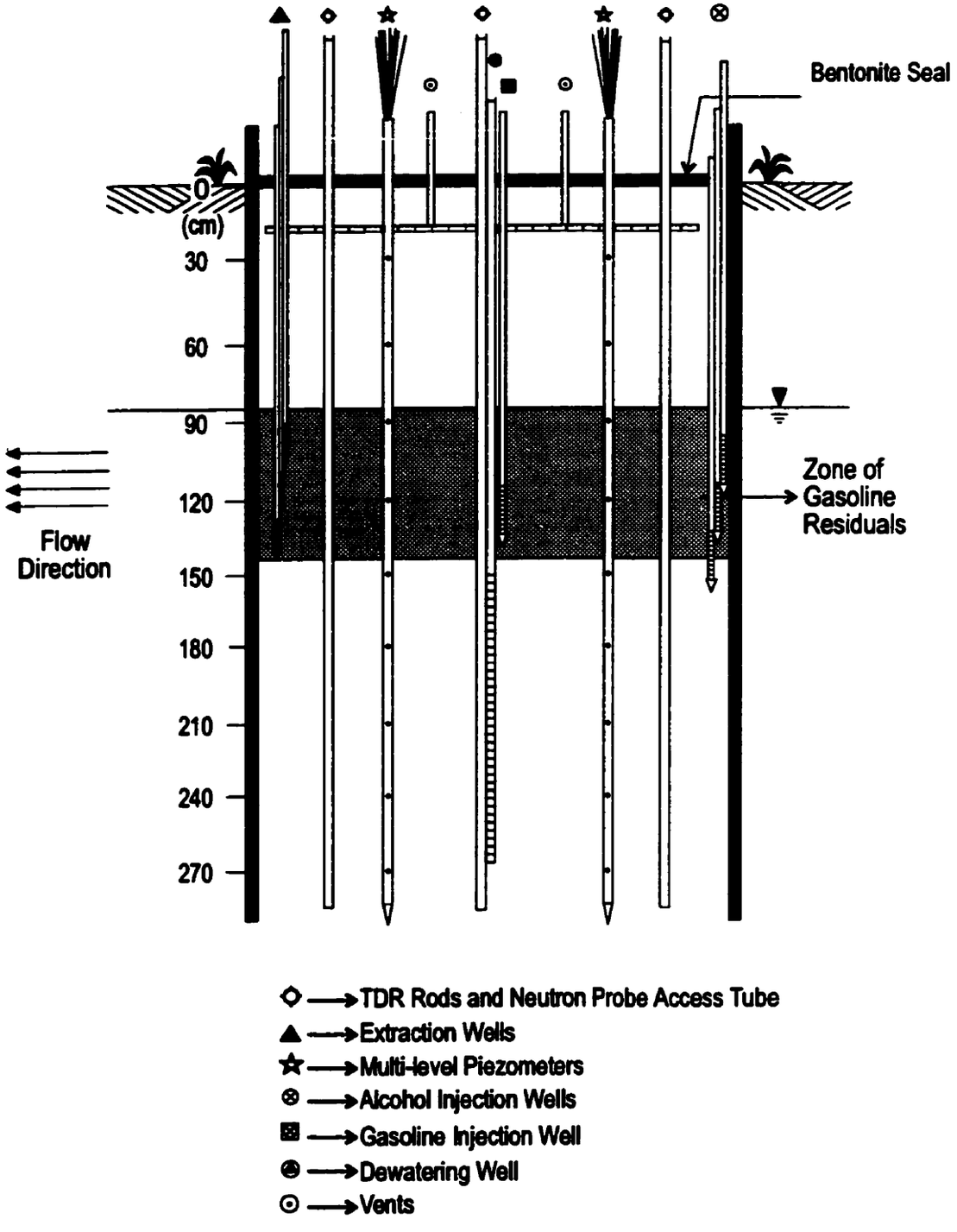

Figure 4-2 - Cell and instrumentation (b) cross section.

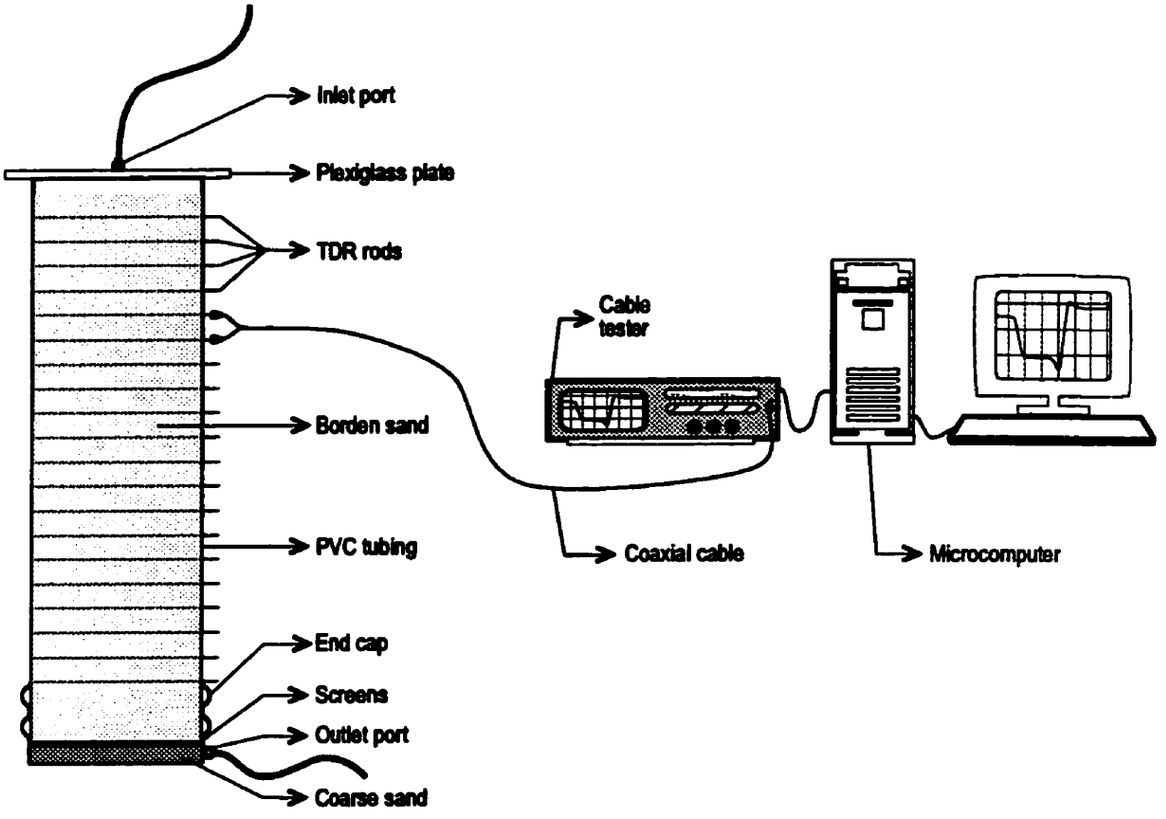

Figure 4-3 - Column setup for evaluation of gasoline residual saturation in the saturated zone due to variations of the water table

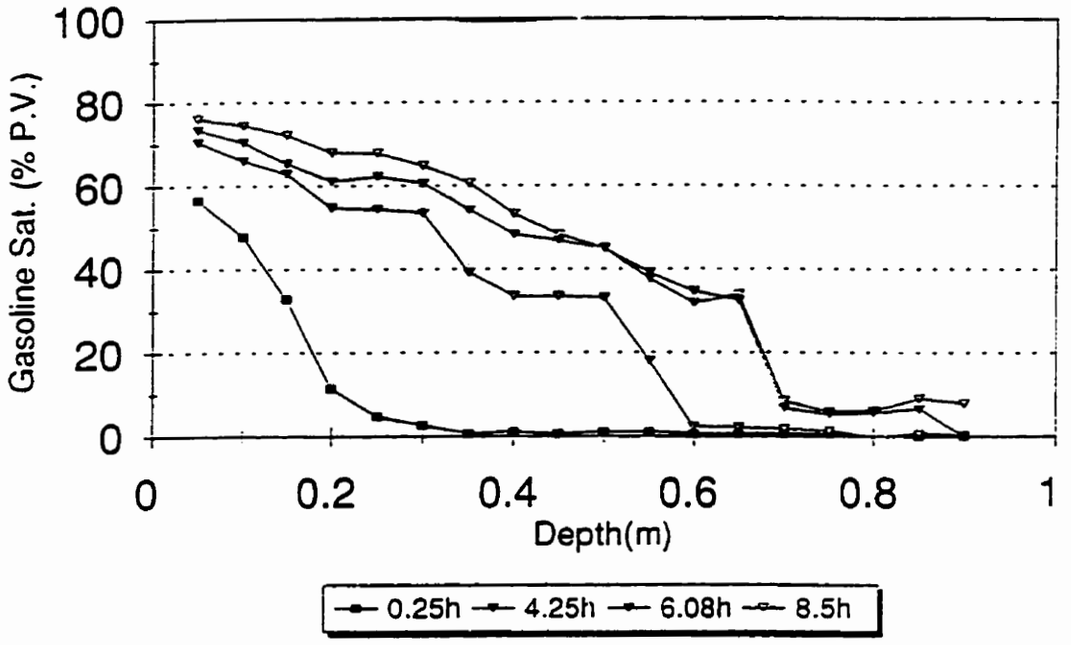

Figure 4-4 - Gasoline saturation versus depth of the column for various times after the experiment started.

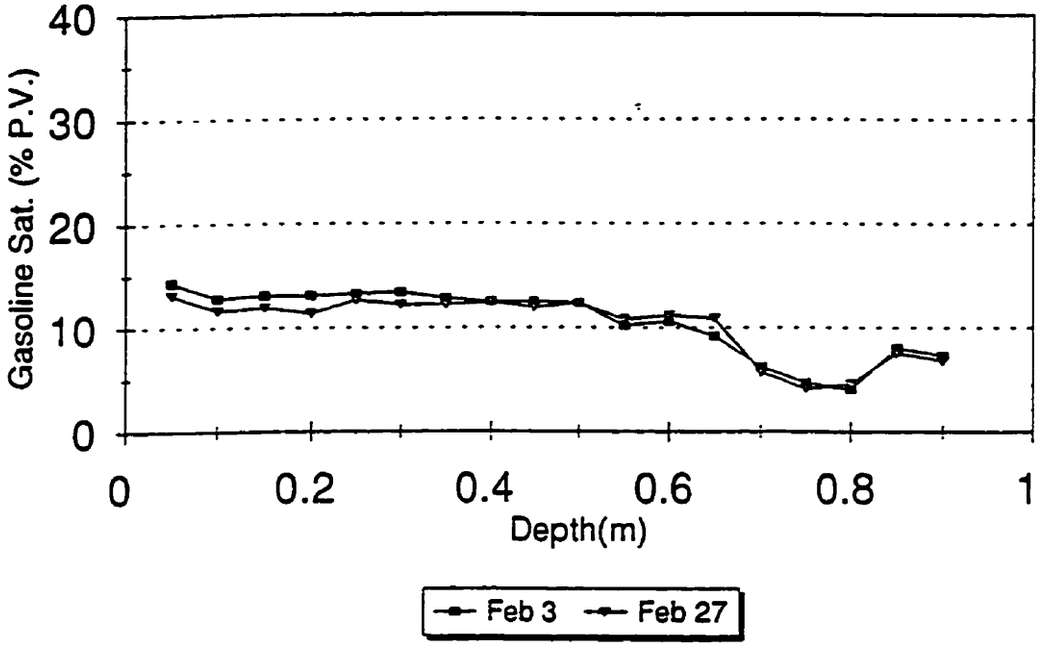

Figure 4-5 - Final gasoline saturation profile after water table fluctuation as determined by TDR measurements.

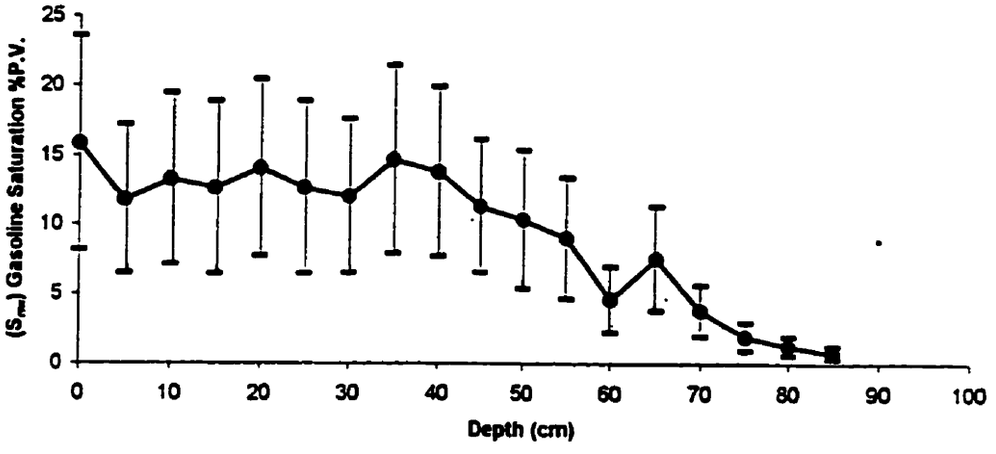

Figure 4-6 - Final gasoline saturation profile after water table fluctuation as calculated based on chromatographic analyses for BTEX compounds and mole fractions of BTEX from the literature.

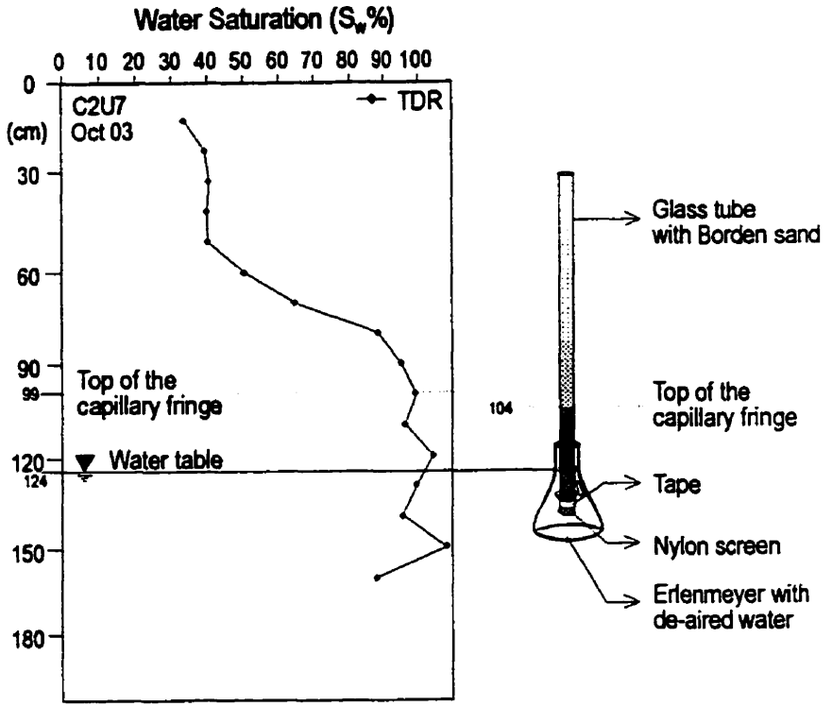

Figure 4-7 - Height of the capillary fringe for Borden sand: comparison between the results of water saturation measured with TDR and visually determination using a glass column in the laboratory.

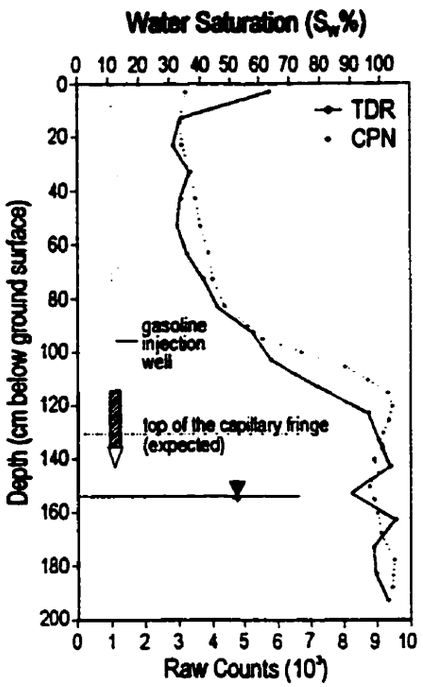

Figure 4-8 - Water saturation profile before gasoline spill as measured by TDR and CPN.

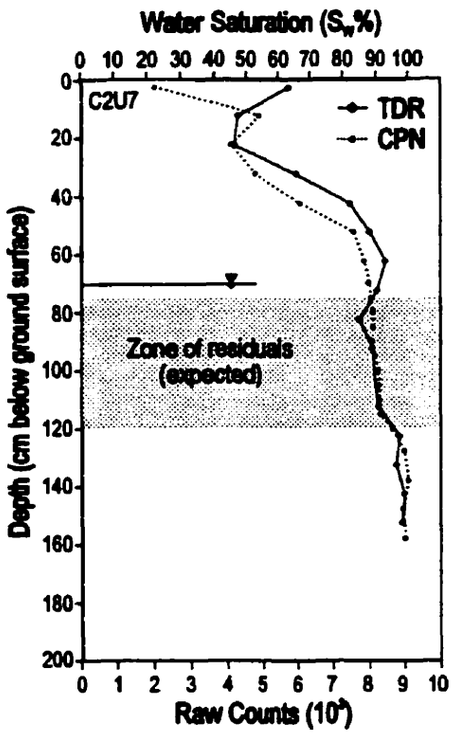

Figure 4-9 - Water saturation profile 13 days after the emplacement of the gasoline residuals.

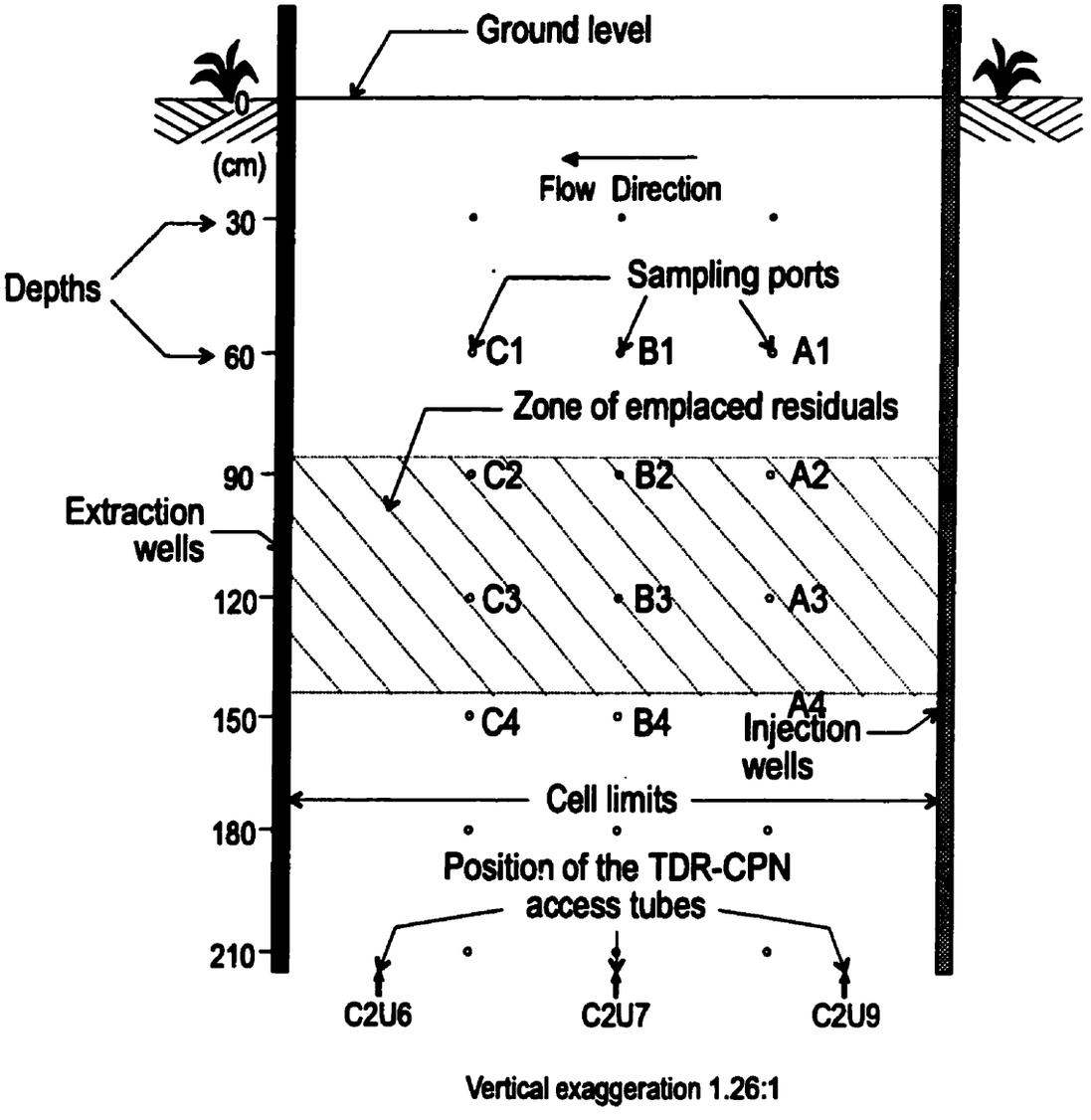

Figure 4-10 - Basic features of the cross section of the cell test used to present the distribution of ethanol and gasoline saturation in Figure 4-11.

The following pages refer to:

Figure 4-11 - Evolution of the ethanol flushing experiment. Cross sections of the cell test presenting the distribution of the ethanol and gasoline saturation and profiles of the TDR and CPN measurements at the three access tubes taken at the same time of the fluid samples.

Figure 4-12

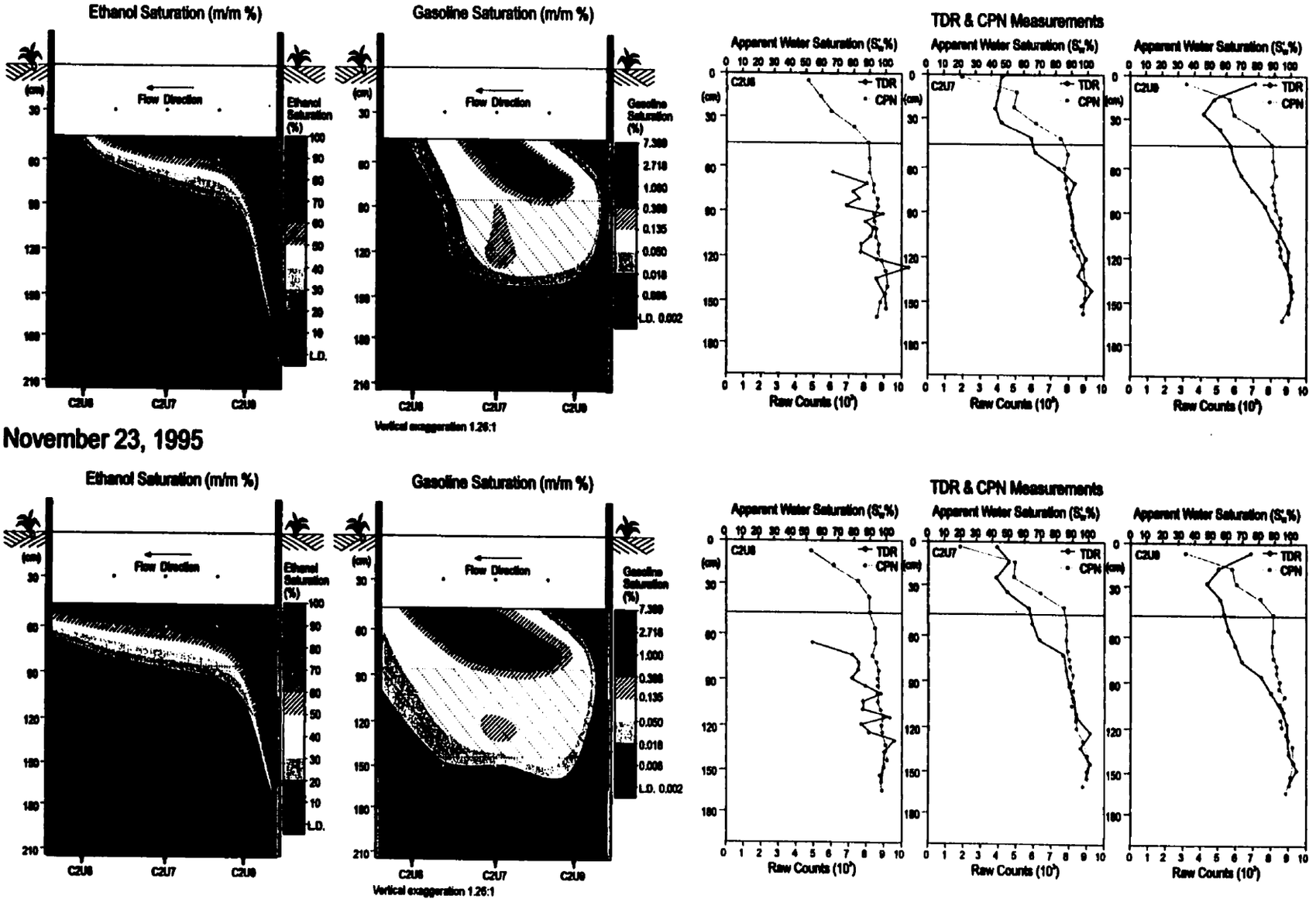
November 21, 1995
Ethanol Saturation (m/m %)
Gasoline Saturation (m/m %)
TDR & CPN Measurements
Flow Direction
Ethanol Saturation (%)
Gasoline Saturation (%)
C2U8
C2U7
C2U9
Vertical exaggeration 1.26:1
Apparent Water Saturation (S'w,%)
TDR
CPN
Raw Counts (10³)
November 23, 1995
Ethanol Saturation (m/m %)
Gasoline Saturation (m/m %)
TDR & CPN Measurements
Flow Direction
Ethanol Saturation (%)
Gasoline Saturation (%)
C2U8
C2U7
C2U9
Vertical exaggeration 1.26:1
Apparent Water Saturation (S'w,%)
TDR
CPN
Raw Counts (10³)

Figure 4-12

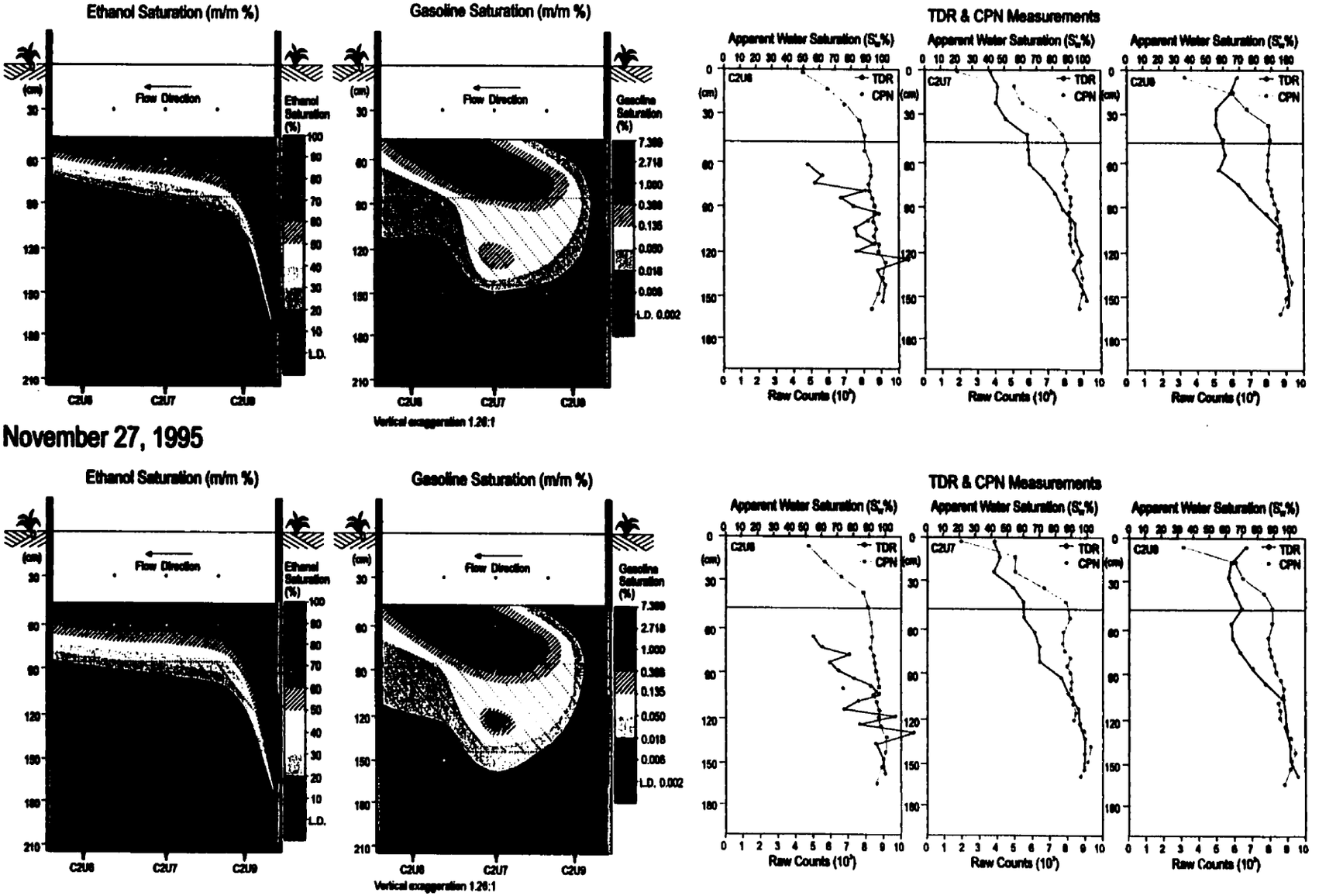
November 25, 1995
Ethanol Saturation (m/m %)
Gasoline Saturation (m/m %)
TDR & CPN Measurements
Flow Direction
Ethanol Saturation (%)
Gasoline Saturation (%)
C2U8
C2U7
C2U9
Vertical exaggeration 1.26:1
Apparent Water Saturation (S'w%)
TDR
CPN
Raw Counts (10³)
November 27, 1995
Ethanol Saturation (m/m %)
Gasoline Saturation (m/m %)
TDR & CPN Measurements
Vertical exaggeration 1.26:1

Figure 4-12

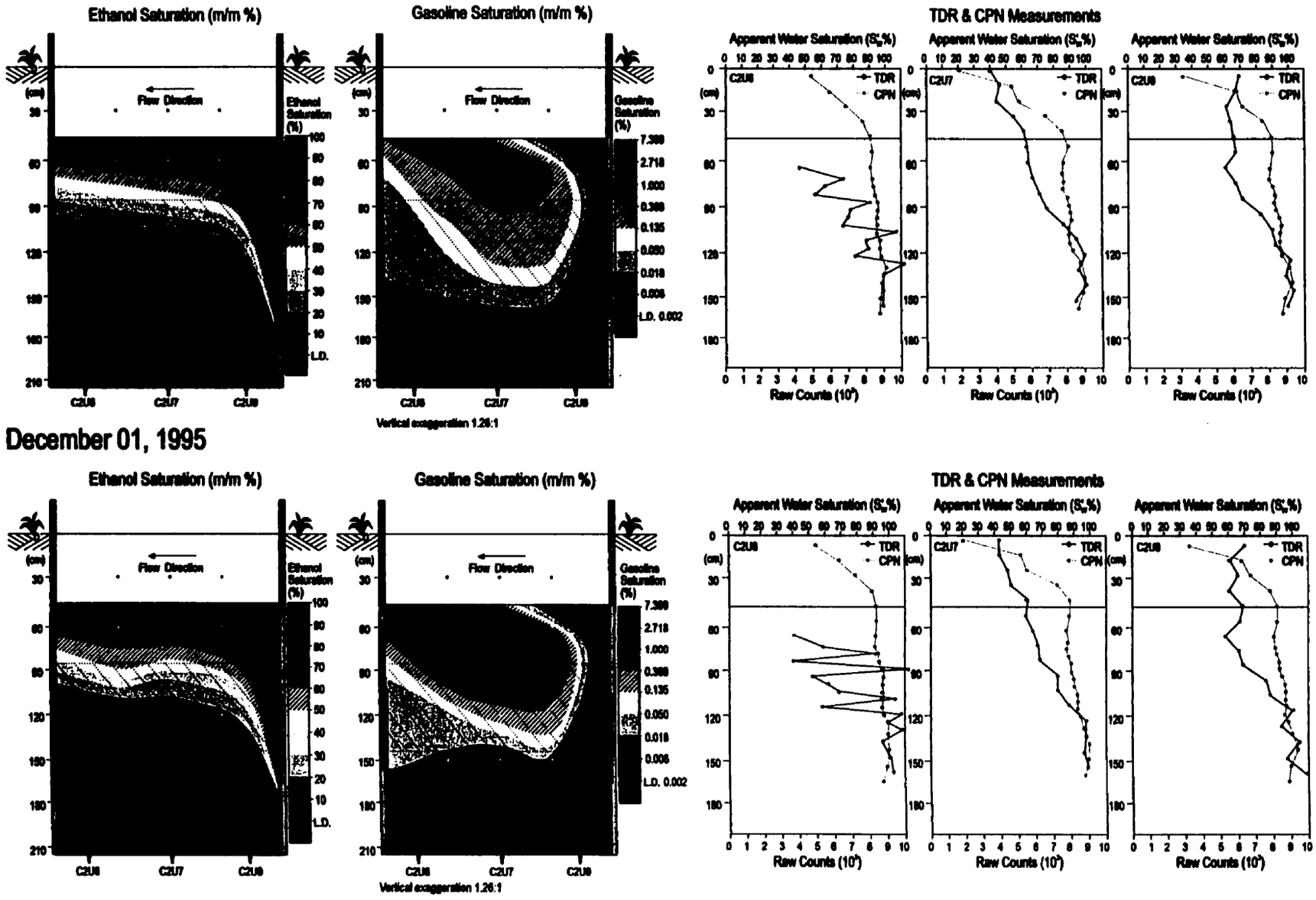
November 29, 1995
Ethanol Saturation (m/m %)
Gasoline Saturation (m/m %)
TDR & CPN Measurements
Flow Direction
Ethanol Saturation (%)
Gasoline Saturation (%)
C2U8
C2U7
C2U9
Vertical exaggeration 1.26:1
Apparent Water Saturation (Sw,%)
TDR
CPN
Raw Counts (10³)
December 01, 1995
Ethanol Saturation (m/m %)
Gasoline Saturation (m/m %)
TDR & CPN Measurements
Flow Direction
Ethanol Saturation (%)
Gasoline Saturation (%)
C2U8
C2U7
C2U9
Vertical exaggeration 1.26:1
Apparent Water Saturation (Sw,%)
TDR
CPN
Raw Counts (10³)

Figure 4-12

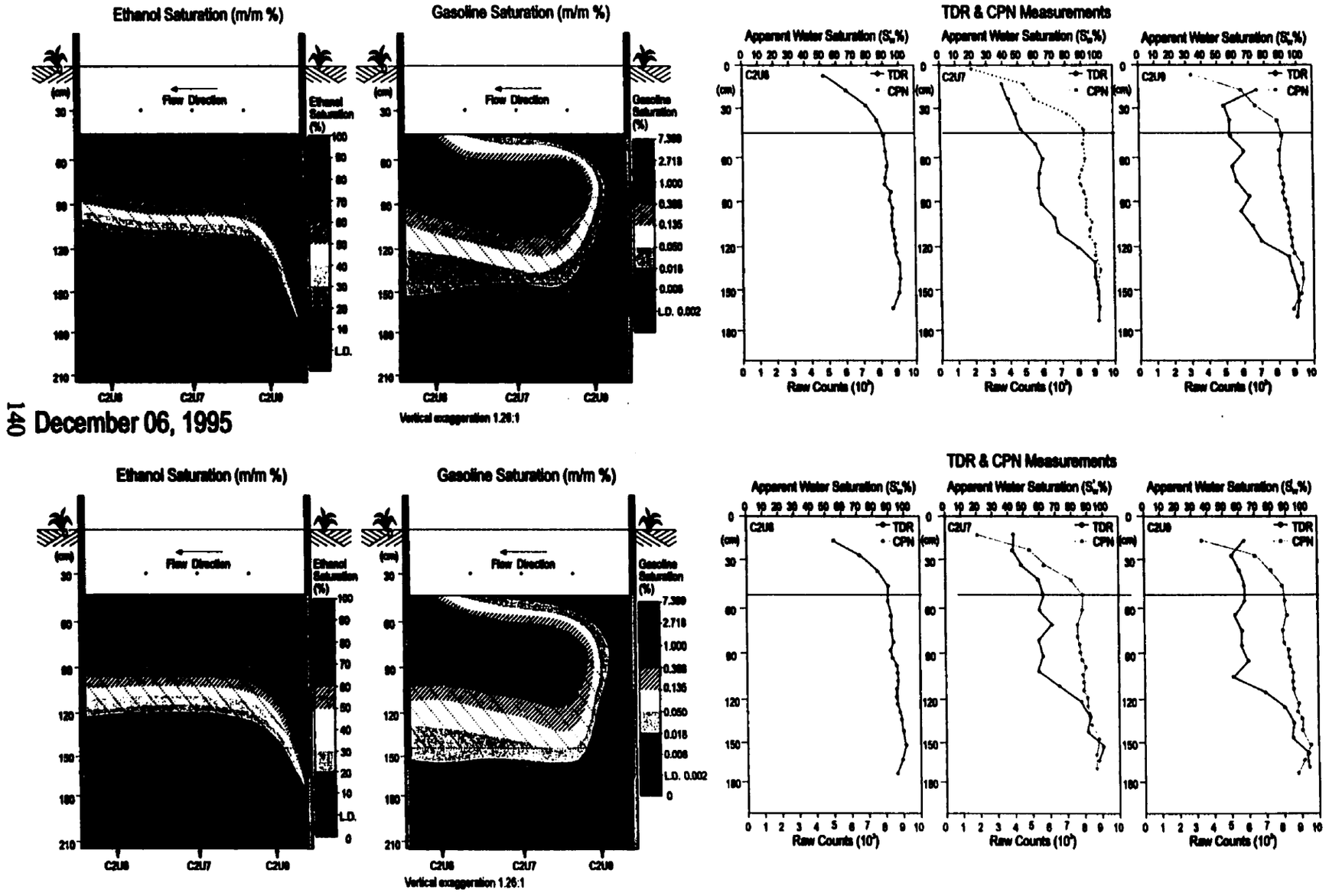
December 04, 1995
Ethanol Saturation (m/m %)
Gasoline Saturation (m/m %)
TDR & CPN Measurements
Flow Direction
C2U8
C2U7
C2U9
Vertical exaggeration 1.26:1
Apparent Water Saturation (S'w,%)
TDR
CPN
Raw Counts (10³)
December 06, 1995
Ethanol Saturation (m/m %)
Gasoline Saturation (m/m %)
TDR & CPN Measurements
Flow Direction
C2U8
C2U7
C2U9
Vertical exaggeration 1.26:1
Apparent Water Saturation (S'w,%)
TDR
CPN
Raw Counts (10³)

Figure 4-12

December 08, 1995

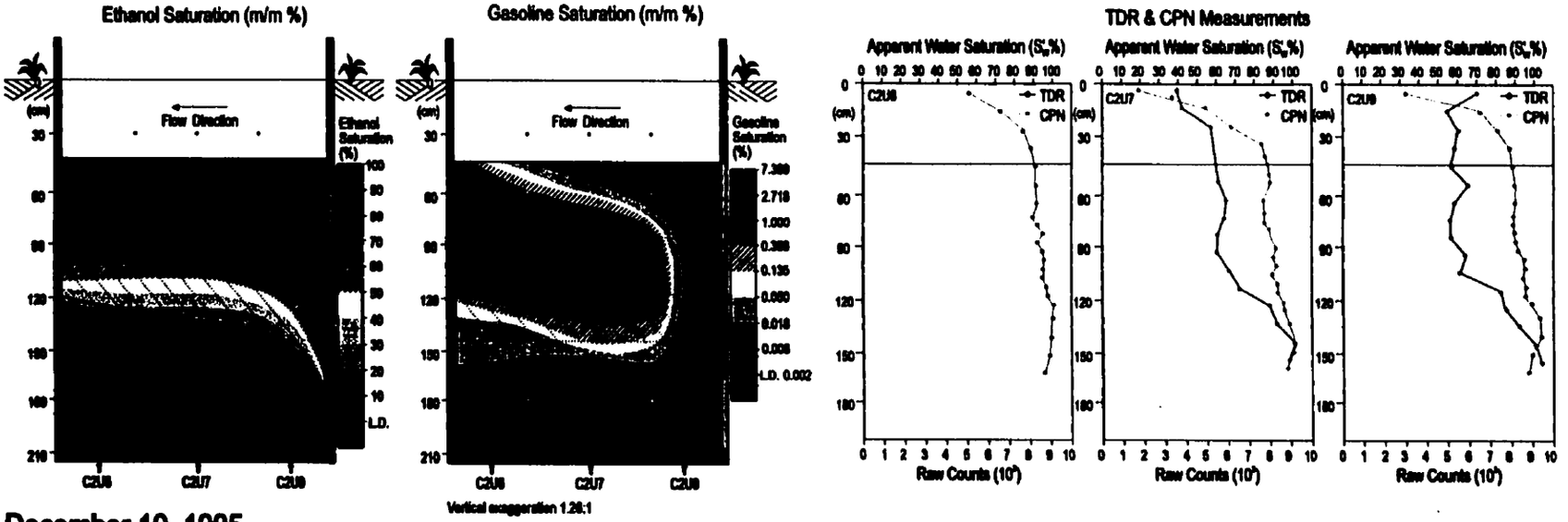

December 10, 1995

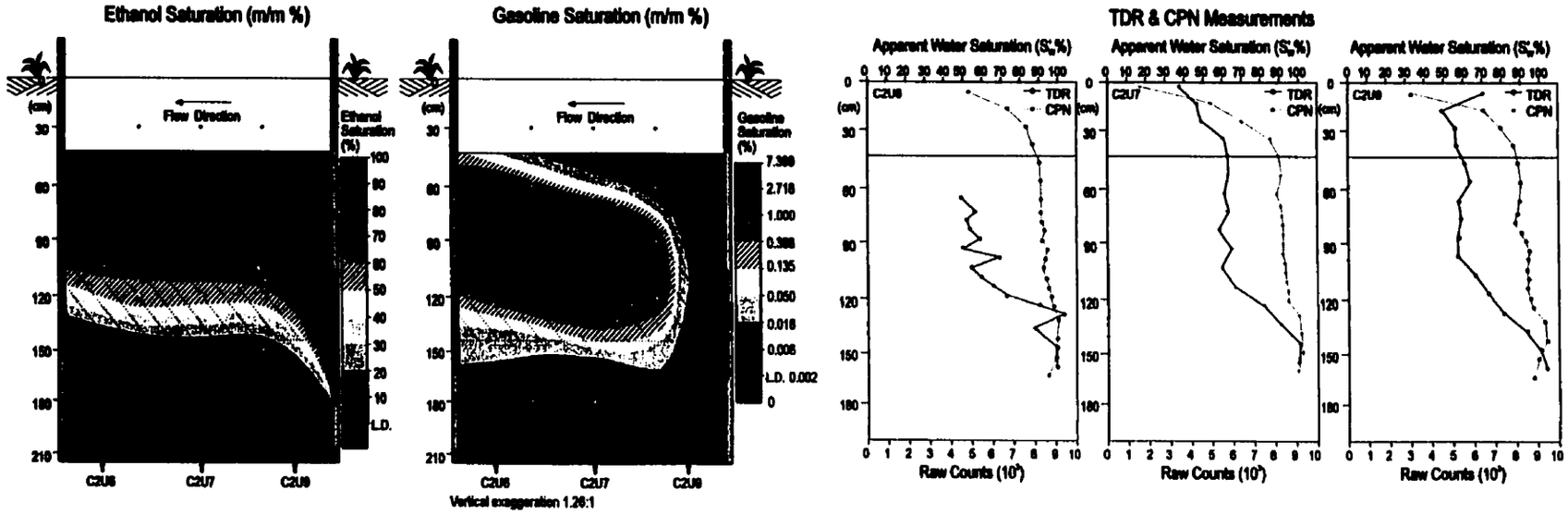

Figure 4-12

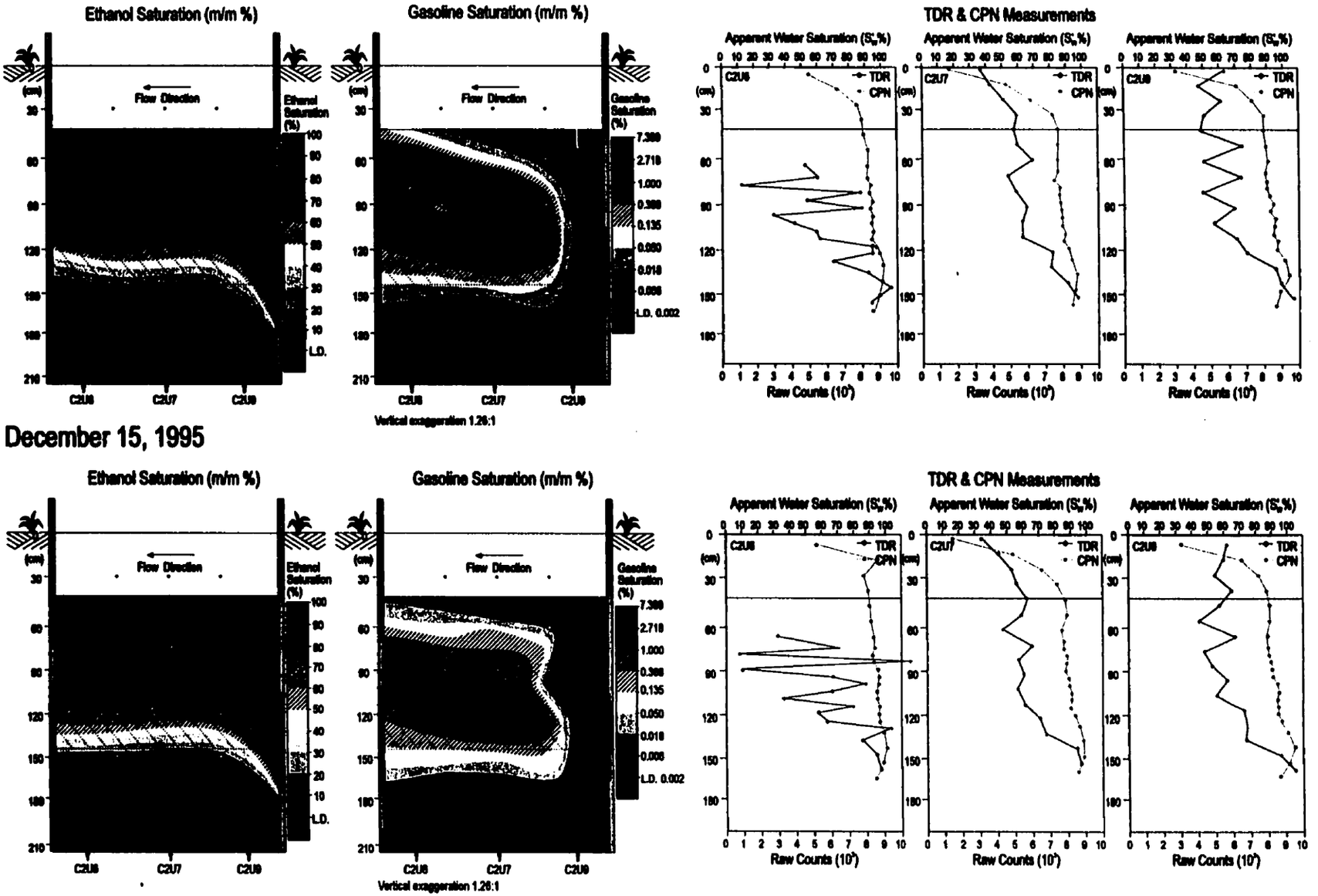
December 12, 1995
Ethanol Saturation (m/m %)
Gasoline Saturation (m/m %)
TDR & CPN Measurements
Flow Direction
Ethanol Saturation (%)
Gasoline Saturation (%)
L.D.
L.D. 0.002
C2U8
C2U7
C2U9
Vertical exaggeration 1.26:1
Apparent Water Saturation (S'w,%)
TDR
CPN
Raw Counts (10³)
December 15, 1995
Ethanol Saturation (m/m %)
Gasoline Saturation (m/m %)
TDR & CPN Measurements
Flow Direction
Ethanol Saturation (%)
Gasoline Saturation (%)
L.D.
L.D. 0.002
C2U8
C2U7
C2U9
Vertical exaggeration 1.26:1
Apparent Water Saturation (S'w,%)
TDR
CPN
Raw Counts (10³)

Figure 4-12

December 17, 1995

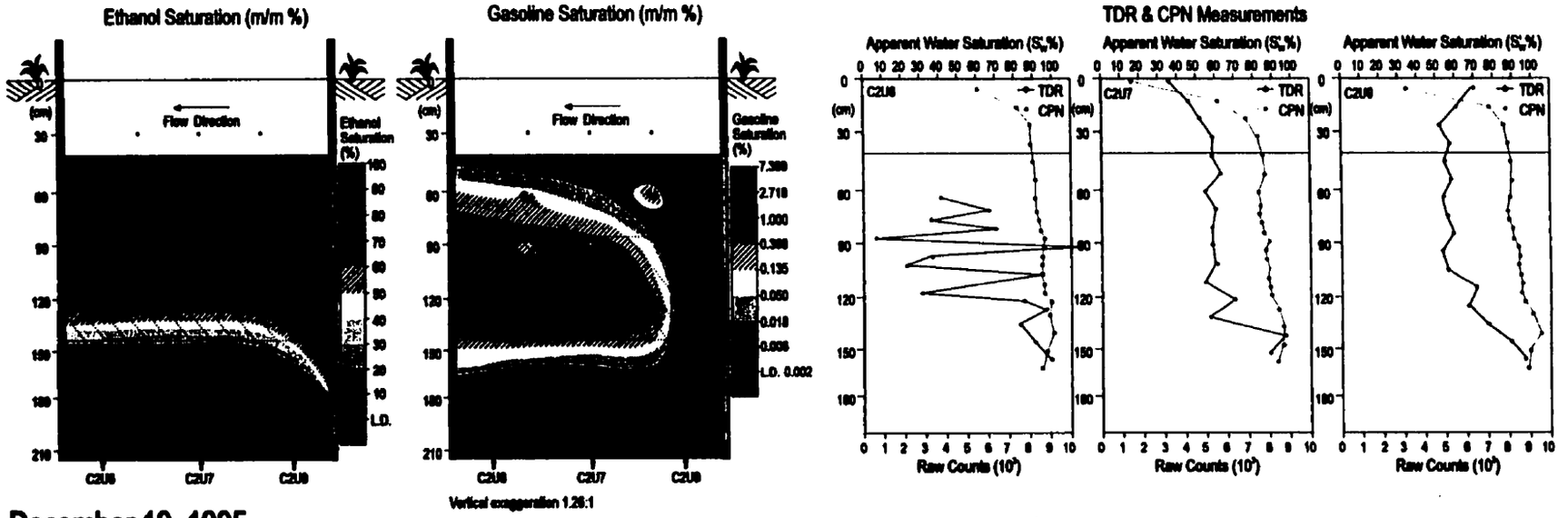

December 19, 1995

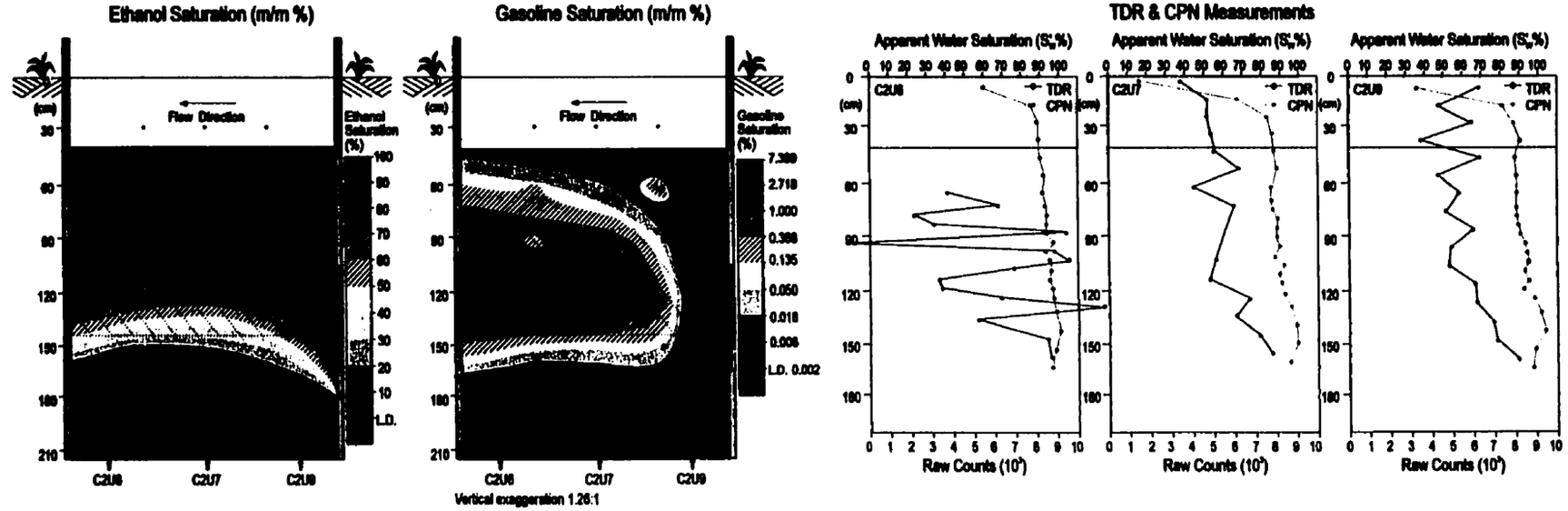

Figure 4-12

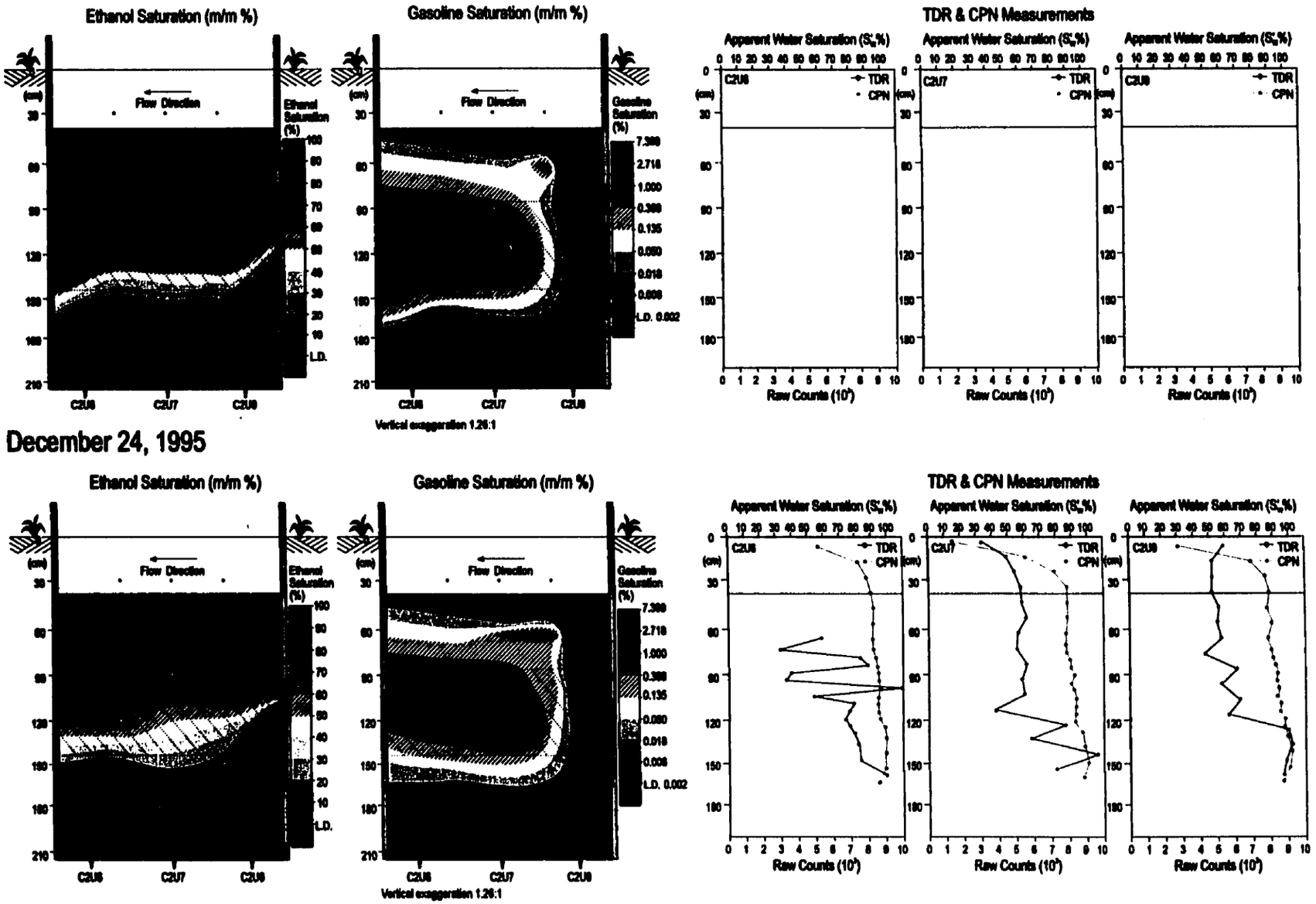
December 22, 1995
Ethanol Saturation (m/m %)
Gasoline Saturation (m/m %)
TDR & CPN Measurements
Apparent Water Saturation (S'w,%)
Flow Direction
Ethanol Saturation (%)
Gasoline Saturation (%)
C2U6
C2U7
C2U8
TDR
CPN
Raw Counts (10³)
Vertical exaggeration 1.26:1
December 24, 1995
Ethanol Saturation (m/m %)
Gasoline Saturation (m/m %)
TDR & CPN Measurements
Apparent Water Saturation (S'w,%)
Flow Direction
Ethanol Saturation (%)
Gasoline Saturation (%)
C2U6
C2U7
C2U8
TDR
CPN
Raw Counts (10³)
Vertical exaggeration 1.26:1

Figure 4-12

December 26, 1995

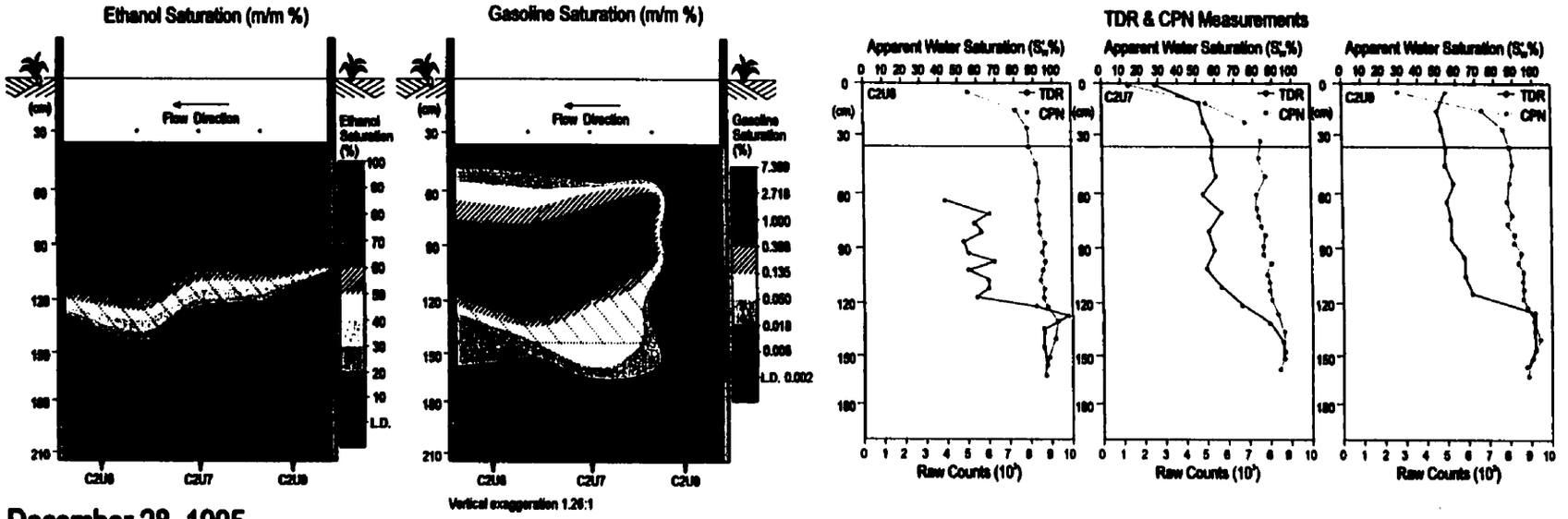

December 28, 1995

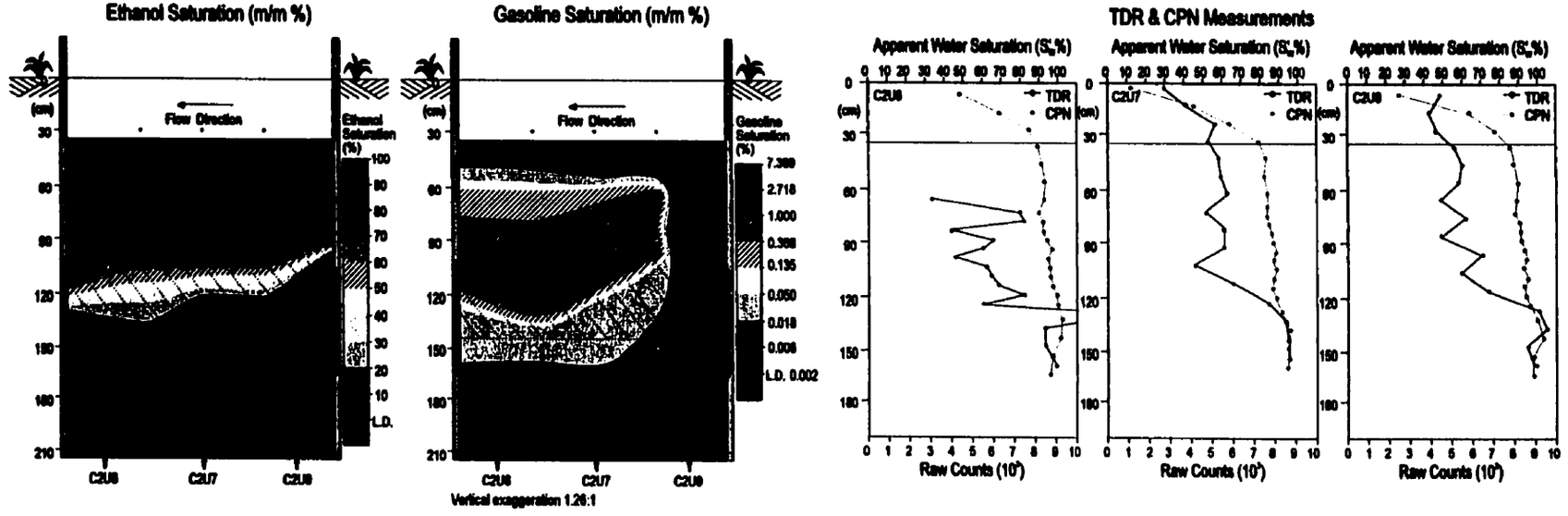

Figure 4-12

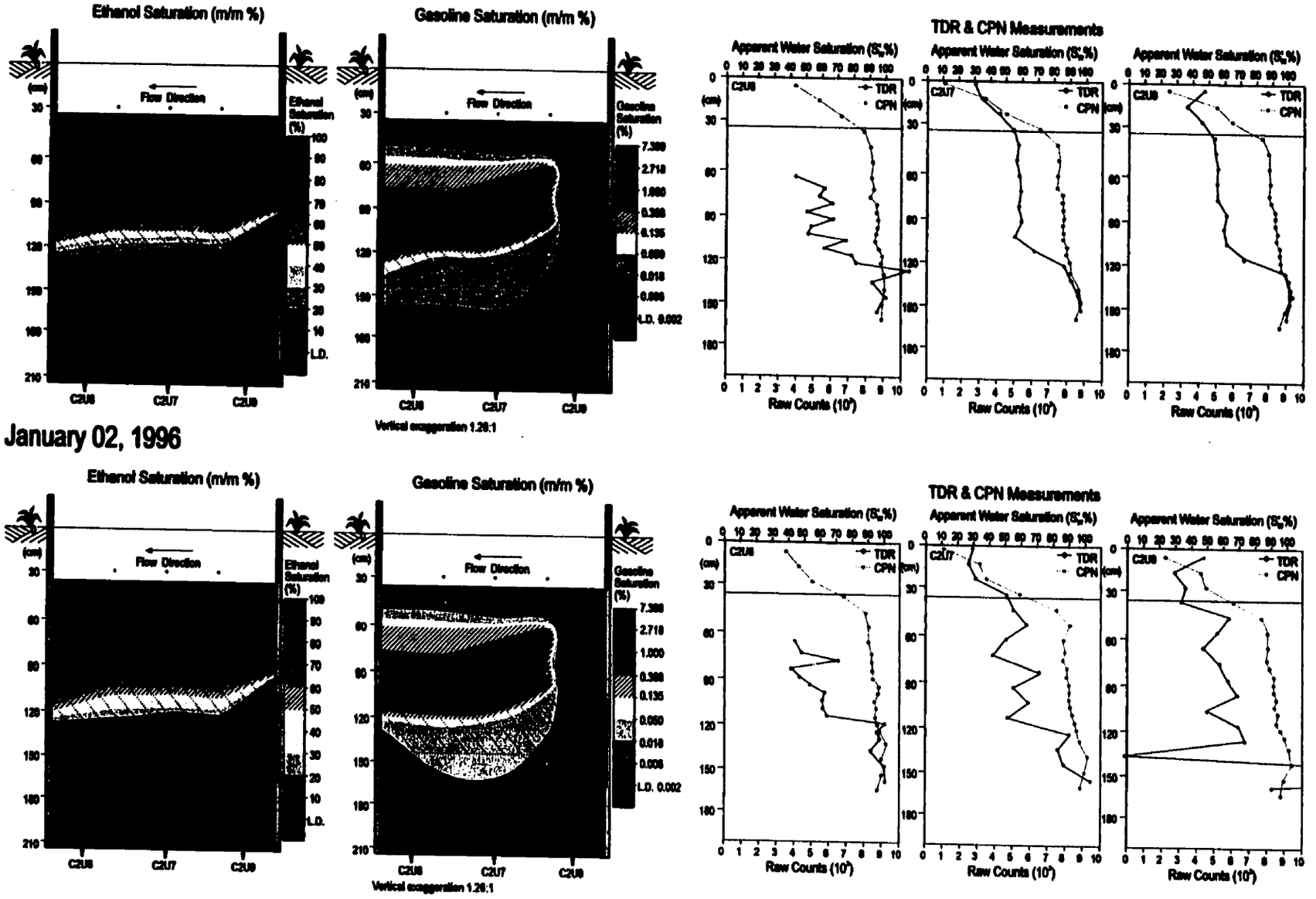
December 30, 1995
Ethanol Saturation (m/m %)
Gasoline Saturation (m/m %)
TDR & CPN Measurements
Apparent Water Saturation (S'w,%)
Flow Direction
C2U8
C2U7
C2U9
TDR
CPN
Raw Counts (10³)
Vertical exaggeration 1.26:1
January 02, 1996
Ethanol Saturation (m/m %)
Gasoline Saturation (m/m %)
TDR & CPN Measurements
Apparent Water Saturation (S'w,%)
Flow Direction
C2U8
C2U7
C2U9
TDR
CPN
Raw Counts (10³)
Vertical exaggeration 1.26:1

Figure 4-12

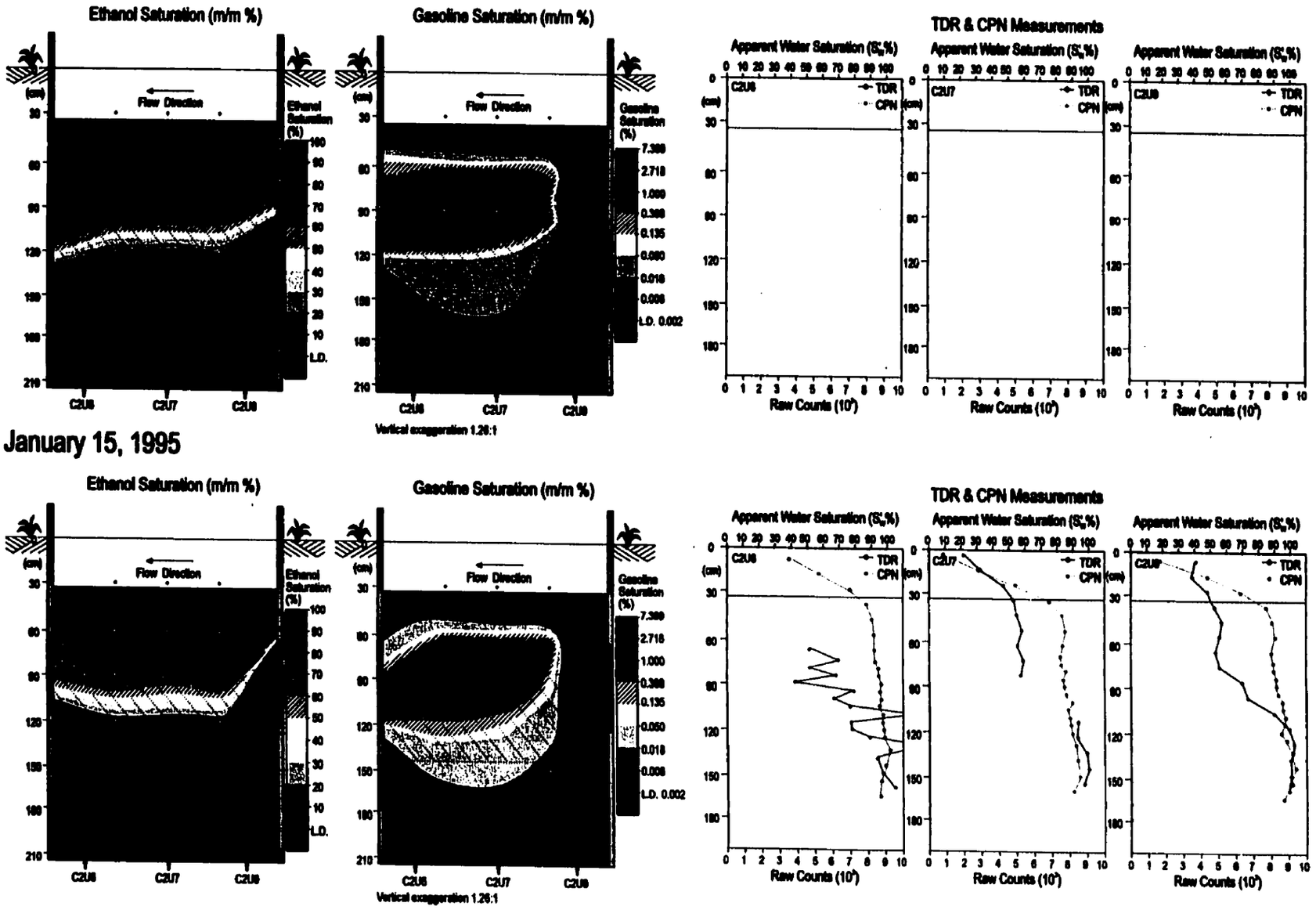
January 05, 1995
Ethanol Saturation (m/m %)
Gasoline Saturation (m/m %)
TDR & CPN Measurements
Flow Direction
Ethanol Saturation (%)
Gasoline Saturation (%)
C2U6
C2U7
C2U8
Vertical exaggeration 1.26:1
Apparent Water Saturation (S'w,%)
TDR
CPN
Raw Counts (10³)
January 15, 1995
Ethanol Saturation (m/m %)
Gasoline Saturation (m/m %)
TDR & CPN Measurements
Flow Direction
Ethanol Saturation (%)
Gasoline Saturation (%)
C2U6
C2U7
C2U8
Vertical exaggeration 1.26:1
Apparent Water Saturation (S'w,%)
TDR
CPN
Raw Counts (10³)

Figure 4-12

January 25, 1995

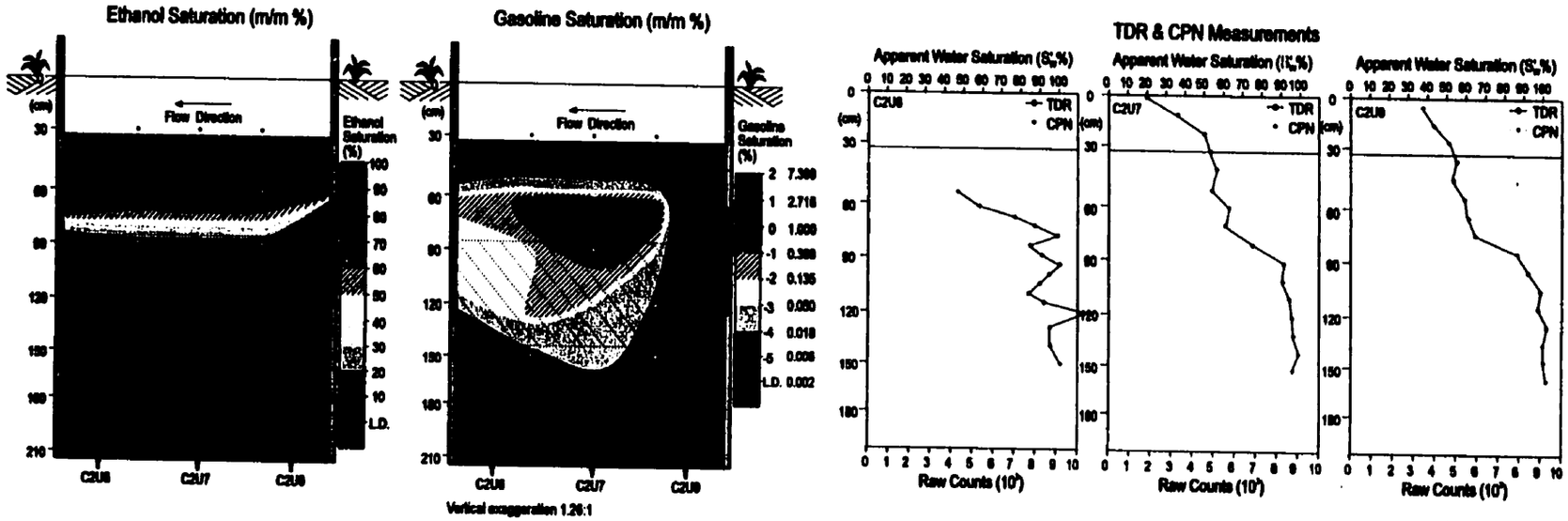

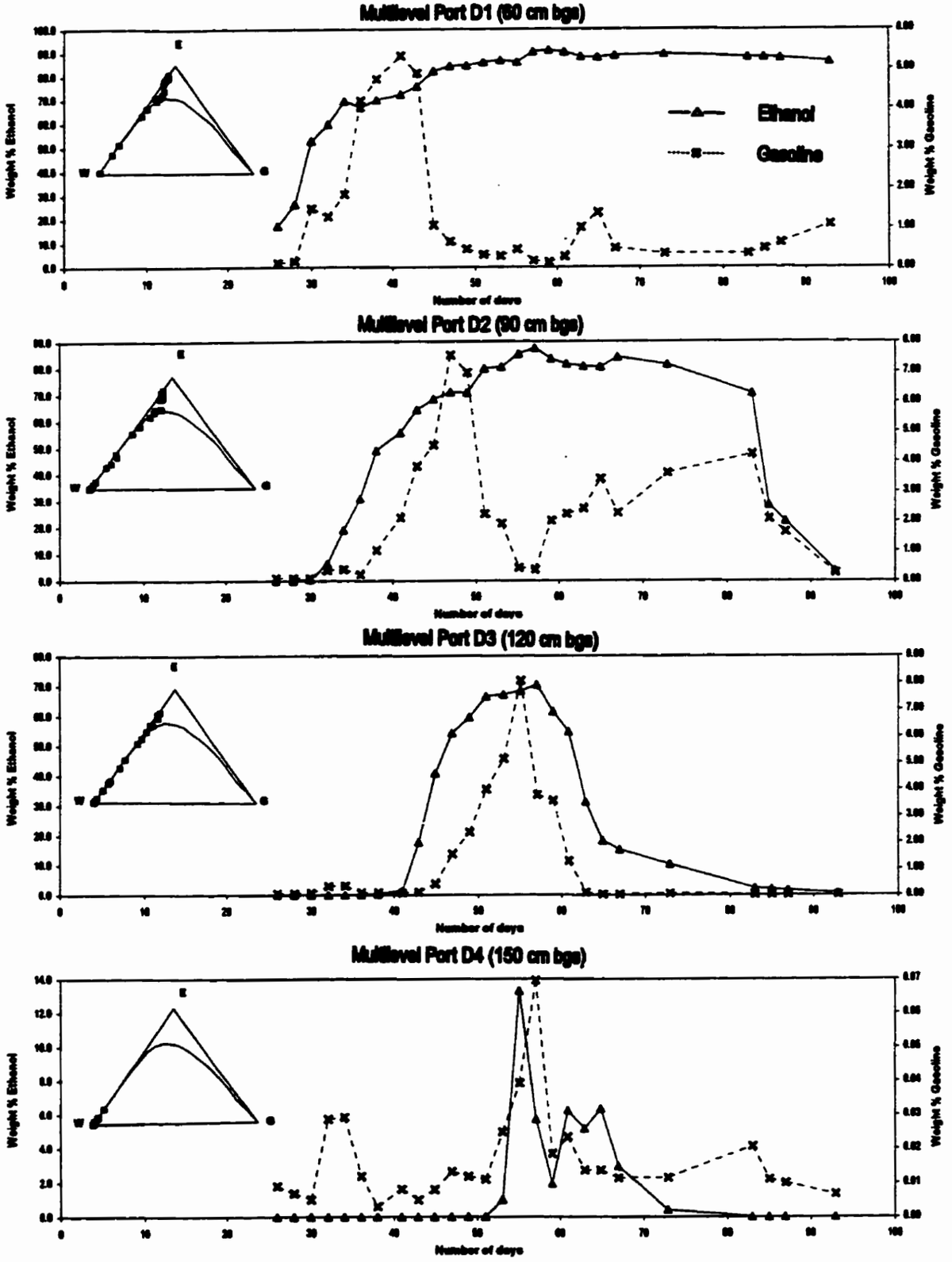

Figure 4-12 - Breakthrough curves for ethanol and gasoline saturation (in weight percent) versus time for the ports of the multilevel well D.

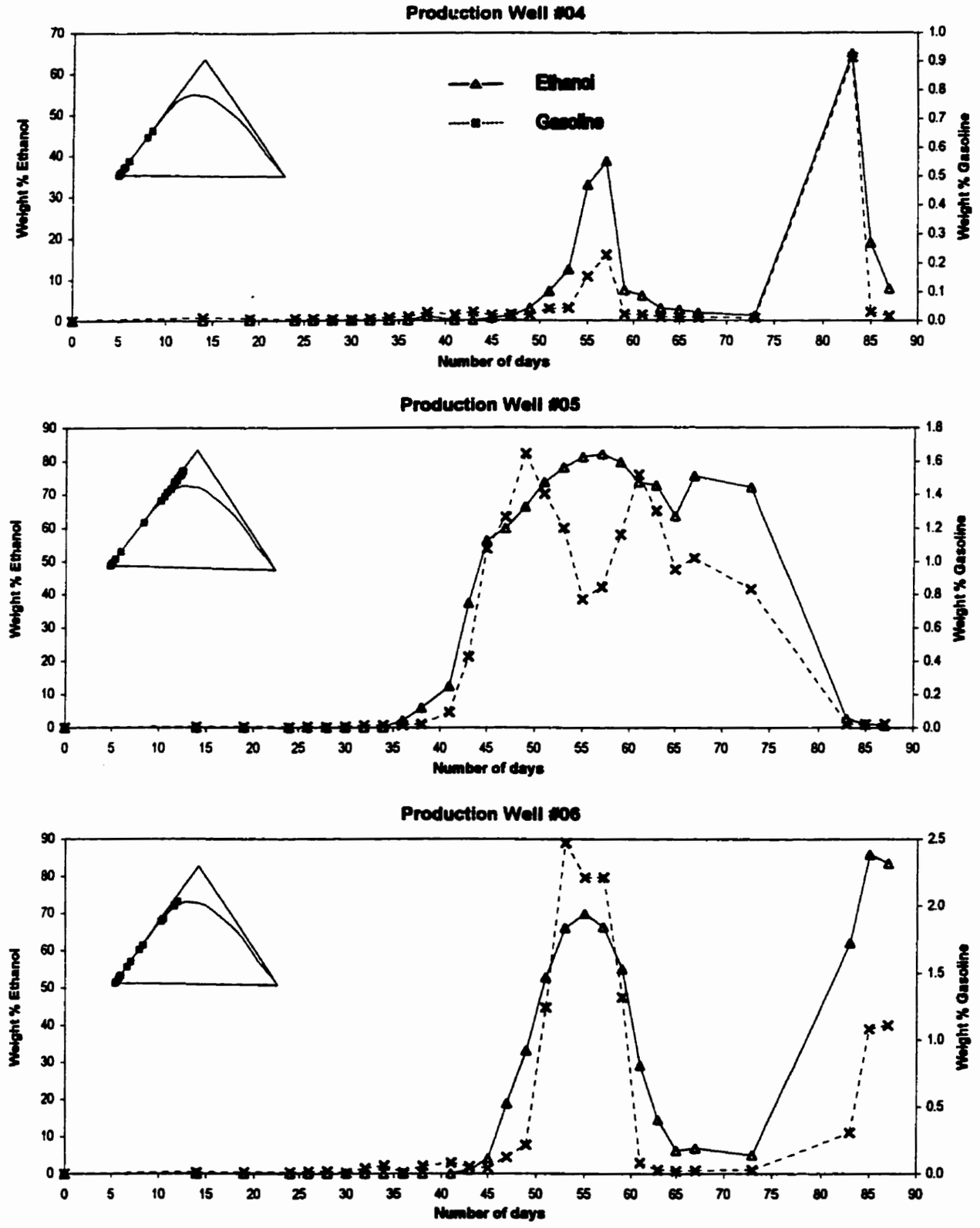

Figure 4-13 - Breakthrough curves for ethanol and gasoline saturation (in weight percent) versus time for the extraction wells 4, 5 and 6.

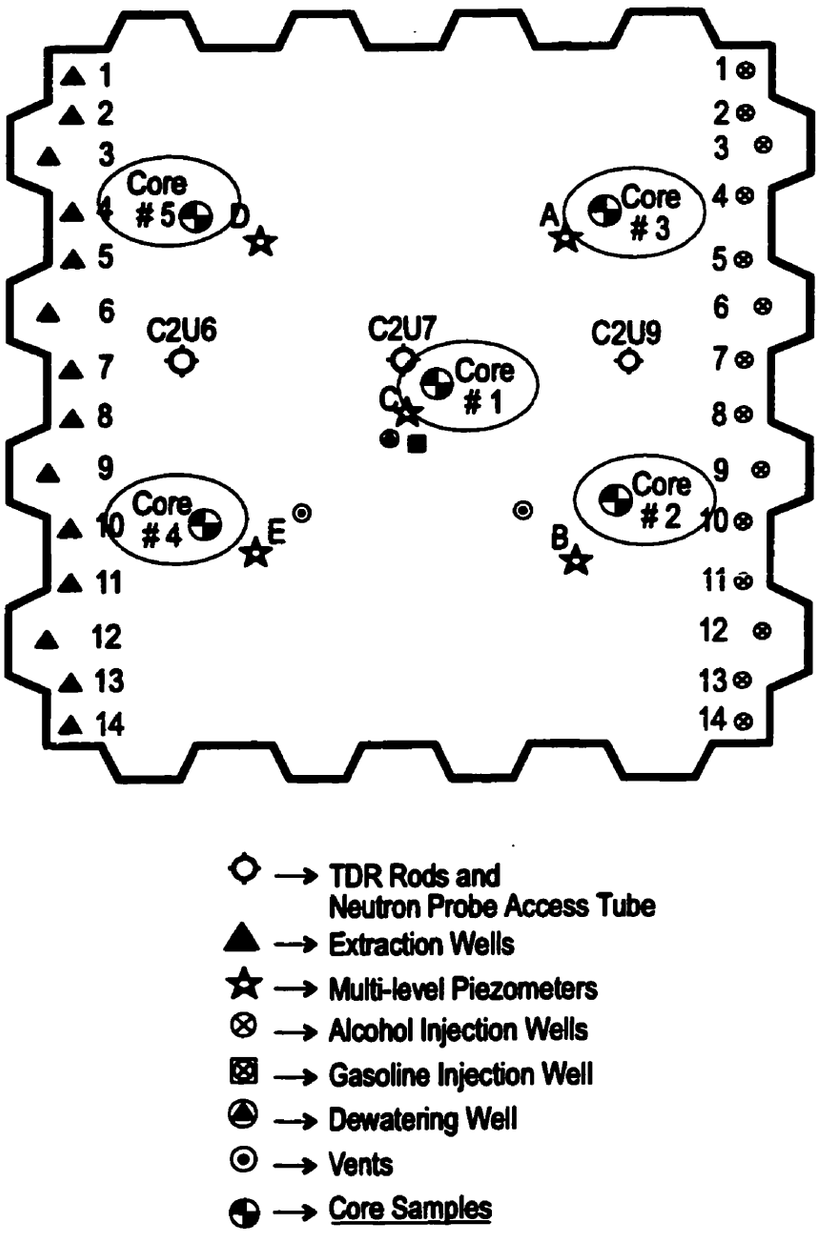

Figure 4-14 - Top view of the cell experiment showing the points from where the core samples were taken.

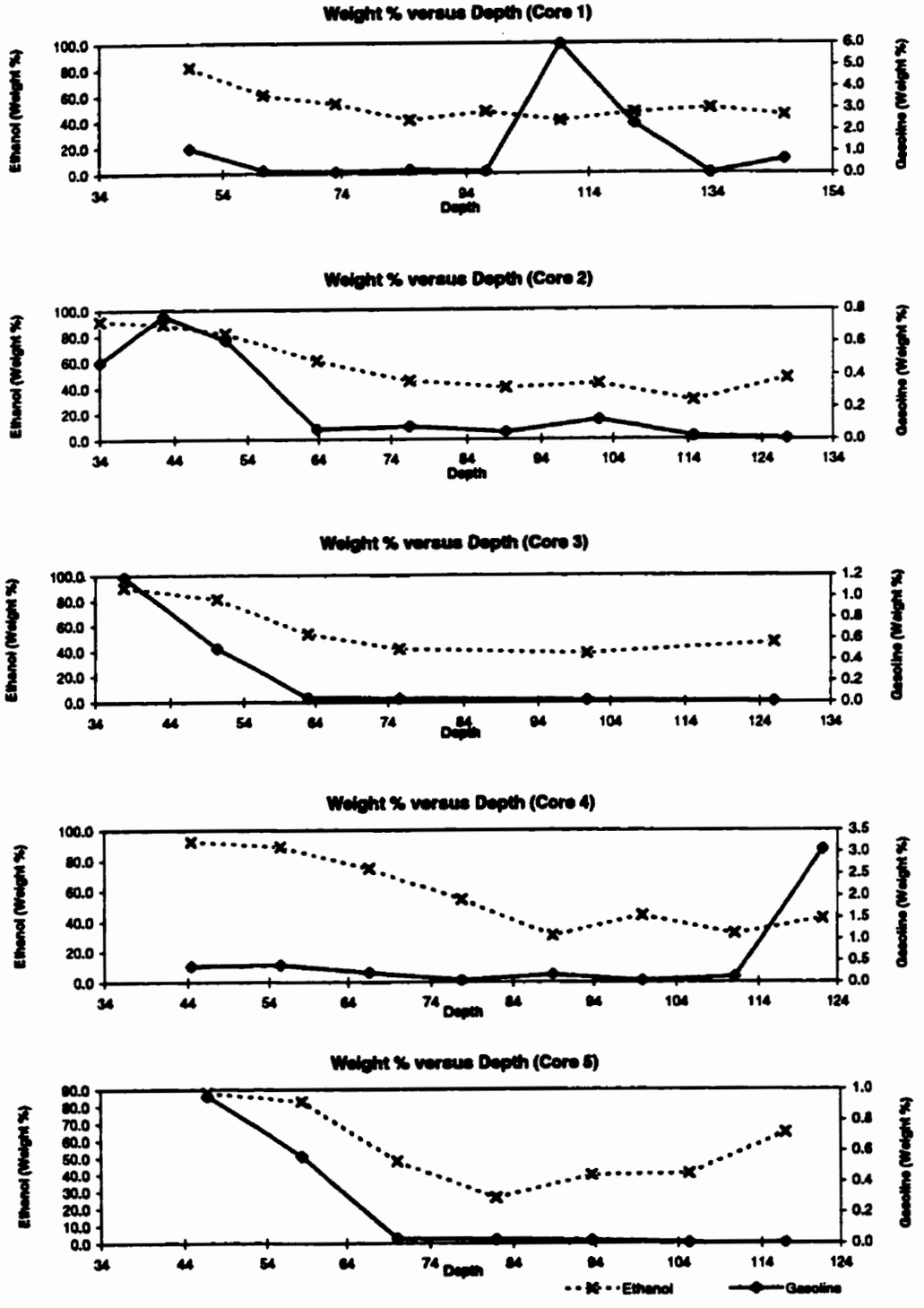

Figure 4-15 - Ethanol and gasoline saturation versus depth as determined by UV analyses of the core samples.

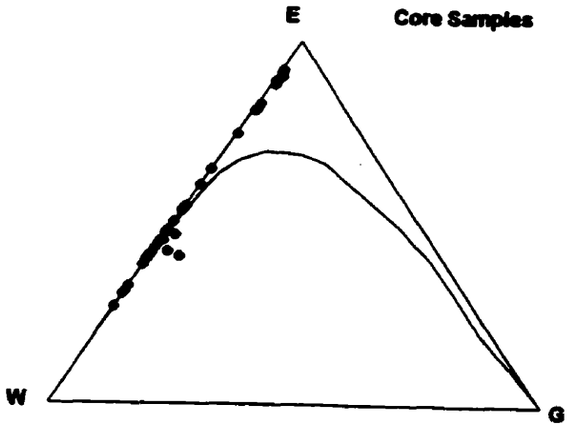

Figure 4-16 - Ternary diagram showing the compositions of the core samples relative to the binodal curve for ethanol-water-gasoline (in weight percent).

5. CONTROL OF THE VERTICAL POSITION OF THE ETHANOL FLUSHING OF GASOLINE RESIDUALS

5.1 Introduction

Following the field trial experiment with the poor performance of ethanol flushing in removing gasoline residuals, the effects of buoyancy forces on flow behavior were investigated further in laboratory scale ethanol flushing experiments. A key concern was the control of buoyancy effects for maximizing the sweep efficiency of gasoline residuals. Unlike miscible displacements in reservoir engineering practice, where the flow behavior is bounded by confining impervious to flow layers at the top and bottom, in a free aquifer scenario, the gravity override aspects of miscible displacements are more pronounced due to the unconfined nature of air-liquid interface at the top of the saturated zone. Of concern to this work is the relative position of the water table location with respect to thickness of the zone of gasoline residuals when an ethanol flushing displacement is carried out. This chapter aims to elucidate the effects of density difference of ethanol with respect to densities of gasoline and water, respectively. In particular, the focus of attention is how one can best establish the conditions of ethanol flushing.

5.2 Objectives

The objectives of this chapter are:

- to provide a basis for minimizing the override of ethanol;
- to explore the conditions for improved sweep efficiency of the ethanol flushing technique;
- to demonstrate improvements in ethanol flushing technology.

5.3 Theoretical Considerations

Figure 5-1 illustrates the hydrostatic equilibrium between ethanol and water in a large diameter tube, where a definite contact between the fluids is assumed. At the equilibrium, the pressure head at the ethanol-water contact (Point A) is equal to the pressure of a point at the same elevation in the water (Point B). A hydrostatic pressure balance gives:

$$\rho_w g h_w = \rho_E g h_E \qquad [5\text{-}1]$$

$$h_E = h_w \frac{\rho_w}{\rho_E} \qquad [5\text{-}2]$$

where h_w and h_E are the height of the water and ethanol columns, respectively. The density of the water is ρ_w = 0.996 g/ml; the density of ethanol is ρ_E = 0.784 g/ml and g is the acceleration of the gravity. Therefore:

$$h_E = 1.27\, h_w \qquad [5\text{-}3]$$

From Equation 5-3, it can be found that 21.3% of the ethanol column will be above the water table; the other 78.7% is below the water table. This proportion does not consider the elevation of ethanol due to differences in interfacial tension. In an aquifer, the vertical positioning of a given column of ethanol will be controlled by the position of the water table

and consequently, artificially controlling the water table allows control of the vertical position of the injected ethanol slug.

The thickness of the ethanol layer in ethanol injection is controlled primarily by the difference between the ethanol and water heads, as illustrated by Equation 5-3. The thickness of the vertical cross-sectional area to be swept by ethanol flushing depends on the thickness of the region contaminated by gasoline residuals and typically corresponds to a few tens of centimeters above and below the zone of residuals for a field situation. For a given thickness of contaminated region, a thickness (h_E) of the ethanol layer and an elevation of the top of ethanol layer (h_L), as displayed in Figure 5-2, the elevation of the water table (h_{WT}) may be calculated from Equation 5-3:

$$h_{WT} = h_L - 0.213h_E \qquad [5\text{-}4]$$

This equation gives the desired location of the water table position for ethanol. Ethanol flushing experiments were performed to test the sweep efficiency of gasoline residual zone using the above relationship.

5.4 Experimental Procedure

The dimensions of the sintered glass bead model used in this experiment were 18×31 cm. The thicknesses of the bead layer and glass plate are 2 mm. Glass bead sizes and porosity are identical to those described in Chapter 3. The connection between the gap and the porous medium is made through several channels (2 mm diameter and 5 mm long). Injection and extraction ports are similar to those described in Chapter 3. The top and bottom sides were not sealed. This was done to allow free vertical flow and mimic water table fluctuations as in a field situation.

To simulate the water table fluctuations, the sintered bead model was immersed in a transparent plexiglass tank. The internal dimensions of the tank were 42 cm of length, 6 cm of width, and 18 cm of depth. The thickness of the plexiglass was 0.96 cm (3/8"). The internal bottom of the model was covered with a 1 cm thick layer of loose glass beads (diameter of 350 to 500 μm).

The experiment was documented using a photographic camera (Nikon FM2 with a 75-300 mm Sigma zoom lens). The setup was backlit as illustrated in Figure 3-17b (Chapter 3).

The model was cleaned following procedures described in Chapter 3. Preparation of the model with CO_2 also followed previously described procedures. Injection and extraction ports were connected at one end to 1/8" (3.175 mm) Teflon tubing through brass fittings (Teflon ferrules, vyton o-rings) and at the other end to the syringe through a larger Tygon fuel tubing. The syringe pump was described previously.

The tank was filled with deionized, de-aired water and the bead layer was rearranged to remain as horizontal as possible. The sintered glass bead model was then carefully inserted into the tank. The unsealed surface was kept horizontal and evenly touched the water surface. The model was further immersed to about 3 mm into the water and rested at this vertical position until capillary equilibrium was reached. The model was then immersed further into the water until the top of the capillary fringe reached to about 0.5 cm below the injection and extraction ports. These points were located at the mid-point in the vertical dimension of the model. The model rested in this position for about 2 hours. Figure 5-3 shows the position of the capillary fringe before gasoline injection.

Fluid injection and extraction was done at a continuous rate of 0.167 ml/min, corresponding to an approximate average linear velocity of 1.2 m/day (about 10 times higher

than groundwater velocity at Borden). Two ml of blue-dyed gasoline was injected at the left-side port and flowed laterally toward the exit end port. When a continuous layer of gasoline was established across the entire length of the model, gasoline flow was stopped and the water table was slowly raised at an average rate of 1 cm/hour, until the complete volume of gasoline was trapped as residual phase in the saturated zone.

Based on the thickness of gasoline residuals and the theory presented, the water table was positioned and a yellow-dyed ethanol was injected from left to right. The extraction pump was maintained off until the ethanol front, moving on the top of the water table, reached the exit port. The extraction pump was then turned on. After 28 ml of ethanol was injected (corresponding to approximately 1.5 pore volumes of the region being swept), water replaced ethanol as the injected fluid.

5.5 Results and Discussion

Figure 5-4 shows the dyed gasoline emplaced at the top of the capillary fringe. The thickness of the gasoline slightly depressed the top of the capillary fringe at the injection point, and in its lateral movement during emplacement encountered different heights of the capillary fringe, which accounted for the irregularities in the thickness of the gasoline layer seen in the Figure 5-4.

The pressure head of gasoline necessary to overcome entry capillary pressure was such that gasoline residuals were trapped lower than the water table position at the connections between the gap edge and the sintered glass beads. These residuals may also be observed in Figure 5-4.

After the water table was raised, gasoline residuals formed below the water table. Figure 5-5 shows the gasoline residuals just moments after ethanol injection started.

The gasoline residuals formed large clusters of blobs in Figure 5-5, in addition to singlet blobs or associations of a few interconnected blobs at the pore scale. Comparing Figure 5-4 to Figure 5-5, it appears that the points where the gasoline layer became disconnected in Figure 5-5 are the same points at where the layer of gasoline was thinered in Figure 5-4. Water invaded first through these regions. Further rise of the water table and the consequent increase in capillary pressure allows water to breakthrough at different points. After water breakthrough through the emplaced gasoline, the water filled the pores above the gasoline layer and the gasoline became trapped as residuals.

The thickness of the zone of residuals was 9 cm and a 12 cm thick layer of ethanol was injected, 1 cm above and cm below the zone of gasoline residuals. Based on Equation 5-3, the water table in the experiment was fixed at 7.4 cm above the bottom of the contaminated zone by extracting water from the container (9.4 cm above the ethanol/water contact). In a real situation, the difference between the thicknesses of the injected ethanol layer and the zone of residuals have to be minimized in order to minimize the volume of ethanol used to cleanup.

The sequence of photographs in Figure 5-6 shows the injected ethanol flowing through the region of high saturation of gasoline residuals. The extraction pump was off until the ethanol front reached the exit port. Figure 5-6a shows that ethanol progresses preferentially above and under the contaminated region, respectively, following the pathways of high permeability. The highly contaminated zone close to the injection point (where gasoline had been released) is completely cleaned in Figure 5-6c. The final step of the

cleanup consists of extracting the injected fluids and injecting water to help remove the ethanol.

The zone of residuals creates a region of much lower permeability to other fluids that acts as a boundary layer affecting the upward movement of ethanol. If the thickness and elevation of the injected ethanol layer is such that it encompasses the zone of residuals, i.e., it extends above and below the residual zone, the preferential pathways for ethanol flow are the regions immediately adjacent to the residual zone, both above and below it.

The preferential flowpath for injected ethanol is around the zone of residuals, both above and below it, which favors the removal of the residuals by the blob ejection mechanism. The high ethanol concentration favors ethanol diffusion through the pore throats adjacent to trapped residuals, facilitating the creation of IFT difference to eject blobs of gasoline. Even if gasoline blobs simply move up, into the residual zone, rather than be swept laterally, eventually they will be contacted later.

Figure 5-7 shows several steps involved in the removal of residuals in the process of cleanup. Point A represents the region where ethanol reaches the lower part of the zone of residuals. At this position ethanol is constantly being mixed with water and consequently, with increasing water content, removed gasoline residuals may undergo phase extraction and be trapped as small blobs of oleic phase. This corresponds to the slightly darker border seen on Figure 5-7. From point A to point D the region of extracted oleic phase is gradually removed by dissolution by higher ethanol content fluid.

A similar phenomenon occurs at the top portion of the zone of residuals (Point A'). Here, without a lower permeability boundary layer represented by trapped gasoline residuals, ethanol can move upward, above the zone of residuals. The upward limit for ethanol

movement will be the air of the unsaturated zone. Ethanol initially displaces the water from higher points, later displacing the water from relatively lower portions adjacent to the top of the zone of residuals. Part of this water is incorporated to the flowing ethanol (aqueous phase). Since the extraction pump is off during this process, to maintain hydrostatic equilibrium, the water initially wedged in between the top flowing ethanol and the zone of residuals that is not incorporated by ethanol has to move downwards, through the residuals (not seen in the Figure).

Residuals are also formed by phase extraction at the top border of the injected ethanol contacting water. Unlike the lower portion of the zone of residuals, the removal of the re-precipitated residuals by the on-coming ethanol is slower due to the slower flow of ethanol through the irregular contact between the top of the capillary fringe and the air.

It is noted from the sequence of photographs in Figure 5-6 that the upper portion of the ethanol injection at the top of the zone of residuals advances faster than the lower portion at the bottom of the residuals. As the lower permeability layer of gasoline residuals is removed, ethanol will be driven by buoyancy forces and move upward, consequently a larger volume of ethanol flows through and to the upper portion. Ethanol, moving faster in the upper portion, displaces water downward through the relatively lower permeability zone of residuals, which slows down the advance of ethanol through the zone of residuals as well as below it.

Points B, B' and C, in Figure 5-7, correspond to the portion of the zone of residuals where the removal by blob ejection happens most efficiently. High content ethanol favors diffusion of ethanol through pore throats adjacent to the trapped residuals, thus favoring blob ejection (see Chapter 3). Point D represent the residuals within the zone of residuals, where

the permeability for ethanol is lower and the flow of ethanol is slower. These residuals are removed later, as the ethanol front (represented by point C) moves toward the exit port.

The optimal injection strategy profits from the buoyancy forces to aim the ethanol flush at the right elevation and thickness of the residuals. With the water table maintained at the desired level, the elevation of the injected ethanol above the water table drives the ethanol laterally, and no extraction of fluids is necessary to achieve the desired regions of gasoline residuals. For this reason, the extraction system is turned on only when the ethanol front reaches the exit port (Figure 5-6c).

After the extraction system was turned on, the injection of ethanol continued until the removal of the original zone of residuals was complete (Figure 5-8a). It is noted in the figure that extracted gasoline remains at the top of the capillary fringe. The water table was then raised to allow flow of ethanol at these higher positions. Figure 5-8b shows the distribution of the residuals at the top of the capillary fringe after the water table was raised, moments before the start of the water flood.

The sequence of photographs of Figure 5-9 shows the water injection. After ethanol injection stopped, the slope of the ethanol-water contact becomes zero and is inverted when the water injection started. The initial volume of injected water dissolved the yellow dye still remaining at the injection port and the front of the injected water may be clearly seen in the photographs. The injected water flows preferentially under the ethanol and only partially displaces it, confirming the underriding behavior of ethanol noticed in the field experiment. Since ethanol moves upwards in a groundwater system, the injection of water creates a hydraulic gradient and ethanol flows towards the exit port. The extraction port had to be placed within the ethanol layer, close to the water-ethanol contact, to allow ethanol

extraction.

The flushed region showed a complete removal of the gasoline residuals. Elevation of the water table after the complete removal of the original zone of residuals is removed allows the removal of the extracted gasoline phase which accumulated at the top of the capillary fringe.

5.6 Conclusions

Laboratory experiments of ethanol flushing confirmed the field experience, that density differences between ethanol and water play a decisive role in the ethanol flushing technique. Furthermore, it suggested that the effects of buoyancy of ethanol in water can be used to position the delivery of the injected ethanol to the zones where gasoline residuals are present.

The deliver of ethanol to the target regions may be precisely controlled by adjusting the level of the water table within the zone of residuals. The thickness of the ethanol layer to be injected may also be controlled to encompass the complete thickness of the zone of residuals.

By controlling the water table complete removal of the gasoline residuals from the target zone was achieved. The flow of the injected ethanol both above and below the zone of residuals favored the removal of the residuals by the blob ejection mechanism.

The preferential pathways for ethanol flow is above and below the zone of residuals. Fingering of ethanol through the zone of residuals may happen in a larger scale experiment, however, under these conditions, fingering does not interfere with the removal of the

residuals.

Some vertical fingering of ethanol from the stream of ethanol flowing below the residual zone will enhance the speed of removal because of increased contact surface area.

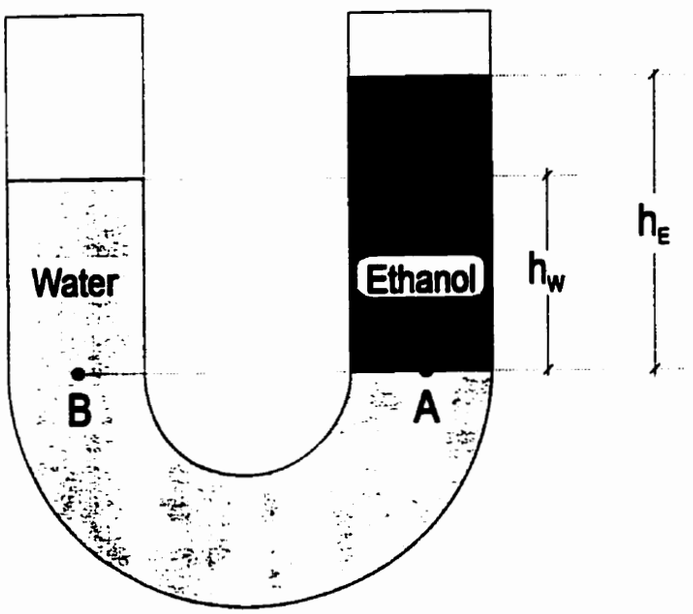

h_w = height of the water column

h_E = height of the ethanol column

Figure 5-1 - Hydrostatic equilibrium between ethanol and water

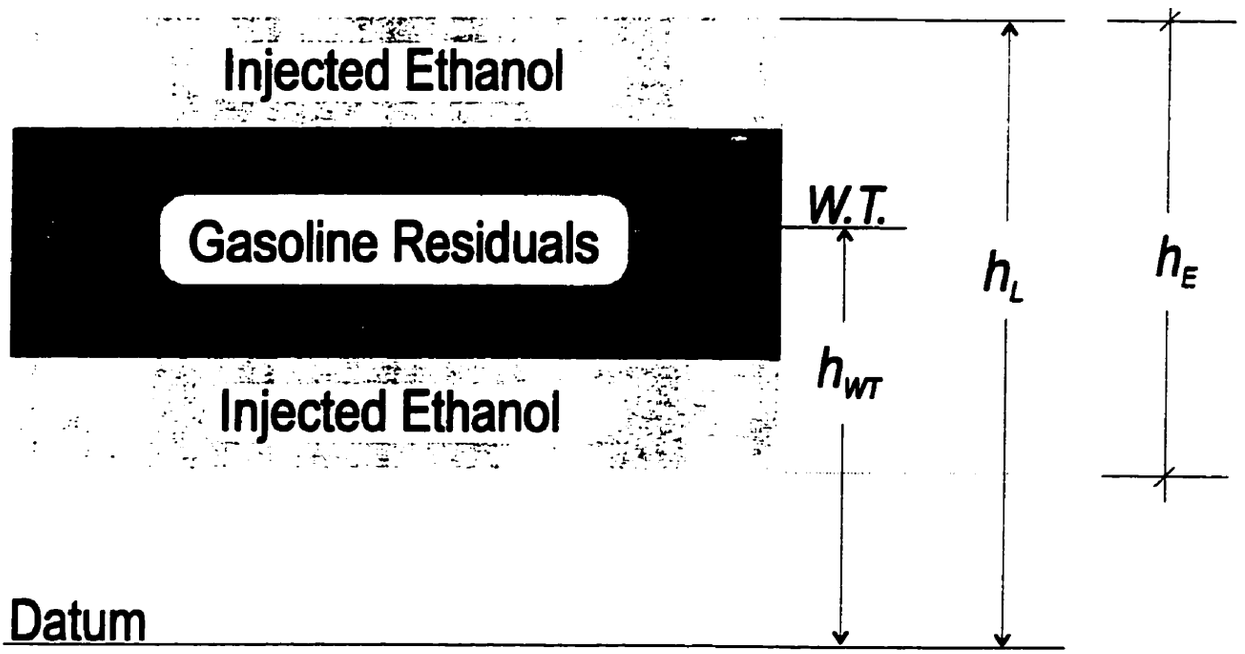

Figure 5-2 - Positioning of the water table with respect to the ethanol layer.

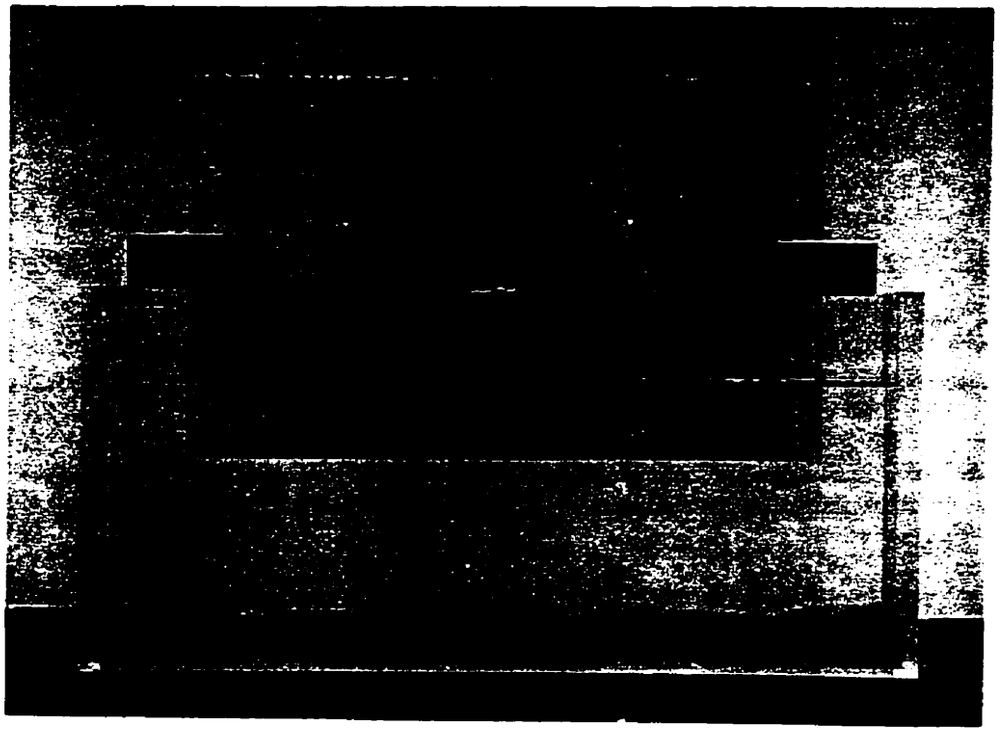

Figure 5-3 - Position of the capillary fringe before gasoline injection.

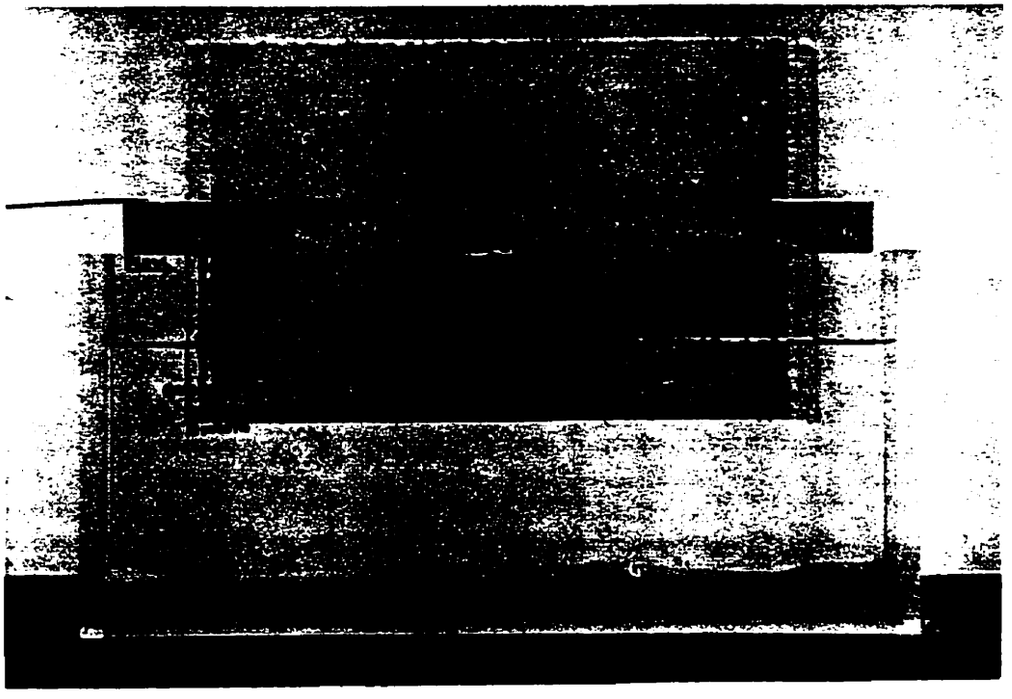

Figure 5-4 - Gasoline emplaced at the top of the capillary fringe.

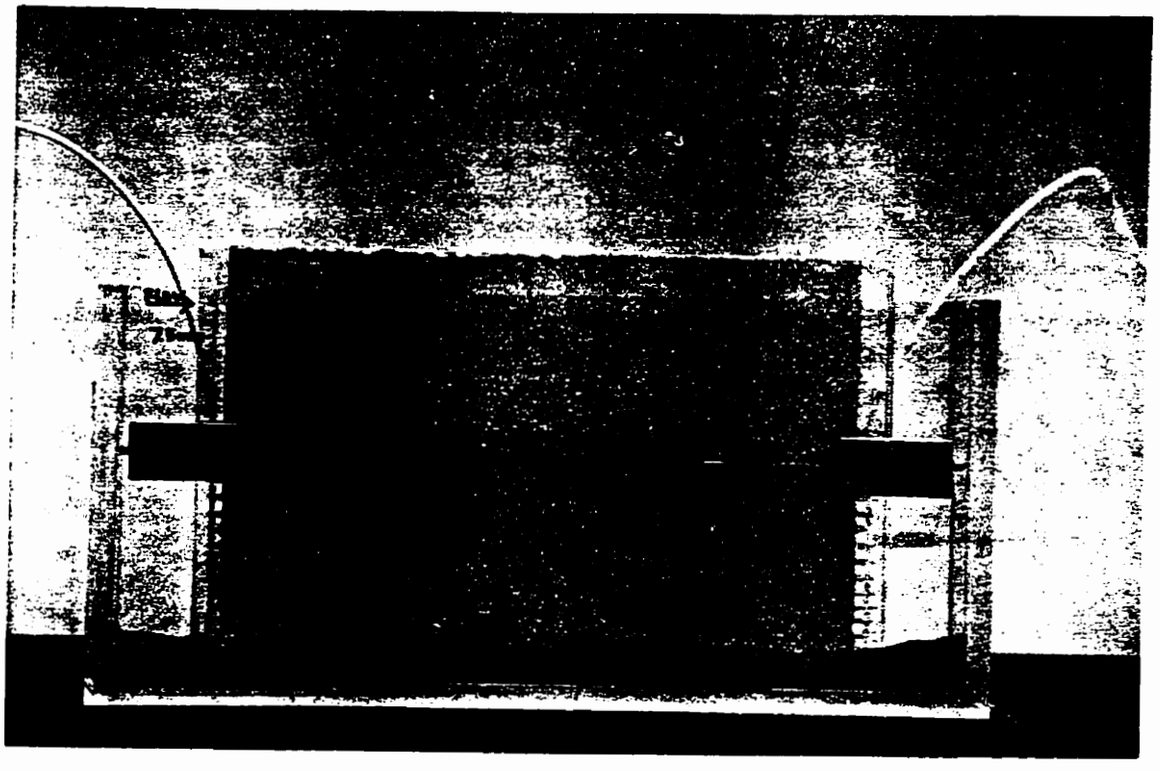

Figure 5-5 - Trapped gasoline residuals moments after ethanol injection start.

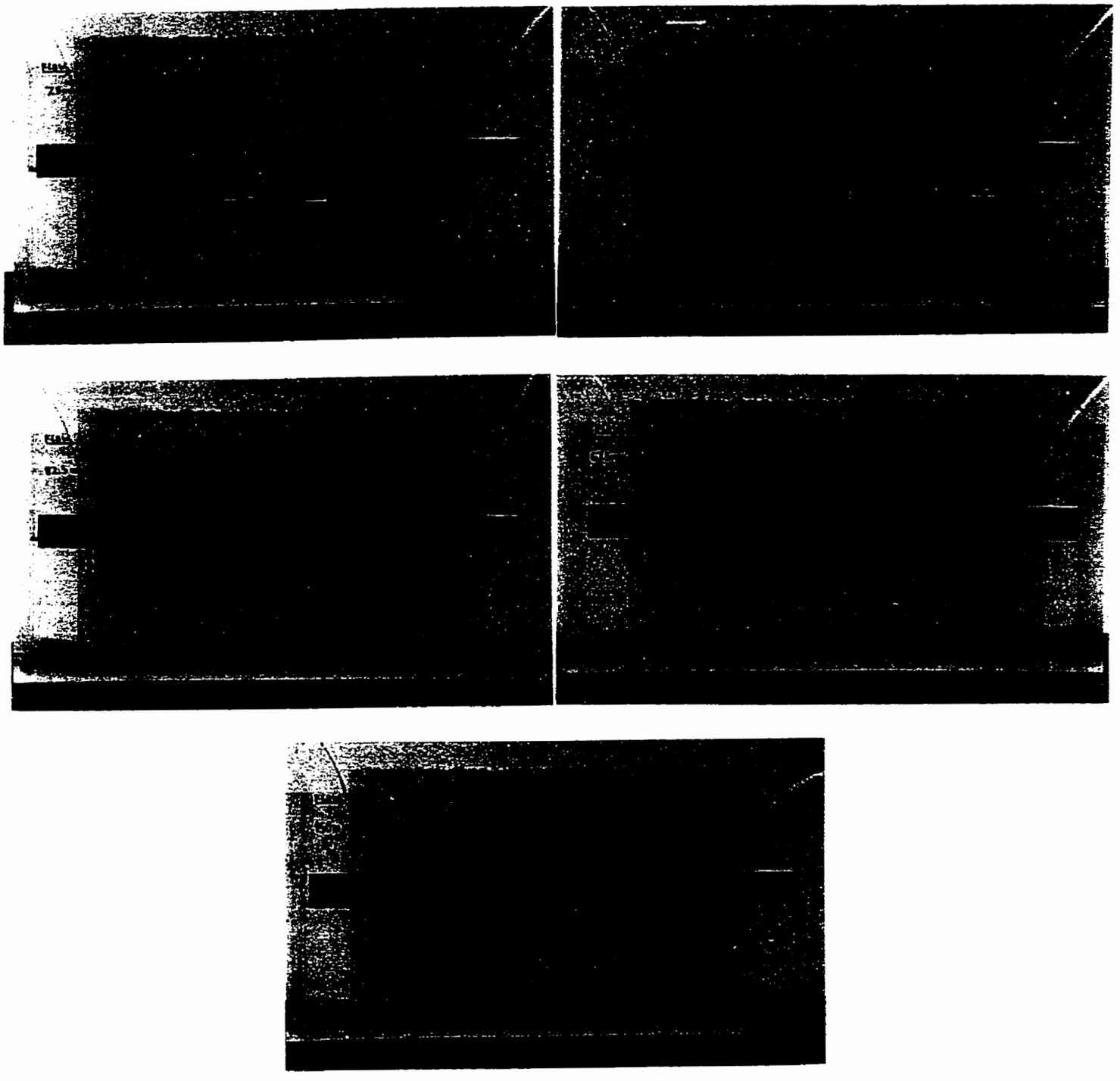

Figure 5-6 - Sequence of photographs showing the hydraulically controlled ethanol flushing of gasoline residuals.

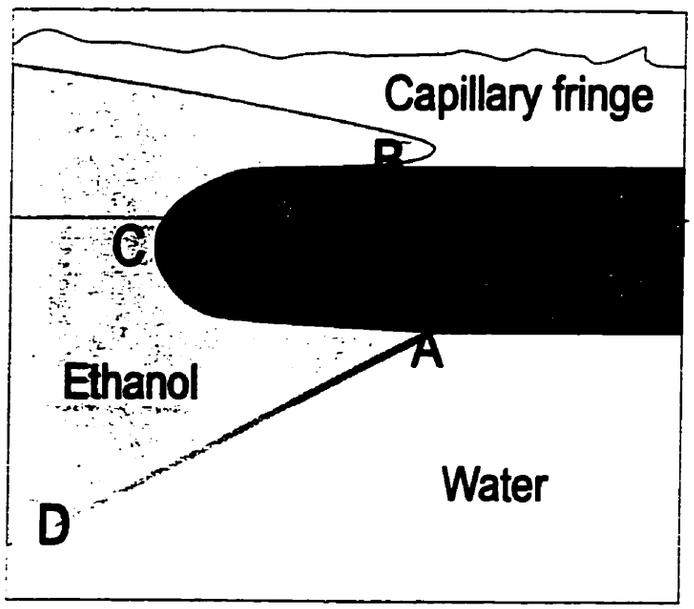

Figure 5-7 - Steps involved in the removal of residuals by lateral ethanol flushing

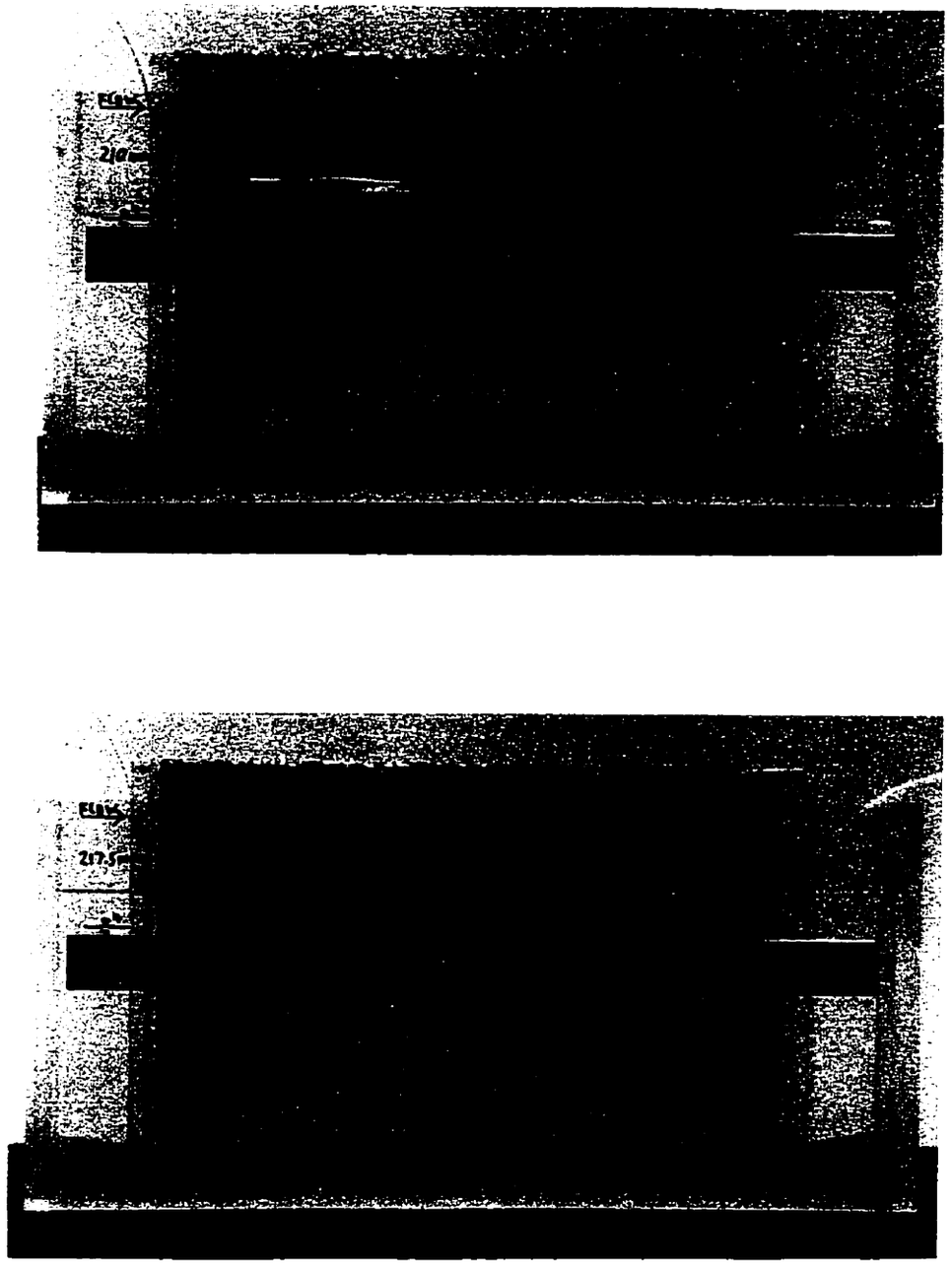

Figure 5-8 - Photograph showing gasoline residuals at the top of the capillary fringe.

a) before water table was raised; b) after water table was raised.

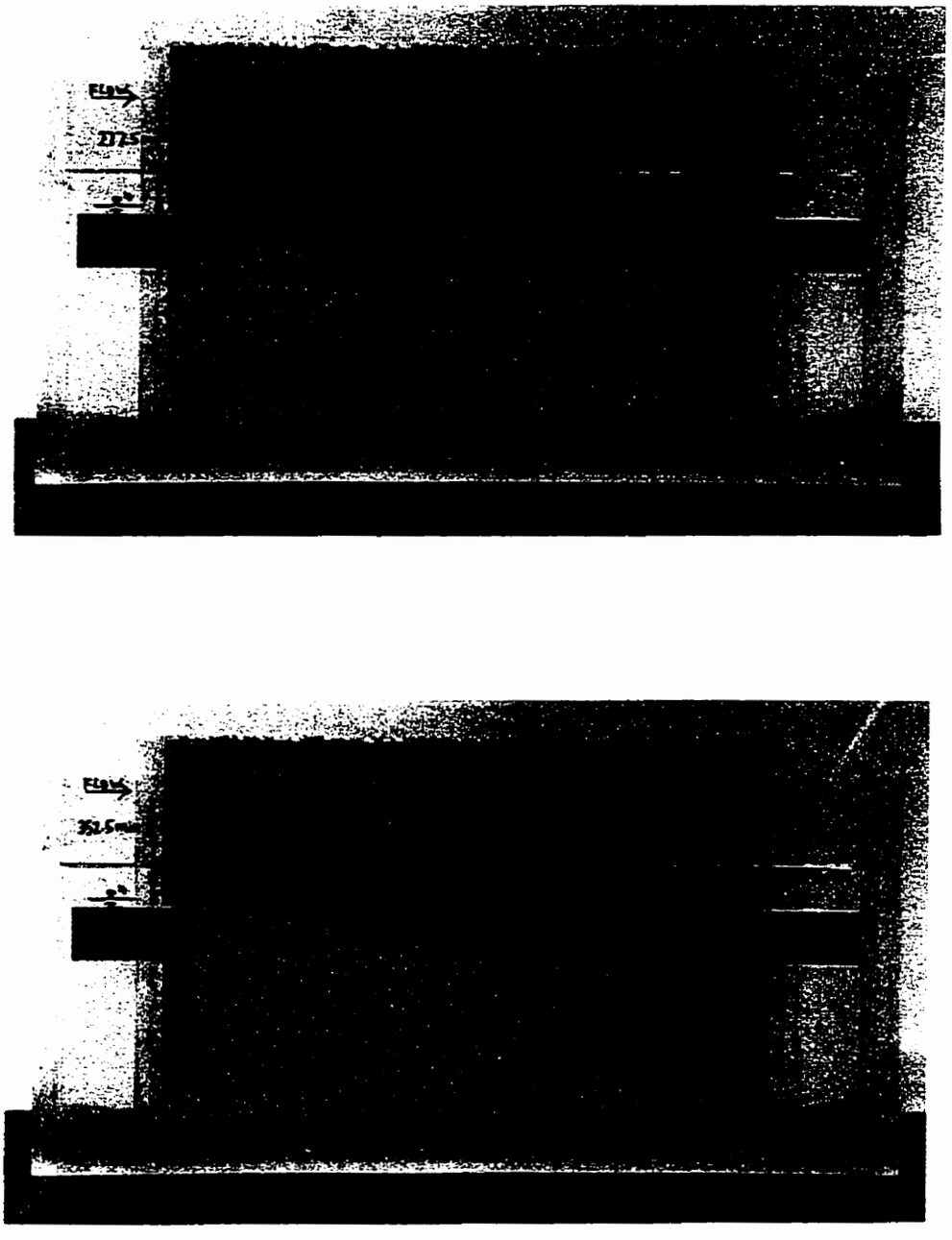

Figure 5-9 - Waterflooding after ethanol injection was terminated

6. CONCLUSIONS AND RECOMMENDATIONS

6.1 Conclusions

1. The pseudoternary system for gasoline-ethanol-water shows that ethanol partitions preferentially to the aqueous phase.
2. For a flushing fluid composed of ethanol and water, the minimum ethanol content necessary to flush the gasoline residuals with complete miscibility is 88 wt% ethanol and 12 wt% water. Considering the percent of water present in commercial alcohols such as ethanol (about 5% by volume), none or little water should be added to commercial ethanol to be used for gasoline residuals cleanup. The presence of methanol in very low percentages in denatured commercial ethanol is not expected to significantly alter the behavior of the ternary diagram, the major problem being that methanol is a regulated compound, as opposed to ethanol that is not.
3. Isodensities plotted on the pseudoternary diagram show that the mixtures of gasoline, water and ethanol that fall within the single phase region of the diagram are always denser than the gasoline phase that originated it. This have a major role on the stability of displacement.
4. The IFT increased exponentially with increasing ethanol content, with a 20-fold decrease from 21.9 to 1.0 mN/m for 0 to 0.65 mole fraction of ethanol in the water phase, respectively.
5. The change in volume during mixing of water and ethanol may lead to the formation of a gas phase. The maximum volume of gas change (and consequently

the volume of gas formed) is 3.4% and occurs for mixtures with 0.55 volume fraction of ethanol relative to water. The maximum mass of BTEX transferred from dissolved phase gasoline to the gas phase is 0.5% of the total mass of BTEX dissolved in water.

6. Small interfacial tension (IFT) differences caused by mass transfer of ethanol and water to gasoline and vice-versa are responsible for small blob of gasoline to move upgradient, against the fluid flow, even for average linear velocities up to 2 orders of magnitude higher than typical groundwater velocities.
7. IFT differences are responsible for gasoline removal by a mechanism described as *blob ejection*. The portion of a trapped blob that is in contact with ethanol has its IFT differentially reduced, and the trapped blob is ejected into flowing ethanol rich fluid.
8. The extent of reduction in IFT necessary to start the ejection depends on the aspect ratio for a given porous medium but is much lower than that predicted by capillary number experiments for blob mobilization.
9. The removal of the trapped residuals takes place at the tips of the blobs or cluster of blobs that are exposed to flowing fluids. For conditions of high ethanol concentration gradients near the blob, gasoline mass removal exclusively by dissolution from the fluid flowing around the blob may be considered minimal when compared to mass removed by ejection.
10. The total mass removed by blob ejection alone could not be assessed in this work, and a visual estimate from the video recording suggests that approximately 40% of the mass is removed by ejection.

11. Pore scale instabilities were responsible for fingering development during the laboratory experiment of ethanol flushing in the downward direction.
12. Larger scale instabilities were responsible for fingering development during the laboratory experiment of ethanol flushing in the upward direction.
13. Lateral flushing laboratory experiment showed ethanol preferentially flowing through regions of higher relative permeability and lower gasoline residual saturation.
14. A typical zone of gasoline residuals originated from a spill will be much more extensive horizontally than vertically and so horizontal flushing presents practical advantages over vertical flushing, i.e., easier to operate injection/extraction system. Experimental results showed that horizontal flushing favorable results for lateral flushing, the relative operational advantage of this direction of flow was decisive to the choice of horizontal flushing for application of ethanol to displace gasoline residuals in the field experiment.
15. During the field experiment, the density difference between ethanol and water caused the segregation of the ethanol from the water with ethanol flowing to the higher portions of the saturated zone, moving upwards in the groundwater system.
16. The field behavior of ethanol flushing was not well predicted from laboratory studies. The design used in this field experiment was not a successful remediation at pilot scale. Most of the ethanol injected missed the target region of residuals, with a consequent poor recovery of the gasoline residuals. Only 36% by weight of the emplaced gasoline was removed from the aquifer (25 liters out of 70 liters),

and only 45% by weight of the injected ethanol (1,068 liters out of 2,400 liters injected) was recovered.

17. The spatial distribution of the core sampling method used in this field experiment offered a reasonable approach to determine the remaining ethanol, but not for the residual gasoline. Core samples for residual gasoline should be closely spaced to be representative.
18. Further laboratory experiments of ethanol flushing suggested that the effects of buoyancy of ethanol in water can be used to position the delivery of the injected ethanol to the zones where gasoline residuals are present. The deliver of ethanol to the target regions may be precisely controlled by adjusting the level of the water table within the zone of residuals. The thickness of the ethanol layer to be injected may also be controlled to encompass the complete thickness of the zone of residuals.
19. By controlling the water table, complete removal of the gasoline residuals from the target zone was achieved. The flow of the injected ethanol both above and below the zone of residuals favored the removal of the residuals by the blob ejection mechanism.
20. The preferential pathways for ethanol flow is above and below the zone of residuals. Fingering of ethanol through the zone of residuals may happen in a larger scale experiment, however, under these conditions, fingering does not interfere with the removal of the residuals.

21. Some vertical fingering of ethanol from the stream of ethanol flowing below the residual zone will enhance the speed of removal because of increased contact surface area.

6.2 Recommendations

Further research in the following areas is recommended:

1. Further study on the effects on the flow pattern caused by the changes in volume when ethanol and water are mixed together.
2. Study of the wettability changes of the trapped gasoline blobs when ethanol is incorporated to the blob.
3. Extend the theoretical work presented for blob ejection mechanism in order to determine the percent of total mass that is transferred from the blob to the injected fluid when compared to dissolution and mobilization.
4. Determine the mechanisms involved in the chop off of the tip of the ejected portion of the blob.
5. Bench scale experiments with controlled water table to determine the efficiency of the horizontal flushing of gasoline residuals by ethanol.

7. REFERENCES

Adamson, A. W. (1967) *"Physical Chemistry of Surfaces"*. Interscience Publishers. New York.

Augustijn, D. C. M.; Dai, D.; Rao, P. S. C. and Wood, A. L. (1994) *"Solvent Flushing Dynamics in Contaminated Soil."* Transport and Reactive Processes in Aquifers. Dracos, T.H. and Stauffer, F. (ed.), pp. 557-562.

Bear, J. (1979) *"Dynamics of Fluids in Porous Media"*. Dover Publications, Inc.. New York. 764 p.

Benhan, A.L.; Dowden, W.E.; and Kunzman, W.J. (1960) *"Miscible Fluid Displacement - Prediction of Miscibility"*. Trans. AIME, 219, 229-237.

Bicalho, K. V. (1997) *"Dissolução de gasolina em presença de água e etanol"*. Ph.D. Thesis. Pontificia Universidade Catolica do Rio de Janeiro. 174 pp, 1997

Boyd, G. L. and Farley, K. J. (1991) *"NAPL Removal from Groundwater by Alcohol Flooding: Laboratory Studies and Applications"*. Calabrese, E. J. And Kostecki, P. T. (Eds.) pp. 437-460.

Brandes, D. and Farley, K. J. (1993) *"Importance of Phase Behavior on the Removal of Residual DNAPLs from Porous Media by Alcohol Flooding"*. Water Environment Research, Vol. 65, No. 7, pp.869-878.

Burns, Charles, M., *"Application of Phase Equilibria"*. Stanford Educational Press, Waterloo, Ontario, 1984.

Brandani, V.; Chianese, A.; and Rossi, M. (1985) *"Ternary Liquid-Liquid Equilibrium data for the Water-Ethanol-Benzene System"*. J. Chem. Eng. Data, vol. 30, pp. 27-29.

Broholm, M. M.; Ingleton, R. A. And Cherry, J. A. (1994) *"The Waterloo Drive Point Profiler. Detailed Profiling of Volatile Organic Compound Plumes in Groundwater Aquifers"*. Transport and Reactive Processes in Aquifers. Dracos, T.H. and Stauffer, F. (ed.), pp. 95-100.

Chatzis, I. and Dullien, F.A.L. (1983) *"Dynamic Immiscible Displacement Mechanisms in Pore Doublets: Theory versus Experiment"* J. Colloid Interface Sci. 91, 199 pp.

Chatzis, I. (1994) *"Theory of Flow in Porous Media with Applications"* - Lecture Notes. University of Waterloo, Department of Chemical Engineering.

Chatzis, I. (1982) *"Photofabrication Technique of Two-dimensiona Glass Micromodels"*. PRRC Rpt. 82-12. Socorro, New Mexico: New Mexico.

Chatzis, I., Morrow, N. R. and Lim H. T. (1983) *"Magnitude and Detailed Structure of Residual Oil Saturation"*. SPE Journal. 23:311-325.

Chatzis , I., Morrow, N. R. (1984) *"Correlation of Capillary Number Relationships for Sandstones"*. SPE Journal, October, pp. 555-562.

Chatzis, I., Kuntamukkula, M. S. and Morrow, N. R. (1988) *"Effect of Capillary Number on the Microstructure of Residual Oil in Strongly Water-Wet Sandstones"*. SPE Reservoir Engineering, August, pp. 902-912.

Clark, N.J.; Shearin, H.M., Schultz, W.P.; Garns, K.; and Moore, J.L. (1958) *"Miscible Drive - Its Theory and Application"*. J. Pet. Tech. (June, 1958).

Cline, P. V.; Delfino, J. J.; and Rao, P. S. C. (1991). *"Partitioning of Aromatic Constituents Into Water from Gasoline and Other Complex solvent Mixtures"*. Environ. Sci. Technol., vol. 25, pp. 914-920.

Conrad, S.H.; Wilson, J.L.; Mason, W.R.; Peplinski, W. (1992) *"Visualization of residual organic liquid trapped in aquifers."* Water Resour. Res. 28:467-478.

Craig, F.F. Jr. (1971) *"The Reservoir Engineering Aspects of Waterflooding."* Society of Petroleum Engineers of AIME, New York.

Crank, J. (1956) *"The Mathematics of Diffusion."* Oxford University Press, Oxford, 347 pp.

DeRick, S.M.; Redman, J.D.; and Annan, A.P. (1993) *"Geophysical Monitoring of a Controlled Kerosene Spill"*. Proceedings of the Symposium on the Applications of Geophysics to Engineering and Environmental Problems, Oakbrook, Illinois, pp. 597-609.

Desnoyers, J. E.; Quirion, F.; Hétu, D.; and Perron, G. (1983) *"Tar Sand Extractions with Microemulsions: I- The Dissolution of Light Hydrocarbons by Microemulsions Using 2-*

Butoxyethanol and Diethylmethylamine as Cosurfactants". Can. J. Chem. Eng., Vol. 61, pp.672-679.

Devlin, J. F. (1994) *"Enhanced In Situ Biodegradation of Carbon Tetrachloride and Trichloroethene Using a Permeable Wall Injection System"*. Ph.D. Thesis. University of Waterloo. Dept. Of Earth Sciences. 633p.

Donaldson, C.R. (1992) *"Oxygenated Fuel Behaviour in the Subsurface - A Quantitative and Qualitative Laboratory Scale Investigation."* M.Sc Thesis. University of Waterloo. Dept. Of Earth Sciences. 297 p..

Dong, M. (1995) *"A Study of Film Transort in Capillaries with an Angular Cross-Section"*. Ph. D. Thesis. Dept. Of Chemical Engineering. University of Waterloo.

Dullien, F.A.L. (1979) *"Porous Media - Fluid Transport and Pore Structure"* - 2nd Edition. Academic Press, Inc.. 574 p.

Ellis, D. V. (1987) *"Well Logging for Earth Scientists"*. Elsevier Science Publishing Co. Inc.

Endres, A. L. , Redman, J. D. and Annan, A. P. (1993) *"Modeling the Electrical Properties of Porous Rocks and Soils Containing Immiscilble Contaminants"*. Proceeding of the Symposium on the Applications of Geophysics to Engineering and Environmental Problems, San Diego, CA.

Freeze, R.A. and Cherry, J.A. (1979) *"Groundwater"*. Prentice Hall, Inc.. Englewwod Cliffs, New Jersey. 604 p.

Gatlin, C. and Slobod, R. L. (1960) *"The Alcohol Slug Process for Increasing Oil Recovery"*. Transaction AIME, vol. 219, pp. 46-53.

Hill, S. (1952) *"Channelling in Packed Columns"*. Chem. Eng. Sci., Vol. 1(6), pp.247.

Holm, L. W. and Csaszar, A. K. (1962) *"Oil Recovery by Solvents Mutually Soluble in Oil and Water"*. Society of Petroleum Engineering Journal, June 1962, pp129-144.

Hunt, J.R.; Sitar, N. and Udell, K. S. (1988) *"Nonaqueous phase transport and cleanup, 1. Analysis and Mechanisms."* Water Resour. Res. 24:1247-1258.

Hvorslev, M. J. (1951) *"Time Lag and Soil Permeability in Groundwater Observations"*. U.S. Army Corps Engrs. Waterways Exp. Sta. Bull. 36, Vicksbourg, Miss.

Lake, L.W. (1989) *"Enhanced Oil Recovery"*. Prentice Hall, Inc.. Englewwod Cliffs, New Jersey. 550 p.

Larson, R.G (1979) *"The Influence of Phase Behavior on Surfactant Flooding"*. Society of Petroleum Engineers Journal, December 1979, pp. 411-422.

Larson, R.G.; Davis, H.T.; and Scriven, L.E. (1982) *"Elementary Mechanisms of Oil Recovery by Chemical Methods"*. Journal of Petroleum Technology, February 1982. pp. 243-258.

Lenormand, R.; Zarcone, C; and Starr, A. (1983) *"Mechanism of the Displacemnt of One Fluid by Another in a Capillary Duct"*. J. Fluid Mechanics. Vol. 135, pp. 337.

Lee, R.C. and Parrish, W.R. (1989) *"Feasibility of Stabilizing Water-Methanol-Gasoline Mixtures by Emulsification"*. Fuel, Vol. 68, 1429-33.

Letcher, T.M.; Heyward, C.; Wooten, S.; and Shuttleworth, B. (1986) *"Ternary Phase Diagrams for Gasoline-Water-Alcohol Mistures"*. Fuel, Vol. 65, pp. 891-894.

Lyman, W.J.; Reehl, W. F.; and Rosenblatt D. H. eds. (1990) *"Handbook of Chemical Properties Estimation Methods"*. McGraw-Hill, New York.

Mackay, D. M; Freyberg, D. L.; Roberts, P. V.; and Cherry, J A. (1986) *"A Natural Gradient Experiment on Solute Transport in a Sand Aquifer. 1. Approach and Overview of Plume Movement"*. Water Res. Research. Vol. 22, No. 13, pp. 2017-2029.

MacFarlane, D. S.; Cherry, J. A.; Gillham, R. W.; and Sudicky, E. A. (1983) "Migration of Contaminants in Groundwater at a Landfill: a Case Study. 1. Groundwater and Plume Delineation". Journal of Hydrology. Vol. 63, pp. 1-29.

McKellar, M. and Wardlaw, N. C. (1982) *"A Method of Viewing Water and Oil Distribution in Native-sate and Restored-state Reservoir Core"*. AAPG Bul. 72:765-771.

Mohanty, K.K.; Davis, H. T.; and Scriven, L. E. (1980) *"Physics of Oil Entrapment in Water-wet Rock"*. Paper SPE 9406, presented at 1980 SPE Annueal Technical Conference and Exhibition, Dallas, TX.

Moore, T.F. and Slobod, R.L. (1956) *"The Effect of Viscosity and Capillarity on the Displacement of Oil by Water,"* Producers Monthly, 20, 20-30.

Morrow, N. R., Chatzis, I. and Taber, J. J. (1988) *"Entrapment and Mobilization of Residual Oil in Bead Packs"*. SPE Reservoir Engineering, August, 937-934.

Nielsen, L. E.(1978) *"Predicting the Properties of Mixtures: Mixtures Rules in Science and Engineering"*. Marcel Dekker, Inc. New York, NY. 96 p.

Nkedi-Kizza, P.; Rao, P.S.C. and Hornsby, A.G. (1985) *"Influence of organic cosolvent on sorption of hydrophobic organic chemicals by soils."* Environ. Sci. Technol. 19:975-979.

Nyer, E.K.; Palmer, P.L.; Suthersan, S.S.; Fam, S.; Johns II, F.J.; Kidd, D.F.; Crossman, T.L.; Boettcher, G. (1996) *"In Situ Treatment Technology"*. Lewis Publishers, NY. 329 p.

Oliveira, E.; Banks, J.; Barker, J.F. (1994) *"Effects of water table fluctuation on the distribution of gasoline residuals from a gasoline-ethanol mixture."* (in preparation).

Padday, J. F. (1969) *"Surface Tension"* in *"Surface and Colloid Science"*, **Matijevic, E.** (editor). Vol. 1. Wiley-Interscience. New York.

Poulsen, M., Lemon, L. and Barker, J.F. (1991) *"Chemical Fate and Impact of Oxygenates in Groundwater: Solubility of BTEX from Gasoline-Oxygenate Compounds."* Health and Environmental Sciences, API Publication No. 4531, 113p.

Redman, J. D. (1997) *"Novel Technique for Continuous Logging of Dielectric Properties Using an Access Tube with an Embedded Transmission Line."* (in preparation)

Redman, J. D. and DeRick, S. M. (1994) *"Monitoring Non-aqueous Phase Liquids in the Subsurface with Multilevel Time Domain Refletometry Probes."* Proceedings of the Symposium and Workshop on Time Domain Reflectometry in Environmental, Infrastructure and Mining Applications. Northwestern University, Evanston, Illinois.

Ross, S. and Patterson, R.E. (1979) *"Surface and Interfacial Tensions of Conjugate Solutions in Ternary Systems"*. J. Chem. Eng. Data, Vol. 24, No. 2, pp.111-115.

Stalkup, F.I. Jr. (1983) *"Miscible Displacement"*. Monograph Vol. 8, Henry Doherty series, Society of Petroleum Engineers, New York, NY, 204 p.

Sudicky, E. A. (1986) *"A Natural Gradient Experiment on Solute Transport in a Sand Aquifer: Spatial Variability of Hydraulic Conductivity and its Role in the Dispersion Process"*. Water Res. Research. Vol. 22, No. 13, 2069-2082.

Sudicky, E. (1993) *"Theory of Flow through Porous Media"* - Lecture Notes. University of Waterloo, Department of Earth Sciences.

Taber, J. J.; Kamath, I. S. K.; and Reed, R. L. (1961) *"Mechanism of Alcohol Displacement of Oil from Porous Media"*. Society of Petroelum Engineering Journal, vol. 1, pp. 195-209.

Taber J. J. and Meyer, W. K. (1964) *"Investigations of Miscible Displacements of Aqueous and Oleic Phases From Porous Media"*. Society of Petroelum Engineering Journal, vol. 4, pp. 37-48.

Topp, G. C.; Davis, J. L. And Annan, A. P. (1980) *"Electromagnetic Determination of Soil Water Content: Measurement in Coaxial Transmission Lines"*. Water Res. Research. Vol. 16, pp. 574-582.

Treybal, Robert E., *Mass-Transfer Operations*, McGraw-Hill Book Company, Inc., USA, 1987.

Varteressian, K.A. and Fenske, M.R. (1936) *"Liquid-Liquid Extraction - Performance of a Packed Extraction Column, Using Continuous Countercurrent Operation"*. Ind. and Eng. Chem., pp. 928-933.

Wan Loosdrecht, M. C. M.; Lyklema, J.; Norde, W.; Schraa, G.; and Zehnder, A. J. B. (1987) *"Electrophoretic Mobility and Hydrophobicity as a Measure to Predict the InitialSteps of Bacterial Adhesion"*. App. Env. Microbiology. Vol. 53, No. 8, pp. 1898-1901.

Wardlaw, N.C. (1982) *"The effect of geometry, wettability, viscosity, and interfacial tension on trapping in single pore throat pairs."* Jour. of Canadian Petro. Tech. 21:21-27.

Wilson, J. L.; and Conrad, S. H. (1984) *"Is Physical displacement of Residual Hydrocarbons a Realistic Possibility in Aquifer Restoration?"*. In Proc. Of Petroleum Hydrocarbons and Organic Chemicals in Groundwater, NWWA, Houston, TX.

Wilson, J.L.; Conrad, S.H.; Hagan, E.; Mason, W.R.; Peplinski (1990) *"Laboratory investigation of residual liquid organics."* Report CR-813571, Ada, Oklahoma. U. S. Environmental Protection Agency.

Wilson, J.L. (1994) *"Visualization of flow and transport at the pore level"*. In: Transport and reactive processes in aquifer, T.H. Dracos and F. Stauffer (editors). V.5, pp19-36.

Yalkowsky, S.H. and Roseman, T. (1981) *"Solubilization of Drugs by Cosolvents"*. In: S.H. Yalkowsky (ed.) Techniques of Solubiliztion of Drugs, pp. 91-134. New York, NY, Marcel Dekker.

APPENDIX I

Analytical methods for chemical analyses

I. ANALYTICAL METHODS

I.1 WATER AND ETHANOL ANALYSIS

I.1.1 Sample Preparation

Samples are collected in 20 ml glass vials, capped with Tegrabond Teflon® septa and aluminum seal (20mm) and stored in a 10 degree C refrigerator until analyzed. A 3 µl aliquot of the solution (a mixture of water, ethanol and gasoline) is sampled for chromatographic analysis.

I.1.2 Spectrophotometric Analysis

The samples are run on a GOW-MAC (series 350) gas chromatograph equipped with a thermal conductivity detector (TCD). The stainless steel column is 6ft x 0.25in o.d., packed with porapak Q. The analysis is run isothermally at 130 C with helium carrier gas at a flow rate of 50 ml/min. The detector temperature at 150 C and the injection port temperature at 150 C. Peak areas are measured by a HP 3380A integrator and a linear regression plot used. Standards were prepared by weighing ethanol ranging in volume from 0-100% (0,10,25,50,75,90,100) with the balance being organic-free water. The method detection limit for ethanol was found to be 1.4% (wt/wt) using the EPA procedure for Method Detection Limit (MDL).

I.1.3 Accuracy and Precision at Check Concentrations

COMPOUND (EtOH)	Xo	X	N	%S	%E
50% (v/v)	44.6	45.5	31	3.0	2.6
75% (v/v)	68.8	72.8	20	2.3	5.9

N - number of replicate determinations

X - mean of replicate determinations

Xo - true value (by weight)

%S - relative standard deviation

%E - relative error

I.2 GASOLINE ANALYSIS

I.2.1 Sample Preparation

Samples are collected in 20 ml glass vials, capped with Tegrabond Teflon® septa and aluminum seal (20mm) and stored in a 10°C refrigerator until analyzed. A 1.5 ml aliquot of the solution (a mixture of water, ethanol and gasoline) is sampled for spectrophotometric analysis.

I.2.2 Spectrophotometric Analysis

The samples are run on a ULTROSPEC Plus(4054) UV/Vis spectophotometer equipped with a deuterium arc and tungsten halogen lamp source. The detector is a single solid-state silicon photocell. An initial wavelength scan was conducted to determine the maximum absorbance peak for gasoline to be 285 nm. Standards and samples were transferred to a cell and placed in the cell holder, the absorbance at a wavelength of 285 nm was recorded. The reference blank used in the analyses was water and ethanol. Standards were prepared by measuring small volumes of gasoline (5,25,100,250and 500 µl) into 100ml of ethanol and the weight of ethanol (calculated based on the measured volume and ethanol density) was recorded. A linear regression plot for the standards (0.005-0.500% wt/wt) was used to determine the concentration of gasoline in the samples. Any samples over 0.5% gasoline were diluted with ethanol to fit the range of the calibration. The method detection limit for gasoline was found to be 0.0015% (wt/wt) using the EPA procedure for Method Detection Limit (MDL).

I.2.3 Accuracy and Precision at Check Concentrations

COMPOUND Gasoline	Xo	X	N	%S	%E
0.48% (v/v)	0.48	0.478	16	0.4	-0.6
0.0048% (v/v)	0.0048	0.0047	11	11.7	-1.5

N - number of replicate determinations

X - mean of replicate determinations

Xo - true value (by weight)

%S - relative standard deviation

%E - relative error

APPENDIX II

Data for pseudoternary diagrams of gasoline-water-ethanol for refractive index method and chemical analyses method

LIST OF TABLES

Table II-3: Composition for the Starting Points of the Tie-lines

Tie-line I.D	Ethanol (ml)	Water (ml)	Gasoline (ml)	Ethanol % (Wt %)	Water % (Wt %)	Gasoline % (Wt %)
1	1.80	8.10	9.00	8.713	49.808	41.479
2	2.70	8.10	8.10	13.043	49.704	37.253
3	3.60	7.20	8.10	17.597	44.706	37.696
4	4.50	6.30	8.10	22.261	39.589	38.150
5	5.40	5.40	8.10	27.039	34.347	38.615
6	6.30	4.50	8.10	31.934	28.975	39.091
7	7.20	3.60	8.10	36.952	23.469	39.579
8	8.10	2.70	8.10	42.097	17.825	40.079
9	8.10	1.80	8.10	44.756	12.634	42.611
10	70.00	7.00	63.00	50.406	6.403	43.191
11	60.20	8.40	71.40	43.357	7.685	48.958
12	61.60	7.00	71.40	44.486	6.421	49.092

Table II-4: Refractive Index Based Compositions for Separate Phases of the Tie-lines (End Points)

Water Phase				
Sample I.D.	Refractive Index	Ethanol % (Wt %)	Water % (Wt %)	Gasoline % (Wt %)
1	1.3359	8.042	91.941	0.017
2	1.3405	14.873	85.093	0.034
3	1.3460	22.981	76.964	0.055
4	1.3506	31.796	68.121	0.083
5	1.3546	40.549	59.246	0.206
6	1.3577	49.403	50.056	0.541
7	1.3602	59.239	39.215	1.546
8	1.3631	7.137	0.522	92.341
9	1.3674	6.803	0.498	92.699
10	1.3786	56.567	7.450	35.983
11	1.3731	63.770	10.432	25.798
12	1.3764	59.405	8.625	31.970
Gasoline Phase				
Sample I.D.	Refractive Index	Ethanol % (Wt %)	Water % (Wt %)	Gasoline % (Wt %)
1	1.4126	3.001	0.220	96.779
2	1.4121	3.502	0.256	96.242
3	1.4120	3.635	0.266	96.099
4	1.4109	4.736	0.347	94.918
5	1.4127	2.901	0.212	96.886
6	1.4110	4.636	0.339	95.025
7	1.4095	6.070	0.444	93.486
8	1.4085	7.321	0.534	92.145
9	1.4088	6.979	0.509	92.512
10	1.3985	23.626	2.425	73.949
11	1.4043	14.444	1.590	83.966
12	1.3996	21.928	2.270	75.802

Table II-3: Composition for the Starting Points of the Tie-lines

Tie-line I.D	Ethanol (ml)	Water (ml)	Gasoline (ml)	Ethanol % (Wt %)	Water % (Wt %)	Gasoline % (Wt %)
1	1.80	8.10	9.00	8.713	49.808	41.479
2	2.70	8.10	8.10	13.043	49.704	37.253
3	3.60	7.20	8.10	17.597	44.706	37.696
4	4.50	6.30	8.10	22.261	39.589	38.150
5	5.40	5.40	8.10	27.039	34.347	38.615
6	6.30	4.50	8.10	31.934	28.975	39.091
7	7.20	3.60	8.10	36.952	23.469	39.579
8	8.10	2.70	8.10	42.097	17.825	40.079
9	8.10	1.80	8.10	44.756	12.634	42.611
10	70.00	7.00	63.00	50.406	6.403	43.191
11	60.20	8.40	71.40	43.357	7.685	48.958
12	61.60	7.00	71.40	44.486	6.421	49.092

Table II-4: Refractive Index Based Compositions for Separate Phases of the Tie-lines (End Points)

Water Phase				
Sample I.D.	Refractive Index	Ethanol % (Wt %)	Water % (Wt %)	Gasoline % (Wt %)
1	1.3359	8.042	91.941	0.017
2	1.3405	14.873	85.093	0.034
3	1.3460	22.981	76.964	0.055
4	1.3506	31.796	68.121	0.083
5	1.3546	40.549	59.246	0.206
6	1.3577	49.403	50.056	0.541
7	1.3602	59.239	39.215	1.546
8	1.3631	7.137	0.522	92.341
9	1.3674	6.803	0.498	92.699
10	1.3786	56.567	7.450	35.983
11	1.3731	63.770	10.432	25.798
12	1.3764	59.405	8.625	31.970
Gasoline Phase				
Sample I.D.	Refractive Index	Ethanol % (Wt %)	Water % (Wt %)	Gasoline % (Wt %)
1	1.4126	3.001	0.220	96.779
2	1.4121	3.502	0.256	96.242
3	1.4120	3.635	0.266	96.099
4	1.4109	4.736	0.347	94.918
5	1.4127	2.901	0.212	96.886
6	1.4110	4.636	0.339	95.025
7	1.4095	6.070	0.444	93.486
8	1.4085	7.321	0.534	92.145
9	1.4088	6.979	0.509	92.512
10	1.3985	23.626	2.425	73.949
11	1.4043	14.444	1.590	83.966
12	1.3996	21.928	2.270	75.802

Table II-5: Tie-line overall compositions (before phase separation)

Sample	Water (ml)	Ethanol (ml)	Gasoline (ml)	Total (ml)	Water (Vol.%)	Ethanol (Vol.%)	Gasoline (Vol.%)
1A	69.0	9.0	42.0	120.0	0.575	0.075	0.350
2A	57.0	21.0	42.0	120.0	0.475	0.175	0.350
3A	48.0	30.0	42.0	120.0	0.400	0.250	0.350
4A	42.0	36.0	42.0	120.0	0.350	0.300	0.350
5A	33.0	45.0	42.0	120.0	0.275	0.375	0.350
6A	25.0	53.0	42.0	120.0	0.208	0.442	0.350
7A	18.0	60.0	42.0	120.0	0.150	0.500	0.350
8A	12.0	66.0	42.0	120.0	0.100	0.550	0.350
Sample	**Water (g)**	**Ethanol (g)**	**Gasoline (g)**	**Total (g)**	**Water (Wt.%)**	**Ethanol (Wt.%)**	**Gasoline (Wt.%)**
1A	68.760	7.061	31.370	107.190	0.641	0.066	0.293
2A	56.802	16.475	31.370	104.646	0.543	0.157	0.300
3A	47.833	23.535	31.370	102.738	0.466	0.229	0.305
4A	41.854	28.242	31.370	101.466	0.412	0.278	0.309
5A	32.885	35.303	31.370	99.557	0.330	0.355	0.315
6A	24.913	41.579	31.370	97.861	0.255	0.425	0.321
7A	17.937	47.070	31.370	96.377	0.186	0.488	0.325
8A	11.958	51.777	31.370	95.105	0.126	0.544	0.330
Sample	n_{water}	$n_{ethanol}$	$n_{gasoline}$	n_{total}	X_{water}	$X_{ethanol}$	$X_{gasoline}$
1A	3.817	0.153	0.350	4.320	0.883	0.035	0.081
2A	3.153	0.357	0.350	3.861	0.817	0.093	0.091
3A	2.655	0.511	0.350	3.516	0.755	0.145	0.100
4A	2.323	0.613	0.350	3.286	0.707	0.186	0.107
5A	1.825	0.766	0.350	2.942	0.621	0.260	0.119
6A	1.383	0.902	0.350	2.635	0.525	0.342	0.133
7A	0.996	1.021	0.350	2.367	0.421	0.431	0.148
8A	0.664	1.123	0.350	2.138	0.311	0.526	0.164

Table II-6: UV analyses results

UV Analyses					
Sample	**Gasoline (Wt%)**	**Water (Wt%)**	**Ethanol (Wt%)**	**Total**	$X_{ethanol}$
9A-A	0.1263	102.7862	0.0000	102.9124	0.0000
1A-A	0.1428	92.4457	10.1534	102.7417	0.2180
2A-A	0.2133	77.2601	24.6286	102.1022	0.4457
3A-A	0.3798	63.5549	34.3488	98.2835	0.5730
4A-A	0.8222	57.1541	42.0352	100.0115	0.6371
5A-A	2.0218	44.0502	51.6998	97.7716	0.7096
6A-A	4.5710	31.9965	59.0916	95.6591	0.7341
7A-A	7.9733	21.8872	69.4407	99.3011	0.7427
8A-A	13.6995	12.8955	68.8988	95.4938	0.6851
9A-G	79.4057	0.0000	0.0000	79.4057	0.0000
1A-G	80.0537	0.0000	0.0000	80.0537	0.0000
2A-G	78.7846	0.0000	0.5780	79.3626	0.0038
3A-G	78.5829	0.0459	1.0564	79.6853	0.0069
4A-G	77.0305	0.1083	0.9247	78.0635	0.0061
5A-G	75.3130	0.0000	1.9459	77.2589	0.0131
6A-G	72.1088	0.0944	2.8802	75.0833	0.0201
7A-G	68.1222	0.0778	4.7427	72.9426	0.0346
8A-G	62.9470	0.2853	9.1868	72.4191	0.0698

NA-A and NA-G (N = 1 to 9) correspond respectively to the aqueous and oleic (gasoline) phases after separation

Wt% = percent by weight

V% = percent by volume

APPENDIX III

Balance of forces acting on a small gasoline blob

moving against the flow of ethanol

LIST OF ILLUSTRATIONS

III. BALANCE OF FORCES ACTING ON A SMALL GASOLINE BLOB MOVING AGAINST THE FLOW OF ETHANOL

Figure shows the of forces acting on a blob that just detached itself from the original blob, as shown in the sequence of photographs of Figure 3-8, Chapter 3. The acting forces on blob moving at a steady state are gravity force, buoyancy force, viscous force (drag) and capillary force.

Gravity force for a spherical blob is given by:

$$F_G = V_O \rho_O g \qquad \text{(IV-1)}$$

where:

F_G = gravity force [F];

ρ_o = density of the blob (oleic phase) [M/L^3];

V_o = volume of the blob [L^3];

g = acceleration of gravity [L/T^2];

Buoyancy force is given by:

$$F_B = V_O \rho_A g \qquad \text{(IV-2)}$$

Where:

F_G = buoyancy force [F];

ρ_A = density of aqueous phase [M/L^3];

The drag force acting on a sphere immersed in a fluid may be calculated by (Granger, 1985):

$$F_D = \frac{1}{2}(\rho_A v^2 A C_{D_T}) \qquad \text{(IV-3)}$$

where:

F_D = drag force [F];

v = flowing fluid velocity [L/T];

A = projected frontal area of blob [L^2];

C_{D_T} = total drag coefficient.

C_{D_T} is variable and depends on the Reynolds number. For low values of Reynolds number (up to about 10), the total drag coefficent for a sphere has an approximate linear behavior and may be calculated by the Stokes law for a sphere (Granger, 1985), $C_{D_T} = 24/R_e$, where R_e is the Reynolds number. Considering that ethanol is the fluid that is being injected, Reynolds number is:

$$R_e = \frac{\rho v L}{\mu} \qquad \text{(IV-4)}$$

where:

R_D = Reynolds number;

L = reference length (diameter) [L];

μ = viscosity of the flowing fluid [FT/L^2].

The viscosity of ethanol is 1.078×10^{-4} N·m/m^2 (very similar to that of the water) and density is 784.5 Kg/m^3. The approximate diameter of the blob observed in the experiment is 3.5×10^{-4} m. For the range of velocities used in the micromodel experiment, 0.69 cm/min to 4.31 cm/min, Reynolds number may be calculated as $0.29 \leq R_D \leq 1.99$ (laminar flow, according to Bear, 1979), and the total drag coefficient $12.1 \leq C_{D_T} \leq 82.7$. The drag force acting on the blob is in the range 2.30×10^{-11} N$\leq F_D \leq 6.13 \times 10^{-9}$ N.

The resultant capillary force acting on the blob is due to differences in capillary forces within the blob from differences in IFT on its frontal side to its rear side. At the front, IFT is being reduced by mass transfer due to the high concentration of ethanol arriving from injected solution. At the rear, mass transfer rate is lower, and consequently the IFT is higher. Figure clarifies this effect. At the front of the blob, the mass transfer results in a shorter tie line, as the ternary diagram on the left shows. At the rear of the blob, the tie line is longer (ternary diagram on the right). As discussed previously, as the tie line decreases in length, interfacial tension is reduced. Assuming a spherical blob, the resultant force due to IFT is:

$$F_C = F_{C_R} - F_{C_F} \tag{IV-5}$$

where:

F_C = resultant force in the blob due to capillary pressure (F);

F_{C_R} = capillary force at the rear of the blob (F);

F_{C_F} = capillary force at the front of the blob (F).

The capillary pressure for each side of the blob is calculated through Laplace's equation for capillary pressure:

$$P_C = \frac{2\sigma_{OA}}{r} \tag{IV-6}$$

where:

P_C = capillary pressure [F/L^2];

σ_{OA} = IFT between oleic and aqueous phase [F/L];

r = radius of the blob [L].

For simplification, it is assumed that the pressure is to a plane surface corresponding to the area of half a sphere. Then force resulting from the capillary pressure at one side of the blob thus exerced is given by:

$$F_{C_i} = P_{C_i} A \tag{IV-7}$$

Where A corresponds to the surface area of half a sphere of radius r. Combining equations IV-5 through IV-7, the resulting capillary force in the blob is given by:

$$F_C = 2r(\sigma_{OA_R} - \sigma_{OA_F}) \tag{IV-8}$$

Solving along the path AB for the forces presented on Figure IV-1, the necessary condition for movement of the blob upgradient is:

$$F_C \cos\theta + F_G \cos\left(\frac{\pi}{2} - \theta\right) \rangle F_D \cos\theta + F_B \cos\left(\frac{\pi}{2} - \theta\right) \tag{IV-9}$$

Substituting equations IV-1, IV-2 and IV-8 and rearranging:

$$\sigma_{OA_R} - \sigma_{OA_F} = \pi r\left[\rho_A v^2 C_{D_T} + (\rho_A - \rho_O)\frac{2}{3} r g \tan\theta\right] \tag{IV-10}$$

The necessary difference in IFT to move the blob depends mainly on the difference of densities and the angle relative to the horizontal plane. The parameters related to the drag force, as shown before, have a minor influence. Drag force is very low for the high velocities of fluid in the micromodel experiment and is much smaller for typical groundwater velocities. Considering the ranges of densities presented on Figure 2-15 (Chapter 2) for oleic and aqueous phases, and $0 \leq \theta \leq \pi/2$, density differences necessary to move a blob are plotted against density differences on Figure . The figure shows that necessary differences in IFT is approximately constant for varying densities (negligible variation is related to the density of the aqueous phase in the drag force formula). For the maximum velocity used in the experiment, the necessary IFT for horizontal movement of the blob is in the order of 10^{-5} N/m and 10^{-7} N/m for the minimum velocity.

For non-horizontal movement of the blob ($\theta \neq 0$), the necessary difference in IFT is of the order of 10^{-2} N/m for both velocities for angles very close to 90° (89.5°). Straight downward movement of the blob is theoretically expectable when density differences tends to zero (close to the plait point), but in this case, coalescence and dissolution of the blob take place.

The phenomenon described above is possible due to differences in composition within the blob. The phenomenon is short-lived due to rapid mixture of the components caused by high concentration gradients within the blob. As observed in the sequence of photographs in Chapter 3, the resulting force is not high enough to push the blob through the narrow opening of the adjacent pore throat from where the injected fluid is coming. The blob remains in front of the pore throat and dissolves away (becomes a single phase).

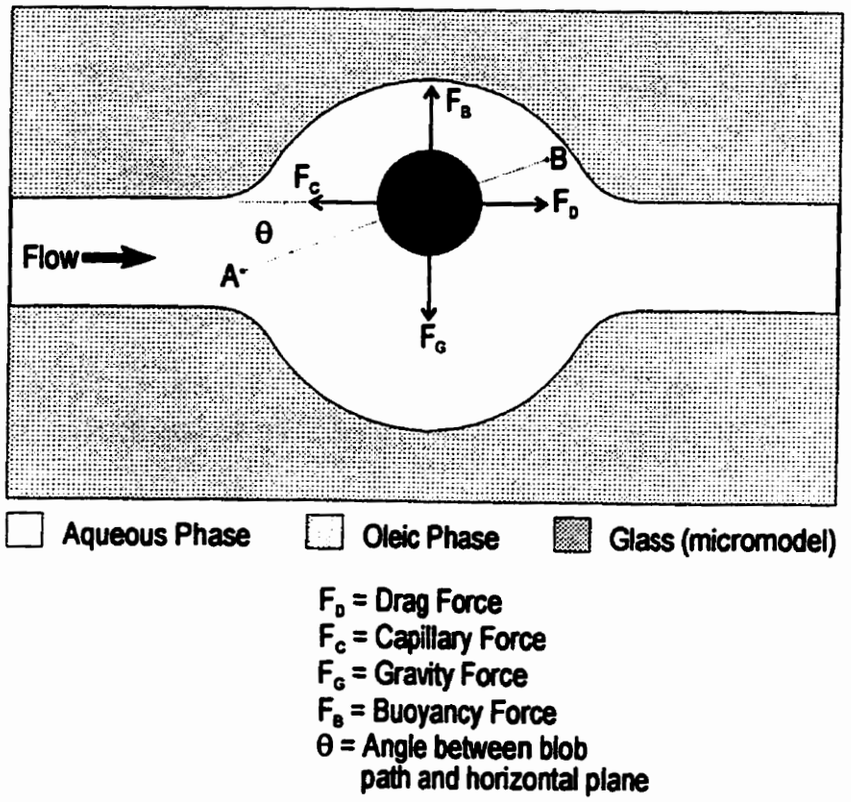

Figure III-1- Balance of forces acting on the blob that moves upgradient on steady state.

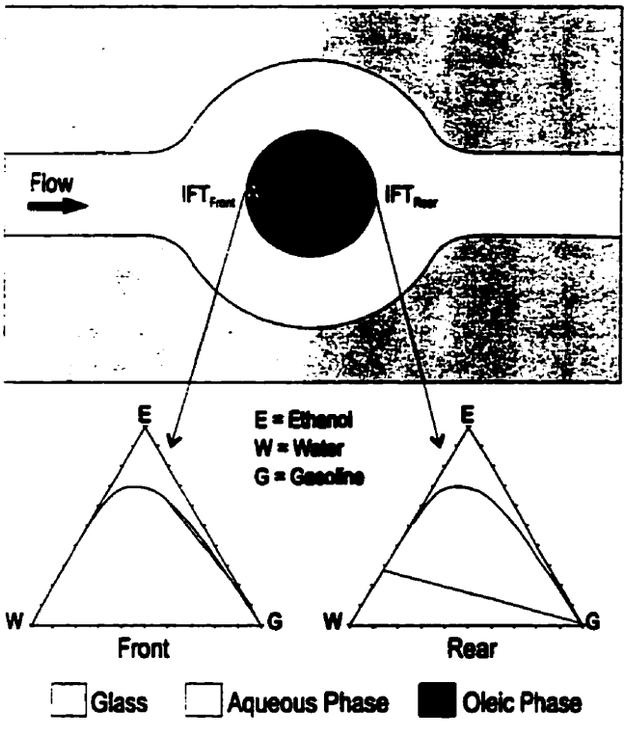

Figure III-2- Differences in interfacial tension acting on a gasoline (oleic phase) blob in flowing aqueous phase (ethanol rich).

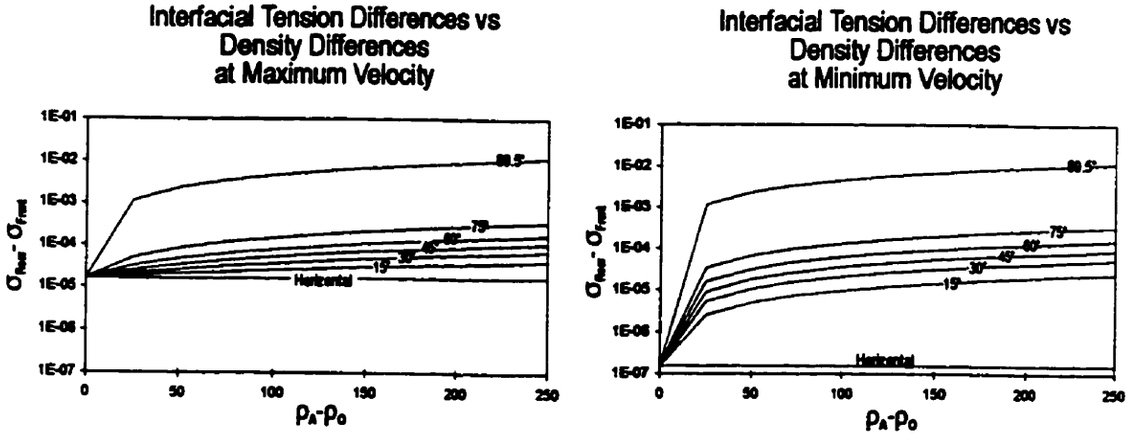

Figure III-3- Differences in interfacial tension versus difference in densities for several different angles of the blob path relative to the horizontal plane.

APPENDIX IV

Unleaded gas analysys summary

UNLEADED GAS ANALYSIS SUMMARY

In the early 1980's a batch of unleaded gasoline was made for health effects testing for the API PS-6 Project. This unleaded gasoline has become known as PS-6. The original batch analysis indicated (MacFarland, 1982) the following results:

Research Octane No.	92.0
Motor Octane No.	84.1
Reid vapor pressure	9.5
Distillation	
IBP/5	93/105
10/20	116/138
30/40	164/190
50/60	216/238
70/80	256/294
90/95	340/388
EP	428
Recovery	97%
Aromatics (Vol.%)	26.1
Olefins	8.4
Saturates	65.5
Benzene content	2.0%

In 1991, additional unleaded gasoline was needed for testing, so a sample designated as API 91-01 was made to replace the old batch of unleaded gasoline in toxicology research. It was the closest (specificationwise) marketed gasoline to PS-6 that was available. It was also used as the "industry average" summer gasoline for the Auto/Oil emissions testing program (reference fuel A).

Attached is a comparison of 4 different analyses done on these two unleaded gas samples.

All unleaded gasoline designated as PS-6 was from 1 batch. The batch of PS-6 sampled in 1989 was from the barrel at the repository used to dispense test article up to that time. Similarly, all unleaded gasoline designated as API 91-01 was from the same batch. The 1991 analysis of API 91-01 was from the sample upon its arrival at the repository. The 1993/94 analysis of the PS-6 sample was from a barrel that had been unopened at the repository and sent to CIIT for research purposes.

The 1993/94 analysis of API 91-01 was from a barrel that had been stored at the repository and used for dispensing since 1991.

An additional batch of unleaded gasoline (same specification - Industry average, RF-A) has been ordered for the Developmental Toxicity Study. It will all be from the same batch and will be given the desingation of API 94-01 upon its arrival.

On the attached table, the 1994 PS-6 analysis is used as the standard for comparison. All components for the 1994 PS-6 analysis are listed in both weight percent (wt%) and volume percent (LV%). The corresponding values for the other analyses, 1989 PS-6, 1991 91-01, and 1994 91-01 are listed as well. If a component of the other three samples was not found in the 1994 PS-6 samples, only those components in wt% or vol% over 0.05% are shown (except 1,2-butadiene).

Wt% or LV% values noted with an asterisk represent only the component(s) asterisked.

It should be noted that in some cases, more generic components (unidentified C9s, Aromatic, paraffin, etc.) were difficult to match between analyses. Only values are reported when there was an exact component match.

In cases where values were not reported they were all below the 0.05 wt.% or LV% limit for reporting.

UNLEADED GAS ANALYSES
(API 91-01, PS-6)

GENERAL CHARACTERISTICS

PS-6	PS-6	PS-6	API 91-01	API 91-01
	1994 Analysis	1989 Analysis	1991 Analysis	1994 Analysis
Bromine number	20.40		24	36.80
Reid Vapor Pressure, psi	8.92	4.9	8.5	8.28
RON (Research Octane Number)	91.70		92.2	91.8
MON (Motor Octane Number)	83.80		82.5	82.1
(R+M)/2	87.80		87.4	87.0
Carbon, wt.%	86.49		85.95	86.4
Hydrogen, wt%	13.51		13.00	13.6
Nitrogen, ppm	10.00		0.0083 wt%	51
Sulfur, ppm	200.00		0.74 wt%	350
Oxygen, wt%	<0.10			<0.10
Molecular Weight	103.00		94.3	101
	Vol%			
MTBE	<0.10		<0.10	<0.10
Methanol	<0.10		<0.10	<0.10
Benzene	1.77		1.03	1.03

BOILING POINT RANGES

	PS-6	PS-6	API 91-01	API 91-01
	1994 Analysis	1989 Analysis	1991 Analysis	1994 Analysis
Distillation, vol%/deg F@ 760mm				
IBP/5	93/112	98/132	98/124	95/116
10/20	127/152	132/168	136/158	131/154
30/40	176/202	192/214	178/201	176/198
50/60	225/245	234/254	224/250	222/246
70/80	266/295	276/306	272/304	270/297
90/95	327/370	350/389	342/376	339/377
EP	433	433	422	420
Rec/Res	98.0/1.0	99.0/1.0	98.0/1.0	98.0/1.0

CONSTITUENTS

	PS-6		PS-6		API 91-01		API 91-01	
	1994 Analysis		1989 Analysis		1991 Analysis		1994 Analysis	
COMPONENT NAME	Wt.%	LV%	Wt.%	LV%	Wt.%	LV%	Wt.%	LV%
Propane	0.02	0.03	-	-	0.01	0.01	0.01	0.01
Isbutane	0.60	0.79	0.29	0.38	0.14	0.19	0.10	0.13
Isobutylene + 1-Butene	0.09	0.11	0.05	0.06	-	-	-	-
n-Butane	3.05	3.82	1.90	2.42	4.88	6.24	3.96	5.08
1,2-Butadiene	-	-	-	-	0.03	0.03	-	-
trans-2-Butene	0.16	0.19	0.12	0.15	-	-	-	-
cis-2-Butene	0.17	0.20	0.12	0.14	-	-	-	-
3-Methyl-1-butene	0.06	0.07	0.04	0.05	0.03	0.04	0.03	0.04
Isopentane	7.95	9.40	6.84	8.14	4.51	5.39	4.09	4.91
1-Pentene	0.18	0.21	0.16	0.18	0.63	0.73	0.18	0.21
2-Methyl-1-butene	0.40	0.45	0.37	0.42	-	-	0.39	0.45
n-Pentane	3.29	3.85	3.07	3.62	3.61	4.27	3.34	3.97
trans-2-Pentene	0.51	0.58	0.48	0.55	0.73	0.83	0.68	0.78
3,3-Dimethyl-1-butene	0.84	0.94	-	-	-	-	-	-
cis-2-Pentene	0.29	0.32	0.27	0.30	0.43	0.49	0.39	0.44
2-methyl-2 butene	-	-	0.81	0.90	1.21	1.35	1.12	1.26
2,2-Dimethylbutane*+ Cyclopentadiene*+ cis-1,3-Pentadiene	-	-	0.19	0.22	1.01*	1.15*	0.96	1.10
Cyclopentene	0.08	0.08	0.08	0.08	0.17	0.16	0.16	0.16
4-Methyl-1-pentene	0.03	0.03	0.03	0.03	0.06	0.07	0.05	0.06
3-Methyl-1-pentene	0.05	0.06	0.05	0.06	0.08	0.09	0.08	0.09
Cyclopentane	0.24	0.24	0.26	0.26	0.23	0.23	0.16	0.16
2,3-Dimethylbutane	1.84	2.04	1.77	1.98	1.65	1.85	1.66	1.87
2,3-Dimethyl-1-butene	0.09	0.10	0.09	0.10	-	-	-	-
4-Methyl-cis-2-pentene	0.09	0.10	0.09	0.10	0.06	0.07	-	-
2-Methylpentane	4.04	4.54	4.01	4.53	5.52	6.27	5.53	6.30
4-Methyl-trans-2-pentene	2.37	2.60	0.09	0.10	0.04	0.04		

	PS-6		PS-6		API 91-01		API 91-014	
	1994 Analysis		1989 Analysis		1991 Analysis		1994 Analysis	
COMPONENT NAME	Wt.%	LV%	Wt.%	LV%	Wt.%	LV%	Wt.%	LV%
3 Methylpentane	-	-	2.51	2.79	3.12	3.48	3.07	3.44
2-Methyl-1-pentene	0.12	0.13	0.12	0.13	0.28	0.31	0.39	0.43
1-Hexene	0.12	0.13	0.12	0.13	0.12	0.13	-	-
n-Hexane*, 2-Ethyl-1-butene	1.71	1.90	1.78	1.99	2.65	2.98	2.63*	2.97*
cis-3-Hexene	0.10	0.11	0.11	0.12	-	-	0.18	0.20
trans-3-Hexene	0.04	0.04	0.04	0.04	0.18	0.20	0.07	0.08
trans-2-Hexene	0.21	0.23	0.22	0.24	0.38	0.42	0.36	0.40
2-Methyl-2-pentene	0.26	0.28	0.28	0.30	-	-	0.33	0.36
3-Methyl-cis-2-pentene	0.21	0.22	0.18	0.19	0.11	0.12	0.36	0.39
4-Methylcyclo-pentene	0.02	0.02	0.02	0.02	0.26	0.25	0.05	0.05
3-Methyl-trans-2-pentene	0.12	0.13	0.12	0.13	0.05	0.05	0.21	0.22
cis-2-Hexene	0.26	0.28	0.28	0.30	0.21	0.23	0.42	0.46
2,2-Dimethylpentane	0.05	0.05	0.05	0.05	0.43	0.47	0.08	0.09
Methylcyclopentane	1.12	1.19	1.12	1.26	1.11	1.19	1.09	1.06
2,4-Dimethylpentane	1.01	1.19	1.05	1.15	0.69	0.76	0.68	0.75
2,2,3-Trimethyl-1-butene	0.01	0.01	0.02	0.02	-	-	-	-
2,2,3-Trimethylbutane	0.07	0.07	0.07	0.07	-	-	-	-
3-Methylcyclopentene	0.16	0.15	0.15	0.14	0.36	0.36	0.38	0.36
C7 Olefin	0.02	0.02	0.02	0.02	0.01	0.01	-	-
Benzene	2.12	1.77	2.23	1.86	1.22	1.03	1.22	1.03
2,3-Dimethylpentane +C7 olefin	0.07	0.07	0.08	0.08	0.14	0.15	0.12	0.13
Cyclohexane*+C7 olefin	0.14	0.13	0.14	0.13	0.28	0.27	0.22*	0.21*
C7 Cyclo-olefin+diolefin	0.02	0.02	0.02	0.02	0.06	0.06	-	-
C7 Olefin	0.03	0.03	0.03	0.03	0.12	0.13	.02	.02
2-Methylhexane* +C7 Olefin	1.56	1.69	1.60	1.74	1.63*	1.78*	1.78*	1.95*
2,3-Dimethyl-pentane*+ C7 olefin	0.84	0.89	0.95	1.01	1.30	1.39	1.31*	1.40*
1,1-Dimethylcyclopen-tane	0.02	0.02	0.02	0.02	0.04	0.04	0.03	0.03
3-Methylhexane	1.59	1.69	1.57	1.69	1.70	1.84	1.76	1.91
C7 Olefin	0.03	0.03	0.03	0.03	0.04	0.04	0.04	0.04
t-1,3-Dimethylcyclopen-tane	0.31	0.30	0.32	0.32	0.32	0.32	0.32	0.32

	PS-6		PS-6		API 91-01		API 91-01	
	1994 Analysis		1989 Analysis		1991 Analysis		1994 Analysis	
COMPONENT NAME	WT.%	LV%	WT.%	LV%	WT.%	LV%	WT.%	LV%
c-1,3-Dimethyl-cyclopentane	0.27	0.27	0.28	0.28	0.28	0.28	0.28	0.28
3-Ethylpentane + C7 olefin	0.15	0.16	0.12	0.13	0.47	0.50	0.24	0.26
t-1,2-Dimethyl-cyclopentane	0.19	0.19	0.18	0.18	1.76	1.74	0.26	0.26
2,2,4-Trimethyl*-pentane + C7 olefin	5.73*	6.08*	6.10*	6.52*	0.21*	0.23*	1.87	2.01
C7 Olefin	0.04	0.04	0.01	0.01	0.11	0.12	0.06	0.06
C7 Olefin	0.07	0.07	0.04	0.04	-	-	0.14	0.15
n-Heptane	0.62	0.67	0.65	0.70	1.30	1.41	1.36	1.48
C7 Olefin	0.06	0.06	0.18	0.19	0.05	0.05	0.14	0.15
C7 Olefin	0.14	0.15	0.07	0.07	0.24	0.25	0.25	0.26
C7 Olefin	0.06	0.06	0.07	0.07	0.11	0.12	0.11	0.12
C7 Olefin	0.04	0.04	0.03	0.03	0.12	0.13	0.13	0.14
C7 Olefin	0.04	0.04	0.12	0.13	0.06	0.06	0.06	0.06
C7 Olefin	0.08	0.08	0.07	0.07	0.13	0.14	0.13	0.14
C8 Olefin	0.04	0.04	-	-	0.09	0.09	0.14	0.15
C8 Olefin	0.04	0.04	-	-	0.09	0.09	0.07	0.07
C8 Olefin	0.03	0.03	-	-	0.08	0.08	0.06	0.06
C8 Olefin	0.02	0.02	-	-	0.05	0.05	0.01	0.01
c-1,2-Dimethyl-cyclopentane	0.16	0.15	0.15	0.14	0.18	0.17	0.15	0.15
Methylcyclopentane	0.35	0.33	0.40	0.38	0.43	0.42	0.44	0.43
2,3-Dimethylhexane	0.03	0.03	-	-	-	-	0.06	0.06
C8 Cyclo-olefin/dio-lefin	0.06	0.06	-	-	-	-	-	-
C8 Cyclo-olefin/diolefin	0.01	0.01	-	-	-	-	-	-
Ethylcyclopentane	-	-	0.16	0.17	0.46	0.46	-	-
2,5-Dimethylhexane* + C8 Naphthene + Ethylcyclopentane	1.20*	1.21*	1.43	1.46	-	-	0.69	0.50
2,2,3-Trimethylpentane + C8 olefin + 2,4-Dimethylhexane	1.24	1.29	0.97	1.02	0.55	0.58	0.57	0.60
1,2,4-Trimethyl-cyclopentane	0.11	0.11	0.11	0.11			0.13	0.13
3,3-Dimethylhexane	0.03	0.03	0.02	0.02			0.06	0.06
C8 Olefin	0.01	0.01	0.03	0.03	0.05	0.06		
1,2,3-Trimethyl-cyclopentane + C8 cyclo-olefin/dio lefin	0.04	0.04	0.06	0.06	0.10	0.10		

	PS-6		PS-6		API 91-01		API 91-01	
	1994 Analysis		1989 Analysis		1991 Analysis		1994 Analysis	
COMPONENT NAME	WT.%	LV%	WT.%	LV%	WT.%	LV%	WT.%	LV%
2,3,4-Trimethylpentane + C8 olefin	3.40	3.47	3.56	3.66	0.73	0.75	0.78	0.82
2,3,3 Trimethylpentane + C8 olefin	3.57	3.61	3.47	3.53	-	-	0.87	0.90
Toluene	3.97	3.36	4.71	4.02	7.68	6.58	6.94	5.97
2,3-Dimethylhexane + C8 olefin	0.90	0.93	1.0	0.98	0.41	0.43	0.41	0.42
1-Methyl-1-ethylpentane	0.08	0.08			-	-	-	-
C8 Olefin	0.02	0.02	0.02	0.02	-	-	0.11	0.11
2-Methylheptane	0.68	0.77	0.73	0.77	0.85	0.90	0.88	0.94
4-Methylheptane	0.27	0.26	0.27	0.28	0.36	0.38	0.38	0.40
3-Methyl-3-ethylpentane + C8 olefin	0.18	0.18	0.22	0.22	-	-	0.14	0.14
3-Methylheptane	0.81	0.84	0.76	0.80	0.02	0.02	0.96	1.01
3-Ethylhexane + C8 olefin	0.13	0.13	-	-	1.21	1.26	0.13	0.14
c-1,4-Dimethylcyclohexane	0.08	0.08	-	-	-	-	0.04	0.04
t-1,4-Dimethylcyclohexane	0.06	0.06	-	-	-	-	0.03	0.03
C8 Naphthene + C8 olefin	0.05	0.05	0.05	0.05	0.14	0.14	-	-
C8 Naphthene +C8 olefin	0.01	0.01	0.14	0.14	0.16	0.16	-	-
C9 Naphthene + C8 olefin	0.06	0.06	0.09	0.09	0.13	0.13	-	-

CONSTITUENTS (CONT)

	PS-6		PS-6		API 91-01		API 91-01	
	1994 Analysis		1989 Analysis		1991 Analysis		1994 Analysis	
COMPONENT NAME	WT.%	LV%	WT.%	LV%	WT.%	LV%	WT.%	LV%
C8 Naphthene + C9 olefin	0.02	0.02	0.04	0.04	-	-	-	-
2,2,4-Trimethylhexane	0.74	0.76	0.72 (2,2,5)	0.74 (2,2,5)	-	-	0.27	0.28
C8 Naphthene	0.12	0.12	-	-	0.09	0.09	0.17	0.17
C8 Naphthene	0.09	0.09	-	-	0.13	0.13	0.12	0.12
Unidentified C8's	0.12	0.12	-	-	-	-	0.65	0.68
n-Octane	0.37	0.39		0.38	0.65	0.69	0.71	0.75
t-1,2-Dimethylcyclohexane	0.01	0.01	-	-	0.12	0.11	0.14	0.13
1,2,3,-Trimethylcyclopentane	0.10	0.09	-	-	-	-	0.05	0.05
C8 Olefin	0.02	0.02	-	-	0.05	0.05	-	-
C8 Olefin	0.01	0.01	-	-	-	-	-	-
C8 Olefin + C9 olefin	0.04	0.04	-	-	-	-	-	-
C9 Naphthene	0.01	0.01	-	-	0.21	0.20	-	-
C9 Paraffin + C8 olefin	0.13	0.13	0.05	0.05	0.05	0.05	0.05	0.05
Diolefin	0.06	0.06	-	-	-	-	-	-
C9 Olefin	0.01	0.01	-	-	0.06	0.06	-	-

	PS-6		PS-6		API 91-01		API 91-01	
	1994 Analysis		1989 Analysis		1991 Analysis		1994 Analysis	
COMPONENT NAME	WT.%	LV%	WT.%	LV%	WT.%	LV%	WT.%	LV%
C8 Olefin	0.02	0.02	-	-	-	-	-	-
C8 Paraffin	0.09	0.09	-	-	0.19	0.19	-	-
Olefin	0.04	0.04	-	-	-	-	-	-
c-1,2-Dimethylcyclohexane + C8 olefin	0.04	0.04	-	-	0.05	0.05	-	-
C8 Paraffin	0.16	0.16	-	-	0.03	0.03	-	-
Ethylcyclohexane	0.02	0.02	0.09	0.09	-	-	-	-
C8 Paraffin	0.22	0.23	-	-	-	-	-	-
C8 Paraffin	0.01	0.01	-	-	-	-	-	-
1,3,5-Trimethylcyclohexane +C8 olefin	0.01	0.01	-	-	-	-	-	-
C8 Naphthene	0.01	0.01	-	-	0.03	0.03	0.04	0.04
C8 Naphthene + C8 olefin	0.01	0.01	-	-	-	-	-	-
Ethylbenzene	1.47	1.56	2.06	1.76	3.37	2.89	3.42	2.94
C8 Olefin	0.04	0.04	-	-	-	-	-	-
m-Xylene + C8 paraffin	5.03	4.28	5.52	4.73	5.31	4.57	5.37	4.64
p-Xylene + C8 paraffin	1.96	1.67	2.23	1.92	2.13	1.84	2.19	1.89
3,4-Dimethylheptane	0.04	0.04	0.04	0.04	-	-	0.05	0.05
2-Methyloctane	0.23	0.23	0.23	0.24	0.28	0.29	0.30	0.31
4-Methyloctane	0.31	0.32	0.31	0.32	0.32	0.33	0.35	0.36
3-Ethyloctane	0.15	0.16	-	-	-	-	-	-
3-Methyloctane	0.31	0.32	0.34	0.35	0.34	0.35	0.36	0.37
3,3-Diethylpentane	0.07	0.07	0.05	0.05	-	-	0.02	0.02
o-Xylene	2.45	2.05	2.72	2.29	2.64	2.21	2.64	2.24
C10 Naphthene	0.11	0.10	-	-	0.04	0.04	0.04	0.04
Naphthene	0.02	0.02	-	-	-	-	-	-
Naphthene	0.05	0.05	-	-	-	-	-	-
Paraffin	0.09	0.08	-	-	-	-	-	-
Naphthene	0.01	0.01	-	-	-	-	-	-
Unidentified C9's	0.07	0.07	-	-	-	-	0.71	0.72
n-Nonane	0.19	0.19	0.21	0.22	0.24	0.25	0.24	0.25
C9 Naphthene	0.05	0.05	0.04	0.04	0.02	0.02	0.02	0.02
Isopropylbenzene	0.11	0.09	0.10	0.09	0.22	0.19	0.16	0.14
C9 Naphthene	0.02	0.02	-	-	0.02	0.02	-	-
Paraffin	0.04	0.04	-	-	-	-	-	-
C10 Paraffin	0.04	0.04	0.03	0.03	-	-	0.03	0.03
C10 Paraffin	0.01	0.01	0.03	0.03	-	-	-	-
C10 Paraffin	0.05	0.05	0.01	0.01	-	-	-	-
C10 Paraffin	0.01	0.01	0.04	0.04	-	-	-	-

	PS-6		PS-6		API 91-01		API 91-01	
	1994 Analysis		1989 Analysis		1991 Analysis		1994 Analysis	
COMPONENT NAME	WT.%	LV%	WT.%	LV%	WT.%	LV%	WT.%	LV%
1,2-Diethylbenzene	0.40	0.33	0.38	0.32	0.44	0.37	0.49	0.42
1,3-Dimethyl-5-ethylbenzene + 1,4-Diethylbenzene	0.01	0.01	0.01	0.01	0.04	0.03	0.05	0.04
C11 Paraffin	0.04	0.04	0.01	0.01	0.01	0.01	0.06	0.06
C11 Paraffin	0.30	0.30	-	-	-	-	-	-
C11 Paraffin	0.01	0.01	-	-	-	-	-	-
Paraffin	0.12	0.10	-	-	-	-	-	-
C11 Paraffin	0.14	0.14	-	-	-	-	-	-
1,3-Dimethyl-4-ethylbenzene + Indane	0.36	0.30	0.29	0.24	0.25	0.21	-	-
Paraffin	0.15	0.12	-	-	-	-	-	-
1,2-Dimethyl-4-ethylbenzene + Indane	0.52	0.44	0.50	0.42	0.62	0.53	0.66	0.56
Paraffin	0.16	0.13	-	-	-	-	-	-
Paraffin	0.01	0.01	-	-	-	-	-	-
Paraffin	0.02	0.02	-	-	-	-	-	-
C11 Aromatic	0.02	0.02	-	-	-	-	1.19	1.04
Unidentified C11's	0.07	0.07	-	-	-	-	0.23	0.23
1,2-Dimethyl-3-ethylbenzene	0.13	0.11	-	-	0.15	0.12	-	-
n-Undecane	0.15	0.15	0.16	0.16	0.06	0.06	0.07	0.07
Aromatic	0.01	0.01	-	-	-	-	-	-
1,2,4,5-Tetramethylbenzene	0.26	0.22	0.23	0.19	0.24	0.20	0.39	0.33
1,2,3,5-Tetramethylbenzene	0.37	0.31	0.32	0.27	0.33	0.28		
Unidentified C12's	0.09	0.09	-	-	-	-	0.23	0.26
Dodecane	0.21	0.20	0.15	0.15	0.05	0.05	-	-
C12 Paraffins	0.17	0.17	-	-	-	-	-	-
C10 Indanes	0.44	0.36	0.21	0.16	-	-	0.70	0.58
Naphthalene	0.39	0.24	0.31	0.20	0.55	0.34	0.63	0.40
C11 Indanes	0.61	0.50	-	-	-	-	1.10	0.91
C13 Paraffins	0.25	0.24	-	-	0.19	0.18	-	-
Tridecane	0.24	0.23	0.16	0.16				
C12 Aromatics	1.00	0.86	0.25(A)	0.25(A)	1.06	0.88	0.15	0.13
C12 Indanes	0.05	0.04	-	-	0.54	0.42	0.13	0.11
C14 + Paraffins	0.23	0.22	-	-	-	-	-	-
Methylnaphthalenes	0.83	0.61	0.64	0.48	0.69	0.45	0.93	0.69
C13 + Aromatics	0.21	0.18	-	-	-	-	-	-
Dimethylnaphthalenes	0.22	0.16	-	-	-	-	-	-

A = ADDITIVE of all C12 Aromatics

	PS-6		PS-6		API 91-01		API 91-01	
	1994 Analysis		1989 Analysis		1991 Analysis		1994 Analysis	
COMPONENT NAME	WT.%	LV%	WT.%	LV%	WT.%	LV%	WT.%	LV%
C10 Naphthene	0.02	0.02	-	-	-	-	-	-
C10 Paraffin	0.00	0.00	-	-	-	-	-	-
3,3-Dimethyloctane	0.07	0.07	-	-	-	-	-	-
n-Propylbenzene	0.54	0.46	0.51	0.44	0.75	0.65	0.77	0.67
1-Methyl-3-ethyl-benzene	2.03	1.72	2.15	1.84	2.34	2.01	2.26	1.95
1-Methyl-4-ethylbenzene	0.89	0.76	0.95	0.85	1.06	1.07	1.02	.088
C11 Paraffin	0.02	0.02	-	-	0.03	0.03	0.03	0.03
1,3,5-Trimethylbenzene	1.13	0.96	1.19	1.02	1.10	0.94	1.04	0.90
4-Methylnonane	0.15	0.15	0.26	0.26	0.11	0.11	0.05	0.05
2-Methylnonane	0.12	0.12	0.15	0.15	0.15	0.15	0.10	0.10
Paraffin	0.23	0.23	-	-	-	-	0.11	0.11
1-Methyl-2-ethylbenzene	0.62	0.52	0.67	0.56	0.72	0.61	0.66	0.56
3-Methylnonane	0.13	0.13	0.14	0.14	-	-	0.13	0.13
Paraffin	0.05	0.04	0.05	0.05	-	-	-	-
Paraffin	0.02	0.02	0.01	0.01	-	-	-	-
1,2,4-Trimethylbenzene	3.30	2.82	3.56	2.96	3.37	2.86	3.04	2.59
Naphthene + Olefin	0.03	0.03	-	-	-	-	-	-
Paraffin	0.02	0.02	-	-	-	-	-	-
C11 Aromatic	0.04	0.03	-	-	-	-	-	-
Unidentified C11's	0.11	0.11	-	-	-	-	0.19	0.19
n-Decane	0.16	0.16	0.13	0.13	-	-	0.05	0.05
Iso-Butylbenzene	0.03	0.02	-	-	-	-	0.04	0.03
Paraffin	0.01	0.01	-	-	-	-	-	-
1,2,3-Trimethylbenzene* + C10 Styrene	0.59	0.49	0.67	0.55	0.66*	0.57*	0.62*	0.52*
C11 Paraffin	0.02	0.02	0.04	0.04	-	-	0.02	0.02
C11 Paraffin	0.07	0.06	0.03	0.03	-	-	-	-
Indane	0.28	0.21	0.26	0.20	0.40	0.31	0.40	0.31
C11 Paraffin	0.14	0.14	0.03	0.03	0.06	0.05	0.02	0.02
Paraffin	0.18	0.17	-	-	-	-	-	-
C11 Paraffin	0.37	0.36	-	-	0.22	0.19	0.04	0.04
1,3-Diethylbenzene	0.14	0.12	* C11 paraffin 0.36	0.33	-	-	0.22	0.19
1-Methyl-3-n-propylbenzene	0.25	0.21	0.35	0.30	0.46	0.41	0.50	0.40
1-Methyl-4-n-propylbenzene	0.22	0.19	0.19	0.16	0.28	0.24	0.30	0.26
n-Butylbenzene	0.08	0.07	0.07	0.06	0.14	0.12	0.16	0.14

	PS-6		PS-6		API 91-01		API 91-01	
	1994 Analysis		1989 Analysis		1991 Analysis		1994 Analysis	
COMPONENT NAME	WT.%	LV%	WT.%	LV%	WT.%	LV%	WT.%	LV%
Unidentified Heavies	0.00	0.00	-	-	0.86	0.89	0.37	0.29
TOTALS	100.00	100.00	100.00	100.00	100.00	100.00	100.00	100.00

HYDROCARBON GROUPINGS								
Paraffins	53.02	57.80	52.79	57.69	41.01	46.38	43.9	49.41
Naphthenes	4.01	3.91	5.13	5.10	6.84	6.72	4.35	4.28
Aromatics	33.52	28.09	35.66	30.29	39.05	33.17	40.74	34.64
Olefins	9.12	9.88	6.22	6.72	11.74	12.47	9.44	10.18
Unknowns	0.33	0.33	0.20	0.20	1.36	1.26	1.56	1.47
Oxygenates	<0.01	<0.01	-	-	-	-	<.01	<.01
TOTALS	100.00	100.00	-	-	100	100	100.00	99.99

APPENDIX V

Time domain reflectometry and chemical analyses results from column experiment to evaluate gasoline residual saturation in Borden sand

LIST OF TABLES

Table V-1: Water saturation measured by TDR (time domain reflectometry) for sand column

Depth	Water Content (%P.V.)									
	9:30 Feb 2	13:36 Feb 2	17:30 Feb 2	19:20 Feb 2	21:07 Feb 2	6:40 Feb 3	8:40 Feb 3	20:00 Feb 3	10:20 Feb 7	2-27 Feb 27
0.075	0.4259	0.1847	0.1262	0.1132	0.1075	0.1019	0.1019	0.3647	0.3725	0.3699
0.125	0.4304	0.2246	0.1468	0.1276	0.1218	0.1103	0.1103	0.3751	0.3853	0.3803
0.175	0.4348	0.2914	0.1618	0.1513	0.1394	0.1218	0.1218	0.3777	0.3904	0.3828
0.225	0.4348	0.3853	0.1969	0.1694	0.1543	0.1394	0.1394	0.3777	0.3853	0.3853
0.275	0.4326	0.4121	0.1969	0.1634	0.1513	0.1394	0.1394	0.3751	0.3803	0.3777
0.325	0.4304	0.4191	0.2000	0.1694	0.1543	0.1513	0.1513	0.3725	0.3777	0.3777
0.375	0.4304	0.4282	0.2614	0.1969	0.1694	0.1694	0.1694	0.3751	0.3777	0.3777
0.425	0.4348	0.4304	0.2884	0.2246	0.1908	0.2031	0.2000	0.3803	0.3803	0.3803
0.475	0.4348	0.4326	0.2884	0.2308	0.2092	0.2246	0.2246	0.3803	0.3828	0.3828
0.525	0.4370	0.4326	0.2914	0.2400	0.2216	0.2400	0.2400	0.3828	0.3879	0.3828
0.575	0.4348	0.4304	0.3566	0.2644	0.2400	0.2704	0.2704	0.3904	0.3953	0.3879
0.625	0.4282	0.4259	0.4180	0.2793	0.2552	0.2914	0.2914	0.3828	0.3828	0.3803
0.675	0.4326	0.4304	0.4237	0.2914	0.2400	0.2854	0.2854	0.3928	0.3904	0.3853
0.725	0.4370	0.4348	0.4293	0.4074	0.3879	0.4002	0.4002	0.4098	0.4098	0.4121
0.775	0.4348	0.4326	0.4293	0.4121	0.4026	0.4098	0.4074	0.4145	0.4145	0.4168
0.825	0.4392	0.4413	0.4403	0.4145	0.4074	0.4121	0.4121	0.4214	0.4191	0.4191
0.875	0.4581	0.4581	0.4550	0.4282	0.4145	0.4168	0.4168	0.4214	0.4237	0.4237
0.925	0.4498	0.4498	0.4488	0.3308	0.4191	0.4145	0.4145	0.4168	0.4191	0.4191

Measured values of saturations were corrected for the total porosity of Borden sand (0.33)

Table V-2: Results of gas chromatography for BTEX

Depth (cm)	Sample ID#	Benzene (mg/l)	Toluene (mg/l)	Ethylbenzene (mg/l)	P-xylene (mg/l)	M-xylene (mg/l)	O-xylene (mg/l)
0	1012	83.39	365.01	62.52	67.81	159.92	80.64
	1013	104.10	447.04	75.96	82.81	194.31	97.71
	1014	94.83	410.12	70.47	76.67	180.52	90.10
	1016	72.55	313.92	54.33	59.35	139.70	72.19
5	1021	104.52	325.12	59.98	66.12	145.12	69.86
	1022	30.43	143.61	25.92	28.70	67.04	33.67
	1023	50.21	222.83	50.11	43.41	99.85	51.45
	1026	47.33	204.70	35.72	39.73	93.05	46.75
10	1031	87.03	368.30	63.96	72.12	169.26	83.67
	1032	106.43	375.59	82.87	74.53	164.50	81.41
	1033	83.23	354.91	60.42	64.82	154.04	78.26
	1036	46.12	199.34	33.69	36.84	90.73	43.55
15	1041	78.78	361.18	64.35	74.34	163.07	72.15
	1042	92.19	397.38	67.94	74.70	176.09	91.64
	1043	52.52	200.97	31.21	32.64	77.98	40.49
	1046	57.43	210.90	35.26	38.29	90.16	45.08
20	1051	79.56	364.39	62.58	69.34	163.61	82.58
	1052	94.42	361.88	89.35	107.87	165.00	83.69
	1053	93.43	399.92	68.26	74.28	175.02	86.02
	1056	43.44	185.50	32.34	35.21	82.95	42.22
25	1061	88.81	412.55	69.32	80.31	179.67	87.48
	1062	70.51	320.88	53.97	60.10	142.82	71.78
	1063	105.22	453.82	76.98	84.10	198.60	99.33
	1066	42.91	166.20	27.79	30.31	71.19	35.38
30	1071	109.42	425.18	76.68	106.02	228.99	95.50
	1072	65.41	294.52	51.84	57.86	134.02	70.97
	1073	68.72	295.43	49.24	53.53	126.24	62.31
	1076	42.65	166.73	25.75	30.35	71.24	36.06
35	1081	96.39	405.52	69.86	76.81	178.07	89.53
	1082	146.72	467.15	102.68	100.07	239.57	104.97
	1083	109.89	462.42	77.16	84.40	200.13	99.90
	1086	33.33	149.93	23.76	26.11	61.60	30.71
40	1091	111.22	400.69	77.84	74.21	173.65	89.56
	1092	170.38	415.92	92.48	98.16	200.06	91.25
	1093	92.22	364.58	60.94	66.07	155.65	76.63
	1096	42.15	174.91	29.82	32.39	75.99	38.52

Table V-2: Results of gas chromatography for BTEX (continued)

Depth (cm)	Sample ID#	Benzene (mg/l)	Toluene (mg/l)	Ethylbenzene (mg/l)	P-xylene (mg/l)	M-xylene (mg/l)	O-xylene (mg/l)
45	1101	127.91	363.09	91.98	109.86	174.98	85.45
	1102	90.76	295.04	49.90	55.25	134.39	66.77
	1103	52.21	194.86	31.29	33.97	79.54	39.82
	1107	59.94	213.97	33.60	36.61	85.12	42.90
50	1111	86.78	318.96	54.92	57.26	132.73	66.47
	1112	71.54	205.03	33.77	39.58	115.81	46.47
	1113	63.14	238.31	35.78	39.78	90.82	45.75
	1116	62.26	274.27	46.63	50.87	119.48	60.57
55	1121	42.56	187.37	32.91	35.79	84.89	42.15
	1122	60.73	242.41	40.40	44.47	103.03	52.06
	1123	50.54	166.67	25.80	28.33	66.85	33.84
	1126	60.82	272.91	47.59	52.08	126.17	63.07
60	1131	9.31	30.33	4.48	4.86	11.32	5.94
	1132	37.52	131.13	19.85	21.69	50.77	25.91
	1133	63.51	232.59	37.72	40.43	95.28	47.96
	1136	17.98	58.46	8.32	9.00	21.80	11.56
65	1141	37.74	152.84	24.06	26.47	61.70	31.09
	1142	30.84	113.31	18.80	19.67	46.10	24.39
	1143	47.02	186.72	29.67	32.25	75.34	38.04
	1146	47.62	234.06	43.35	47.29	110.73	55.60
70	1151	43.89	185.12	31.46	34.47	81.19	41.45
	1152	18.53	73.64	12.34	13.84	31.61	15.96
	1153	21.91	89.16	15.92	17.42	40.95	20.62
	1156	17.77	77.28	12.30	13.66	32.29	16.68
75	1161	21.72	76.59	11.96	12.90	29.90	14.84
	1162	16.95	62.77	9.37	10.29	24.32	12.48
	1163	6.88	25.60	3.73	4.43	11.10	5.19
80	1171	9.54	41.40	6.72	7.53	17.70	9.08
	1172	17.04	63.73	9.17	10.20	24.18	12.39
	1174	4.41	15.11	1.87	2.10	4.83	2.47
	1176	6.58	26.44	4.40	4.73	11.22	5.93
85	1181	5.27	22.78	2.83	2.93	6.90	3.76
	1183	4.66	18.24	2.55	2.83	6.63	3.57
	1184	5.04	16.61	2.03	1.93	5.28	2.76
	1186	2.94	13.06	2.28	2.30	5.46	2.89

Table V-3: BTEX concentration in pore water

Depth (cm)	Sample ID#	Bulk Soil (g)	Water in Bottle (ml)	Benzene (mg/l)	Toluene (mg/l)	Ethylbenzen (mg/l)	P-xylene (mg/l)	M-xylene (mg/l)	O-xylene (mg/l)
0	1012	3.13	15.91	2324.92	10176.29	1743.12	1890.54	4458.53	2248.11
	1013	3.55	15.66	2518.70	10816.18	1837.93	2003.49	4701.27	2364.16
	1014	3.44	15.36	2322.41	10043.98	1725.85	1877.60	4421.11	2206.50
	1016	2.97	16.02	2146.53	9287.37	1607.39	1755.90	4133.03	2135.61
5	1021	3.45	15.75	2617.21	8140.80	1501.86	1655.69	3633.68	1749.17
	1022	1.60	15.59	1626.14	7674.84	1385.39	1533.63	3582.74	1799.45
	1023	2.29	15.21	1829.01	8117.82	1825.45	1581.40	3637.46	1874.50
	1026	3.65	15.79	1123.12	4857.01	847.55	942.80	2207.95	1109.31
10	1031	3.63	15.82	2080.25	8803.71	1528.91	1723.89	4045.85	1999.92
	1032	3.56	15.78	2587.57	9131.44	2014.82	1811.97	3999.31	1979.27
	1033	3.51	15.92	2070.42	8829.13	1503.16	1612.50	3832.13	1946.79
	1036	2.76	15.63	1432.42	6191.54	1046.33	1144.38	2818.06	1352.75
15	1041	3.10	15.71	2189.89	10039.41	1788.55	2066.22	4532.63	2005.53
	1042	3.57	15.98	2263.49	9756.28	1667.91	1833.96	4323.28	2249.96
	1043	2.80	16.31	1678.03	6420.84	997.21	1042.77	2491.48	1293.77
	1046	3.03	15.87	1649.73	6058.69	1012.89	1099.91	2590.14	1294.92
20	1051	3.28	15.84	2107.45	9651.90	1657.64	1836.65	4333.61	2187.40
	1052	3.24	15.90	2541.56	9740.47	2405.07	2903.44	4441.20	2252.55
	1053	3.34	15.77	2419.53	10356.69	1767.73	1923.59	4532.38	2227.62
	1056	3.46	15.18	1045.38	4463.82	778.27	847.21	1996.12	1016.02
25	1061	3.73	16.00	2089.48	9706.27	1630.93	1889.49	4227.19	2058.19
	1062	3.86	15.78	1581.04	7194.92	1210.08	1347.64	3202.43	1609.47
	1063	3.83	15.22	2293.33	9891.50	1677.98	1833.05	4328.74	2164.96
	1066	2.66	16.20	1433.42	5551.61	928.43	1012.60	2377.90	1181.91
30	1071	3.95	15.34	2330.76	9056.65	1633.35	2258.23	4877.71	2034.28
	1072	3.25	15.77	1740.95	7838.51	1379.74	1539.92	3566.90	1888.87
	1073	3.12	16.42	1983.76	8527.87	1421.40	1545.23	3643.96	1798.71
	1076	3.41	15.94	1093.39	4274.78	660.32	778.19	1826.45	924.44
35	1081	3.30	14.77	2366.15	9955.02	1715.06	1885.53	4371.49	2197.92
	1082	3.84	15.85	3321.65	10575.88	2324.61	2265.54	5423.77	2376.55
	1083	3.75	15.01	2412.51	10151.97	1693.94	1852.81	4393.73	2193.21
	1086	2.52	16.78	1217.29	5475.61	867.65	953.71	2249.60	1121.41
40	1091	3.84	15.75	2502.07	9014.04	1751.03	1669.35	3906.54	2014.76
	1092	3.51	15.38	4094.89	9995.86	2222.70	2359.01	4808.20	2192.98
	1093	3.38	15.60	2334.49	9229.31	1542.61	1672.62	3940.13	1939.74
	1096	3.36	15.92	1095.31	4545.50	774.92	841.72	1974.75	1001.00

Table V-3: BTEX concentration in pore water (continued)

Depth (cm)	Sample ID#	Bulk Soil (g)	Water in Bottle (ml)	Benzene (mg/l)	Toluene (mg/l)	Ethylbenzen (mg/l)	P-xylene (mg/l)	M-xylene (mg/l)	O-xylene (mg/l)
45	1101	3.39	16.04	3319.47	9422.82	2387.11	2851.09	4541.07	2217.54
	1102	3.27	15.81	2406.94	7823.90	1323.22	1465.14	3563.91	1770.60
	1103	3.88	16.13	1190.51	4443.07	713.54	774.54	1813.56	908.02
	1107	3.77	14.91	1300.31	4641.52	728.91	794.16	1846.38	930.49
50	1111	3.39	15.52	2178.98	8009.27	1378.97	1437.79	3332.95	1669.11
	1112	3.34	15.78	1853.95	5313.05	875.17	1025.67	3000.98	1204.26
	1113	3.79	15.87	1450.15	5473.20	821.64	913.56	2085.87	1050.85
	1116	3.28	15.61	1625.13	7159.23	1217.15	1327.98	3118.80	1581.13
55	1121	2.96	15.77	1243.64	5475.24	961.59	1045.94	2480.70	1231.68
	1122	3.46	15.68	1509.60	6025.32	1004.26	1105.43	2560.86	1293.91
	1123	3.54	16.27	1273.93	4201.52	650.47	714.04	1685.07	852.97
	1126	3.32	15.60	1567.54	7033.39	1226.59	1342.30	3251.59	1625.53
60	1131	3.60	16.05	227.74	741.63	109.49	118.74	276.89	145.26
	1132	3.13	15.48	1017.81	3557.04	538.52	588.31	1377.21	702.77
	1133	3.38	15.81	1629.29	5967.18	967.64	1037.20	2444.46	1230.47
	1136	3.15	15.99	500.55	1627.61	231.60	250.55	607.01	321.90
65	1141	2.71	16.27	1242.79	5033.03	792.29	871.49	2031.87	1023.79
	1142	3.83	16.04	708.33	2602.71	431.95	451.86	1058.84	560.31
	1143	2.75	16.33	1531.39	6081.42	966.38	1050.25	2453.95	1239.11
	1146	3.55	15.59	1147.08	5637.71	1044.10	1139.05	2667.15	1339.23
70	1151	3.89	14.90	922.03	3889.23	660.95	724.21	1705.73	870.80
	1152	3.54	15.77	452.67	1799.41	301.61	338.12	772.28	389.89
	1153	3.90	15.77	486.02	1977.45	352.99	386.36	908.25	457.42
	1156	3.44	15.75	446.36	1940.73	308.82	343.07	810.81	418.80
75	1161	3.53	15.44	520.98	1837.40	286.92	309.54	717.42	356.04
	1162	4.01	15.66	362.98	1344.60	200.67	220.40	520.86	267.41
	1163	3.71	15.80	160.65	598.03	87.24	103.45	259.33	121.32
80	1171	3.64	15.45	222.21	963.74	156.43	175.40	412.15	211.37
	1172	3.70	15.12	381.92	1428.39	205.46	228.56	541.91	277.71
	1174	3.58	14.87	100.43	344.17	42.64	47.77	109.93	56.25
	1176	3.74	15.11	145.70	585.97	97.54	104.84	248.59	131.35
85	1181	2.54	15.26	173.66	750.50	93.23	96.44	227.39	123.84
	1183	3.87	15.52	102.59	401.11	56.15	62.15	145.79	78.56
	1184	3.91	15.98	112.98	372.41	45.60	43.35	118.37	61.77
	1186	1.79	16.06	144.79	642.77	112.02	113.00	268.55	142.35

ρ_b = bulk mass density (1.81 g/ml)

Table V-4: Volume of BTEX in pore space

Depth (cm)	Sample ID#	Benzene (ml)	Toluene (ml)	thylbenzen (ml)	P-xylene (ml)	M-xylene (ml)	O-xylene (ml)
0	1012	1.51E-03	6.70E-03	1.15E-03	1.22E-03	2.94E-03	1.46E-03
	1013	1.86E-03	8.08E-03	1.37E-03	1.47E-03	3.52E-03	1.74E-03
	1014	1.66E-03	7.27E-03	1.25E-03	1.34E-03	3.21E-03	1.57E-03
	1016	1.33E-03	5.80E-03	1.00E-03	1.08E-03	2.59E-03	1.31E-03
5	1021	1.88E-03	5.91E-03	1.09E-03	1.18E-03	2.64E-03	1.25E-03
	1022	5.41E-04	2.58E-03	4.66E-04	5.08E-04	1.21E-03	5.96E-04
	1023	8.71E-04	3.91E-03	8.79E-04	7.49E-04	1.76E-03	8.89E-04
	1026	8.53E-04	3.73E-03	6.51E-04	7.12E-04	1.70E-03	8.39E-04
10	1031	1.57E-03	6.72E-03	1.17E-03	1.29E-03	3.10E-03	1.50E-03
	1032	1.92E-03	6.84E-03	1.51E-03	1.33E-03	3.00E-03	1.46E-03
	1033	1.51E-03	6.52E-03	1.11E-03	1.17E-03	2.84E-03	1.42E-03
	1036	8.22E-04	3.59E-03	6.07E-04	6.54E-04	1.64E-03	7.73E-04
15	1041	1.41E-03	6.55E-03	1.17E-03	1.33E-03	2.96E-03	1.29E-03
	1042	1.68E-03	7.33E-03	1.25E-03	1.35E-03	3.26E-03	1.66E-03
	1043	9.77E-04	3.78E-03	5.87E-04	6.04E-04	1.47E-03	7.50E-04
	1046	1.04E-03	3.86E-03	6.45E-04	6.90E-04	1.66E-03	8.13E-04
20	1051	1.44E-03	6.66E-03	1.14E-03	1.25E-03	3.00E-03	1.49E-03
	1052	1.71E-03	6.64E-03	1.64E-03	1.95E-03	3.04E-03	1.51E-03
	1053	1.68E-03	7.27E-03	1.24E-03	1.33E-03	3.19E-03	1.54E-03
	1056	7.52E-04	3.25E-03	5.66E-04	6.07E-04	1.46E-03	7.28E-04
25	1061	1.62E-03	7.61E-03	1.28E-03	1.46E-03	3.33E-03	1.59E-03
	1062	1.27E-03	5.84E-03	9.82E-04	1.08E-03	2.61E-03	1.29E-03
	1063	1.83E-03	7.97E-03	1.35E-03	1.45E-03	3.50E-03	1.72E-03
	1066	7.93E-04	3.11E-03	5.19E-04	5.57E-04	1.33E-03	6.51E-04
30	1071	1.92E-03	7.52E-03	1.36E-03	1.85E-03	4.06E-03	1.66E-03
	1072	1.18E-03	5.36E-03	9.43E-04	1.04E-03	2.45E-03	1.27E-03
	1073	1.29E-03	5.60E-03	9.33E-04	9.98E-04	2.40E-03	1.16E-03
	1076	7.76E-04	3.07E-03	4.74E-04	5.49E-04	1.31E-03	6.53E-04
35	1081	1.62E-03	6.91E-03	1.19E-03	1.29E-03	3.04E-03	1.50E-03
	1082	2.65E-03	8.54E-03	1.88E-03	1.80E-03	4.39E-03	1.89E-03
	1083	1.88E-03	8.01E-03	1.34E-03	1.44E-03	3.48E-03	1.70E-03
	1086	6.38E-04	2.90E-03	4.60E-04	4.97E-04	1.20E-03	5.85E-04
40	1091	2.00E-03	7.28E-03	1.41E-03	1.33E-03	3.16E-03	1.60E-03
	1092	2.99E-03	7.38E-03	1.64E-03	1.71E-03	3.56E-03	1.59E-03
	1093	1.64E-03	6.56E-03	1.10E-03	1.17E-03	2.81E-03	1.36E-03
	1096	7.66E-04	3.21E-03	5.48E-04	5.85E-04	1.40E-03	6.97E-04

Table V-4: Volume of BTEX in pore space (continued)

Depth (cm)	Sample ID#	Benzene (mg/l)	Toluene (mg/l)	thylbenzen (mg/l)	P-xylene (mg/l)	M-xylene (mg/l)	O-xylene (mg/l)
45	1101	2.34E-03	6.72E-03	1.70E-03	2.00E-03	3.25E-03	1.56E-03
	1102	1.64E-03	5.38E-03	9.10E-04	9.91E-04	2.46E-03	1.20E-03
	1103	9.61E-04	3.63E-03	5.82E-04	6.22E-04	1.48E-03	7.30E-04
	1107	1.02E-03	3.68E-03	5.78E-04	6.20E-04	1.47E-03	7.27E-04
50	1111	1.54E-03	5.71E-03	9.83E-04	1.01E-03	2.38E-03	1.17E-03
	1112	1.29E-03	3.73E-03	6.15E-04	7.09E-04	2.11E-03	8.33E-04
	1113	1.14E-03	4.36E-03	6.55E-04	7.16E-04	1.67E-03	8.25E-04
	1116	1.11E-03	4.94E-03	8.40E-04	9.01E-04	2.16E-03	1.07E-03
55	1121	7.66E-04	3.41E-03	5.99E-04	6.41E-04	1.55E-03	7.55E-04
	1122	1.09E-03	4.38E-03	7.31E-04	7.91E-04	1.87E-03	9.27E-04
	1123	9.38E-04	3.13E-03	4.84E-04	5.23E-04	1.26E-03	6.25E-04
	1126	1.08E-03	4.91E-03	8.56E-04	9.22E-04	2.28E-03	1.12E-03
60	1131	1.71E-04	5.62E-04	8.29E-05	8.85E-05	2.10E-04	1.08E-04
	1132	6.63E-04	2.34E-03	3.54E-04	3.81E-04	9.09E-04	4.56E-04
	1133	1.15E-03	4.24E-03	6.88E-04	7.25E-04	1.74E-03	8.61E-04
	1136	3.28E-04	1.08E-03	1.53E-04	1.63E-04	4.03E-04	2.10E-04
65	1141	7.01E-04	2.87E-03	4.52E-04	4.89E-04	1.16E-03	5.75E-04
	1142	5.64E-04	2.10E-03	3.48E-04	3.58E-04	8.56E-04	4.45E-04
	1143	8.76E-04	3.52E-03	5.59E-04	5.98E-04	1.42E-03	7.06E-04
	1146	8.47E-04	4.21E-03	7.79E-04	8.37E-04	2.00E-03	9.85E-04
70	1151	7.46E-04	3.18E-03	5.41E-04	5.83E-04	1.40E-03	7.02E-04
	1152	3.33E-04	1.34E-03	2.25E-04	2.48E-04	5.77E-04	2.86E-04
	1153	3.94E-04	1.62E-03	2.89E-04	3.12E-04	7.47E-04	3.70E-04
	1156	3.19E-04	1.40E-03	2.23E-04	2.44E-04	5.88E-04	2.98E-04
75	1161	3.83E-04	1.36E-03	2.13E-04	2.26E-04	5.34E-04	2.60E-04
	1162	3.03E-04	1.13E-03	1.69E-04	1.83E-04	4.41E-04	2.22E-04
	1163	1.24E-04	4.67E-04	6.81E-05	7.94E-05	2.03E-04	9.32E-05
80	1171	1.68E-04	7.38E-04	1.20E-04	1.32E-04	3.17E-04	1.59E-04
	1172	2.94E-04	1.11E-03	1.60E-04	1.75E-04	4.23E-04	2.13E-04
	1174	7.48E-05	2.59E-04	3.21E-05	3.54E-05	8.30E-05	4.17E-05
	1176	1.13E-04	4.61E-04	7.67E-05	8.11E-05	1.96E-04	1.02E-04
85	1181	9.18E-05	4.01E-04	4.98E-05	5.07E-05	1.22E-04	6.52E-05
	1183	8.26E-05	3.26E-04	4.57E-05	4.98E-05	1.19E-04	6.30E-05
	1184	9.19E-05	3.06E-04	3.75E-05	3.51E-05	9.76E-05	5.00E-05
	1186	5.39E-05	2.42E-04	4.22E-05	4.19E-05	1.01E-04	5.28E-05

d_{benz} = 0.8765 mg/l $d_{p\text{-}xyl}$ = 0.8811 mg/l (after Poulsen, 1991)

d_{tol} = 0.8669 mg/l $d_{m\text{-}xyl}$ = 0.8642 mg/l

d_{ethz} = 0.8670 mg/l $d_{o\text{-}xyl}$ = 0.8802 mg/l

Table V-5: BTEX-based volume of gasoline in pore space

Depth (cm)	Sample ID#	Benzene based (ml)	Toluene based (ml)	thyibenzen based (ml)	P-xylene based (ml)	M-xylene based (ml)	O-xylene based (ml)
0	1012	7.27E-02	1.90E-01	7.31E-02	6.77E-02	7.23E-02	6.98E-02
	1013	8.93E-02	2.29E-01	8.74E-02	8.14E-02	8.65E-02	8.33E-02
	1014	7.98E-02	2.06E-01	7.95E-02	7.39E-02	7.88E-02	7.53E-02
	1016	6.37E-02	1.65E-01	6.39E-02	5.97E-02	6.36E-02	6.29E-02
5	1021	9.02E-02	1.68E-01	6.94E-02	6.53E-02	6.49E-02	5.99E-02
	1022	2.60E-02	7.34E-02	2.97E-02	2.81E-02	2.97E-02	2.86E-02
	1023	4.18E-02	1.11E-01	5.60E-02	4.14E-02	4.32E-02	4.26E-02
	1026	4.10E-02	1.06E-01	4.14E-02	3.94E-02	4.18E-02	4.02E-02
10	1031	7.54E-02	1.91E-01	7.43E-02	7.16E-02	7.61E-02	7.20E-02
	1032	9.20E-02	1.94E-01	9.61E-02	7.38E-02	7.38E-02	6.99E-02
	1033	7.26E-02	1.85E-01	7.07E-02	6.47E-02	6.97E-02	6.78E-02
	1036	3.95E-02	1.02E-01	3.87E-02	3.61E-02	4.03E-02	3.70E-02
15	1041	6.78E-02	1.86E-01	7.43E-02	7.33E-02	7.28E-02	6.17E-02
	1042	8.07E-02	2.08E-01	7.98E-02	7.49E-02	8.00E-02	7.97E-02
	1043	4.69E-02	1.07E-01	3.74E-02	3.34E-02	3.61E-02	3.59E-02
	1046	4.99E-02	1.10E-01	4.11E-02	3.81E-02	4.07E-02	3.89E-02
20	1051	6.91E-02	1.89E-01	7.28E-02	6.89E-02	7.36E-02	7.12E-02
	1052	8.23E-02	1.89E-01	1.04E-01	1.08E-01	7.46E-02	7.24E-02
	1053	8.07E-02	2.07E-01	7.91E-02	7.35E-02	7.84E-02	7.38E-02
	1056	3.61E-02	9.23E-02	3.61E-02	3.35E-02	3.58E-02	3.49E-02
25	1061	7.79E-02	2.16E-01	8.15E-02	8.06E-02	8.17E-02	7.62E-02
	1062	6.10E-02	1.66E-01	6.26E-02	5.95E-02	6.40E-02	6.16E-02
	1063	8.78E-02	2.26E-01	8.61E-02	8.03E-02	8.59E-02	8.23E-02
	1066	3.81E-02	8.83E-02	3.31E-02	3.08E-02	3.28E-02	3.12E-02
30	1071	9.20E-02	2.14E-01	8.64E-02	1.02E-01	9.98E-02	7.97E-02
	1072	5.65E-02	1.52E-01	6.01E-02	5.72E-02	6.01E-02	6.09E-02
	1073	6.18E-02	1.59E-01	5.94E-02	5.51E-02	5.89E-02	5.57E-02
	1076	3.73E-02	8.71E-02	3.02E-02	3.04E-02	3.23E-02	3.13E-02
35	1081	7.80E-02	1.96E-01	7.58E-02	7.12E-02	7.47E-02	7.20E-02
	1082	1.27E-01	2.43E-01	1.20E-01	9.95E-02	1.08E-01	9.05E-02
	1083	9.04E-02	2.28E-01	8.51E-02	7.95E-02	8.54E-02	8.16E-02
	1086	3.06E-02	8.25E-02	2.93E-02	2.75E-02	2.94E-02	2.80E-02
40	1091	9.60E-02	2.07E-01	9.01E-02	7.33E-02	7.77E-02	7.67E-02
	1092	1.44E-01	2.10E-01	1.04E-01	9.47E-02	8.74E-02	7.64E-02
	1093	7.88E-02	1.86E-01	6.98E-02	6.47E-02	6.90E-02	6.50E-02
	1096	3.68E-02	9.13E-02	3.49E-02	3.24E-02	3.44E-02	3.34E-02

Table V-5: BTEX-based volume of gasoline in pore space (continued)

Depth (cm)	Sample ID#	Benzene based (ml)	Toluene based (ml)	thylbenzen based (ml)	P-xylene based (ml)	M-xylene based (ml)	O-xylene based (ml)
45	1101	1.12E-01	1.91E-01	1.08E-01	1.11E-01	7.98E-02	7.46E-02
	1102	7.86E-02	1.53E-01	5.80E-02	5.48E-02	6.04E-02	5.74E-02
	1103	4.61E-02	1.03E-01	3.71E-02	3.44E-02	3.65E-02	3.50E-02
	1107	4.90E-02	1.05E-01	3.68E-02	3.42E-02	3.61E-02	3.48E-02
50	1111	7.38E-02	1.62E-01	6.26E-02	5.58E-02	5.85E-02	5.61E-02
	1112	6.19E-02	1.06E-01	3.92E-02	3.92E-02	5.19E-02	3.99E-02
	1113	5.49E-02	1.24E-01	4.17E-02	3.96E-02	4.10E-02	3.95E-02
	1116	5.33E-02	1.40E-01	5.35E-02	4.98E-02	5.30E-02	5.14E-02
55	1121	3.68E-02	9.69E-02	3.81E-02	3.54E-02	3.80E-02	3.62E-02
	1122	5.22E-02	1.25E-01	4.65E-02	4.38E-02	4.59E-02	4.44E-02
	1123	4.51E-02	8.89E-02	3.08E-02	2.89E-02	3.09E-02	3.00E-02
	1126	5.20E-02	1.40E-01	5.45E-02	5.10E-02	5.59E-02	5.35E-02
60	1131	8.19E-03	1.60E-02	5.28E-03	4.89E-03	5.16E-03	5.19E-03
	1132	3.18E-02	6.65E-02	2.26E-02	2.11E-02	2.23E-02	2.18E-02
	1133	5.50E-02	1.21E-01	4.38E-02	4.01E-02	4.28E-02	4.13E-02
	1136	1.58E-02	3.06E-02	9.77E-03	9.03E-03	9.91E-03	1.01E-02
65	1141	3.36E-02	8.15E-02	2.88E-02	2.70E-02	2.85E-02	2.75E-02
	1142	2.71E-02	5.96E-02	2.22E-02	1.98E-02	2.10E-02	2.13E-02
	1143	4.21E-02	1.00E-01	3.56E-02	3.30E-02	3.50E-02	3.38E-02
	1146	4.07E-02	1.20E-01	4.96E-02	4.63E-02	4.91E-02	4.72E-02
70	1151	3.58E-02	9.04E-02	3.44E-02	3.22E-02	3.44E-02	3.36E-02
	1152	1.60E-02	3.81E-02	1.43E-02	1.37E-02	1.42E-02	1.37E-02
	1153	1.89E-02	4.61E-02	1.84E-02	1.72E-02	1.84E-02	1.77E-02
	1156	1.53E-02	3.99E-02	1.42E-02	1.35E-02	1.45E-02	1.43E-02
75	1161	1.84E-02	3.88E-02	1.36E-02	1.25E-02	1.31E-02	1.25E-02
	1162	1.45E-02	3.22E-02	1.08E-02	1.01E-02	1.08E-02	1.06E-02
	1163	5.95E-03	1.33E-02	4.34E-03	4.39E-03	4.98E-03	4.47E-03
80	1171	8.08E-03	2.10E-02	7.63E-03	7.30E-03	7.77E-03	7.63E-03
	1172	1.41E-02	3.16E-02	1.02E-02	9.67E-03	1.04E-02	1.02E-02
	1174	3.59E-03	7.36E-03	2.04E-03	1.96E-03	2.04E-03	2.00E-03
	1176	5.44E-03	1.31E-02	4.89E-03	4.48E-03	4.82E-03	4.87E-03
85	1181	4.41E-03	1.14E-02	3.17E-03	2.80E-03	2.99E-03	3.12E-03
	1183	3.97E-03	9.28E-03	2.91E-03	2.75E-03	2.92E-03	3.02E-03
	1184	4.41E-03	8.70E-03	2.39E-03	1.94E-03	2.40E-03	2.40E-03
	1186	2.59E-03	6.88E-03	2.69E-03	2.31E-03	2.49E-03	2.53E-03

Table V-6: BTEX-based gasoline saturation (in % of the pore volume)

Depth (cm)	Sample ID#	Benzene based (%PV)	Toluene based (%PV)	thylbenzen based (%PV)	P-xylene based (%PV)	M-xylene based (%PV)	O-xylene based (%PV)	Average (%PV)
0	1012	12.74	33.36	12.81	11.86	12.67	12.23	15.94
	1013	13.80	35.46	13.50	12.57	13.36	12.86	16.93
	1014	12.73	32.92	12.68	11.78	12.56	12.01	15.78
	1016	11.76	30.44	11.81	11.02	11.74	11.62	14.73
5	1021	14.34	26.69	11.03	10.39	10.33	9.52	13.72
	1022	8.91	25.16	10.18	9.62	10.18	9.79	12.31
	1023	10.02	26.61	13.41	9.92	10.34	10.20	13.42
	1026	6.15	15.92	6.23	5.92	6.27	6.04	7.75
10	1031	11.40	28.86	11.23	10.82	11.50	10.88	14.11
	1032	14.18	29.93	14.80	11.37	11.36	10.77	15.40
	1033	11.35	28.94	11.04	10.12	10.89	10.59	13.82
	1036	7.85	20.30	7.69	7.18	8.01	7.36	9.73
15	1041	12.00	32.91	13.14	12.96	12.88	10.91	15.80
	1042	12.40	31.98	12.25	11.51	12.29	12.24	15.45
	1043	9.20	21.05	7.33	6.54	7.08	7.04	9.71
	1046	9.04	19.86	7.44	6.90	7.36	7.05	9.61
20	1051	11.55	31.64	12.18	11.52	12.31	11.90	15.18
	1052	13.93	31.93	17.67	18.22	12.62	12.26	17.77
	1053	13.26	33.95	12.99	12.07	12.88	12.12	16.21
	1056	5.73	14.63	5.72	5.32	5.67	5.53	7.10
25	1061	11.45	31.82	11.98	11.85	12.01	11.20	15.05
	1062	8.66	23.59	8.89	8.45	9.10	8.76	11.24
	1063	12.57	32.42	12.33	11.50	12.30	11.78	15.48
	1066	7.85	18.20	6.82	6.35	6.76	6.43	8.74
30	1071	12.77	29.69	12.00	14.17	13.86	11.07	15.59
	1072	9.54	25.69	10.14	9.66	10.14	10.28	12.57
	1073	10.87	27.95	10.44	9.69	10.36	9.79	13.18
	1076	5.99	14.01	4.85	4.88	5.19	5.03	6.66
35	1081	12.97	32.63	12.60	11.83	12.42	11.96	15.73
	1082	18.20	34.67	17.08	14.21	15.41	12.93	18.75
	1083	13.22	33.28	12.44	11.62	12.49	11.93	15.83
	1086	6.67	17.95	6.37	5.98	6.39	6.10	8.25
40	1091	13.71	29.55	12.86	10.47	11.10	10.96	14.78
	1092	22.44	32.77	16.33	14.80	13.66	11.93	18.66
	1093	12.79	30.25	11.33	10.49	11.20	10.55	14.44
	1096	6.00	14.90	5.69	5.28	5.61	5.45	7.16

Table V-6: BTEX-based gasoline saturation (in % of the pore volume) - continued

Depth (cm)	Sample ID#	Benzene based (%PV)	Toluene based (%PV)	thylbenzen based (%PV)	P-xylene based (%PV)	M-xylene based (%PV)	O-xylene based (%PV)	
45	1101	127.91	363.09	91.98	109.86	174.98	85.45	158.88
	1102	90.76	295.04	49.90	55.25	134.39	66.77	115.35
	1103	52.21	194.86	31.29	33.97	79.54	39.82	71.95
	1107	59.94	213.97	33.60	36.61	85.12	42.90	78.69
50	1111	86.78	318.96	54.92	57.26	132.73	66.47	119.52
	1112	71.54	205.03	33.77	39.58	115.81	46.47	85.37
	1113	63.14	238.31	35.78	39.78	90.82	45.75	85.60
	1116	62.26	274.27	46.63	50.87	119.48	60.57	102.35
55	1121	42.56	187.37	32.91	35.79	84.89	42.15	70.95
	1122	60.73	242.41	40.40	44.47	103.03	52.06	90.52
	1123	50.54	166.67	25.80	28.33	66.85	33.84	62.00
	1126	60.82	272.91	47.59	52.08	126.17	63.07	103.77
60	1131	9.31	30.33	4.48	4.86	11.32	5.94	11.04
	1132	37.52	131.13	19.85	21.69	50.77	25.91	47.81
	1133	63.51	232.59	37.72	40.43	95.28	47.96	86.25
	1136	17.98	58.46	8.32	9.00	21.80	11.56	21.19
65	1141	37.74	152.84	24.06	26.47	61.70	31.09	55.65
	1142	30.84	113.31	18.80	19.67	46.10	24.39	42.18
	1143	47.02	186.72	29.67	32.25	75.34	38.04	68.17
	1146	47.62	234.06	43.35	47.29	110.73	55.60	89.77
70	1151	43.89	185.12	31.46	34.47	81.19	41.45	69.60
	1152	18.53	73.64	12.34	13.84	31.61	15.96	27.65
	1153	21.91	89.16	15.92	17.42	40.95	20.62	34.33
	1156	17.77	77.28	12.30	13.66	32.29	16.68	28.33
75	1161	21.72	76.59	11.96	12.90	29.90	14.84	27.99
	1162	16.95	62.77	9.37	10.29	24.32	12.48	22.70
	1163	6.88	25.60	3.73	4.43	11.10	5.19	9.49
80	1171	9.54	41.40	6.72	7.53	17.70	9.08	15.33
	1172	17.04	63.73	9.17	10.20	24.18	12.39	22.78
	1174	4.41	15.11	1.87	2.10	4.83	2.47	5.13
	1176	6.58	26.44	4.40	4.73	11.22	5.93	9.88
85	1181	5.27	22.78	2.83	2.93	6.90	3.76	7.41
	1183	4.66	18.24	2.55	2.83	6.63	3.57	6.41
	1184	5.04	16.61	2.03	1.93	5.28	2.76	5.61
	1186	2.94	13.06	2.28	2.30	5.46	2.89	4.82

Table V-7: Depth-averaged BTEX-based gasoline saturation (in % of the pore volume)

Depth (cm)	Final average (%PV)
0	15.85
5	11.80
10	13.27
15	12.64
20	14.07
25	12.63
30	12.00
35	14.64
40	13.76
45	11.30
50	10.33
55	8.97
60	4.58
65	7.53
70	3.79
75	1.92
80	1.26
85	0.78

APPENDIX VI

TDR - time domain reflectometry and CPN - water moisture content probe measurements during the field experiment

LIST OF TABLES

Table VI - 1

TDR - CPN Access Tube C2U6

TDR measurements for various depths at different dates

Depth (m b.g.s.)	TDR Measurement (water content)									
	Sep. 28A	Sep. 28B	Oct. 03	Oct. 05	Oct. 06A	Oct. 06B	Oct. 11	Oct. 13	Oct 18	Oct. 30
6			16.28	15.61	15.62	15.79	21.75	15.38	20.12	24.72
16			14.7	14	14.38	13.69	23.95	25.55	25.27	25.59
26			15.04	14.54	12.61	13.67	23.07	23.01	23.56	33.05
36			18.23	14.59	15.88	14.7	27.6	27.05	27.36	33.99
46			18.6	15.68	15.55	15.33	32.01	35	32.94	38.78
56			18.83	15.82	16.81	16.18	34.02	33.9	35.24	38.24
66			23	15.88	15.02	17.78	36.92	37.27	37.92	40.28
76			32.17	16.6	18.49	19.07		35.36	35.38	38.64
86			36.82	19.34	21.44	23.67		38.14	38.52	39.3
96			43.37	23.12	21.61	24.02	37.1	38.66	39.8	39.47
106			43.75	24.77	17.37	20.07	36.55	38.91	42.11	40.86
116			45.56	34.01	15.81	19.29	40.92	41.36		39.56
126			43.26	43.42	23.59	26.6	35.65	41.87		41.03
136			45.34	45.11	30.02	36.57	43.13	42.71	42.88	45.05
146			45.39	45.23	45.56	15.62	44.96	43.41	46.29	
156			43.99	43.69	43.39		41.69	47.51	44.58	
166			43.91	43.3	43.2		15.79	43.72	15.38	20.12
176			15.61	45.76	46.11					
186				41.09	40.58					
196				45.56	16.28					

Table VI - 1

TDR - CPN Access Tube C2U6

TDR measurements for various depths at different dates (continued)

Depth (m b.g.s.)	TDR Measurement (water content)								
	Nov. 08	Nov. 10	Nov. 17	Nov. 19	Nov. 21	Nov. 23	Nov. 25	Nov. 27	Nov. 29
6	25.8		26.62	25.17	22.63	26.5	25.88	27.31	25.97
16	25.68		25.02	25.94	26.07	25.42	28.58	27.73	28.73
26	16.88		20.27	21.06	20.92	23.03	23.88	22.93	23.34
36	17.19		25.29	25.34	27.48	27.12	25.73	29.68	27.1
46	28.27		31.5	30.23	29.76	26.83	29.14	43.62	27.87
56	36.98		33.71	33.16	28.97	28.88	27.1	7.76	28.42
66	35.86		34.12	31.54	30.34	24.54	26.03	24.99	21.12
73.5	43.53		40.01	42.43	40.2	35.86	29.59	27.36	33.55
78.5	35.88		40.58	39.09	36.24	37.84	27.72	35.2	28.41
83.5	41.19		37.28	37.43	37.95	37.59	41.02	29.57	25.71
88.5	37.84		42.22	42.9	34.09	35.69	34.58	32.26	41.42
93.5	39.07		36.29	35.59	44.61	39.48	37.97	36.75	35.68
98.5	39.96		41.1	42	39.63	43.76	44.59	41.53	34.96
103.5	37.27		42	41.66	42.27	38.85	41.62	43.58	33.33
108.5	40.34	35.94	42.29	40.68	41.38	38.85	38.3	37.68	48.64
113.5	37.51	40.63	37.68	39.08	38.5	46.24	38.87	33.49	40.02
118.5	54.12	44.5	40.47	41.15	38.5	38.39	43.34	48.35	40.75
123.5	901.24	33.89	41.34	43.68	42.94	40.77	38.38	38.2	36.96
128.5	33.05	52.41	50.62	49.58	52.07	47.74	52.03	53.5	50.98
136	35.63	41.98	44.04	42.96	42.71	44.93	43.92	42.86	45.1
146	37.91	47.08	46.6	45.67	45.34	44.77	46.11	44.95	44.84
156	38.55	43.22	45.26	44.82	45.79	44	45.34	45.36	44.83

Table VI - 1

TDR - CPN Access Tube C2U6

TDR measurements for various depths at different dates (continued)

Depth (m b.g.s.)	TDR Measurement (water content)								
	Dec. 01	Dec.04	Dec. 06	Dec. 08	Dec. 10	Dec. 12	Dec. 15	Dec. 17	Dec. 19
6	27.84	28.76	28	28.44	28.98	28.02		25.53	25.82
16	30.84	29.04	29.2	31.04	31.74	28.8	24.7	22.74	21.96
26	24.14	25.24	25.71	25.1	25.71	25.13	30.31	26.51	26.44
36	29.05	26.97	26.81	26.68	25.82	26.29	24.26	25.14	25.65
46	23.76	26.45	26.33	26.76	26.88	26.91	25.38	27.59	23.13
56	31.46	27.41	25.78	26.56	26.47	23.93	28.78	27.45	28
66	18.6	28.32	27	25.6	22.54	23.78	14.89	19.02	18.61
73.5	26.89				25.86	27.48	32.31	30.47	30.87
78.5	41.44	28.47		28.24	23.66	5.48	4.02	16.65	10.69
83.5	18.45				24.65	39.24	52.55	32.04	15.32
88.5	50.7	32.21		25.3	27.03	24.4	4.69	3.71	47.3
93.5	23.94				22.84	39.92	30.42	52.23	-5.3
98.5	28.18	33.66	28.1	26.53	31.38	14.71	39.48	16.56	44.14
103.5	31.24				24.79	20.41	30.44	10.31	47.96
108.5	46.95	34.4	29.37	31	27.13	26.91	16.41	42.83	34.75
113.5	26.45				30	27.86	36.38	30.23	16.55
118.5	49.06	39.8	40.53	33.14	33.41	42.79	25.99	14.06	17.42
123.5	44.87				41.13	42.98	28.93	38.75	31.54
128.5	49.21	38.54	36.45	36.12	47.19	31.66	46.99	44	56.23
136	43.37	44.89	43.88	42.98	39.77	41.57	39	37.67	25.89
146	45.89	46.11	48.39	46.9	45.61	48.23	42.87	41.25	42.24
156	46.57	44.02	42.85	42.74	45.18	42.63	44.06	45.26	43.32

Table VI - 1

TDR - CPN Access Tube C2U6

TDR measurements for various depths at different dates (continued)

Depth (m b.g.s.)	TDR Measurement (water content)								
	Dec. 24	Dec. 26	Dec. 28	Dec. 30	Jan. 02	Jan. 15	Jan. 17	Jan. 19	Jan. 25
6		25.15	20.93	20.05	16.34	21.73	21.9	23.27	22.46
16	24.63	25.06	23.28	20.74	14.71	17.92	21.17	23.08	20.36
26	25.17	26.26	24.48	23.75	21.12	25.74	23.08	23.05	6.02
36	25.63	26.05	22.87	25.62	24.08	23.23	24.45	23.59	
46	24.38	28.53	27.85	28.65	26.63	24.55	24.22	27.19	
56	28.34	27.7	27.72	27.39	26.43	24.86	25.76	26.3	26.01
66	26.63	19.48	15.07	20	20.19	23.44	22.14	20.46	21.43
73.5	14.76	30.1	36.04	28.33	22.24	31.94	26.26	29.91	26.72
78.5	37.66	26.46	37.11	28.77	32.45	23.34	28.7	22.27	34.97
83.5	40.06	28.4	19.86	30.52	19.14	30.96	26.59	36.31	39.82
88.5	18.04	24.13	30.06	23.13	21.59	19.4	35.05	40.68	45.37
93.5	16.47	25.03	27.37	30.7	24.7	35.7	36.6	43.79	38.44
98.5	49.43	31.58	20.8	24.45	28.74	30.4	40.55	39.35	41.41
103.5	24.52	25.15	28.36	23.45	27.99	35.06	42.38	42.34	45.72
108.5	36.01	30.07	29.44	34.5	28.29	53.43	42.89	43.05	43.15
113.5	34.79	29.98	31.34	28.08	29.53	35.1	41.66	42.53	40.86
118.5	33.57	26.87	37.2	35.92	45.93	35.53	40.82	41.64	38.28
123.5	34.68429	41.33	27.38	37.5	43.84	40.24	38.38	40.05	42.05
128.5	35.79857	49.09	61.99	52.35	44.51	55.73	52.7	52.03	52.04
136	37.47	43.34	42.13	41.82	41.72	42.51	42.61	43.34	43.28
146	37.9	43.18	42.26	45.79	45.59	44.09	46.08	44.79	43.41
156	45.13	43.97	44.93	43.45	46.1	47.67	43.78	46.69	45.79

Table VI - 2 **TDR - CPN Access Tube C2U7**

TDR measurements for various depths at different dates

Depth (m b.g.s.)	TDR Measurement (water content)									
	Sep. 28A	Sep. 28B	Oct. 03	Oct. 05	Oct. 06A	Oct. 06B	Oct. 11	Oct. 13	Oct 18	Oct. 30
2.8	29.72	28.29	29.66	28.89	13.37	28.72	0.94	30.12	28.65	22.99
12.8	17.45	17.04	15.18	15.23	17.91	13.33	41.84	21.16	21.34	23.59
22.8	22.89	19.56	17.77	14.32	24.25	15.22	42.9	22.04	20.87	30.02
32.8	28.73	23.1	18.19	16.82	11.52	16.12	21.56	26.12	29.75	38.54
42.8	29.62	30.25	18.05	15.34	15.09	14.9	33.88	36.28	37.25	41.67
52.8	30.93	30.51	18.15	14.82	14.51	15.94		40.8	39.97	42.12
62.8	30.54	31.05	22.87	16.17	16.26	16.67		40.54	42.23	42.31
72.8	30.92	30.12	29.3	18.69	17.89	19.12		40.69	41.02	40.8
82.8	38.61	39.79	39.98	20.77	25.31	29.53	36.43	39.53	38.5	39.36
92.8	44.43	43.67	43.08	26.34	33.56	40.35	40.59	40.46	40.34	41.58
102.8	45.12	44.27	44.91	29.06	36.64	39.7	41.65	40.73	40.64	41.08
112.8		44.64	43.5	36.07	40.28	41.17	41.84	41.94	41.19	41.81
122.8		44.86	47.14	43.86	44.04	45.56	45.39	44.35	44.18	44.73
132.8			44.93	45.4	46.45	42.65	45.48	42.13	43.79	42.9
142.8			43.34	47.13	44.47		46.04	45.48	44.89	44.93
152.8			48.85	41.23	45.99		44.45	44.43	44.67	43.92
162.8			39.65	47.88	45.77					
172.8				44.63	45.77					
182.8				44.94	44.34					
192.8				46.77						

Table VI - 2 **TDR - CPN Access Tube C2U7**

TDR measurements for various depths at different dates (continued)

Depth (m b.g.s.)	TDR Measurement (water content)								
	Nov. 08	Nov. 10	Nov. 17	Nov. 19	Nov. 21	Nov. 23	Nov. 25	Nov. 27	Nov. 29
2.8	21.34	18.61	20.87	19.4	21.29	19.39	18.6	18.97	16.22
12.8	25.4	28.44	23.8	23.35	20.47	22.95	21.15	20.81	21
22.8	32.78	33.08	21.66	19.96	19.47	19.29	20.59	18.92	19.97
32.8	39.35	39.85	19.42	19.98	21.01	22.62	23.45	24.52	24.78
42.8	43.9	42.52	27.17	28.23	29.39	28.57	29.3	27.36	28.03
52.8	40.63	43.11	37.32	34.66	30.76	29.7	29.63	27.5	28.78
62.8	42.96	42.13	41.44	40.03	37.38	31.38	29.89	30.62	29.15
72.8	41.48	41.4	42.38	41.29	41.79	38.41	34.14	31.72	30.4
82.8	38.01	38.92	40.1	40.66	39.98	39.06	37.17	32	32.27
92.8	42.34	40.92	40.77	41.7	41.04	40.06	39.21	38.15	34.52
102.8	41.74	41.77	41.52	40.88	41.31	41.12	42.89	40.01	39.01
112.8	40.8	42.94	44.37	42.34	43.03	41.99	43.04	43.1	42.65
122.8	46.49	41.87	43.04	43.79	44.83	45.9	44.71	43.51	45.18
132.8	42.02	45.79	41.73	43.9	42.68	43.25	42.47	44.72	43.46
142.8	45.41	45.76	46.21	45.21	46.8	45.84	44.46	44.89	45.52
152.8	44.82	41.4	44.67	44.4	43.78	44.76	46.12	44.68	42.34

Table VI - 2 **TDR - CPN Access Tube C2U7**

TDR measurements for various depths at different dates (continued)

Depth (m b.g.s.)	TDR Measurement (water content)								
	Dec. 01	Dec.04	Dec. 06	Dec. 08	Dec. 10	Dec. 12	Dec. 15	Dec. 17	Dec. 19
2.8	19.72	18.32	19.43	17.36	16.95	16.6	15.46	16.5	17.15
12.8	19.66	19.9	19.01	18.7	20.96	19.4	20.18	21.2	23.73
22.8	22.05	21.92	21.74	25.52	21.95	23.14	24.05	24.1	23.47
32.8	23.16	23.3	26.69		27.09	27.03	25.38	26.9	24.5
42.8	27.66	27.45	27.91		27.97	26.09	28.47	26.71	25.51
52.8	27.04	29.27	26.67	27.23	27.96	27.17	26.93	28.71	31.28
62.8	29.11	28.3	30.37	29.03	27.15	31.42	21.36	25.05	20.1
72.8	30.73	28.03	26.65	28.61	28.08	24.3	29.99	27.56	29.63
82.8	31.41	28.84	27.97	27.14	26.08	26.69	25.93	26.82	
92.8	36.19	32.83	26.45	27.07	28.75	29.78	27.76	26.68	
102.8	36.17	33.24	32.51	29.76	26.59	28.48	25.79	27.39	25.61
112.8	39.49	39.16	38.59	32.38	29.48	28.46	27.94	24.79	24.05
122.8	44.19	43.39	41.48	39.42	35.9	37.02	32.17	31.88	33.48
132.8	44.31	43.67	40.81	41.08	39.6	38.58	33.63	25.93	30.15
142.8	43.74	44.47	45.04	45.41	43.76	41.05	42.62	44.04	35.81
152.8	44.71	44.51	43.52	43.9	43.33	44.07	43.75	40.05	38.86

Table VI - 2 **TDR - CPN Access Tube C2U7**

TDR measurements for various depths at different dates (continued)

Depth (m b.g.s.)	TDR Measurement (water content)								
	Dec. 24	Dec. 26	Dec. 28	Dec. 30	Jan. 02	Jan. 15	Jan. 17	Jan. 19	Jan. 25
2.8	15.41	13.05	13.2	13.73	13.59	9.86	10.1	23.27	8.93
12.8	22.48	23.53	18.62	15.53	12.1	14.53	15.02	23.08	16.37
22.8	24.75	24.58	25.8	20.94	14.41	21.18	22.82	23.05	22.93
32.8	26.56	26.61	24.01	24.92	23.32	24.19	24.51	23.59	24.42
42.8	26.64	26.4	26.7	26.43	25.16	25	27.04	27.19	25.82
52.8	28.07	27.39	27.06	25.77	28.74	26.54	23.95	26.3	24.51
62.8	25.57	24.14	28.62	26.62	23.06	25.31	24.17	27.38	28.61
72.8	25.3	28.79	23.49	27.07	19.07	26.86	28.44	28.83	27.71
82.8	27.96	25.65	27.9	26.37	32.51	26.37	27.24	37.09	34.35
92.8	26.75	27.16	27.93	27.41	25		34.04	41.44	41.66
102.8	27.38	25.07	20.67	25.32	29.39		38.61	43.2	41.36
112.8	18.94	28.54	30.11	30.67	23.52	42.47	42.39	42.33	43.04
122.8	39.1	33.56	38.59	39.38	41.01	42.22	44.61	40.28	43.5
132.8	29.32	40	42.48	41.33	37.71	45.03	43.35	43.34	43.86
142.8	48.27	43.27	43.33	43.37	39.34	45.66	44.53	44.79	45.13
152.8	36.15	43.36	43.51	44.2	46.91	44.27	44.96	46.69	43.62

Table VI - 3

TDR - CPN Access Tube C2U9

TDR measurements for various depths at different dates

Depth (m b.g.s.)	TDR Measurement (water content)									
	Sep. 28A	Sep. 28B	Oct. 03	Oct. 05	Oct. 06A	Oct. 06B	Oct. 11	Oct. 13	Oct 18	Oct. 30
6.4			21.74	22.41	20.66	20.83	35.83	34.4	30.6	32.28
16.4			18.88	17.48	18	16.83	21.33	21.74	23.2	22
26.4			16.52	16.18	14.91	15.49	19.64	21.2	21.65	26.08
36.4			16.54	15.09	14.74	14.7	27.39	25.77	25.29	32.07
46.4			17.03	15.14	15.8	15.29	32.4	34.6	34.61	32.48
56.4			21.48	16.08	15.8	16.4		41.51	41.66	21.52
66.4			26.28	16.39	16.03	17.94		38.73	40.43	32.33
76.4			33.29	17.54	19.48	21.32		40.93	40.45	40.02
86.4			39.26	23.8	24.25	31.02	37.49	39.85	40.26	41.12
96.4			42.79	22.89	33.01	39.48	40.3	42.99	42.44	43.09
106.4			47.35	30.72	39.32	40.75	43.06	43.35	44.1	
116.4			45.11	32.01	40.97	40.86	42.94	44.28	43.66	
126.4			45.54	43.83	44.26	45.69	43.87	44.6	44.45	44.56
136.4			45.85	45.96	44.8	44.66	45.18	43.84	45.79	44.97
146.4			46.25	46.21	46.35		47.01	46.9	45.21	45.89
156.4			45.39	44.81	44.2		46.51		46.02	
166.4			45.08	46.16	45.55					
176.4				45.68	47.06					
186.4				44.94	44.55					
196.4				47.55						

Table VI - 3

TDR - CPN Access Tube C2U9

TDR measurements for various depths at different dates (continued)

Depth (m b.g.s.)	TDR Measurement (water content)								
	Nov. 08	Nov. 10	Nov. 17	Nov. 19	Nov. 21	Nov. 23	Nov. 25	Nov. 27	Nov. 29
6.4	32.34	32.09	34.83	33.12	35.52	34.06	31.28	33.27	31.59
16.4	22.57	23.85	24.29	26.13	24.02	25.28	29.5	29.01	30.38
26.4	20.96	23.03	22.97	21.02	20.74	21.71	25.45	28.17	28.06
36.4	17.79	21.62	25.37	26.58	25.25	25.72	25.26	30.13	29.3
46.4	23.04	24.65	31.09	29.48	28.69	26.86	27.18	31.87	30.21
56.4	33.36	28.59	30.07	31.34	29.6	27.99	27.97	29.05	30.71
66.4	35.82	32.19	37.02	32.95	31.6	29.89	26.12	29.37	27.63
76.4	38.51	34.05	39.86	37.29	34.96	31.61	31.77	31.66	30.67
86.4	42.25	39.69	41.09	40.53	38.57	37.13	35.2	34.93	32.59
96.4	41.51	40.93	44.4	41.78	40.45	39.78	39.52	38.63	37.75
106.4	44.71	42.42	43.87	43.61	43.11	42.73	43.8	43.66	40.73
116.4	42.34	43.7	43.68	43.71	45.3	44.34	44.38	44.44	42.02
126.4	44.95	46.07	45.81	46.27	44.82	44.76	44.67	44.45	46.06
136.4	45.08	44.47	46.6	46.31	45.88	45.01	45.21	45.59	44.93
146.4	45.2	45.85	45.27	46.89	46.09	47.31	46	45.81	47.2
156.4	44.67	44.88	45.94	44.74	45.15	44.98	45.63	47.77	45.38

Table VI - 3 **TDR - CPN Access Tube C2U9**

TDR measurements for various depths at different dates (continued)

Depth (m b.g.s.)	TDR Measurement (water content)								
	Dec. 01	Dec.04	Dec. 06	Dec. 08	Dec. 10	Dec. 12	Dec. 15	Dec. 17	Dec. 19
6.4	32.05	34.22	28.72	32.04	32.13	28.93	28.19	31.56	31.27
16.4	27.55	24.61	24.76	24.91	22.6	21.48	27.13	27.65	21.53
26.4	29.99	26.24	27.27	27.38	25.71	27.92	24.75	23.68	29.75
36.4	27.59	26.38	28.59	26.57	25.95	22.95	29.66	26	17.31
46.4	31.43	30.54	28.64	25.78	27.88	22.06	26.16	24.67	31.65
56.4	30.57	26.92	25.93	29.79	29.09	33.81	20.21	26.51	21.55
66.4	26.33	28.06	27.96	26.56	26.42	22.66	30.8	24.55	26.65
76.4	30.27	31.81	27.77	25.49	27	33.51	21.51	25.48	23.47
86.4	31.38	29.24	29.88	25.72	26.44	22.78	24.16	26.98	30.15
96.4	37.88	32.71	25.26	29.04	26.19	31.72	28.42	24.17	24.65
106.4	39.22	35.16	34.44	27.82	30.2	25.76	25.11	25.58	24.2
116.4	45.7	43.03	40.02	37.45	33.28	32.18	33.04	32.34	30.44
126.4	42.18	43.9	42.84	38.68	36.96	35.15	34.02	30.43	30.75
136.4	47.5	45.39	42.15	42.11	42.45	43.27	33.5	35.03	34.69
146.4	43.73	45.87	46.56	45.86	45.77	44.9	43.57	40.56	35.68
156.4	49.14	45.11	46.67	47.43	47.13	48.4	47.62	44.18	40.78

Table VI - 3 **TDR - CPN Access Tube C2U9**

TDR measurements for various depths at different dates (continued)

Depth (m b.g.s.)	TDR Measurement (water content)								
	Dec. 24	Dec. 26	Dec. 28	Dec. 30	Jan. 02	Jan. 15	Jan. 17	Jan. 19	Jan. 25
6.4	26.89	24.92	22.28	21.52	21.51	18.68	18.47	19.2	17.06
16.4	23.64	22.73	19.62	16.61	13.34	17.44	17.75	22.47	19.61
26.4	23.66	23.77	21.26	20.92	16.89	21.91	23.52	24.08	23.33
36.4	23.49	24.82	25.81	24.37	15.57	23.89	24.14	24.4	25.04
46.4	25.48	24.57	27.55	24.8	29.48	26.04	26.25	24.64	24.24
56.4	24.96	26.76	26.5	25.51	25.88	25.34	25.46	24.92	26.93
66.4	26.28	24.92	22.35	25.42	21.78	24.22	25.06	28.67	27.77
76.4	21.31	25.93	28.36	25.5	26.38	25.5	26.51	27.73	29.43
86.4	30.69	25.91	22.45	27.94	29.01	31.89	32.52	33.15	39.24
96.4	26.17	29.17	32.22	27.2	31.51	33.42	38.64	41.58	42.08
106.4	31.42	29.26	27.3	28.17	22.85	40.87	43.83	43.67	44.95
116.4	28.15	30.95	33.75	33.03	31.87	45.04	45.9	45.83	44.22
126.4	45.24	45.98	45.72	44.81	33.84	46.67	44.35	46.42	46.53
136.4	46.15	45.84	47.59	45.92	-0.74	45.67	45.59	44.73	45.43
146.4	44.47	46.17	43.13	45.86	121.15	45.64	47.3	46.55	45.6
156.4	43.55	44.07	45.06	45.03	41.61	44.96	45.57	45.22	46.12

Table VI - 4

TDR - CPN Access Tube C2U6

Neutron Counts for various depths at different dates

Depth (m b.g.s.)	Neutron Count Sept. 28 11am	Depth (m b.g.s.)	Neutron Count Sept. 28 5pm	Depth (m b.g.s.)	Neutron Count Oct. 3 9am	Depth (m b.g.s.)	Neutron Count Oct. 5 7pm	Depth (m b.g.s.)	Neutron Count Oct. 6 6am	Depth (m b.g.s.)	Neutron Count Oct. 6 3pm
6.4	7628	6.4	6357	6.4	3996	6.4	3354	6.4	3174	6.4	3182
16.4	8444	16.4	7822	16.4	4335	16.4	3231	16.4	3294	16.4	3265
26.4	8726	26.4	8395	26.4	4963	26.4	3314	26.4	3341	26.4	3237
36.4	8683	36.4	8803	36.4	6093	36.4	3476	36.4	3484	36.4	3553
46.4	8755	46.4	8976	46.4	7240	46.4	3554	46.4	3590	46.4	3962
53.9	8970	53.9	9114	53.9	8068	56.4	3609	56.4	3804	56.4	4256
58.9	8999	58.9	9295	58.9	8693	66.4	3731	66.4	4387	58.9	4548
63.9	9301	63.9	9360	63.9	8886	76.4	4236	76.4	6102	63.9	5003
68.9	9207	68.9	8943	68.9	9034	86.4	5246	86.4	7835	68.9	6055
73.9	9196	73.9	9199	73.9	9060	93.9	6581	93.9	8294	73.9	7047
78.9	9261	78.9	9108	78.9	9267	98.9	7610	98.9	8562	78.9	7638
86.4	9194	83.9	9310	83.9	9245	103.9	8244	103.9	8715	83.9	8082
96.4	9186	88.9	9317	88.9	9238	108.9	8997	108.9	8745	88.9	8321
106.4	9287	93.9	9084	93.9	9267	113.9	8982	113.9	8901	93.9	8365
116.4	8925	98.9	9105	98.9	9186	118.9	9073	118.9	8894	98.9	8473
		106.4	9233	103.9	9343	123.9	8849	123.9	8963	103.9	8834
		116.4	9102	108.9	9274	128.9	9098	128.9	8967	108.9	8821
		126.4	8657	113.9	9059	133.9	8600	133.9	8876	113.9	9065
		136.4	8573	118.9	9084	138.9	8688	138.9	8563	121.4	9199
				123.9	8835	143.9	8609	143.9	8427	131.4	8753
				128.9	8729	148.9	8835	148.9	8497	141.4	8544
				136.4	8607	153.9	8800	156.4	9015	151.4	8647
				146.4	8648	158.9	8979	166.4	9066	161.4	9197
				156.4	9258	163.9	9060	176.4	9019		
						171.4	9123				
						181.4	9222				
						191.4	8975				

Table VI - 4

TDR - CPN Access Tube C2U6

Neutron Counts for various depths at different dates (continued)

Depth (m b.g.s.)	Neutron Count Oct. 11 12pm	Neutron Count Oct. 13 9:30am	Neutron Count Oct. 18	Neutron Count Oct. 30	Neutron Count Nov. 8	Neutron Count Nov. 10	Neutron Count Nov. 17	Neutron Count Nov. 19	Neutron Count Nov. 21	Neutron Count Nov. 23
6.4	4533	4654	4807	4510	4473	4612	4673	4777	4661	4808
16.4	5667	5822	4528	4995	4716	5007	5389	5312	5410	6077
26.4	6921	7271	4281	5404	4384	4807	6076	5612	6024	7463
36.4	7863	7940	5371	6850	5060	6185	7441	7243	7307	8148
46.4	8010	8033	6961	7934	6873	7848	8134	8126	8167	8162
56.4	8116	8087	7977	8128	7983	8166	8394	8419	8198	8428
66.4	8321	8506	8114	8358	8192	8440	8315	8221	8194	8494
73.9	8494	8390	8078	8258	8323	8211	8283	8400	8419	8279
78.9	8587	8529	8155	8419	8307	8452	8358	8304	8421	8527
83.9	8488	8476	8320	8379	8411	8494	8495	8462	8626	8655
88.9	8496	8426	8437	8623	8549	8562	8677	8550	8672	8595
93.9	8606	8672	8532	8496	8650	8702	8693	8684	8466	8651
98.9	8820	8825	8414	8552	8763	8657	8894	8607	8483	8665
103.9	9176	8923	8498	8607	8575	8537	8456	8513	8568	8588
108.9	9023	9156	8419	8759	8836	8573	8514	8550	8581	8736
113.9	9140	9132	8680	8643	8857	8707	8590	8724	8758	8896
118.9	9137	9189	8681	8887	8753	8852	8874	8707	8707	8790
123.9	9082	9077	8899	8782	8987	8966	8866	8690	8886	8839
131.4	8897	8897	9215	8971	9028	9008	9199	9045	9157	9039
141.4	8811	8697	9112	9103	9152	9048	9241	9118	9225	9117
151.4	8506	8708	8899	8843	8987	8762	8747	8635	8810	8723
161.4	9114	8861	8544	8672	8706	8855	8823	8583	8609	8819

Table VI - 4

TDR - CPN Access Tube C2U6

Neutron Counts for various depths at different dates (continued)

Depth (m b.g.s.)	Neutron Count Nov.25	Neutron Count Nov. 27	Neutron Count Oct. 29	Neutron Count Dec. 01	Neutron Count Dec. 04	Neutron Count Dec. 06	Neutron Count Dec. 08	Neutron Count Dec. 10	Neutron Count Dec. 12	Neutron Count Dec. 15
6.4	4924	4716	4902	4938	4739	4982	5111	4820	4956	5193
16.4	6186	5638	5939	6220	6045	6494	6654	6689	6640	8675
26.4	7138	6621	6910	7162	7210	7513	7672	7586	7749	7851
36.4	7873	7857	7821	8113	7870	8132	8092	7893	7995	8140
46.4	8150	8143	8300	8310	8234	8101	8310	8247	8095	8200
56.4	8151	8268	8390	8367	8292	8293	8293	8290	8357	8283
66.4	8469	8361	8313	8312	8422	8277	8373	8335	8305	8404
73.9	8487	8273	8364	8280	8301	8440	8168	8318	8311	8466
78.9	8381	8451	8446	8489	8269	8237	8359	8345	8510	8367
83.9	8402	8516	8543	8488	8624	8351	8667	8511	8388	8410
88.9	8558	8619	8685	8715	8543	8566	8376	8355	8588	8679
93.9	8695	8724	8725	8743	8706	8647	8613	8626	8471	8770
98.9	8668	8721	8663	8708	8690	8663	8689	8504	8635	8678
103.9	8567	8407	8661	8715	8622	8592	8652	8414	8544	8623
108.9	8797	8588	8648	8709	8710	8588	8637	8575	8670	8656
113.9	8592	8740	8830	8698	8802	8656	8821	8651	8534	8774
118.9	8853	8726	8801	8768	8838	8750	8884	8787	8903	8715
123.9	8888	8812	8881	8985	8880	8854	9148	8864	9030	8764
131.4	9258	9169	9179	9039	9087	8946	9084	9128	9217	9063
141.4	9058	9137	8941	9108	9128	9097	9021	9071	9121	9174
151.4	8847	8903	8862	8973	9059	8888	8934	8980	8964	9003
161.4	8497	8626	8787	8716	8682	8648	8700	8631	8631	8542

Table VI - 4

TDR - CPN Access Tube C2U6

Neutron Counts for various depths at different dates (continued)

Depth (m b.g.s.)	Neutron Count Dec. 17	Neutron Count Dec. 20	Neutron Count Dec. 24	Neutron Count Dec. 26	Neutron Count Dec. 28	Neutron Count Dec. 30	Neutron Count Jan. 02	Neutron Count Jan. 15	Neutron Count Jan. 17	Neutron Count Jan. 19
6.4	5502	5475	5191	5038	4366	3949	3505	3495	3613	4025
16.4	7447	7755	7469	7331	6285	5291	4220	5211	5820	7001
26.4	8084	8066	7968	7904	7707	6586	5015	6965	7247	7681
36.4	8088	8117	8137	7972	8148	7903	6862	7955	7928	7935
46.4	8250	8196	8350	8309	8302	8256	8033	8252	8172	8154
56.4	8334	8400	8271	8455	8450	8387	8247	8340	8356	8330
66.4	8368	8293	8290	8287	8391	8321	8274	8355	8442	8454
73.9	8360	8450	8302	8435	8166	8469	8442	8409	8568	8480
78.9	8444	8512	8493	8437	8371	8253	8420	8579	8427	8371
83.9	8543	8483	8514	8444	8336	8636	8492	8604	8583	8541
88.9	8749	8456	8579	8701	8564	8637	8484	8754	8387	8661
93.9	8670	8825	8635	8558	8759	8715	8853	8669	8746	8813
98.9	8664	8452	8726	8733	8611	8717	8777	8751	8653	8813
103.9	8648	8671	8611	8600	8684	8606	8595	8610	8785	8592
108.9	8536	8708	8581	8480	8710	8519	8718	8853	8697	8646
113.9	8730	8627	8631	8665	8806	8737	8586	8819	8774	8679
118.9	8740	8784	8686	8617	9031	8961	8775	8893	8773	8680
123.9	9008	8828	8940	8832	9035	8862	8873	8955	8863	8823
131.4	8998	8935	9037	9264	9280	9038	9272	9227	9103	9082
141.4	9118	9158	9036	9159	9209	9079	8990	9051	9021	9038
151.4	8824	8895	8995	8835	8788	8931	9010	8716	8868	8868
161.4	8643	8702	8610	8678	8692	8920	8739	8720	8564	8842

Table VI - 5

TDR - CPN Access Tube C2U7

Neutron Counts for various depths at different dates

Depth (m b.g.s.)	Neutron Count Sept. 28 11am	Depth (m b.g.s.)	Neutron Count Sept. 28 5pm	Depth (m b.g.s.)	Neutron Count Oct. 3 9am	Depth (m b.g.s.)	Neutron Count Oct. 5 7pm	Depth (m b.g.s.)	Neutron Count Oct. 6 6am	Depth (m b.g.s.)	Neutron Count Oct. 6 3pm
2.8	6579	2.8	5238	2.8	3528	2.8	3218	2.8	3249	2.8	3119
12.8	8127	12.8	6659	12.8	3859	12.8	3074	12.8	3036	12.8	2979
22.8	8414	22.8	7956	22.8	4505	22.8	3097	22.8	3097	22.8	3080
32.8	8536	32.8	8488	32.8	5367	32.8	3318	32.8	3202	32.8	3408
42.8	8557	42.8	8585	42.8	7143	42.8	3504	42.8	3455	42.8	3841
50.3	8626	50.3	8694	50.3	8110	52.8	3642	52.8	3856	52.8	4278
55.3	8996	55.3	8846	55.3	8505	62.8	3873	62.8	4127	55.3	4770
60.3	8931	60.3	8979	60.3	8733	72.8	4019	72.8	5117	60.3	5575
65.3	8920	65.3	9008	65.3	8958	82.8	4378	82.8	6837	65.3	6273
70.3	9089	70.3	9168	70.3	8951	90.3	5110	90.3	7964	70.3	7066
75.3	9165	75.3	9054	75.3	9221	95.3	5559	95.3	8413	75.3	7785
82.8	9331	80.3	9166	80.3	9205	100.3	6743	100.3	8776	80.3	8161
92.8	9158	85.3	9314	85.3	9285	105.3	8043	105.3	8996	85.3	8328
102.8	9408	90.3	9211	90.3	9312	110.3	8724	110.3	9311	90.3	8459
112.8	9404	95.3	9378	95.3	9353	115.3	9329	115.3	9488	95.3	8747
		102.8	9321	100.3	9473	120.3	9474	120.3	9405	100.3	8774
		112.8	9395	105.3	9419	125.3	9376	125.3	9253	105.3	9185
		122.8	9219	110.3	9216	130.3	9199	130.3	9301	110.3	9342
		132.8	8913	115.3	9272	135.3	9187	135.3	9077	117.8	9317
				120.3	9213	140.3	8913	140.3	8919	127.8	9144
				125.3	9143	145.3	9068	145.3	8836	137.8	8992
				132.8	8879	150.3	8791	152.8	8709	147.8	9122
				142.8	8932	155.3	8922	162.8	9189	157.8	8875
				152.8	8741	160.3	9020	172.8	9448		
						167.8	9120				
						177.8	9522				
						187.8	9459				

Table VI - 5

TDR - CPN Access Tube C2U7

Neutron Counts for various depths at different dates (continued)

Depth (m b.g.s.)	Neutron Count Oct. 11 12pm	Neutron Count Oct. 13 9:30am	Neutron Count Oct. 18	Neutron Count Oct. 30	Neutron Count Nov. 8	Neutron Count Nov. 10	Neutron Count Nov. 17	Neutron Count Nov. 19	Neutron Count Nov. 21	Neutron Count Nov. 23
2.8	3936	4044	2037	1657	1741	1932	2006	1352	1963	1851
12.8	4935	5137	4966	5125	5188	5569	5396	5100	5280	5078
22.8	6478	6640	4157	5252	5210	5929	5254	4894	5040	4982
32.8	7564	7851	4854	6339	5554	7075	6658	6109	6351	6611
42.8	8000	7786	6163	7731	7080	7878	7824	7633	7826	7889
52.8	7979	8092	7725	8282	7878	8349	8287	8188	8221	8144
62.8	8212	8221	8005	8140	8351	8102	8190	8249	8035	8074
70.3	8354	8320	8151	8082	8164	8104	8148	8228	8063	8158
75.3	8357	8286	8188	8106	7964	8202	8073	8105	8193	8202
80.3	8297	8402	8240	8255	8101	8172	8361	8198	8244	8260
85.3	8441	8492	8238	8170	8366	8244	8343	8140	8368	8499
90.3	8383	8608	8225	8270	8374	8377	8521	8449	8399	8294
95.3	8554	8676	8315	8492	8393	8511	8557	8494	8500	8494
100.3	8925	8920	8398	8469	8374	8281	8513	8612	8449	8467
105.3	9223	8913	8432	8525	8544	8517	8408	8558	8633	8392
110.3	9210	9270	8444	8549	8487	8617	8507	8649	8407	8630
115.3	9188	9169	8469	8704	8492	8705	8825	8748	8576	8678
120.3	9228	9419	8836	8910	8687	8762	8905	8823	8854	8630
127.8	9397	9175	9164	8945	8971	8995	9084	8825	9091	9038
137.8	8976	8966	9277	9216	9305	9471	9601	9257	9227	9235
147.8	8756	9009	9144	9404	9361	9324	9418	9210	9215	9278
157.8	8979	8774	9188	9127	9026	9155	9150	9154	9093	9016

Table VI - 5

TDR - CPN Access Tube C2U7

Neutron Counts for various depths at different dates (continued)

Depth (m b.g.s.)	Neutron Count Nov.25	Neutron Count Nov. 27	Neutron Count Oct. 29	Neutron Count Dec. 01	Neutron Count Dec. 04	Neutron Count Dec. 06	Neutron Count Dec. 08	Neutron Count Dec. 10	Neutron Count Dec. 12	Neutron Count Dec. 15
2.8	1933	2011	1967	1973	1862	1920	1748	1799	1680	1537
12.8	5284	5191	5080	5411	5154	5149	5174	5055	5125	5092
22.8	5744	5161	5527	5770	5615	6093	6403	6474	6612	6852
32.8	7319	6789	7100	7534	7503	7654	7884	7818	7977	7796
42.8	8102	8165	8100	8271	8414	8436	8134	8219	8286	8284
52.8	8421	8399	8459	8232	8334	8399	8273	8324	8276	8376
62.8	8089	7992	8137	8077	8448	8126	7964	8103	8260	8052
70.3	8363	7980	8077	8156	8241	8091	8064	8298	8238	8180
75.3	8211	8075	8150	8047	8093	8200	7983	8359	8044	8196
80.3	8355	8393	8129	8203	8147	8261	8266	8427	8375	8396
85.3	8591	8200	8341	8330	8371	8371	8391	8430	8355	8330
90.3	8567	8446	8476	8360	8478	8510	8568	8419	8375	8302
95.3	8504	8509	8571	8521	8450	8457	8433	8383	8485	8525
100.3	8561	8392	8582	8519	8525	8495	8572	8524	8556	8548
105.3	8534	8554	8424	8703	8800	8492	8374	8508	8535	8666
110.3	8556	8550	8433	8730	8707	8671	8618	8589	8727	8650
115.3	8488	8738	8548	8708	8680	8698	8688	8640	8590	8612
120.3	8707	8576	8677	8894	9001	8798	8912	8667	8897	8849
127.8	9089	9211	9146	9083	8984	8958	9066	9151	9080	9128
137.8	9262	9588	9352	9416	9284	9374	9371	9246	9419	9339
147.8	9278	9473	9284	9354	9091	9250	9408	9308	9282	9382
157.8	9047	8962	8988	9159	9070	9184	9093	9071	9098	8998

Table VI - 5

TDR - CPN Access Tube C2U7

Neutron Counts for various depths at different dates (continued)

Depth (m b.g.s.)	Neutron Count Dec. 17	Neutron Count Dec. 20	Neutron Count Dec. 24	Neutron Count Dec. 26	Neutron Count Dec. 28	Neutron Count Dec. 30	Neutron Count Jan. 02	Neutron Count Jan. 15	Neutron Count Jan. 17	Neutron Count Jan. 19
2.8	1677	1525	1425	1372	1252	1103	1015	856	849	857
12.8	5987	6434	5717	5431	4434	3637	3126	3021	3072	3953
22.8	7468	7908	7412	7418	6242	4942	3569	5288	5641	6730
32.8	8030	8143	8137	8253	7753	7030	5506	7365	7428	8026
42.8	8330	8256	8144	8164	8149	8167	7664	8177	8183	8100
52.8	8422	8440	8179	8479	8028	8205	8454	8405	8234	8294
62.8	8078	8103	8067	8049	8173	8129	8106	8239	8192	8174
70.3	8183	8093	8063	8009	8194	8095	8176	8111	8254	7935
75.3	8115	8201	8088	8150	8167	8396	8085	8137	8256	8107
80.3	8289	8364	8322	8250	8305	8435	8282	8444	8205	8274
85.3	8361	8376	8377	8417	8422	8399	8335	8257	8484	8481
90.3	8637	8426	8574	8369	8500	8506	8363	8341	8594	8479
95.3	8402	8523	8297	8354	8635	8455	8477	8445	8526	8523
100.3	8472	8351	8532	8731	8517	8484	8390	8801	8392	8553
105.3	8608	8785	8684	8519	8652	8480	8485	8591	8639	8498
110.3	8545	8520	8632	8722	8497	8692	8588	8679	8572	8613
115.3	8651	8643	8623	8663	8473	8657	8770	8762	8664	8667
120.3	8680	8732	8599	8749	8618	8850	8843	8822	8800	8791
127.8	9092	9103	9080	9033	8906	8924	9013	9061	9106	9116
137.8	9369	9359	9205	9379	9377	9389	9498	9169	9165	9364
147.8	9316	9437	9379	9423	9260	9574	9318	9281	9170	9423
157.8	9063	9057	9075	9177	9238	9231	9071	8925	9034	8971

Table VI - 6

TDR - CPN Access Tube C2U9

Neutron Counts for various depths at different dates

Depth (m b.g.s.)	Neutron Count Sept. 28 11am	Depth (m b.g.s.)	Neutron Count Sept. 28 5pm	Depth (m b.g.s.)	Neutron Count Oct. 3 9am	Depth (m b.g.s.)	Neutron Count Oct. 5 7pm	Depth (m b.g.s.)	Neutron Count Oct. 6 6am	Depth (m b.g.s.)	Neutron Count Oct. 6 3pm
6.4	6912	6.4	5689	6.4	3856	6.4	3426	6.4	3409	6.4	3524
16.4	7724	16.4	6505	16.4	3994	16.4	3326	16.4	3306	16.4	3338
26.4	8134	26.4	7614	26.4	4527	26.4	3193	26.4	3192	26.4	3208
36.4	8191	36.4	8241	36.4	5756	36.4	3331	36.4	3180	36.4	3273
46.4	8333	46.4	8324	46.4	6519	46.4	3378	46.4	3233	46.4	3533
53.9	8691	53.9	8464	53.9	7348	56.4	3324	56.4	3410	56.4	3808
58.9	8754	58.9	8869	58.9	7838	66.4	3617	66.4	3863	58.9	4110
63.9	9018	63.9	8962	63.9	8154	76.4	3877	76.4	4924	63.9	4698
68.9	9200	68.9	9156	68.9	8650	86.4	4757	86.4	6903	68.9	5337
73.9	9076	73.9	9014	73.9	8841	93.9	5665	93.9	8165	73.9	6097
78.9	9083	78.9	9160	78.9	9001	98.9	6319	98.9	8580	78.9	6946
86.4	9216	83.9	9254	83.9	9067	103.9	7301	103.9	8690	83.9	7594
96.4	9347	88.9	9353	88.9	9134	108.9	8169	108.9	8939	88.9	8035
106.4	9538	93.9	9356	93.9	9171	113.9	8969	113.9	9148	93.9	8512
116.4	9086	98.9	9354	98.9	9507	118.9	9216	118.9	9349	98.9	8549
		106.4	9412	103.9	9455	123.9	8919	123.9	9177	103.9	8773
		116.4	9056	108.9	9578	128.9	8975	128.9	9061	108.9	9157
		126.4	8782	113.9	9138	133.9	8878	133.9	8927	113.9	9442
		136.4	8762	118.9	9171	138.9	8721	138.9	8783	121.4	9204
				123.9	8833	143.9	8809	143.9	8807	131.4	8945
				128.9	8721	148.9	8799	148.9	8873	141.4	8893
				136.4	8680	153.9	8795	156.4	8796	151.4	8794
				146.4	8822	158.9	8817	166.4	8857	161.4	8782
				156.4	8904	163.9	8879	176.4	9000		
						171.4	8861				
						181.4	8961				
						191.4	9664				

Table VI - 6

TDR - CPN Access Tube C2U9

Neutron Counts for various depths at different dates (continued)

Depth (m b.g.s.)	Neutron Count Oct. 11 12pm	Neutron Count Oct. 13 9:30am	Neutron Count Oct. 16	Neutron Count Oct. 30	Neutron Count Nov. 8	Neutron Count Nov. 10	Neutron Count Nov. 17	Neutron Count Nov. 19	Neutron Count Nov. 21	Neutron Count Nov. 23
6.4	4477	4508	3313	3024	2856	2944	2921	3111	3161	3164
16.4	4896	5216	5248	5245	5316	5374	5734	5640	5677	5788
26.4	5810	6076	4502	5035	4801	5179	5811	5572	5918	6006
36.4	7292	7610	4765	6002	4854	5966	7286	6913	7297	7403
46.4	7613	7799	5760	6903	5822	7231	8139	7902	8158	8164
56.4	7928	7760	7233	7572	7517	7776	8192	8256	8166	8143
66.4	7955	8012	7921	7782	8034	8191	7950	8278	8323	8062
73.9	8236	8438	7953	7841	8057	8194	8148	8026	8106	8134
78.9	8537	8456	7901	8058	8341	8179	8327	8052	8204	8326
83.9	8366	8544	8078	8079	8196	8234	8168	8322	8291	8317
88.9	8509	8552	8248	8284	8330	8232	8367	8423	8310	8480
93.9	8346	8427	8410	8346	8448	8487	8470	8612	8549	8471
98.9	8462	8488	8464	8338	8461	8524	8659	8584	8606	8779
103.9	8938	8904	8426	8461	8565	8744	8641	8649	8531	8475
108.9	8956	9081	8637	8661	8818	8504	8675	8673	8441	8736
113.9	9351	9360	8589	8644	8643	8690	8567	8578	8627	8578
118.9	9260	9443	8552	8795	8651	8680	8793	8640	8587	8635
123.9	9269	9242	8730	8802	8638	8815	8710	8795	8820	8891
131.4	8983	8957	8950	8888	9073	9058	9168	9272	9159	9220
141.4	9020	8748	9247	9385	9240	9431	9446	9382	9314	9237
151.4	8768	8829	9222	9032	8993	9014	9109	8884	9102	9088
161.4	8709	8842	8781	8785	8836	8803	8794	8875	8664	8830

Table VI - 6

TDR - CPN Access Tube C2U9

Neutron Counts for various depths at different dates (continued)

Depth (m b.g.s.)	Neutron Count Nov.25	Neutron Count Nov. 27	Neutron Count Oct. 29	Neutron Count Dec. 01	Neutron Count Dec. 04	Neutron Count Dec. 06	Neutron Count Dec. 08	Neutron Count Dec. 10	Neutron Count Dec. 12	Neutron Count Dec. 15
6.4	3306	3139	3121	3234	3066	3249	3018	2996	2994	3038
16.4	6000	5998	6164	6271	5961	6378	6528	6443	6460	6488
26.4	6765	6475	6511	6663	6724	7208	7386	7290	7369	7438
36.4	8054	7674	7698	7870	7987	7894	7927	7888	8009	7938
46.4	8123	8135	8198	8221	8236	8015	8051	8140	8009	8082
56.4	8039	8136	8214	8270	8088	8156	8174	8172	8111	8106
66.4	7975	7898	8085	8015	8108	7883	8208	8186	8242	7920
73.9	7966	7931	8012	8088	8205	7970	8078	8046	8092	7982
78.9	8155	8067	8242	8179	8297	8199	8125	7916	8145	8026
83.9	8248	8257	8390	8350	8267	8294	8135	8249	8193	8186
88.9	8377	8355	8303	8351	8377	8333	8227	8433	8324	8259
93.9	8543	8623	8428	8514	8521	8466	8343	8646	8564	8277
98.9	8478	8750	8622	8657	8630	8451	8636	8609	8352	8526
103.9	8691	8714	8735	8704	8629	8524	8684	8499	8689	8625
108.9	8603	8459	8653	8679	8645	8649	8589	8584	8614	8525
113.9	8575	8576	8647	8755	8729	8841	8700	8518	8560	8601
118.9	8559	8540	8643	8676	8785	8716	8696	8683	8803	8567
123.9	8831	8837	8767	8876	8920	9048	8988	8760	8738	8764
131.4	9078	9190	9203	9099	9313	9011	9350	9354	9229	9147
141.4	9361	9449	9341	9377	9423	9441	9403	9436	9457	9524
151.4	9011	9142	8935	9018	9282	9069	9037	9022	8961	9218
161.4	8691	8797	8743	8869	8851	8743	8823	8797	8704	8657

Table VI - 6

TDR - CPN Access Tube C2U9

Neutron Counts for various depths at different dates (continued)

Depth (m b.g.s.)	Neutron Count Dec. 17	Neutron Count Dec. 20	Neutron Count Dec. 24	Neutron Count Dec. 26	Neutron Count Dec. 28	Neutron Count Dec. 30	Neutron Count Jan. 02	Neutron Count Jan. 15	Neutron Count Jan. 17	Neutron Count Jan. 19
6.4	3154	3247	2808	2701	2451	2265	2176	1699	1590	1812
16.4	7112	7393	6907	6719	5867	5042	4189	4386	4596	5636
26.4	7840	7931	7747	7722	7087	5920	4481	6289	6732	7386
36.4	7984	8256	7977	8009	7829	7627	6104	7740	7904	7881
46.4	8159	8011	7822	8154	8014	8005	7734	8105	8187	7972
56.4	8171	8072	8130	8034	8183	8035	8043	8222	8181	8228
66.4	8107	8079	7850	7912	8108	8072	8060	7994	8019	8012
73.9	7966	8042	8110	8114	8048	8016	7988	8107	8014	8064
78.9	8055	8101	8117	7907	8252	8103	8159	8176	8198	8090
83.9	8228	8112	8323	8223	8281	8354	8387	8322	8283	8229
88.9	8283	8280	8406	8256	8320	8348	8341	8294	8356	8332
93.9	8473	8467	8362	8583	8491	8372	8415	8403	8642	8622
98.9	8557	8581	8528	8392	8595	8538	8532	8644	8785	8652
103.9	8486	8654	8436	8663	8453	8435	8417	8662	8657	8686
108.9	8573	8452	8630	8632	8634	8625	8651	8787	8719	8617
113.9	8683	8608	8582	8632	8465	8634	8527	8768	8619	8765
118.9	8629	8435	8841	8659	8587	8681	8795	8592	8550	8589
123.9	8772	8939	8799	8810	8774	8700	9019	8873	8817	8798
131.4	9166	9201	9001	9176	9125	9074	9242	9205	9321	9227
141.4	9554	9444	9206	9436	9379	9339	9424	9359	9378	9339
151.4	9033	8951	9098	9069	8882	8929	8945	9153	8776	8899
161.4	8922	8858	8719	8839	8869	8610	8772	8732	8739	8760

APPENDIX VII

Results of the UV chemical analyses of the water samples collected during the field experiment

Sampling Session # 01
Date: Tuesday, November 07, 1995
Time: 4:00pm

Sample ID	Ethanol (m/m)%	Gasoline (m/m)%	Water (m/m)%	Total (m/m)%
1-1	0.000	0.009	99.990	99.999
2-1	0.000	0.011	N/A	N/A
3-1	0.000	0.009	103.120	103.129
4-1	0.000	0.009	N/A	N/A
5-1	0.000	0.007	102.740	102.747
6-1	0.000	0.011	N/A	N/A
7-1	0.000	0.009	101.400	101.409
8-1	0.000	0.033	N/A	N/A
9-1	0.000	0.019	102.090	102.109
10-1	0.000	0.011	N/A	N/A
11-1	0.000	0.014	101.550	101.564
12-1	0.000	0.008	N/A	N/A
13-1	0.000	0.014	99.180	99.194
14-1	0.000	0.007	N/A	N/A
A1-1	N/A	N/A	N/A	N/A
A2-1	N/A	N/A	N/A	N/A
A3-1	N/A	N/A	N/A	N/A
A4-1	N/A	N/A	N/A	N/A
B1-1	N/A	N/A	N/A	N/A
B2-1	N/A	N/A	N/A	N/A
B3-1	N/A	N/A	N/A	N/A
B4-1	N/A	N/A	N/A	N/A
C1-1	N/A	N/A	N/A	N/A
C2-1	N/A	N/A	N/A	N/A
C3-1	N/A	N/A	N/A	N/A
C4-1	N/A	N/A	N/A	N/A
D1-1	N/A	N/A	N/A	N/A
D2-1	N/A	N/A	N/A	N/A
D3-1	N/A	N/A	N/A	N/A
D4-1	N/A	N/A	N/A	N/A
E1-1	N/A	N/A	N/A	N/A
E2-1	N/A	N/A	N/A	N/A
E3-1	N/A	N/A	N/A	N/A
E4-1	N/A	N/A	N/A	N/A

Sampling Session # 02
Date: Thursday, November 12, 1995
Time: 2:00pm to 4:30pm

Sample ID	Ethanol (m/m)%	Gasoline (m/m)%	Water (m/m)%	Total (m/m)%
1-2	0.000	0.005	100.800	100.805
2-2	0.000	0.006	N/A	N/A
3-2	0.000	0.007	N/A	N/A
4-2	0.000	0.006	N/A	N/A
5-2	0.000	0.007	N/A	N/A
6-2	0.000	0.012	100.600	100.612
7-2	0.000	0.026	N/A	N/A
8-2	0.000	0.014	N/A	N/A
9-2	0.000	0.017	N/A	N/A
10-2	0.000	0.009	N/A	N/A
11-2	0.000	0.014	N/A	N/A
12-2	0.000	0.009	N/A	N/A
13-2	0.000	0.007	N/A	N/A
14-2	0.000	0.007	99.700	99.707
A1-2	N/A	N/A	N/A	N/A
A2-2	N/A	N/A	N/A	N/A
A3-2	N/A	N/A	N/A	N/A
A4-2	N/A	N/A	N/A	N/A
B1-2	N/A	N/A	N/A	N/A
B2-2	N/A	N/A	N/A	N/A
B3-2	N/A	N/A	N/A	N/A
B4-2	N/A	N/A	N/A	N/A
C1-2	N/A	N/A	N/A	N/A
C2-2	N/A	N/A	N/A	N/A
C3-2	N/A	N/A	N/A	N/A
C4-2	N/A	N/A	N/A	N/A
D1-2	N/A	N/A	N/A	N/A
D2-2	N/A	N/A	N/A	N/A
D3-2	N/A	N/A	N/A	N/A
D4-2	N/A	N/A	N/A	N/A
E1-2	N/A	N/A	N/A	N/A
E2-2	N/A	N/A	N/A	N/A
E3-2	N/A	N/A	N/A	N/A
E4-2	N/A	N/A	N/A	N/A

Sampling Session # 03
Date: Friday, November 17, 1995
Time: 2:00pm to 4:30pm

Sample ID	Ethanol (m/m)%	Gasoline (m/m)%	Water (m/m)%	Total (m/m)%
1-3	N/A	0.006	N/A	N/A
2-3	N/A	0.007	N/A	N/A
3-3	N/A	0.006	N/A	N/A
4-3	N/A	0.007	N/A	N/A
5-3	N/A	0.004	N/A	N/A
6-3	N/A	0.009	N/A	N/A
7-3	N/A	0.006	100.400	N/A
8-3	N/A	0.016	N/A	N/A
9-3	N/A	0.019	N/A	N/A
10-3	N/A	0.009	N/A	N/A
11-3	N/A	0.018	N/A	N/A
12-3	N/A	0.012	N/A	N/A
13-3	N/A	0.013	N/A	N/A
14-3	N/A	0.010	100.300	N/A
A1-3	N/A	N/A	N/A	N/A
A2-3	N/A	N/A	N/A	N/A
A3-3	N/A	N/A	N/A	N/A
A4-3	N/A	N/A	N/A	N/A
B1-3	N/A	N/A	N/A	N/A
B2-3	N/A	N/A	N/A	N/A
B3-3	N/A	N/A	N/A	N/A
B4-3	N/A	N/A	N/A	N/A
C1-3	N/A	N/A	N/A	N/A
C2-3	N/A	N/A	N/A	N/A
C3-3	N/A	N/A	N/A	N/A
C4-3	N/A	N/A	N/A	N/A
D1-3	N/A	N/A	N/A	N/A
D2-3	N/A	N/A	N/A	N/A
D3-3	N/A	N/A	N/A	N/A
D4-3	N/A	N/A	N/A	N/A
E1-3	N/A	N/A	N/A	N/A
E2-3	N/A	N/A	N/A	N/A
E3-3	N/A	N/A	N/A	N/A
E4-3	N/A	N/A	N/A	N/A

Sampling Session # 04
Date: Sunday, November 19, 1995
Time: 2:00pm to 4:30pm

Sample ID	Ethanol (m/m)%	Gasoline (m/m)%	Water (m/m)%	Total (m/m)%
1-4	N/A	0.005	N/A	N/A
2-4	N/A	0.005	N/A	N/A
3-4	N/A	0.004	N/A	N/A
4-4	N/A	0.006	N/A	N/A
5-4	N/A	0.005	N/A	N/A
6-4	N/A	0.014	N/A	N/A
7-4	N/A	0.007	99.500	N/A
8-4	N/A	0.026	N/A	N/A
9-4	N/A	0.029	N/A	N/A
10-4	N/A	0.008	N/A	N/A
11-4	N/A	0.025	N/A	N/A
12-4	N/A	0.015	N/A	N/A
13-4	N/A	0.018	N/A	N/A
14-4	N/A	0.012	100.500	N/A
A1-4	53.200	0.785	43.000	96.985
A2-4	5.500	0.073	93.400	98.973
A3-4	0.000	0.063	101.300	101.363
A4-4	0.000	0.009	98.800	98.809
A5-4	0.000	0.011	100.700	100.711
A6-4	0.000	0.006	N/A	N/A
B1-4	50.700	0.904	47.700	99.304
B2-4	2.500	0.033	96.500	99.033
B3-4	0.000	0.039	100.000	100.039
B4-4	0.000	0.006	100.000	100.006
B5-4	0.000	0.006	99.000	99.006
B6-4	0.000	0.005	N/A	N/A
C1-4	34.300	0.176	66.000	100.476
C2-4	0.800	0.123	101.600	102.323
C3-4	0.100	0.213	101.600	101.913
C4-4	0.000	0.011	101.200	101.211
C5-4	N/A	0.016	N/A	N/A
C6-4	N/A	0.007	N/A	N/A
D1-4	17.700	0.110	83.700	101.510
D2-4	0.000	0.105	100.400	100.505
D3-4	0.000	0.062	100.800	100.862
D4-4	N/A	0.009	N/A	N/A
D5-4	N/A	0.009	N/A	N/A
D6-4	N/A	0.006	N/A	N/A
E1-2	14.200	0.034	87.900	102.134
E2-4	0.000	0.007	100.800	100.807
E3-4	0.000	0.010	100.900	100.910
E4-4	N/A	0.010	N/A	N/A
E5-4	N/A	0.009	N/A	N/A
E6-4	N/A	0.005	N/A	N/A

Sampling Session # 05
Date: Tuesday, November 21, 1995
Time: 12:30 to 13:55

Sample ID	Ethanol (m/m)%	Gasoline (m/m)%	Water (m/m)%	Total (m/m)%
1-5	0.000	0.005	101.600	101.605
2-5	0.000	0.003	N/A	N/A
3-5	0.000	0.003	N/A	N/A
4-5	0.000	0.005	N/A	N/A
5-5	0.000	0.004	N/A	N/A
6-5	0.000	0.018	N/A	N/A
7-5	0.000	0.006	100.800	100.806
8-5	0.000	0.034	N/A	N/A
9-5	0.000	0.034	N/A	N/A
10-5	0.000	0.007	N/A	N/A
11-5	0.000	0.034	N/A	N/A
12-5	0.000	0.016	N/A	N/A
13-5	0.000	0.015	101.700	101.715
14-5	0.000	0.009	N/A	N/A
A1-5	64.300	0.486	33.700	98.486
A2-5	11.900	0.052	89.000	100.952
A3-5	0.000	0.065	100.100	100.165
A4-5	0.000	0.007	101.300	101.307
B1-5	60.500	1.407	37.700	99.607
B2-5	6.200	0.031	95.600	101.831
B3-5	0.000	0.042	100.600	100.642
B4-5	0.000	0.007	100.700	100.707
C1-5	49.200	1.019	51.500	101.719
C2-5	2.100	0.114	99.400	101.614
C3-5	0.000	0.193	100.400	100.593
C4-5	0.000	0.008	99.700	99.708
D1-5	26.400	0.148	73.200	99.748
D2-5	0.000	0.104	101.500	101.604
D3-5	0.000	0.055	100.700	100.755
D4-5	0.000	0.007	102.400	102.407
E1-5	23.000	0.060	82.700	105.760
E2-5	0.000	0.012	102.900	102.912
E3-5	0.000	0.018	101.500	101.518
E4-5	0.000	0.008	101.100	101.108

Sampling Session # 06
Date: Thusday, November 23, 1995
Time: 10:30 to 12:30

Sample ID	Ethanol (m/m)%	Gasoline (m/m)%	Water (m/m)%	Total (m/m)%
1-6	0.000	0.005	98.700	98.705
2-6	0.000	0.008	N/A	N/A
3-6	0.000	0.007	N/A	N/A
4-6	0.000	0.003	N/A	N/A
5-6	0.000	0.005	N/A	N/A
6-6	0.000	0.004	N/A	N/A
7-6	0.000	0.024	101.500	101.524
8-6	0.000	0.004	N/A	N/A
9-6	0.000	0.042	N/A	N/A
10-6	0.000	0.038	N/A	N/A
11-6	0.000	0.006	N/A	N/A
12-6	0.000	0.055	N/A	N/A
13-6	0.000	0.024	100.200	100.224
14-6	0.000	0.016	N/A	N/A
A1-6	74.400	0.125	21.000	95.525
A2-6	26.100	0.063	78.300	104.463
A3-6	0.000	0.074	103.100	103.174
A4-6	0.000	0.072	102.200	102.272
A5-6	0.000	0.004	99.000	99.004
B1-6	73.300	1.181	26.000	100.481
B2-6	17.100	0.030	84.300	101.430
B3-6	1.200	0.041	102.200	103.441
B4-6	2.500	0.017	100.600	103.117
B5-6	0.000	0.003	102.300	102.303
C1-6	60.900	2.972	35.600	99.472
C2-6	11.100	0.073	90.900	102.073
C3-6	0.000	0.174	101.600	101.774
C4-6	0.000	0.006	100.100	100.106
C5-6	0.000	0.006	100.600	100.606
D1-6	51.000	1.434	44.100	96.534
D2-6	0.600	0.096	99.900	100.596
D3-6	0.000	0.068	101.700	101.768
D4-5	0.000	0.005	100.400	100.405
D5-6	0.000	0.004	97.400	97.404
E1-6	53.000	1.415	42.700	97.115
E2-6	1.700	0.060	95.500	97.260
E3-6	0.000	0.043	100.600	100.643
E4-6	0.000	0.016	100.300	100.316
E5-6	0.000	0.017	100.800	100.817

Sampling Session # 07
Date: Saturday, November 25, 1995
Time: 10:30 to 12:30

Sample ID	Ethanol (m/m)%	Gasoline (m/m)%	Water (m/m)%	Total (m/m)%
1-7	0.000	0.007	99.800	99.807
2-7	0.000	0.010	N/A	N/A
3-7	0.000	0.004	N/A	N/A
4-7	0.000	0.006	N/A	N/A
5-7	0.000	0.014	N/A	N/A
6-7	0.000	0.039	N/A	N/A
7-7	0.000	0.010	100.000	100.010
8-7	0.000	0.051	N/A	N/A
9-7	0.000	0.046	N/A	N/A
10-7	0.000	0.009	N/A	N/A
11-7	0.000	0.089	N/A	N/A
12-7	0.000	0.026	N/A	N/A
13-7	N/A	N/A	N/A	N/A
14-7	0.000	0.015	99.600	99.615
A1-7	78.000	0.142	19.100	97.242
A2-7	33.700	0.141	69.900	103.741
A3-7	0.100	0.081	100.700	100.881
A4-7	0.000	0.006	99.700	99.706
B1-7	77.100	0.505	21.900	99.505
B2-7	20.200	0.193	83.400	103.793
B3-7	0.000	0.160	100.900	101.060
B4-7	0.000	0.028	100.300	100.328
C1-7	66.200	3.821	31.000	101.021
C2-7	14.500	0.072	85.400	99.972
C3-7	0.000	0.182	99.600	99.782
C4-7	0.000	0.008	100.800	100.808
D1-7	58.200	1.246	38.300	97.746
D2-7	6.200	0.356	91.900	98.456
D3-7	0.000	0.326	98.000	98.326
D4-7	0.000	0.029	100.700	100.729
E1-7	64.500	1.804	35.700	102.004
E2-7	6.300	0.022	92.500	98.822
E3-7	0.000	0.011	100.900	100.911
E4-7	0.000	0.008	100.900	100.908

Sampling Session # 08
Date: Monday, November 27, 1995
Time: 1:30 to 3:30

Sample ID	Ethanol (m/m)%	Gasoline (m/m)%	Water (m/m)%	Total (m/m)%
1-8	0.000	0.004	97.500	97.504
2-8	N/A	0.011	N/A	N/A
3-8	N/A	0.005	N/A	N/A
4-8	N/A	0.009	N/A	N/A
5-8	N/A	0.014	N/A	N/A
6-8	N/A	0.061	N/A	N/A
7-8	0.000	0.004	101.600	101.604
8-8	N/A	0.057	N/A	N/A
9-8	N/A	0.054	N/A	N/A
10-8	N/A	0.005	N/A	N/A
11-8	N/A	0.074	N/A	N/A
12-8	0.000	0.028	98.400	98.428
13-8	1.500	0.028	97.600	99.128
14-8	0.000	0.009	100.300	100.309
A1-8	75.400	0.145	19.500	95.045
A2-8	33.100	0.145	66.200	99.445
A3-8	0.000	0.080	98.100	98.180
A4-8	0.000	0.004	99.100	99.104
B1-8	77.200	0.126	21.200	98.526
B2-8	26.800	0.051	74.600	101.451
B3-8	0.000	0.040	97.700	97.740
B4-8	0.000	0.011	98.700	98.711
C1-8	65.100	1.486	23.900	90.486
C2-8	22.800	0.273	78.500	101.573
C3-8	0.000	0.635	99.700	100.335
C4-8	0.000	0.026	101.200	101.226
D1-8	67.400	1.791	28.100	97.291
D2-8	18.700	0.386	78.400	97.486
D3-8	0.000	0.348	98.800	99.148
D4-8	0.000	0.029	98.900	98.929
E1-8	69.900	0.661	26.900	97.461
E2-8	17.500	0.027	81.600	99.127
E3-8	0.000	0.021	98.600	98.621
E4-8	0.000	0.006	99.500	99.506

Sampling Session # 09
Date: November 29, 1995
Time: 1:15 pm

Sample ID	Ethanol (m/m)%	Gasoline (m/m)%	Water (m/m)%	Total (m/m)%
1-9	0.000	0.009	99.500	99.509
2-9	3.600	0.090	94.700	98.390
3-9	0.000	0.007	100.000	100.007
4-9	0.000	0.013	100.600	100.613
5-9	2.100	0.014	97.500	99.614
6-9	0.000	0.006	100.200	100.206
7-9	2.900	0.007	97.100	100.007
8-9	3.700	0.068	95.800	99.568
9-9	0.000	0.046	97.500	97.546
10-9	0.000	0.007	100.700	100.707
11-9	4.300	0.071	94.800	99.171
12-9	0.000	0.026	100.300	100.326
13-9	3.300	0.033	99.900	103.233
14-9	0.000	0.017	101.600	101.617
A1-9	78.400	0.486	18.800	97.686
A2-9	46.500	2.844	50.100	99.444
A3-9	0.400	0.092	96.600	97.092
A4-9	0.000	0.015	97.600	97.615
B1-9	76.900	0.006	17.200	94.106
B2-9	40.300	0.321	59.200	99.821
B3-9	0.000	0.043	99.500	99.543
B4-9	0.800	0.009	98.200	99.009
C1-9	69.800	3.443	22.900	96.143
C2-9	36.500	0.283	62.100	98.883
C3-9	0.000	0.149	99.700	99.849
C4-9	0.050	0.015	100.100	100.165
D1-9	67.100	4.195	29.200	100.495
D2-9	30.700	0.214	68.100	99.014
D3-9	0.000	0.089	99.600	99.689
D4-9	0.000	0.012	100.000	100.012
E1-9	71.700	0.510	24.900	97.110
E2-9	28.000	0.092	70.300	98.392
E3-9	0.000	0.019	98.100	98.119
E4-9	0.000	0.007	97.400	97.407

Sampling Session # 07
Date: Saturday, November 25, 1995
Time: 10:30 to 12:30

Sample ID	Ethanol (m/m)%	Gasoline (m/m)%	Water (m/m)%	Total (m/m)%
1-7	0.000	0.007	99.800	99.807
2-7	0.000	0.010	N/A	N/A
3-7	0.000	0.004	N/A	N/A
4-7	0.000	0.006	N/A	N/A
5-7	0.000	0.014	N/A	N/A
6-7	0.000	0.039	N/A	N/A
7-7	0.000	0.010	100.000	100.010
8-7	0.000	0.051	N/A	N/A
9-7	0.000	0.046	N/A	N/A
10-7	0.000	0.009	N/A	N/A
11-7	0.000	0.069	N/A	N/A
12-7	0.000	0.026	N/A	N/A
13-7	N/A	N/A	N/A	N/A
14-7	0.000	0.015	99.600	99.615
A1-7	78.000	0.142	19.100	97.242
A2-7	33.700	0.141	69.900	103.741
A3-7	0.100	0.081	100.700	100.881
A4-7	0.000	0.006	99.700	99.706
B1-7	77.100	0.505	21.900	99.505
B2-7	20.200	0.193	83.400	103.793
B3-7	0.000	0.160	100.900	101.060
B4-7	0.000	0.028	100.300	100.328
C1-7	66.200	3.821	31.000	101.021
C2-7	14.500	0.072	85.400	99.972
C3-7	0.000	0.182	99.600	99.782
C4-7	0.000	0.008	100.800	100.808
D1-7	58.200	1.246	38.300	97.746
D2-7	6.200	0.356	91.900	98.456
D3-7	0.000	0.326	98.000	98.326
D4-7	0.000	0.029	100.700	100.729
E1-7	64.500	1.804	35.700	102.004
E2-7	6.300	0.022	92.500	98.822
E3-7	0.000	0.011	100.900	100.911
E4-7	0.000	0.008	100.900	100.908

Sampling Session # 08
Date: Monday, November 27, 1995
Time: 1:30 to 3:30

Sample ID	Ethanol (m/m)%	Gasoline (m/m)%	Water (m/m)%	Total (m/m)%
1-8	0.000	0.004	97.500	97.504
2-8	N/A	0.011	N/A	N/A
3-8	N/A	0.005	N/A	N/A
4-8	N/A	0.009	N/A	N/A
5-8	N/A	0.014	N/A	N/A
6-8	N/A	0.061	N/A	N/A
7-8	0.000	0.004	101.600	101.604
8-8	N/A	0.057	N/A	N/A
9-8	N/A	0.054	N/A	N/A
10-8	N/A	0.005	N/A	N/A
11-8	N/A	0.074	N/A	N/A
12-8	0.000	0.028	98.400	98.428
13-8	1.500	0.028	97.600	99.128
14-8	0.000	0.009	100.300	100.309
A1-8	75.400	0.145	19.500	95.045
A2-8	33.100	0.145	66.200	99.445
A3-8	0.000	0.060	98.100	98.160
A4-8	0.000	0.004	99.100	99.104
B1-8	77.200	0.126	21.200	98.526
B2-8	26.800	0.051	74.600	101.451
B3-8	0.000	0.040	97.700	97.740
B4-8	0.000	0.011	96.700	96.711
C1-8	65.100	1.486	23.900	90.486
C2-8	22.800	0.273	78.500	101.573
C3-8	0.000	0.635	99.700	100.335
C4-8	0.000	0.026	101.200	101.226
D1-8	67.400	1.791	28.100	97.291
D2-8	18.700	0.386	78.400	97.486
D3-8	0.000	0.348	98.800	99.148
D4-8	0.000	0.029	98.900	98.929
E1-8	69.900	0.661	26.900	97.461
E2-8	17.500	0.027	81.600	99.127
E3-8	0.000	0.021	98.600	98.621
E4-8	0.000	0.006	99.500	99.506

Sampling Session # 09
Date: November 29, 1995
Time: 1:15 pm

Sample ID	Ethanol (m/m)%	Gasoline (m/m)%	Water (m/m)%	Total (m/m)%
1-9	0.000	0.009	99.500	99.509
2-9	3.600	0.090	94.700	98.390
3-9	0.000	0.007	100.000	100.007
4-9	0.000	0.013	100.600	100.613
5-9	2.100	0.014	97.500	99.614
6-9	0.000	0.006	100.200	100.206
7-9	2.900	0.007	97.100	100.007
8-9	3.700	0.068	95.800	99.568
9-9	0.000	0.046	97.500	97.546
10-9	0.000	0.007	100.700	100.707
11-9	4.300	0.071	94.800	99.171
12-9	0.000	0.026	100.300	100.326
13-9	3.300	0.033	99.900	103.233
14-9	0.000	0.017	101.600	101.617
A1-9	78.400	0.486	18.800	97.686
A2-9	46.500	2.844	50.100	99.444
A3-9	0.400	0.092	96.600	97.092
A4-9	0.000	0.015	97.600	97.615
B1-9	76.900	0.006	17.200	94.106
B2-9	40.300	0.321	59.200	99.821
B3-9	0.000	0.043	99.500	99.543
B4-9	0.800	0.009	98.200	99.009
C1-9	69.800	3.443	22.900	96.143
C2-9	36.500	0.283	62.100	98.883
C3-9	0.000	0.149	99.700	99.849
C4-9	0.050	0.015	100.100	100.165
D1-9	67.100	4.195	29.200	100.495
D2-9	30.700	0.214	68.100	99.014
D3-9	0.000	0.089	99.600	99.689
D4-9	0.000	0.012	100.000	100.012
E1-9	71.700	0.510	24.900	97.110
E2-9	28.000	0.092	70.300	98.392
E3-9	0.000	0.019	98.100	98.119
E4-9	0.000	0.007	97.400	97.407

Sampling Session # 10
Date: December 01, 1995
Time: 12:00 pm

Sample ID	Ethanol (m/m)%	Gasoline (m/m)%	Water (m/m)%	Total (m/m)%
1-10	0.000	0.007	99.900	99.907
2-10	5.500	0.011	93.700	99.211
3-10	0.000	0.010	98.500	98.510
4-10	1.000	0.028	98.700	99.728
5-10	5.800	0.019	92.200	98.019
6-10	0.000	0.054	97.700	97.754
7-10	0.000	0.007	99.000	99.007
8-10	9.000	0.072	92.100	101.172
9-10	0.000	0.065	98.100	98.165
10-10	0.000	0.008	99.200	99.208
11-10	5.000	0.074	95.200	100.274
12-10	0.000	0.027	101.400	101.427
13-10	5.600	0.037	94.100	99.737
14-10	0.000	0.010	100.000	100.010
A1-10	78.000	0.875	17.900	96.775
A2-10	55.300	1.652	41.500	98.452
A3-10	2.600	0.112	101.100	103.812
A4-10	0.000	0.003	101.700	101.703
B1-10	83.900	0.497	15.800	100.197
B2-10	50.100	0.823	51.200	102.123
B3-10	0.500	0.052	100.400	100.952
B4-10	0.000	0.010	100.000	100.010
C1-10	73.600	0.857	19.600	94.057
C2-10	35.700	1.179	33.800	70.679
C3-10	0.000	0.152	98.600	98.752
C4-10	0.000	0.004	101.500	101.504
D1-10	65.000	4.401	23.800	93.201
D2-10	48.900	1.017	50.000	99.917
D3-10	0.100	0.087	102.100	102.287
D4-10	0.000	0.003	102.100	102.103
E1-10	74.900	0.554	21.300	96.754
E2-10	48.300	0.806	46.000	95.106
E3-10	0.900	0.024	98.900	99.824
E4-10	0.000	0.008	101.400	101.408

Sampling Session # 11
Date: December 04, 1995
Time: 11:05 am

Sample ID	Ethanol (m/m)%	Gasoline (m/m)%	Water (m/m)%	Total (m/m)%
1-11	0.000	0.006	102.000	102.006
2-11	17.700	0.084	83.100	100.884
3-11	0.500	0.012	98.400	98.912
4-11	0.000	0.019	100.500	100.519
5-11	12.500	0.094	88.300	100.894
6-11	0.000	0.079	99.700	99.779
7-11	0.000	0.007	99.700	99.707
8-11	19.600	0.227	82.900	102.727
9-11	0.600	0.055	99.500	100.155
10-11	0.000	0.009	98.900	98.909
11-11	16.600	0.107	85.200	101.907
12-11	0.000	0.026	101.200	101.226
13-11	13.400	0.080	89.500	102.980
14-11	0.000	0.006	100.000	100.006
A1-11	79.400	1.091	17.700	98.191
A2-11	64.400	3.606	33.300	101.306
A3-11	10.900	0.051	87.900	98.851
A4-11	0.000	0.007	99.000	99.007
B1-11	83.700	0.008	14.700	98.408
B2-11	63.300	0.750	34.800	98.850
B3-11	7.300	0.390	91.800	99.490
B4-11	0.000	0.004	98.500	98.504
C1-11	82.500	0.312	19.200	102.012
C2-11	62.000	2.835	36.700	101.535
C3-11	2.300	0.127	97.200	99.627
C4-11	0.000	0.009	99.100	99.109
D1-11	69.900	5.160	21.700	96.760
D2-11	54.700	2.067	41.400	98.167
D3-11	1.400	0.075	98.500	99.975
D4-11	0.000	0.008	98.700	98.708
E1-11	74.200	0.392	23.100	97.692
E2-11	59.200	0.625	37.000	96.825
E3-11	3.600	0.045	95.200	98.845
E4-11	0.000	0.005	101.100	101.105

Sampling Session # 12
Date: December 06, 1995
Time: 1 pm

Sample ID	Ethanol (m/m)%	Gasoline (m/m)%	Water (m/m)%	Total (m/m)%
1-12	0.000	0.008	99.000	99.008
2-12	40.800	0.474	58.700	99.974
3-12	3.000	0.010	95.700	98.710
4-12	0.000	0.030	99.600	99.630
5-12	38.000	0.430	63.100	101.530
6-12	1.000	0.051	94.000	95.051
7-12	0.000	0.007	97.100	97.107
8-12	71.900	0.962	58.200	131.062
9-12	1.200	0.053	99.100	100.353
10-12	0.000	0.008	100.200	100.208
11-12	41.500	0.859	58.400	100.759
12-12	2.500	0.026	97.500	100.026
13-12	44.400	0.605	60.000	105.005
14-12	0.000	0.010	101.100	101.110
A1-12	89.800	0.037	7.900	97.737
A2-12	69.400	4.990	23.700	98.090
A3-12	31.700	0.121	71.600	103.421
A4-12	0.000	0.024	101.700	101.724
B1-12	91.600	0.004	9.900	101.504
B2-12	76.800	0.284	26.500	103.584
B3-12	18.700	0.040	80.200	98.940
B4-12	0.000	0.006	99.000	99.006
C1-12	81.300	0.476	16.600	98.376
C2-12	68.800	5.034	27.700	101.534
C3-12	15.800	0.095	84.500	100.395
C4-12	0.000	0.020	100.700	100.720
D1-12	73.100	4.714	18.700	96.514
D2-12	66.100	3.953	32.800	102.853
D3-12	18.700	0.117	87.600	106.417
D4-12	0.000	0.005	100.600	100.605
E1-12	79.800	0.734	18.800	99.334
E2-12	70.200	0.268	30.300	100.768
E3-12	17.500	0.038	85.000	102.538
E4-12	0.700	0.020	100.700	101.420

Sampling Session # 10
Date: December 01, 1995
Time: 12:00 pm

Sample ID	Ethanol (m/m)%	Gasoline (m/m)%	Water (m/m)%	Total (m/m)%
1-10	0.000	0.007	99.900	99.907
2-10	5.500	0.011	93.700	99.211
3-10	0.000	0.010	98.500	98.510
4-10	1.000	0.028	98.700	99.728
5-10	5.800	0.019	92.200	98.019
6-10	0.000	0.054	97.700	97.754
7-10	0.000	0.007	99.000	99.007
8-10	9.000	0.072	92.100	101.172
9-10	0.000	0.065	98.100	98.165
10-10	0.000	0.008	99.200	99.208
11-10	5.000	0.074	95.200	100.274
12-10	0.000	0.027	101.400	101.427
13-10	5.600	0.037	94.100	99.737
14-10	0.000	0.010	100.000	100.010
A1-10	78.000	0.875	17.900	96.775
A2-10	55.300	1.652	41.500	98.452
A3-10	2.600	0.112	101.100	103.812
A4-10	0.000	0.003	101.700	101.703
B1-10	83.900	0.497	15.800	100.197
B2-10	50.100	0.823	51.200	102.123
B3-10	0.500	0.052	100.400	100.952
B4-10	0.000	0.010	100.000	100.010
C1-10	73.600	0.857	19.600	94.057
C2-10	35.700	1.179	33.800	70.679
C3-10	0.000	0.152	98.600	98.752
C4-10	0.000	0.004	101.500	101.504
D1-10	65.000	4.401	23.800	93.201
D2-10	48.900	1.017	50.000	99.917
D3-10	0.100	0.087	102.100	102.287
D4-10	0.000	0.003	102.100	102.103
E1-10	74.900	0.554	21.300	96.754
E2-10	48.300	0.806	46.000	95.106
E3-10	0.900	0.024	98.900	99.824
E4-10	0.000	0.008	101.400	101.408

Sampling Session # 11
Date: December 04, 1995
Time: 11:05 am

Sample ID	Ethanol (m/m)%	Gasoline (m/m)%	Water (m/m)%	Total (m/m)%
1-11	0.000	0.006	102.000	102.006
2-11	17.700	0.084	83.100	100.884
3-11	0.500	0.012	98.400	98.912
4-11	0.000	0.019	100.500	100.519
5-11	12.500	0.094	88.300	100.894
6-11	0.000	0.079	99.700	99.779
7-11	0.000	0.007	99.700	99.707
8-11	19.600	0.227	82.900	102.727
9-11	0.600	0.055	99.500	100.155
10-11	0.000	0.009	98.900	98.909
11-11	16.600	0.107	85.200	101.907
12-11	0.000	0.026	101.200	101.226
13-11	13.400	0.080	89.500	102.980
14-11	0.000	0.006	100.000	100.006
A1-11	79.400	1.091	17.700	98.191
A2-11	64.400	3.606	33.300	101.306
A3-11	10.900	0.051	87.900	98.851
A4-11	0.000	0.007	99.000	99.007
B1-11	83.700	0.008	14.700	98.408
B2-11	63.300	0.750	34.800	98.850
B3-11	7.300	0.390	91.800	99.490
B4-11	0.000	0.004	98.500	98.504
C1-11	82.500	0.312	19.200	102.012
C2-11	62.000	2.835	36.700	101.535
C3-11	2.300	0.127	97.200	99.627
C4-11	0.000	0.009	99.100	99.109
D1-11	69.900	5.160	21.700	96.760
D2-11	54.700	2.067	41.400	98.167
D3-11	1.400	0.075	98.500	99.975
D4-11	0.000	0.008	98.700	98.708
E1-11	74.200	0.392	23.100	97.692
E2-11	59.200	0.625	37.000	96.825
E3-11	3.600	0.045	95.200	98.845
E4-11	0.000	0.005	101.100	101.105

Sampling Session # 12
Date: December 06, 1995
Time: 1 pm

Sample ID	Ethanol (m/m)%	Gasoline (m/m)%	Water (m/m)%	Total (m/m)%
1-12	0.000	0.006	99.000	99.006
2-12	40.800	0.474	58.700	99.974
3-12	3.000	0.010	95.700	98.710
4-12	0.000	0.030	99.600	99.630
5-12	38.000	0.430	63.100	101.530
6-12	1.000	0.051	94.000	95.051
7-12	0.000	0.007	97.100	97.107
8-12	71.900	0.962	58.200	131.062
9-12	1.200	0.053	99.100	100.353
10-12	0.000	0.008	100.200	100.208
11-12	41.500	0.859	58.400	100.759
12-12	2.500	0.026	97.500	100.026
13-12	44.400	0.605	60.000	105.005
14-12	0.000	0.010	101.100	101.110
A1-12	89.800	0.037	7.900	97.737
A2-12	69.400	4.990	23.700	98.090
A3-12	31.700	0.121	71.600	103.421
A4-12	0.000	0.024	101.700	101.724
B1-12	91.600	0.004	9.900	101.504
B2-12	76.800	0.284	26.500	103.584
B3-12	8.700	0.040	80.200	98.940
B4-12	0.000	0.006	99.000	99.006
C1-12	81.300	0.476	16.600	98.376
C2-12	68.800	5.034	27.700	101.534
C3-12	15.800	0.095	84.500	100.395
C4-12	0.000	0.020	100.700	100.720
D1-12	73.100	4.714	18.700	96.514
D2-12	66.100	3.953	32.800	102.853
D3-12	18.700	0.117	87.600	106.417
D4-12	0.000	0.005	100.600	100.605
E1-12	79.800	0.734	18.800	99.334
E2-12	70.200	0.268	30.300	100.768
E3-12	17.500	0.038	85.000	102.538
E4-12	0.700	0.020	100.700	101.420

Sampling Session # 13
Date: December 08, 1995
Time: 12 pm

Sample ID	Ethanol (m/m)%	Gasoline (m/m)%	Water (m/m)%	Total (m/m)%
1-13	0.000	0.008	101.000	101.008
2-13	52.500	0.941	43.300	96.741
3-13	8.800	0.012	93.100	101.912
4-13	0.600	0.019	100.700	101.319
5-13	53.900	1.029	40.700	95.629
6-13	4.000	0.042	96.400	100.442
7-13	0.000	0.019	100.400	100.419
8-13	59.400	2.029	36.700	98.129
9-13	5.500	0.066	96.200	101.766
10-13	0.000	0.009	101.600	101.609
11-13	45.500	1.663	38.200	85.363
12-13	7.100	0.056	93.600	100.756
13-13	54.900	1.731	40.500	97.131
14-13	0.000	0.008	100.000	100.008
A1-13	90.200	0.010	6.800	97.010
A2-13	75.800	1.335	17.200	94.335
A3-13	48.700	0.819	48.100	97.619
A4-13	0.000	0.010	103.900	103.910
A5-13	0.000	0.006	101.100	101.106
B1-13	89.800	0.004	6.500	96.304
B2-13	84.600	0.018	15.700	100.318
B3-13	39.100	0.022	62.800	101.922
B4-13	0.000	8.106	101.700	109.806
B5-13	0.000	0.005	100.300	100.305
C1-13	84.800	0.231	13.100	98.131
C2-13	71.700	6.156	21.000	98.856
C3-13	37.800	0.262	61.300	99.162
C4-13	0.000	0.010	101.400	101.410
C5-13	0.000	0.013	100.800	100.813
D1-13	77.900	1.009	16.000	94.909
D2-13	66.900	4.444	26.700	98.044
D3-13	40.500	0.416	58.300	99.216
D4-13	0.000	0.008	101.100	101.108
D5-13	0.000	0.005	101.400	101.405
E1-13	79.400	0.749	19.200	99.349
E2-13	78.100	0.672	25.000	103.772
E3-13	38.300	0.228	62.800	101.328
E4-13	0.000	0.006	100.800	100.806
E5-13	0.000	0.005	99.900	99.905

Sampling Session # 14
Date: December 10, 1995
Time: 11:00 am

Sample ID	Ethanol (m/m)%	Gasoline (m/m)%	Water (m/m)%	Total (m/m)%
1-14	0.000	0.011	100.600	100.611
2-14	61.800	1.663	31.900	95.363
3-14	19.200	0.074	82.600	101.874
4-14	1.100	0.021	97.200	98.321
5-14	56.100	1.186	36.500	93.786
6-14	N/A	N/A	N/A	N/A
7-14	0.000	0.014	98.500	98.514
8-14	68.200	2.802	29.000	99.802
9-14	18.600	0.130	82.700	101.430
10-14	0.200	0.011	98.100	98.311
11-14	61.500	2.724	29.500	93.724
12-14	15.100	0.063	88.000	103.163
13-14	60.200	2.568	32.800	95.568
14-14	0.000	0.010	98.600	98.610
A1-14	89.200	0.084	7.200	96.484
A2-14	86.000	0.289	10.600	96.889
A3-14	54.200	1.958	37.700	93.858
A4-14	0.000	0.014	98.300	98.314
B1-14	91.000	0.005	5.900	96.905
B2-14	86.100	0.025	10.800	96.925
B3-14	50.600	0.450	50.800	101.850
B4-14	0.000	0.006	99.900	99.906
C1-14	88.400	0.035	10.200	98.635
C2-14	76.400	2.583	15.500	94.483
C3-14	49.600	1.097	46.500	97.197
C4-14	0.000	0.010	100.400	100.410
D1-14	84.000	0.645	15.000	99.645
D2-14	69.300	7.381	21.200	97.681
D3-14	52.800	1.501	43.100	97.401
D4-14	0.000	0.013	98.400	98.413
E1-14	82.900	0.427	15.200	98.527
E2-14	77.200	0.393	21.000	98.593
E3-14	54.600	0.889	42.000	97.489
E4-14	0.000	0.011	99.000	99.011
A5-14	0.000	0.006	98.700	98.706

Sampling Session # 15
Date: December 12, 1995
Time: 11:00 am

Sample ID	Ethanol (m/m)%	Gasoline (m/m)%	Water (m/m)%	Total (m/m)%
1-15	0.144	0.011	97.294	97.450
2-15	71.569	2.157	27.872	101.598
3-15	31.282	0.177	67.743	99.202
4-15	2.871	0.017	94.858	97.745
5-15	66.974	1.661	32.308	100.942
6-15	33.508	0.217	67.605	101.330
7-15	0.122	0.016	98.079	98.217
8-15	67.079	2.400	28.525	98.004
9-15	29.191	0.227	70.839	100.258
10-15	0.499	0.014	98.652	99.164
11-15	64.992	3.182	31.693	99.868
12-15	21.746	0.089	78.060	99.896
13-15	64.461	2.696	34.112	101.269
14-15	0.000	0.009	100.353	100.363
A1-15	91.504	0.043	8.042	99.589
A2-15	85.844	0.407	11.363	97.615
A3-15	60.673	2.768	34.173	97.613
A4-15	0.429	0.014	96.610	97.052
B1-15	90.802	0.064	8.403	99.270
B2-15	86.706	0.063	11.132	97.903
B3-15	56.656	0.267	41.868	98.791
B4-15	0.000	0.008	100.469	100.477
C1-15	87.257	0.044	11.380	98.682
C2-15	77.035	1.685	17.943	96.663
C3-15	55.345	1.635	41.265	98.244
C4-15	0.000	0.010	98.644	98.654
D1-15	82.273	0.439	14.533	97.244
D2-15	68.073	6.718	21.607	96.399
D3-15	57.483	2.290	37.074	96.848
D4-15	0.000	0.012	101.484	101.496
E1-15	83.626	0.854	19.249	103.729
E2-15	84.227	0.213	18.703	103.143
E3-15	61.061	0.702	36.405	98.167
E4-15	0.000	0.009	98.931	98.940

Sampling Session # 16
Date: December 15, 1995
Time: 11:00 am

Sample ID	Ethanol (m/m)%	Gasoline (m/m)%	Water (m/m)%	Total (m/m)%
1-16	1.551	0.011	97.347	98.909
2-16	89.496	2.166	25.571	97.232
3-16	54.511	0.370	42.083	96.964
4-16	6.949	0.040	90.345	97.334
5-16	71.807	1.370	24.389	97.566
6-16	51.551	1.213	44.794	97.558
7-16	0.125	0.035	95.936	96.096
8-16	73.117	2.291	25.221	100.629
9-16	48.153	1.568	47.448	97.169
10-16	1.331	0.013	92.915	94.259
11-16	67.227	3.458	26.143	96.828
12-16	48.942	0.976	51.620	101.537
13-16	67.303	2.623	27.940	97.865
14-16	0.947	0.013	93.095	94.055
A1-16	91.297	0.020	7.457	98.774
A2-16	91.037	0.003	7.892	98.931
A3-16	66.634	2.680	27.938	97.252
A4-16	1.503	0.036	97.166	98.704
B1-16	88.368	0.258	9.317	97.941
B2-16	90.459	0.006	7.194	97.659
B3-16	68.001	0.009	34.241	102.251
B4-16	0.000	0.050	97.614	97.664
C1-16	83.631	0.105	9.046	92.781
C2-16	84.583	0.355	13.160	98.099
C3-16	59.689	3.446	34.766	97.901
C4-16	0.073	0.017	99.356	99.446
D1-16	86.386	0.316	13.818	100.519
D2-16	77.813	2.186	17.623	97.622
D3-16	67.142	4.026	29.938	101.105
D4-16	0.000	0.011	101.167	101.178
E1-16	86.978	0.072	13.189	100.239
E2-16	84.224	0.398	17.305	101.927
E3-16	68.396	1.676	30.699	100.771
E4-16	0.000	0.019	97.110	97.130

Sampling Session # 17
Date: December 17, 1995
Time: 11:00 am

Sample ID	Ethanol (m/m)%	Gasoline (m/m)%	Water (m/m)%	Total (m/m)%
1-17	3.657	0.009	91.031	94.698
2-17	77.818	2.041	22.730	102.589
3-17	65.190	0.636	36.993	102.819
4-17	12.319	0.043	87.754	100.116
5-17	76.799	1.181	20.478	98.458
6-17	64.269	2.401	30.468	97.138
7-17	2.257	0.020	95.890	98.167
8-17	74.085	2.123	20.304	96.512
9-17	62.688	3.659	30.153	96.500
10-17	3.287	0.017	96.563	99.867
11-17	70.341	3.413	22.588	96.342
12-17	56.107	2.005	38.450	96.562
13-17	69.776	2.562	24.620	96.978
14-17	2.304	0.009	95.015	97.328
A1-17	86.526	0.284	8.900	95.710
A2-17	88.433	0.063	6.528	95.025
A3-17	73.411	0.459	20.539	94.406
A4-17	14.532	0.027	85.185	99.744
B1-17	89.137	0.165	7.650	96.952
B2-17	90.137	0.001	6.701	96.839
B3-17	70.371	0.016	24.305	94.693
B4-17	1.206	0.014	92.782	94.003
C1-17	94.288	0.023	7.829	102.140
C2-17	86.666	0.290	11.181	98.137
C3-17	66.829	4.764	29.855	101.448
C4-17	1.469	0.029	97.685	99.183
D1-17	86.460	0.274	12.892	99.626
D2-17	75.690	1.795	16.752	94.236
D3-17	65.977	5.058	27.413	98.447
D4-17	1.003	0.025	99.168	100.196
E1-17	86.251	0.362	11.835	98.448
E2-17	82.286	0.099	14.672	97.058
E3-17	72.824	2.026	23.960	98.810
E4-17	0.802	0.012	96.718	97.532

Sampling Session # 18
Date: December 19, 1995
Time: 11:00 am

Sample ID	Ethanol (m/m)%	Gasoline (m/m)%	Water (m/m)%	Total (m/m)%
1-18	8.231	0.036	88.596	96.863
2-18	77.127	2.041	20.079	99.247
3-18	72.729	0.709	29.270	102.709
4-18	33.118	0.154	67.439	100.711
5-18	80.058	0.761	17.946	98.766
6-18	71.867	2.275	28.752	102.894
7-18	8.248	0.069	87.699	96.017
8-18	74.594	1.788	17.929	94.310
9-18	69.529	4.120	27.555	101.204
10-18	6.831	0.050	88.827	95.709
11-18	75.655	3.030	20.929	99.615
12-18	68.661	2.584	27.577	98.823
13-18	75.171	2.355	24.856	102.385
14-18	10.043	0.065	87.053	97.160
A1-18	87.361	0.452	10.268	98.081
A2-18	93.639	0.002	7.387	101.228
A3-18	82.660	0.012	14.996	97.868
A4-18	41.984	0.325	60.368	102.677
B1-18	93.799	0.073	7.384	101.256
B2-18	88.500	0.001	6.528	95.029
B3-18	77.145	0.162	18.151	95.459
B4-18	11.299	0.024	89.589	100.912
C1-18	86.186	0.028	9.353	95.568
C2-18	89.940	0.472	11.014	101.427
C3-18	66.639	4.040	23.207	93.886
C4-18	14.991	0.049	80.396	95.436
D1-18	84.240	0.439	13.221	97.899
D2-18	82.704	0.432	13.800	96.936
D3-18	67.241	7.944	23.140	98.325
D4-18	13.813	0.041	90.080	103.935
E1-18	91.235	0.122	9.993	101.350
E2-18	83.900	0.095	13.727	97.722
E3-18	76.065	0.817	19.625	96.507
E4-18	9.041	0.030	91.756	100.827

Sampling Session # 19
Date: December 22, 1995
Time: 11:00 am

Sample ID	Ethanol (m/m)%	Gasoline (m/m)%	Water (m/m)%	Total (m/m)%
1-19	3.649	0.010	95.486	99.145
2-19	76.292	1.814	17.782	95.888
3-19	66.567	0.453	32.575	99.594
4-19	39.170	0.230	61.936	101.336
5-19	77.884	0.801	16.312	94.997
6-19	62.627	2.088	29.607	94.322
7-19	4.147	0.043	94.349	98.539
8-19	77.001	2.012	17.077	96.090
9-19	66.716	4.095	29.393	100.204
10-19	4.636	0.053	93.437	98.126
11-19	76.313	2.587	17.867	96.767
12-19	68.346	3.344	30.836	102.527
13-19	77.466	1.810	19.201	98.478
14-19	1.264	0.039	98.142	99.445
A1-19	85.350	0.877	13.819	100.046
A2-19	88.707	0.014	8.060	96.781
A3-19	72.728	0.054	28.475	101.258
A4-19	9.304	0.018	89.249	98.571
B1-19	91.817	0.008	6.872	98.697
B2-19	90.229	0.010	6.867	97.106
B3-19	64.656	0.445	34.889	99.990
B4-19	8.616	0.021	90.299	98.936
C1-19	91.394	0.186	10.284	101.865
C2-19	83.444	1.581	12.277	97.302
C3-19	63.904	4.201	34.932	103.038
C4-19	16.055	0.053	93.663	109.771
D1-19	89.986	0.158	9.350	99.495
D2-19	84.645	0.362	11.686	96.692
D3-19	71.371	3.842	26.367	101.580
D4-19	5.804	0.071	95.628	101.502
E1-19	88.855	0.034	8.254	97.144
E2-19	83.664	0.369	12.885	96.918
E3-19	76.942	0.083	22.866	99.891
E4-19	4.739	0.019	91.612	96.369

Sampling Session # 20
Date: December 24, 1995
Time: 11:00 am

Sample ID	Ethanol (m/m)%	Gasoline (m/m)%	Water (m/m)%	Total (m/m)%
1-20	2.540	0.004	95.900	98.444
2-20	74.503	1.705	17.520	93.728
3-20	45.177	0.167	51.847	97.191
4-20	7.311	0.020	92.093	99.424
5-20	76.981	1.122	18.689	96.792
6-20	53.826	1.289	42.573	97.687
7-20	1.150	0.009	99.646	100.806
8-20	76.409	2.980	18.895	98.284
9-20	54.319	2.119	40.367	96.806
10-20	0.000	0.006	96.215	96.222
11-20	78.900	3.426	19.476	101.802
12-20	51.256	1.202	46.649	99.107
13-20	75.914	2.340	22.033	100.287
14-20	0.000	0.009	98.484	98.493
A1-20	90.440	0.431	13.251	104.122
A2-20	92.250	0.147	9.429	101.826
A3-20	55.004	0.055	49.017	104.077
A4-20	13.345	0.023	88.888	102.257
B1-20	97.382	0.003	6.179	103.564
B2-20	90.867	0.074	8.207	99.148
B3-20	19.697	0.017	83.053	102.767
B4-20	0.554	0.008	98.955	99.517
C1-20	88.648	0.281	10.392	99.321
C2-20	76.407	3.663	13.730	93.800
C3-20	47.572	0.937	48.255	96.763
C4-20	20.094	0.041	80.217	100.351
D1-20	89.999	0.119	8.775	98.893
D2-20	83.202	2.006	14.484	99.692
D3-20	61.885	3.592	35.261	100.738
D4-20	1.900	0.018	96.999	98.917
E1-20	91.895	0.075	8.822	100.792
E2-20	85.322	0.477	13.649	99.448
E3-20	70.050	0.265	32.987	103.302
E4-20	3.798	0.012	94.092	97.901

Sampling Session # 21
Date: December 26, 1995
Time: 11:00 am

Sample ID	Ethanol (m/m)%	Gasoline (m/m)%	Water (m/m)%	Total (m/m)%
1-21	0.988	0.005	97.756	98.749
2-21	75.200	1.433	23.214	99.847
3-21	14.155	0.012	87.333	101.500
4-21	5.838	0.020	92.470	98.328
5-21	75.459	1.556	25.511	102.526
6-21	30.420	0.083	73.939	104.442
7-21	2.271	0.017	96.931	99.219
8-21	75.919	3.200	22.037	101.155
9-21	38.546	0.341	62.492	101.379
10-21	1.012	0.016	100.722	101.750
11-21	73.430	2.980	20.644	97.055
12-21	72.508	2.417	23.176	98.100
13-21	43.761	0.921	54.517	99.198
14-21	0.487	0.017	99.625	100.129
A1-21	88.152	0.356	11.298	99.806
A2-21	92.034	0.373	11.951	104.358
A3-21	19.359	0.011	83.776	103.146
A4-21	21.074	0.020	82.091	103.184
B1-21	95.583	0.003	5.942	101.509
B2-21	92.926	0.120	10.586	103.632
B3-21	0.417	0.005	98.284	98.706
B4-21	0.000	0.007	101.501	101.508
C1-21	91.464	0.193	9.192	100.848
C2-21	84.263	3.528	15.049	102.840
C3-21	20.383	0.031	84.872	105.285
C4-21	14.696	0.025	88.701	103.422
D1-21	94.116	0.278	9.881	104.275
D2-21	80.199	2.204	16.147	98.550
D3-21	57.380	1.362	46.150	104.892
D4-21	6.309	0.024	94.364	100.697
E1-21	94.074	0.068	9.544	103.686
E2-21	87.355	0.717	14.720	102.792
E3-21	53.035	0.727	49.092	102.854
E4-21	0.000	0.011	100.781	100.792

Sampling Session # 22
Date: December 28, 1995
Time: 11:00 am

Sample ID	Ethanol (m/m)%	Gasoline (m/m)%	Water (m/m)%	Total (m/m)%
1-22	0.731	0.006	101.763	102.501
2-22	76.307	1.163	25.226	102.696
3-22	8.138	0.008	95.980	104.126
4-22	2.909	0.012	99.237	102.158
5-22	73.301	1.313	26.346	100.960
6-22	15.001	0.030	88.358	103.389
7-22	2.161	0.014	100.976	103.151
8-22	72.766	2.822	26.997	102.585
9-22	20.201	0.071	86.634	106.905
10-22	0.000	0.011	102.613	102.624
11-22	72.000	2.602	23.275	97.877
12-22	15.970	0.069	86.104	102.143
13-22	68.873	1.816	27.245	97.934
14-22	0.000	0.011	102.533	102.544
A1-22	92.425	0.300	10.817	103.542
A2-22	94.818	0.360	11.986	107.165
A3-22	13.169	0.012	91.775	104.956
A4-22	9.926	0.010	94.283	104.218
B1-22	95.203	0.011	6.018	101.232
B2-22	90.332	0.096	10.792	101.220
B3-22	0.836	0.008	99.551	100.395
B4-22	0.000	0.012	103.282	103.294
C1-22	93.020	0.186	9.311	102.517
C2-22	92.008	1.048	15.546	108.600
C3-22	10.896	0.018	94.197	105.112
C4-22	4.867	0.017	96.984	101.849
D1-22	91.181	1.028	11.035	103.244
D2-22	80.829	2.420	17.047	100.297
D3-22	30.995	0.093	67.939	99.027
D4-22	5.215	0.014	95.278	100.506
E1-22	91.174	0.115	9.598	100.888
E2-22	88.669	0.442	14.547	103.657
E3-22	32.115	0.650	72.048	104.813
E4-22	0.551	0.015	100.200	100.766

Sampling Session # 23
Date: December 30, 1995
Time: 11:00 am

Sample ID	Ethanol (m/m)%	Gasoline (m/m)%	Water (m/m)%	Total (m/m)%
1-23	0.407	0.016	97.816	98.239
2-23	66.753	1.486	30.870	99.109
3-23	3.846	0.065	101.719	105.630
4-23	N/A	N/A	N/A	N/A
5-23	63.292	0.948	35.357	99.597
6-23	6.518	0.020	97.915	104.453
7-23	0.444	0.019	97.652	98.115
8-23	74.366	2.485	26.667	103.519
9-23	8.983	0.029	94.102	103.115
10-23	0.000	0.017	96.185	96.202
11-23	64.758	2.291	33.054	100.104
12-23	4.076	0.026	93.345	97.446
13-23	51.403	0.839	45.847	98.090
14-23	0.000	0.026	96.424	96.451
A1-23	91.286	0.266	10.524	102.076
A2-23	91.283	0.269	10.995	102.548
A3-23	19.458	0.012	80.047	99.517
A4-23	11.176	0.008	91.916	103.100
B1-23	92.271	0.071	7.381	99.723
B2-23	91.399	0.135	12.496	104.030
B3-23	4.663	0.009	95.219	99.892
B4-23	0.000	0.009	98.755	98.765
C1-23	93.322	0.211	9.214	102.747
C2-23	84.688	0.871	13.192	98.751
C3-23	10.605	0.014	90.606	101.226
C4-23	0.765	0.013	97.767	98.545
D1-23	83.530	1.304	10.047	94.881
D2-23	75.701	3.215	15.326	94.242
D3-23	19.212	0.026	86.524	105.763
D4-23	6.133	0.013	90.715	96.861
E1-23	93.186	0.190	10.015	103.390
E2-23	87.286	0.305	13.310	100.901
E3-23	19.355	0.024	87.233	106.612
E4-23	3.322	0.016	90.247	93.586

Sampling Session # 24
Date: January 02, 1996
Time: 11:00 am

Sample ID	Ethanol (m/m)%	Gasoline (m/m)%	Water (m/m)%	Total (m/m)%
1-24	0.583	0.005	101.701	102.289
2-24	74.252	2.306	23.753	100.310
3-24	5.736	0.006	94.642	100.384
4-24	1.837	0.010	98.388	100.235
5-24	73.826	0.997	23.001	97.825
6-24	6.898	0.024	94.609	101.531
7-24	0.792	0.010	99.787	100.589
8-24	75.327	2.161	21.838	99.326
9-24	7.722	0.027	89.449	97.198
10-24	0.000	0.010	95.500	95.510
11-24	70.268	2.682	23.990	96.940
12-24	4.178	0.029	94.625	98.832
13-24	55.373	0.836	46.326	102.534
14-24	0.410	0.009	98.449	98.868
A1-24	92.369	0.322	11.250	103.941
A2-24	92.763	0.237	11.333	104.333
A3-24	20.903	0.013	78.695	99.611
A4-24	2.485	0.006	95.114	97.605
B1-24	93.220	0.185	8.161	101.566
B2-24	87.259	0.194	11.707	99.161
B3-24	8.120	0.010	92.094	100.224
B4-24	0.000	0.009	97.906	97.915
C1-24	88.773	0.237	8.895	97.906
C2-24	84.802	0.677	11.723	97.202
C3-24	10.199	0.018	89.488	99.704
C4-24	0.000	0.015	100.103	100.118
D1-24	85.109	0.453	10.165	95.727
D2-24	81.286	2.190	13.220	96.675
D3-24	15.063	0.014	83.839	98.915
D4-24	2.950	0.011	96.343	99.304
E1-24	92.571	0.261	9.866	102.697
E2-24	88.450	0.337	12.428	101.215
E3-24	20.180	0.076	84.650	105.107
E4-24	0.000	0.013	97.491	97.504

Sampling Session # 25
Date: January 05, 1996
Time: 11:00 am

Sample ID	Ethanol (m/m)%	Gasoline (m/m)%	Water (m/m)%	Total (m/m)%
1-25	0.467	0.010	103.396	103.873
2-25	65.918	1.067	37.581	104.566
3-25	3.281	0.009	94.500	97.790
4-25	1.076	0.008	96.568	97.652
5-25	73.959	0.854	27.773	102.585
6-25	5.092	0.027	97.012	102.131
7-25	0.000	0.012	98.924	98.936
8-25	71.527	2.016	22.969	96.512
9-25	6.017	0.022	95.475	101.514
10-25	0.820	0.012	93.781	94.612
11-25	73.142	2.277	23.348	98.767
12-25	7.934	0.026	91.764	99.724
13-25	54.374	1.026	41.552	96.952
14-25	0.434	0.012	98.951	99.398
A1-25	90.272	0.212	10.317	100.801
A2-25	83.149	0.311	11.213	94.674
A3-25	15.991	0.010	85.425	101.425
A4-25	1.279	0.006	98.995	100.281
B1-25	86.492	0.246	10.443	97.182
B2-25	85.085	0.168	12.399	97.651
B3-25	5.546	0.010	96.913	102.469
B4-25	0.000	0.006	99.778	99.783
C1-25	84.514	0.243	10.318	95.075
C2-25	83.310	0.457	12.320	96.087
C3-25	6.473	0.012	92.429	98.914
C4-25	0.609	0.014	99.849	100.472
D1-25	86.035	0.325	9.788	96.148
D2-25	78.707	3.498	14.633	96.839
D3-25	10.024	0.047	86.324	96.395
D4-25	0.400	0.012	100.673	101.084
E1-25	86.335	0.263	9.961	96.559
E2-25	84.992	0.480	12.618	98.089
E3-25	11.507	0.020	91.794	103.321
E4-25	1.343	0.025	98.606	99.973

Sampling Session # 26
Date: January 15, 1996
Time: 11:00 am

Sample ID	Ethanol (m/m)%	Gasoline (m/m)%	Water (m/m)%	Total (m/m)%
1-26	55.373	0.916	46.146	102.435
2-26	3.663	0.027	98.584	102.274
3-26	70.328	0.411	29.106	99.844
4-26	65.744	0.924	34.460	101.128
5-26	2.781	0.024	99.623	102.428
6-26	62.137	0.305	37.718	100.160
7-26	49.091	0.303	48.035	97.430
8-26	6.310	0.027	96.538	102.875
9-26	69.245	1.272	28.438	98.954
10-26	61.204	1.769	35.074	98.047
11-26	3.590	0.034	102.564	106.188
12-26	73.720	0.792	22.343	96.854
13-26	12.890	0.045	91.940	104.875
14-26	0.434	0.012	98.951	99.398
A1-26	88.210	0.298	10.121	98.629
A2-26	81.075	0.042	19.948	101.066
A3-26	1.679	0.012	99.370	101.060
A4-26	0.575	0.006	97.221	97.803
B1-26	85.005	0.471	10.408	95.884
B2-26	70.289	0.217	30.234	100.740
B3-26	0.000	0.016	98.723	98.738
B4-26	0.000	0.013	100.100	100.112
C1-26	88.019	0.286	10.996	99.301
C2-26	67.225	4.614	27.866	99.705
C3-26	2.029	0.048	98.615	100.691
C4-26	0.000	0.014	100.722	100.736
D1-26	86.804	0.340	11.296	98.441
D2-26	74.258	4.468	26.704	105.430
D3-26	2.421	0.028	100.977	103.425
D4-26	0.000	0.021	101.155	101.176
E1-26	86.802	0.408	11.062	98.272
E2-26	79.292	0.336	22.165	101.793
E3-26	1.618	0.201	100.412	102.231
E4-26	0.000	0.016	99.829	99.845

Obs.: Wells raised

Sampling Session # 27
Date: January 17, 1996
Time: 11:00 am

Sample ID	Ethanol (m/m)%	Gasoline (m/m)%	Water (m/m)%	Total (m/m)%
1-27	10.027	0.022	95.598	105.647
2-27	0.526	0.016	100.590	101.132
3-27	87.186	0.474	12.806	100.466
4-27	19.825	0.031	85.021	104.876
5-27	1.009	0.020	98.842	99.872
6-27	83.561	1.055	12.744	97.360
7-27	16.767	0.051	87.284	104.101
8-27	0.953	0.025	100.460	101.439
9-27	86.380	0.291	12.948	99.618
10-27	26.599	0.084	75.002	101.685
11-27	2.581	0.025	98.516	101.122
12-27	84.963	1.230	14.035	100.248
13-27	0.606	0.024	103.330	103.961
14-27	N/A	N/A	N/A	N/A
A1-27	86.963	0.322	10.514	97.800
A2-27	58.636	0.237	43.182	102.055
A3-27	0.000	0.013	100.343	100.356
A4-27	0.000	0.006	98.628	98.633
B1-27	83.026	0.185	11.106	94.317
B2-27	29.392	0.194	74.038	103.624
B3-27	0.000	0.010	100.289	100.299
B4-27	0.000	0.009	99.162	99.171
C1-27	86.294	0.237	11.384	97.915
C2-27	29.343	0.677	73.974	103.993
C3-27	0.000	0.018	104.879	104.897
C4-27	0.494	0.015	100.845	101.353
D1-27	85.197	0.453	10.956	96.607
D2-27	30.052	2.190	73.293	105.535
D3-27	2.008	0.014	98.427	100.450
D4-27	0.000	0.011	101.845	101.857
E1-27	86.021	0.261	11.088	97.369
E2-27	32.807	0.337	65.866	99.010
E3-27	0.934	0.076	94.658	95.668
E4-27	0.000	0.013	101.211	101.224

Obs.: Wells raised

Sampling Session # 28
Date: January 19, 1996
Time: 11:00 am

Sample ID	Ethanol (m/m)%	Gasoline (m/m)%	Water (m/m)%	Total (m/m)%
1-28	3.227	0.011	97.490	100.728
2-28	0.000	0.007	99.649	99.656
3-28	82.663	0.772	14.729	98.164
4-28	7.949	0.017	94.381	102.348
5-28	0.637	0.022	99.793	100.452
6-28	82.983	1.103	15.339	99.425
7-28	6.448	0.029	96.255	102.732
8-28	0.584	0.034	101.617	102.235
9-28	80.378	2.970	14.859	98.206
10-28	7.884	0.025	92.799	100.708
11-28	0.000	0.019	103.276	103.295
12-28	84.411	1.298	13.906	99.615
13-28	0.795	0.017	101.407	102.220
14-25	0.434	0.012	98.951	99.398
A1-28	N/A	N/A	N/A	N/A
A2-28	N/A	N/A	N/A	N/A
A3-28	N/A	N/A	N/A	N/A
A4-28	N/A	N/A	N/A	N/A
B1-28	84.719	0.969	11.953	97.641
B2-28	12.039	0.024	90.944	103.008
B3-28	0.000	0.022	99.620	99.643
B4-28	0.000	0.009	100.802	100.811
C1-28	N/A	N/A	N/A	N/A
C2-28	N/A	N/A	N/A	N/A
C3-28	N/A	N/A	N/A	N/A
C4-28	N/A	N/A	N/A	N/A
D1-28	N/A	N/A	N/A	N/A
D2-28	N/A	N/A	N/A	N/A
D3-28	N/A	N/A	N/A	N/A
D4-28	N/A	N/A	N/A	N/A
E1-28	N/A	N/A	N/A	N/A
E2-28	N/A	N/A	N/A	N/A
E3-28	N/A	N/A	N/A	N/A
E4-28	N/A	N/A	N/A	N/A

Obs.: Wells raised

Sampling Session # 29
Date: January 25, 1996
Time: 11:00 am

Sample ID	Ethanol (m/m)%	Gasoline (m/m)%	Water (m/m)%	Total (m/m)%
1-29	N/A	N/A	N/A	N/A
2-29	N/A	N/A	N/A	N/A
3-29	N/A	N/A	N/A	N/A
4-29	N/A	N/A	N/A	N/A
5-29	N/A	N/A	N/A	N/A
6-29	N/A	N/A	N/A	N/A
7-29	N/A	N/A	N/A	N/A
8-29	N/A	N/A	N/A	N/A
9-29	N/A	N/A	N/A	N/A
10-29	N/A	N/A	N/A	N/A
11-29	N/A	N/A	N/A	N/A
12-29	N/A	N/A	N/A	N/A
13-29	N/A	N/A	N/A	N/A
14-29	N/A	N/A	N/A	N/A
A1-29	93.030	0.362	12.227	105.619
A2-29	9.606	0.017	92.898	102.521
A3-29	0.490	0.006	100.292	100.788
A4-29	0.000	0.006	99.459	99.465
B1-29	84.257	0.964	14.380	99.601
B2-29	3.426	0.015	97.958	101.397
B3-29	0.359	0.010	101.326	101.695
B4-29	0.000	0.007	100.257	100.264
C1-29	84.564	0.467	13.239	98.270
C2-29	3.028	0.262	99.475	102.765
C3-29	0.000	0.014	100.676	100.690
C4-29	0.000	0.012	101.236	101.248
D1-29	83.865	1.049	12.129	97.043
D2-29	4.035	0.283	99.620	103.937
D3-29	0.628	0.013	101.704	102.345
D4-29	0.000	0.007	104.104	104.111
E1-29	88.787	0.273	13.100	102.160
E2-29	6.776	0.021	98.135	104.932
E3-29	0.000	0.116	100.374	100.490
E4-29	0.000	0.011	96.980	96.991

Obs.: Wells raised

APPENDIX VIII

Breakthrough curves for all the sampling points (multilevel ports and extraction wells) of the field experiment

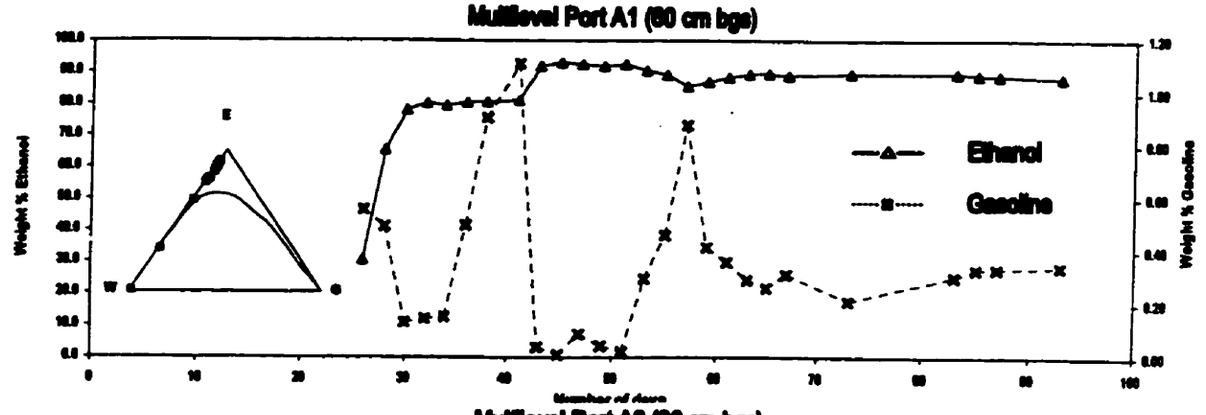
Multilevel Port A1 (80 cm bgs)
Ethanol
Gasoline
Weight % Ethanol
Weight % Gasoline
Number of days

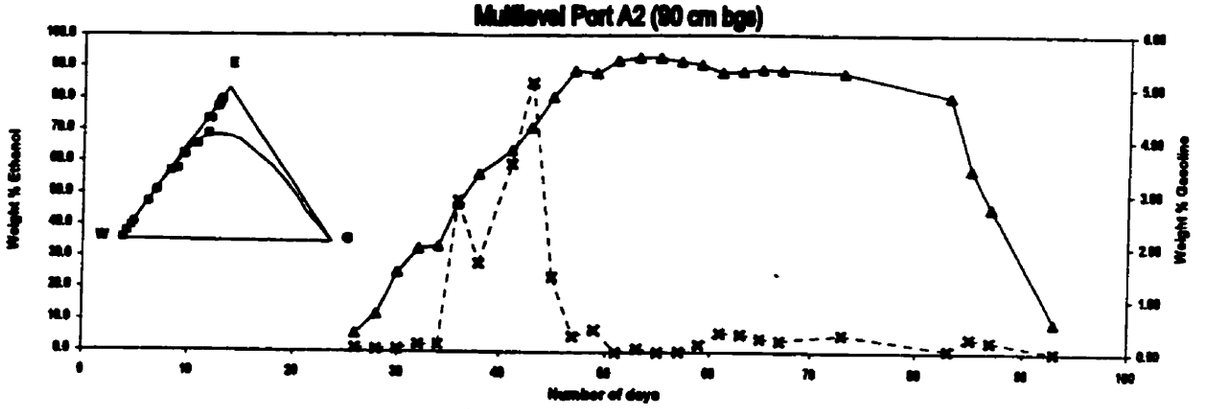
Multilevel Port A2 (90 cm bgs)
Weight % Ethanol
Weight % Gasoline
Number of days

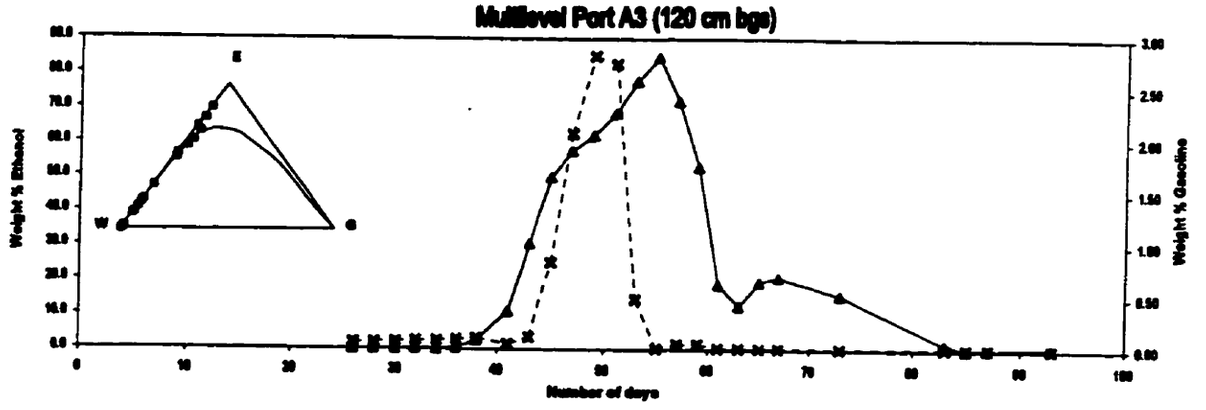
Multilevel Port A3 (120 cm bgs)
Weight % Ethanol
Weight % Gasoline
Number of days

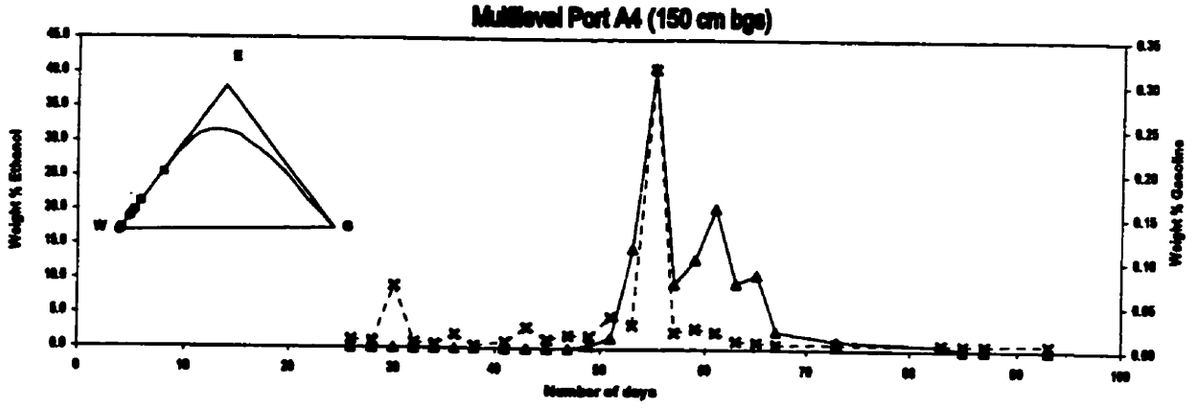
Multilevel Port A4 (150 cm bgs)
Weight % Ethanol
Weight % Gasoline
Number of days

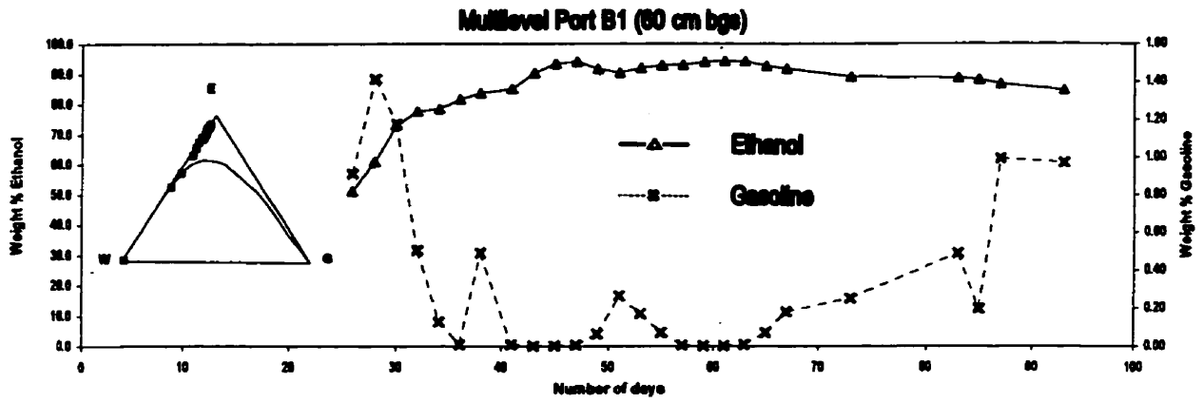
Multilevel Port B1 (60 cm bgs)
Ethanol
Gasoline
Weight % Ethanol
Weight % Gasoline
Number of days

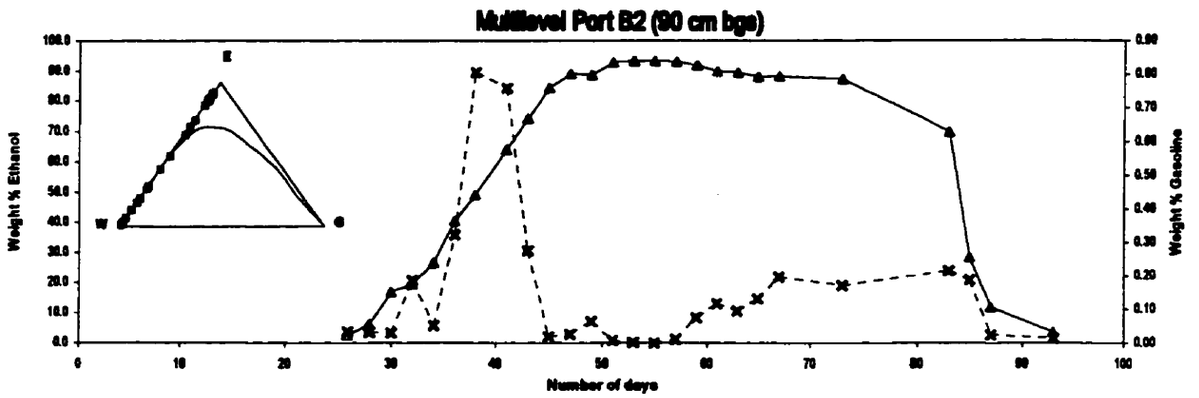
Multilevel Port B2 (90 cm bgs)
Weight % Ethanol
Weight % Gasoline
Number of days

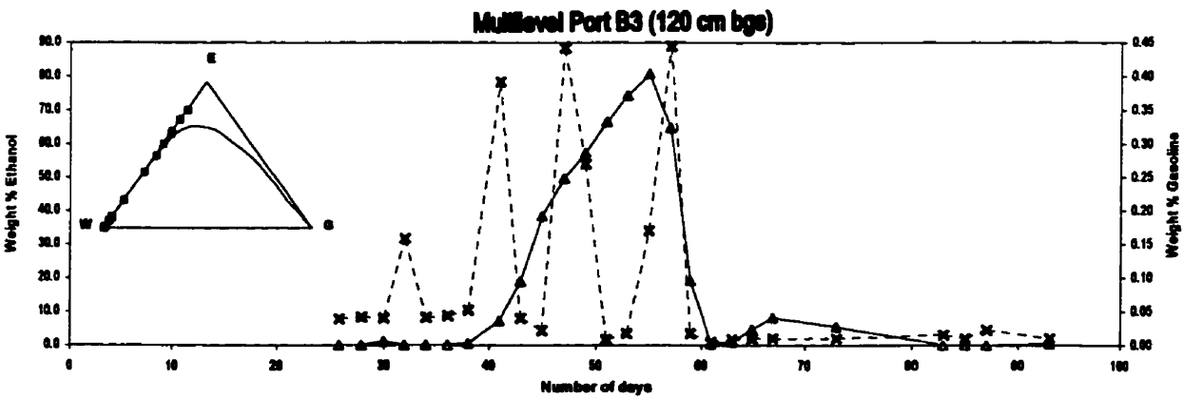
Multilevel Port B3 (120 cm bgs)
Weight % Ethanol
Weight % Gasoline
Number of days

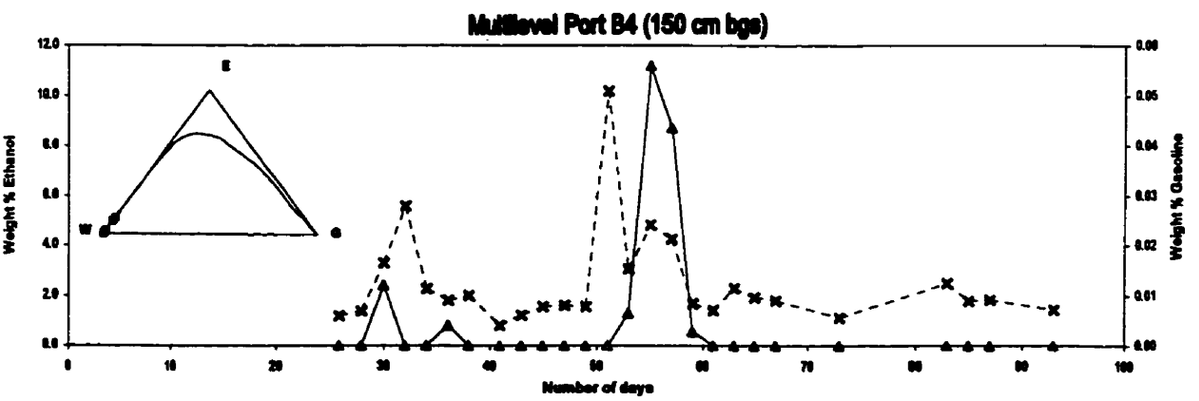
Multilevel Port B4 (150 cm bgs)
Weight % Ethanol
Weight % Gasoline
Number of days

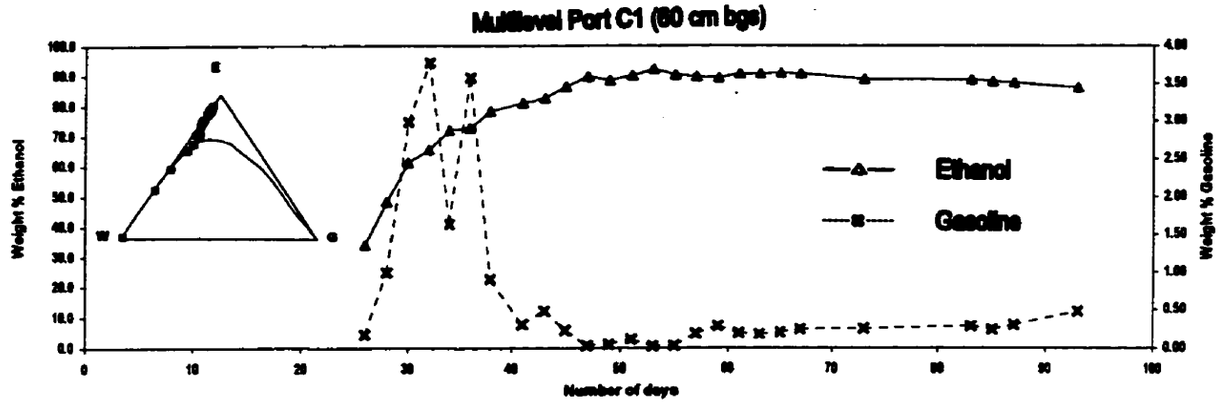
Multilevel Port C1 (60 cm bgs)
Weight % Ethanol
Weight % Gasoline
Number of days
Ethanol
Gasoline
E
W
G

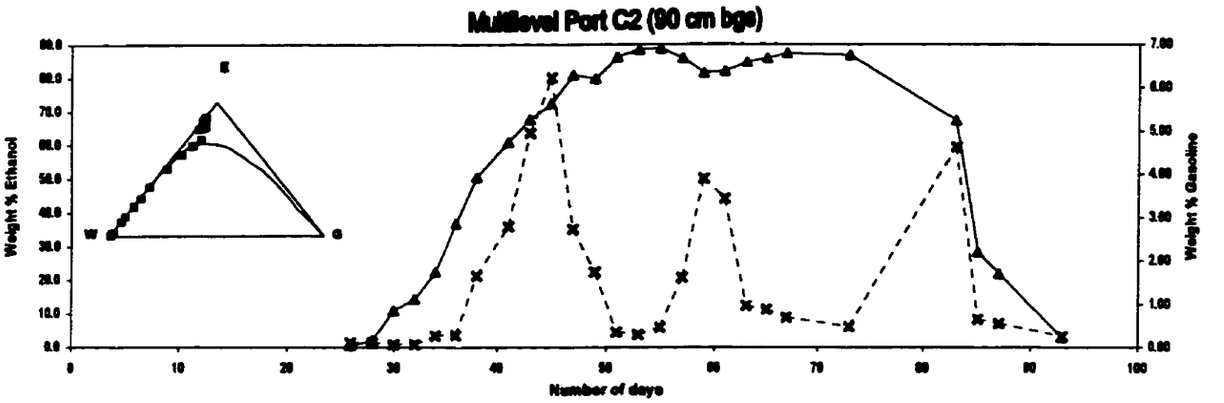
Multilevel Port C2 (90 cm bgs)
Weight % Ethanol
Weight % Gasoline
Number of days
E
W
G

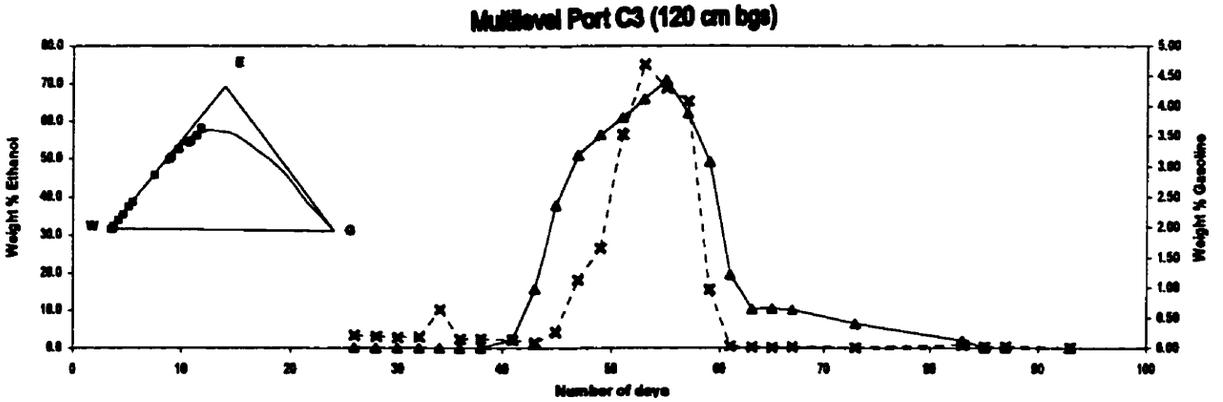
Multilevel Port C3 (120 cm bgs)
Weight % Ethanol
Weight % Gasoline
Number of days
E
W
G

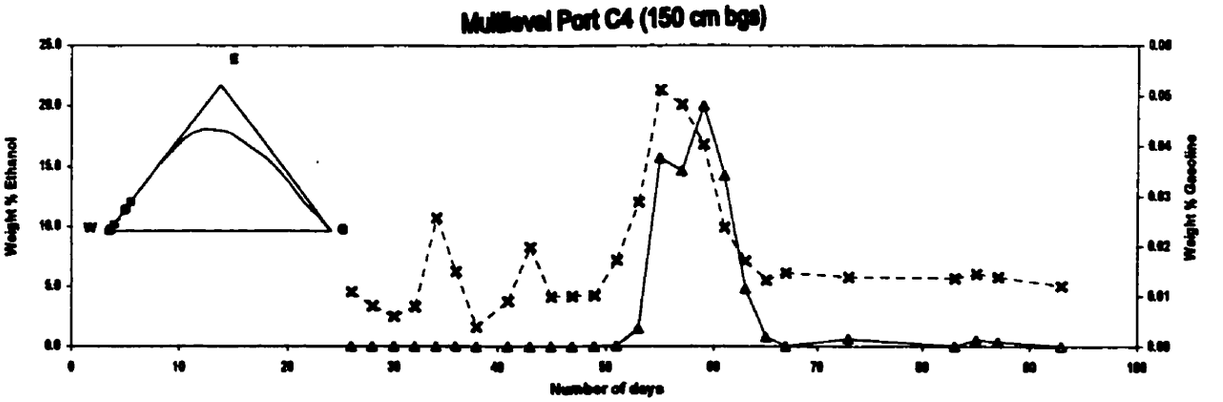
Multilevel Port C4 (150 cm bgs)
Weight % Ethanol
Weight % Gasoline
Number of days
E
W
G

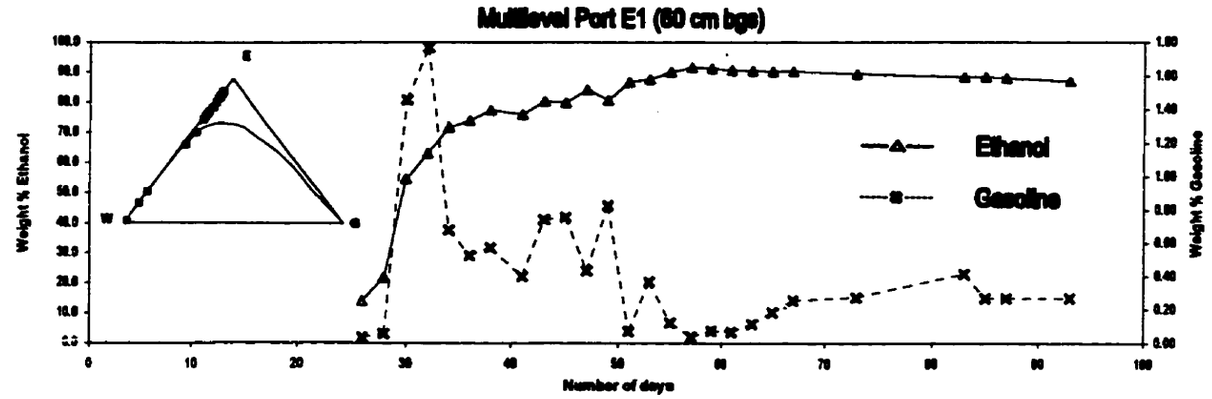
Multilevel Port E1 (60 cm bgs)
Weight % Ethanol
Weight % Gasoline
Number of days
Ethanol
Gasoline
E
W
e

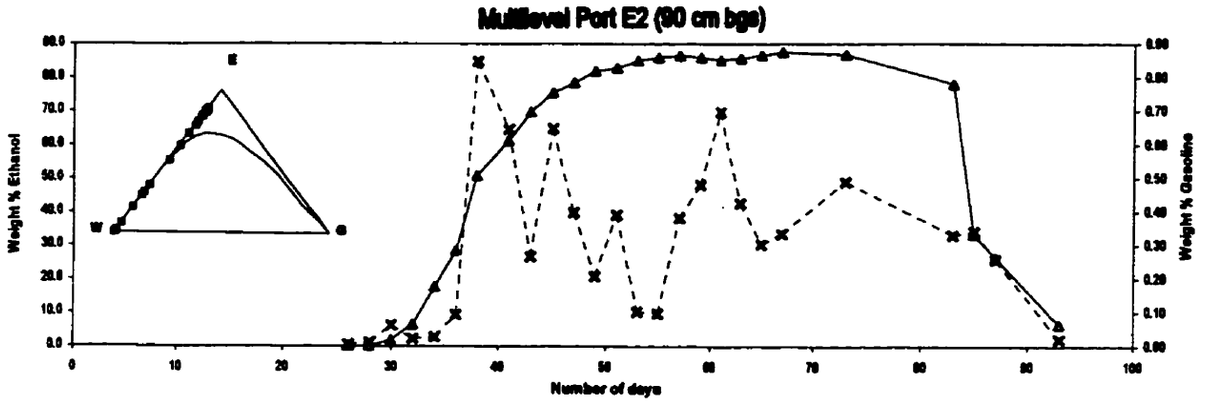
Multilevel Port E2 (90 cm bgs)
Weight % Ethanol
Weight % Gasoline
Number of days
E
W
e

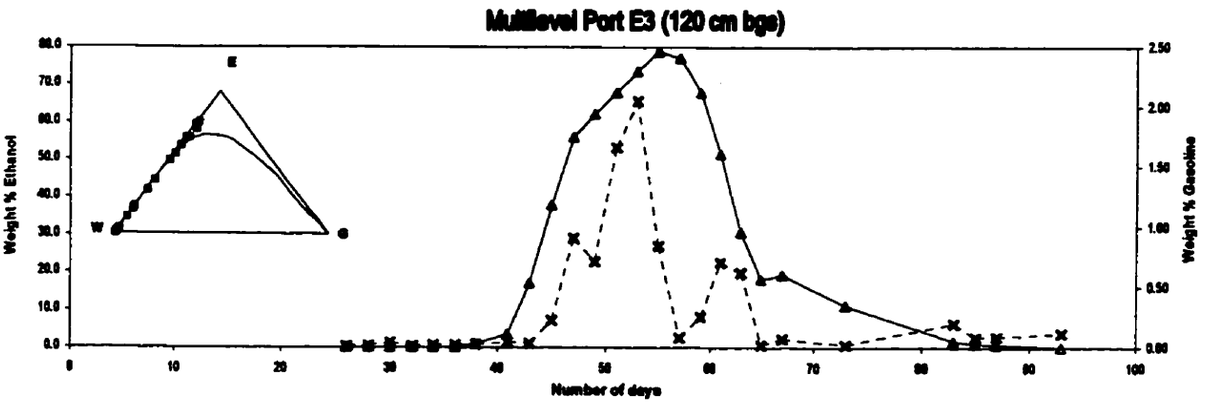
Multilevel Port E3 (120 cm bgs)
Weight % Ethanol
Weight % Gasoline
Number of days
E
W
e

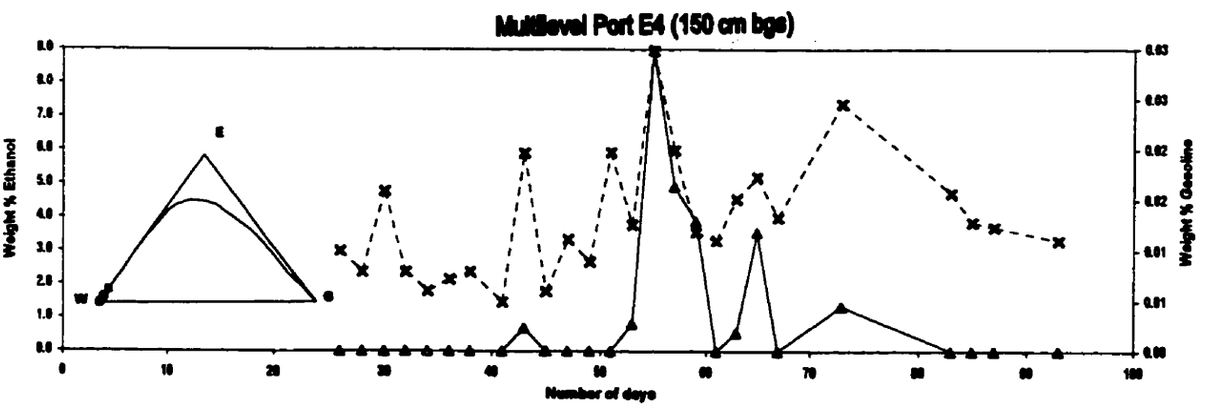
Multilevel Port E4 (150 cm bgs)
Weight % Ethanol
Weight % Gasoline
Number of days
E
W
e

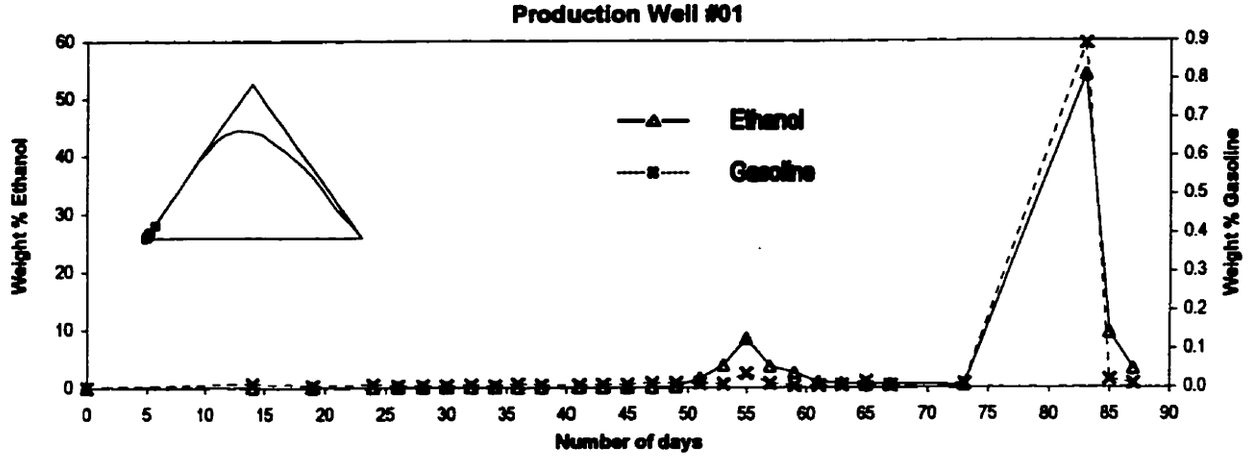
Production Well #01
Ethanol
Gasoline
Weight % Ethanol
Weight % Gasoline
Number of days

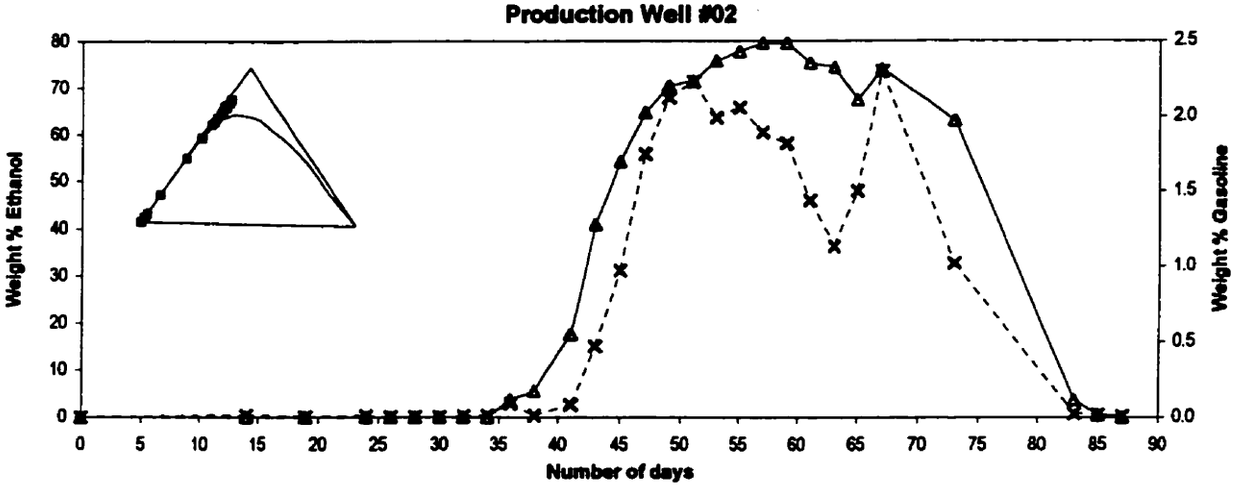
Production Well #02
Weight % Ethanol
Weight % Gasoline
Number of days

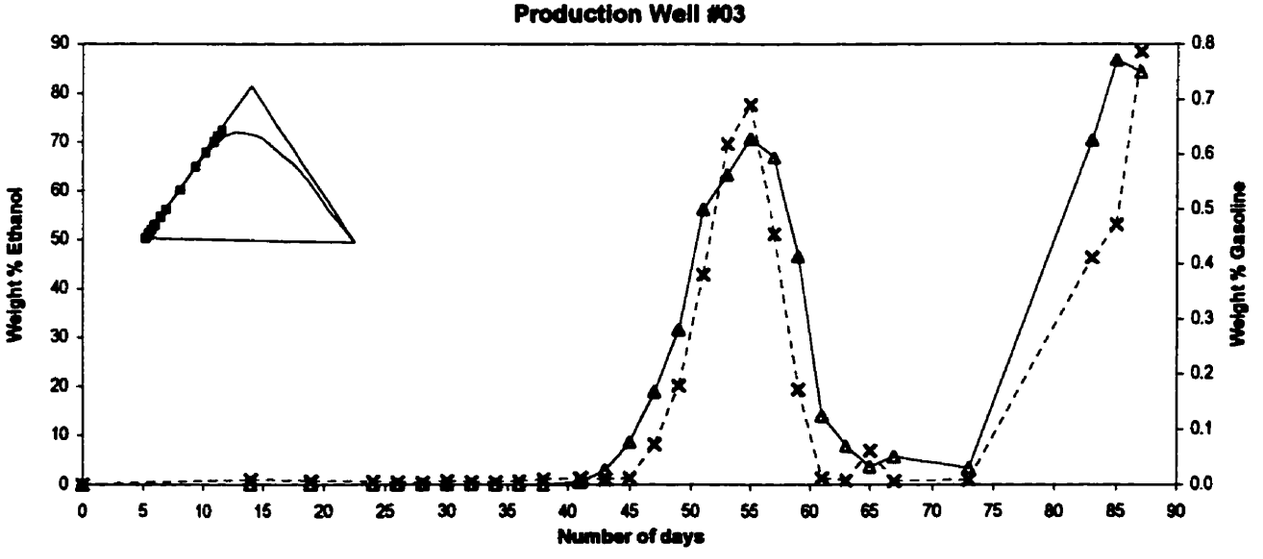
Production Well #03
Weight % Ethanol
Weight % Gasoline
Number of days

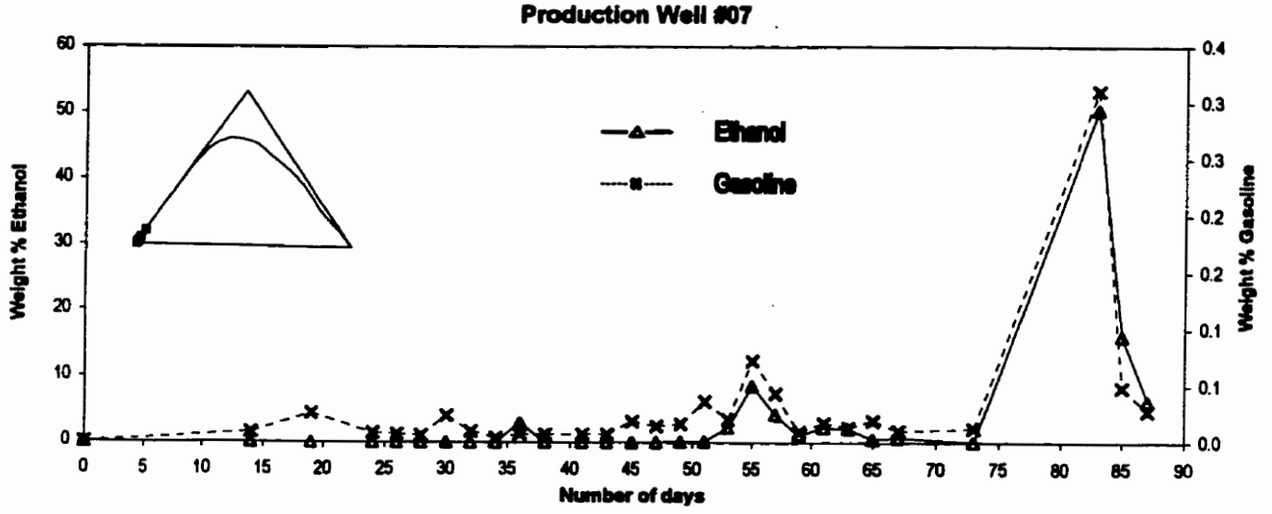
Production Well #07
Ethanol
Gasoline
Weight % Ethanol
Weight % Gasoline
Number of days

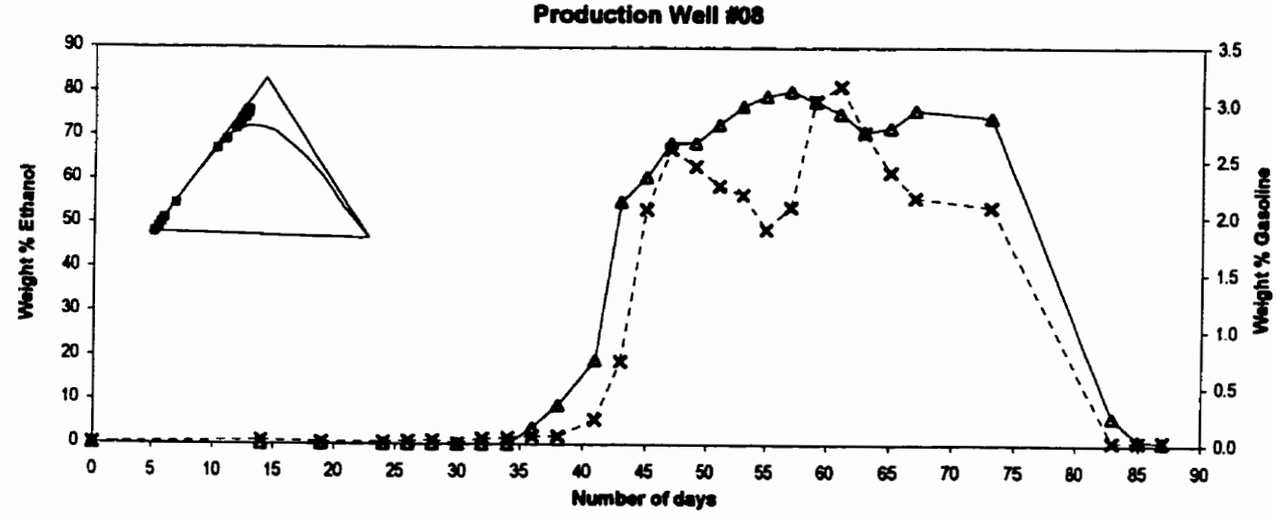
Production Well #08
Weight % Ethanol
Weight % Gasoline
Number of days

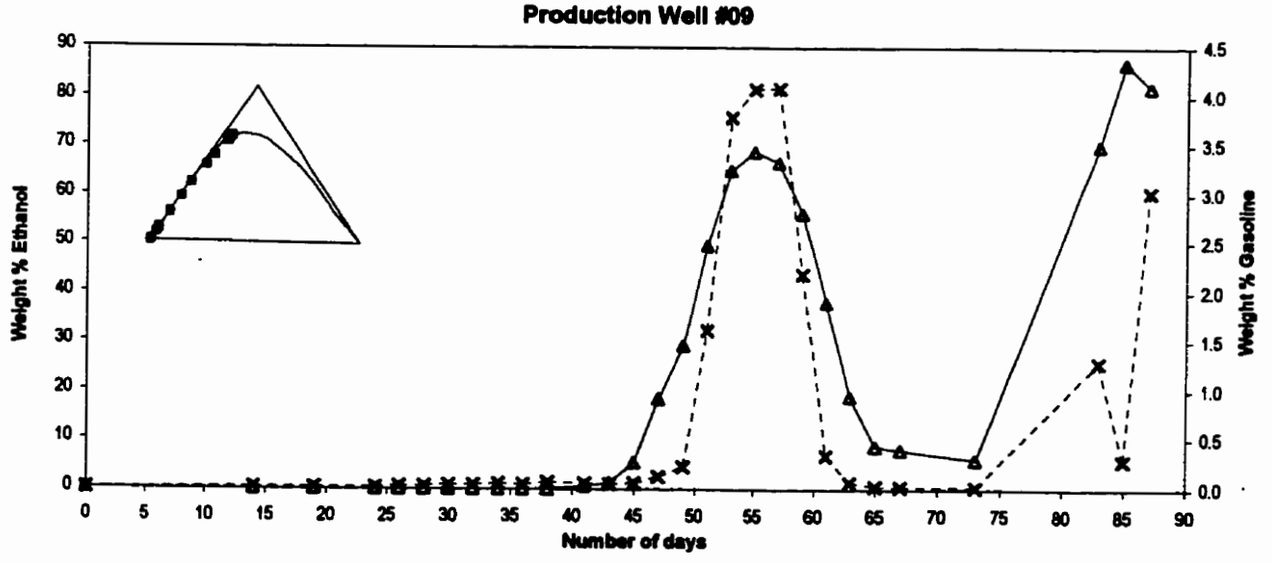
Production Well #09
Weight % Ethanol
Weight % Gasoline
Number of days

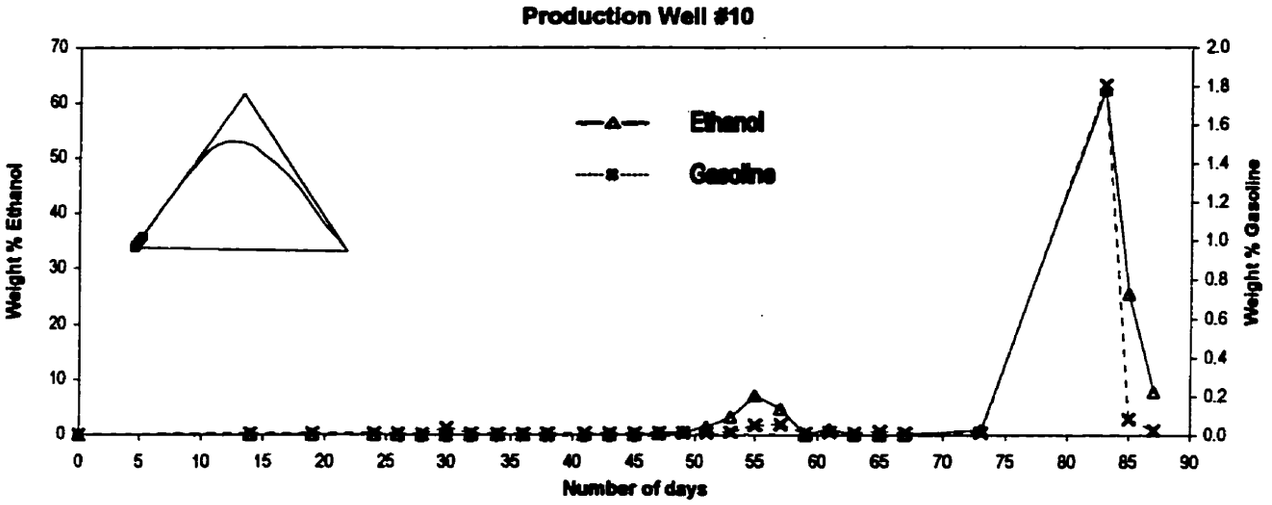
Production Well #10
Ethanol
Gasoline
Weight % Ethanol
Weight % Gasoline
Number of days

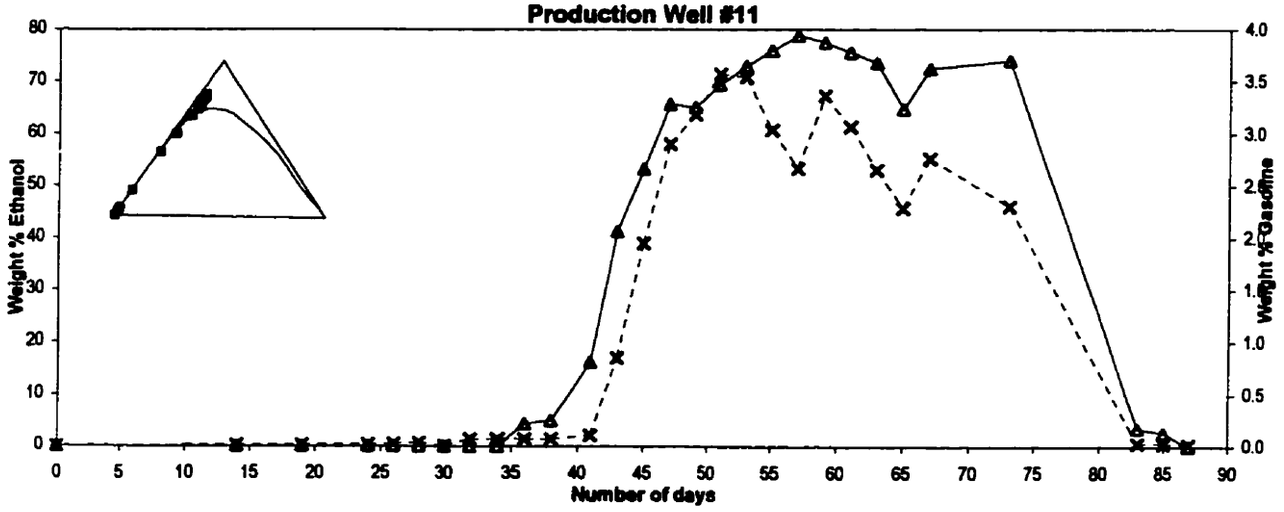
Production Well #11
Weight % Ethanol
Weight % Gasoline
Number of days

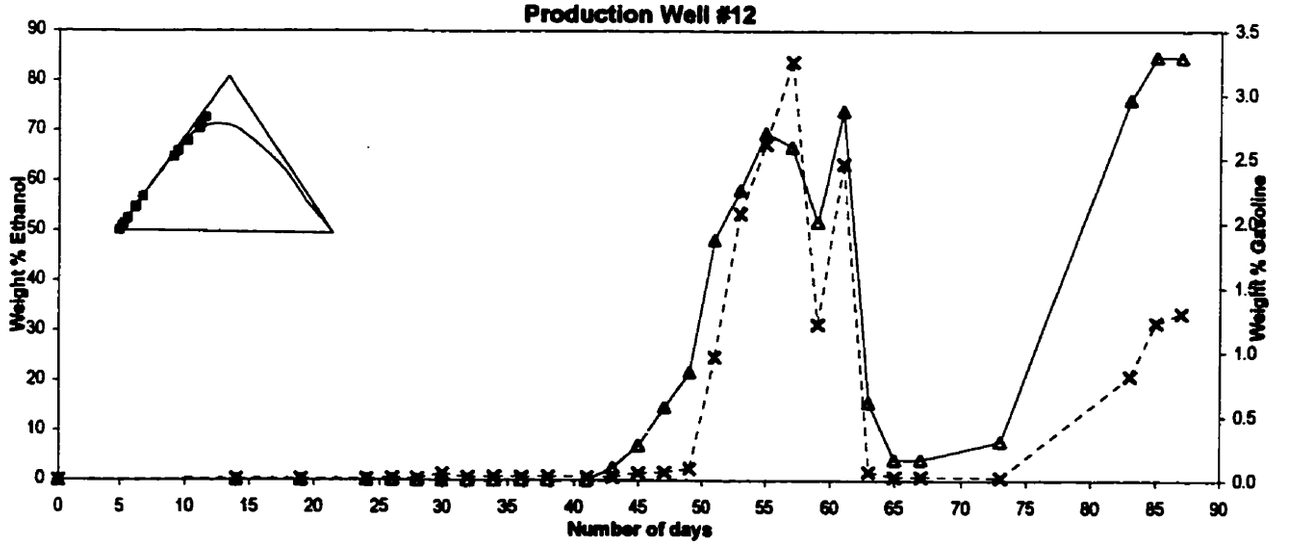
Production Well #12
Weight % Ethanol
Weight % Gasoline
Number of days

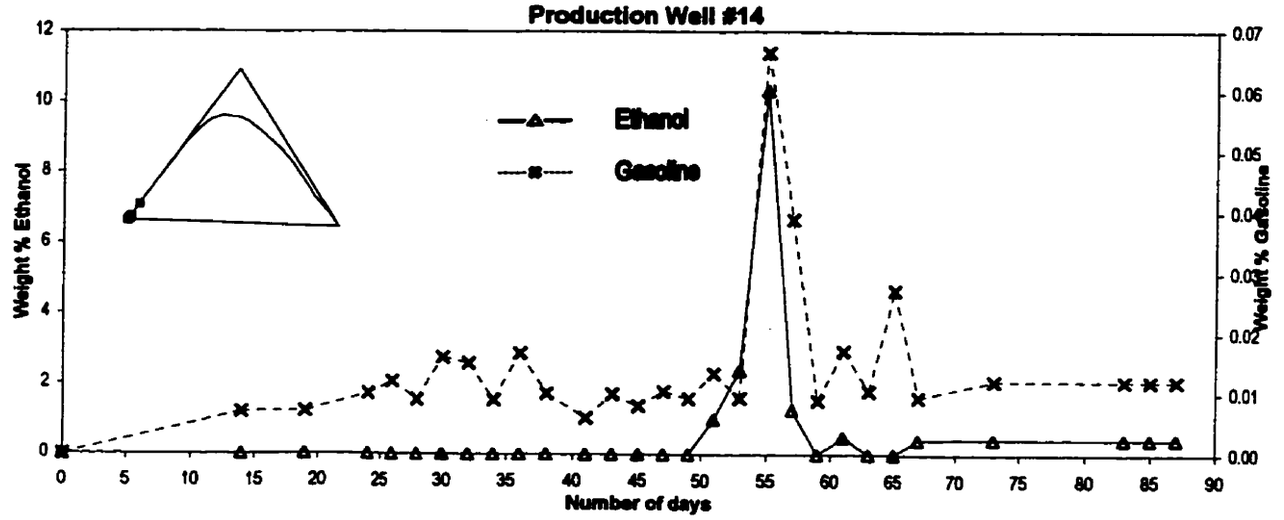
Production Well #14
Ethanol
Gasoline
Weight % Ethanol
Weight % Gasoline
Number of days

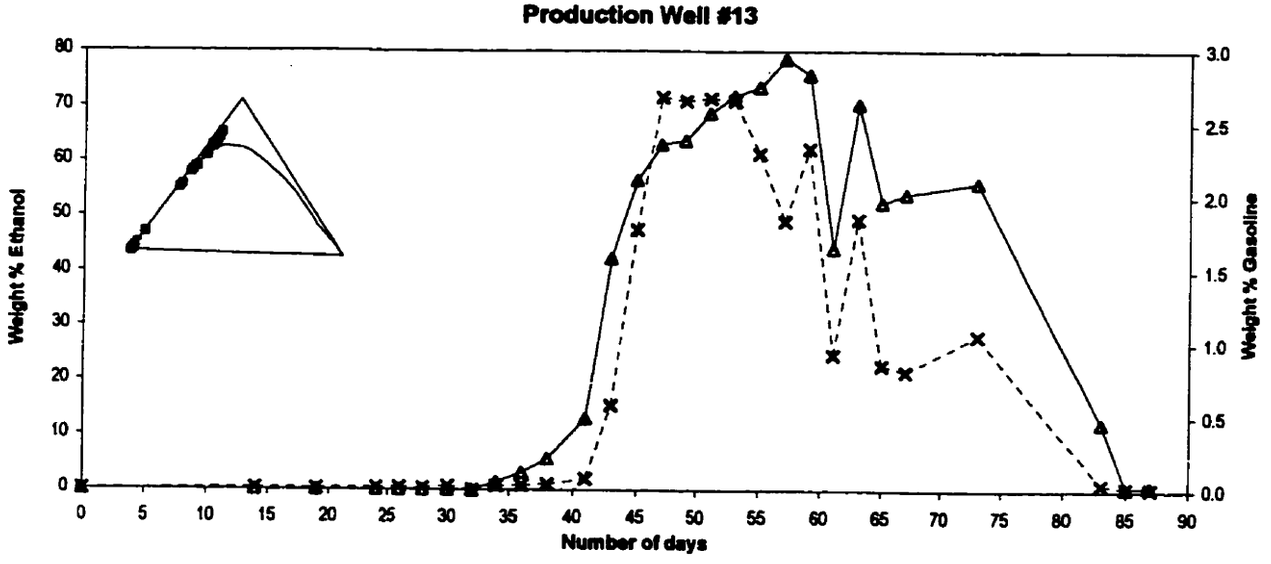
Production Well #13
Weight % Ethanol
Weight % Gasoline
Number of days

APPENDIX IX

Results of the UV chemical analyses of the core samples

collected after the field experiment was terminated

Table IX-1 - Chemical analyses of the core samples

Core #	sample I.D.	Raw Depths (cm bgs)	Corrected Depths (cm bgs)	Empty Bottle (g)	Bottle + sand+ soil fluid + 40 mL Ethanol	Bottle+ sand (Dry) (g)	Gasoline %Wt in diluted sample	Water %Wt in diluted sample	Ethanol %Wt in diluted sample	Gasoline %Wt in soil fluid	Water %Wt in soil fluid	Ethanol %Wt in soil fluid
	1	60	49	119.28	240.82	194.56	0.36	5.63	92.22	1.146	17.164	81.690
	2	75	61	119.54	219.76	175.93	0.03	11.29	87.22	0.123	39.591	60.287
	3	90	73	121.53	248.43	199.00	0.02	17.23	82.99	0.058	46.566	53.377
	4	105	85	121.30	220.85	176.03	0.04	17.68	81.57	0.145	58.725	41.130
1	5	120	97	121.36	242.82	194.91	0.03	18.05	80.58	0.080	52.474	47.446
	6	135	109	121.67	226.44	181.96	1.77	16.04	82.90	5.987	53.396	40.617
F_c = 0.81	7	150	122	121.22	239.02	191.34	0.76	17.33	79.78	2.275	51.251	46.474
	8	165	134	121.55	259.82	207.08	0.00	19.97	78.17	0.012	49.826	50.161
	9*	180	146	120.93	225.97	174.23	0.25	21.77	78.95	0.641	54.340	45.019
	10	40	34	121.22	261.47	211.95	0.18	3.11	96.94	0.479	7.940	91.582
	11	50	43	121.41	252.86	204.29	0.27	3.86	94.77	0.761	10.451	88.787
	12	60	51	120.75	262.93	212.73	0.23	6.77	91.53	0.613	17.819	81.568
	13	75	64	120.55	261.57	208.69	0.02	16.08	82.99	0.062	39.487	60.451
2	14	90	77	121.27	259.86	208.38	0.03	22.00	79.56	0.078	55.019	44.904
	15	105	89	121.39	256.04	206.81	0.02	22.35	79.27	0.043	60.153	39.803
F_c = 0.85	16	120	102	121.24	254.54	205.97	0.04	20.62	80.51	0.121	57.074	42.805
	17	135	115	121.24	253.45	204.82	0.01	25.36	76.30	0.016	69.817	30.167
	18	150	128	121.11	262.72	210.37	0.00	21.49	79.62	0.004	52.636	47.360
	19	45	38	120.70	260.13	211.70	0.41	3.21	95.65	1.185	8.596	90.220
	20	60	50	121.64	261.93	211.84	0.18	6.98	91.29	0.503	18.471	81.027
3	21	75	63	121.61	263.54	209.80	0.02	19.54	80.56	0.039	46.507	53.454
	22	90	76	121.51	251.06	200.75	0.01	22.25	78.06	0.030	58.472	41.498
F_c = 0.84	23	120	101	120.95	254.73	204.83	0.01	23.39	77.91	0.014	61.734	38.252
	24	150	126	121.21	258.92	208.41	0.00	20.26	79.99	0.007	52.896	47.097
	25	60	44	121.46	259.01	208.88	0.14	2.89	95.19	0.368	7.345	92.287
	26	75	56	121.53	259.20	209.33	0.14	3.99	93.57	0.392	10.495	89.112
	27	90	67	120.91	265.38	213.13	0.09	10.23	89.61	0.223	25.174	74.603
	28	105	78	120.41	268.10	215.76	0.01	17.88	79.55	0.036	45.394	54.569
4	29	120	89	121.13	233.40	187.01	0.05	22.68	77.99	0.165	69.011	30.824
	30	135	100	120.43	261.71	210.67	0.01	21.85	78.79	0.026	55.911	44.064
F_c = 0.74	31	150	111	120.54	252.08	203.38	0.04	24.61	77.08	0.121	67.509	32.370
	32	165	122	120.75	259.10	209.09	1.14	20.71	78.49	3.057	54.933	42.009
	33	60	47	120.99	253.01	205.66	0.31	3.76	92.68	0.957	10.917	88.126
	34	75	59	120.99	265.66	216.00	0.21	6.38	94.66	0.564	16.577	82.860
	35	90	70	120.90	253.62	205.50	0.01	18.25	81.54	0.027	52.038	47.935
5	36	105	82	121.05	247.54	198.54	0.01	26.68	73.76	0.025	73.379	26.596
	37	120	94	120.83	247.73	199.90	0.01	20.96	79.43	0.016	60.160	39.824
F_c = 0.78	38	135	105	121.10	256.74	207.37	0.00	21.70	77.87	0.005	59.310	40.685
	39	150	117	120.39	271.35	212.80	0.00	16.40	82.69	0.004	35.322	64.674
Ethanol	40	-	-	-	-	-	0.00	0.23	95.91	-	-	-

F_c = Correction factor for compaction (length recovered/lenght sampled)

APPENDIX X

Evaluation of the geophysical methods employed in the field experiment

TABLE OF CONTENTS

LIST OF ILLUSTRATIONS

X. EVALUATION OF THE GEOPHYSICAL METHODS EMPLOYED IN THE FIELD EXPERIMENT

X.1 Objectives

The objectives of the research described in this appendix are:

- to evaluate the novel technique for continuous logging of dielectric properties using an access tube with an embedded transmission line for TDR (time domain reflectometry);
- to evaluate the combined use of TDR and CPN soil moisture probe to monitor the distribution of fluids during ethanol flushing of gasoline residuals.

X.2 Experimental Procedure for TDR and CPN Monitoring

Variation of the water saturation within the cell was monitored using TDR and CPN methods. Three TDR/CPN access tubes were built of 2" (5.08 cm) OD SCH 40 PVC pipe 2.75 m in length, fitted with a machined 1¼" (31.75 mm) PVC SCH 80 end cap as a seal. Solid 1/8" (3.175 mm) stainless steel rods were laid into U-shaped grooves 1.75 mm deep spaced 1" (2.54 mm) apart on opposite sides of the PVC tube and attached with nylon straps (2-pair stainless steel rods). The stainless steel rods extended 1 cm above the top of the PVC tube. The TDR access tubes were jetted into the ground to a depth of 2.45 m using a 4" (10.16 cm) standard steel casing. Figure X-1 schematically shows the design used for this access tubes. The TDR rods had a fixed length, and distinct depth intervals of the aquifer could be evaluated by lowering a solid aluminum probe down the access tube. This system was developed by Redman (1997) and was tested for the first time in the field during this experiment. The rods were connected to a

Tektronics model 1502B cable tester through a 300 ohm shielded cable. The TDR waveform was captured, transferred to a microcomputer, and analyzed using a software developed by D. Redman of the Physical Properties laboratory in the Department of Earth Sciences of the University of Waterloo. The relationship of Topp et al. (1980) was used to calculate a water saturation given the dielectric permittivity of the soil as determined by the TDR waveform. This method depends on the dielectric permittivities of the soil components and their relative proportions. The dielectric permittivity of the components present in this experiment include water 80, ethanol 20, soil grains 5.2, gasoline 2 and air 1. The points were selected from the waveform using the software developed by D. Redman. Measurements were taken at 10 cm intervals from the depth of 2.8 cm to 172.8 cm.

The dielectric permittivities of different proportions of ethanol and water were determined in the laboratory by immersing a 14 mm, 50Ω coaxial air line in the liquid and measuring the traveltime on this coaxial line with the model 1502B TDR instrument, as described in Redman and DeRyck (1994).

The same access tubes installed for TDR readings were used CPN measurements. The soil moisture probe (CPN Corporation Model 503 DR Probe) was used to measure the hydrogen content of the medium based on thermalized neutron counts. The measurement is based on the fact that hydrogen, with its relatively large scattering cross section and small mass, is very efficient in the slowing-down of fast neutrons. Neutrons are emitted from a source within the probe and transported and scattered through the porous medium back to the detector within the same probe. The properties of the material will affect the transport process, influencing the spatial and energy distribution of the

neutron population and, consequently, the counting rate at any detector location (Ellis, 1987). The presence of ethanol or gasoline in the system soil+fluids decreases the number of hydrogen atoms per unit volume of the system when compared to a fully water saturated system. The ratio of hydrogen content for ethanol to water is 0.93:1 and for gasoline to water is 0.91:1. Therefore changes in counts can be related to changes in proportions of ethanol and water and the presence of gasoline and/or ethanol are likely to be determined. See Appendix IV for detailed composition and average molecular weight of the gasoline used in the field experiment.

X.3 Results and Discussion

Results obtained with the use of TDR (time domain reflectometry) and the moisture content probe CPN were already displayed in Chapter 4.

The use of TDR in the column experiment to determine the gasoline residual saturation confirmed the effectiveness of the method for monitoring the variation in saturation of an immiscible fluid of low dielectric permittivity such as gasoline. The use of TDR in columns with horizontal rods has been addressed by other authors (e. g., Redman and DeRick, 1994; DeRick, 1994).

The continuous logging of dielectric properties using an access tube with an embedded transmission line (Redman, 1997) proved accurate to determine the relative saturation of air and gasoline. The presence of gasoline or air is determined as a decrease in the water saturation of the medium, i.e., the difference between the water saturation before and after the presence of the residuals. Figure 4-9 (Chapter 4), presents the water saturation profile within the cell before gasoline spill. The TRD profile shows a good

agreement with the measurements of moisture content done with CPN and allowed the determination of the top of the capillary fringe after the cell was dewatered. Figure 4-10 (Chapter 4), presents the water saturation profile 13 days after the emplacement of the gasoline residuals. TDR readings in this figure showed a decrease of about 10% P.V. in water saturation, in agreement with expected gasoline residual saturation (12%) determined in the laboratory. Although the hydrogen content of gasoline relative to water (0.91:1) does not predict a good contrast for 12% gasoline saturation in soil, CPN measurements showed it differently, with a similar decrease in water saturation as indicated by TDR measurements. No explanation was found for this success.

Most of the data collected using TDR and CPN during the experiment dealt with the monitoring of the ethanol flushing process, ethanol being a miscible fluid with an intermediate value of dielectric permittivity (20), between the values of water (80) and the grains of the soil (5.2). The determination of water content in this case provides an apparent water saturation, where the dielectric permittivity of the fluid varies according to the proportions of ethanol, gasoline and water. The transformation of the values of water content as determined by the relationship of Topp et al. (1980) to water saturation was done using the average water content for the saturated zone as being the porosity of the medium. The use of another tool, the soil moisture probe, was devised to help interpret the changes in dielectric permittivity introduced by the mixing of ethanol and water. The results are compared to the determination of ethanol and water from UV analyses in Figure X-2, showing plots of the ethanol and water saturation in time for four different depths (60 cm, 90 cm, 120 cm and 150 cm below ground surface). Each plot present ethanol and water saturation as determined by chemical analyses, apparent water

saturation as determined by TDR and CPN readings. The access tube C2U7 and the multilevel C were chosen to this comparison for their proximity to each other within the test cell.

Figure X-2 shows that the behavior of the CPN data is constant at the four plots, reflecting the variation of the hydrogen content in water due to either the presence of dissolved ethanol and gasoline or to the almost complete replacement of the water by ethanol only, as showed in the plot for depth of 60 cm. The differences in hydrogen content proved too small to be distinguish these possibilities.

The apparent water saturation as measured by TDR showed a reasonable agreement to the water saturation as measured by the chemical analyses. The overall shape of the TDR curve agrees to that of the water saturation determined by chemical analyses, but the values of water saturation inferred from TDR data are somehow higher.

A relationship between the ethanol saturation and the apparent water saturation as measured by TDR is presented by Bicalho (1997). A series of measurements of dielectric permittivity for different proportions of ethanol and water in Ottawa sand was carried out by this author in the Physical Properties Laboratory, University of Waterloo. The results are summarized in Figure X-3, where water and ethanol saturation as determined by UV analyses, apparent water saturation (TDR-based) and raw counts (CPN) are plotted against time in days, as breakthrough curves.

The ethanol saturation in the fiels is estimated from the measured apparent water saturation and the relationship between ethanol saturation (in percent by volume) and apparent water saturation presented on the diagram of Figure X-3. The results were comparable to the ethanol saturation measured by chemical analyses (Figure X-4).

The results showed a good qualitative result, but the estimated values of ethanol saturation based on the TDR measurements are usually lower than those measured by chemical analyses by as much as 30%.

For low ethanol saturation, the TDR-based ethanol saturation either matched or is higher than the value obtained by chemical analysis. At low ethanol saturation, the saturation of gasoline is expected to be higher because they are not removed at the same rate as at high ethanol saturation. The presence of the gasoline residuals decreases the apparent water saturation measured by TDR, and consequently increases the TDR-based ethanol saturation, since the presence of gasoline is not considered in the calculation. Although at a much smaller proportion, the presence of dissolved gasoline may also affect the TDR measurements, with a tendency of a slight decrease on the value of the apparent water saturation. An eventual presence of gasoline phase, like the halo that forms around the pathway of ethanol flowing through the zone of residuals, also decreases the apparent water saturation, and so does the presence of any gas phase. These factors all shift the TDR-based ethanol saturation to higher values, which explains the deviation in the measurements at low ethanol saturation. In the presence of gasoline residuals or other separate phase of low dielectric permittivity, the values of ethanol saturation are bound to be overestimated by TDR measurements alone. CPN measurements could circumvent the problem, but as discussed earlier, were not feasible.

For high ethanol saturation, the problem of having gasoline residuals is concealed either by the decrease in the dielectric permittivity caused by the high ethanol saturation or by the actual removal of the residuals. Reduction in water saturation is not consistent with the lower values of TDR-based ethanol saturation measured for all the situations. It

is likely that the relationship between ethanol saturation and apparent water saturation changes for this type of probe used as opposed to the one determined by Bicalho (1997). This fact should be tested to improve the quantitative results obtained for ethanol saturation after dielectric permittivity measurements using the continuous logging TDR technique.

Based on the behavior of TDR measurements for the presence of ethanol just presented, it is convenient to review the first two sets of Figure 4-12 (Chapter 4). In this figure, the profiles of TDR and CPN measurements are plotted side by side with the ethanol and gasoline concentration distribution during the evolution of the ethanol flushing process.

The first two sets, November 21 and November 23, 1995, show that the ethanol flowing upward and to the left is well described by the TDR curves on access tubes C2U9 and C2U7 (C2U6 data is not reliable, as mentioned previously). On November 21, 1995, the profile of C2U9 shows a gradual decrease of apparent water saturation from the lower portions to higher positions, indicating the increase in ethanol saturation. The decrease in the apparent water saturation measured by the access tube C2U7 is sharper, and reflects the higher ethanol saturation at that point compared to that at access tube C2U9.

X.4 Conclusions

The use of the continuous logging of dielectric properties using an access tube with an embedded transmission line (Redman, 1997) proved accurate to determine the presence of immiscible fluid of low dielectric permittivity, such as air and gasoline.

TDR measurements using the continuous logging technique were useful to monitor the positioning of the ethanol slug. Since the ethanol floats over water, TDR monitoring using the continuous logging technique, although only qualitative, is a cost-effective tool to monitor the evolution of the ethanol flushing in the field.

CPN (soil moisture probe) was useful to determine total fluid saturation, but the hydrogen content of the fluids involved (gasoline, ethanol and water) was of insufficient contrast to permit their differentiation.

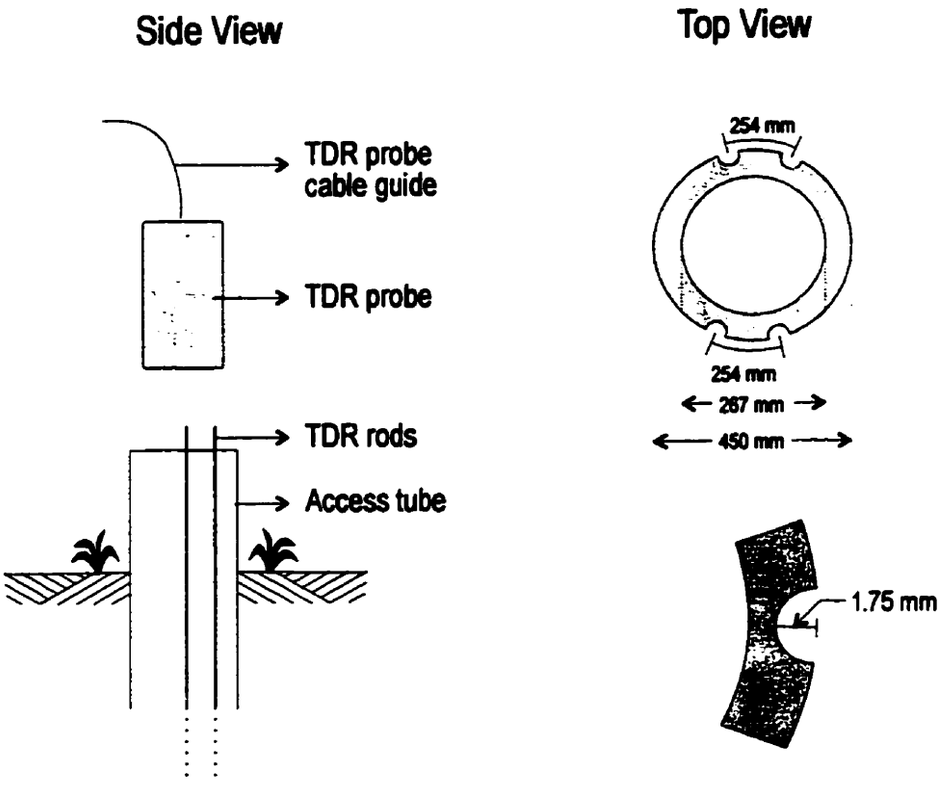

Figure X-1 - Time domain reflectometry and soil moisture probe access tube.

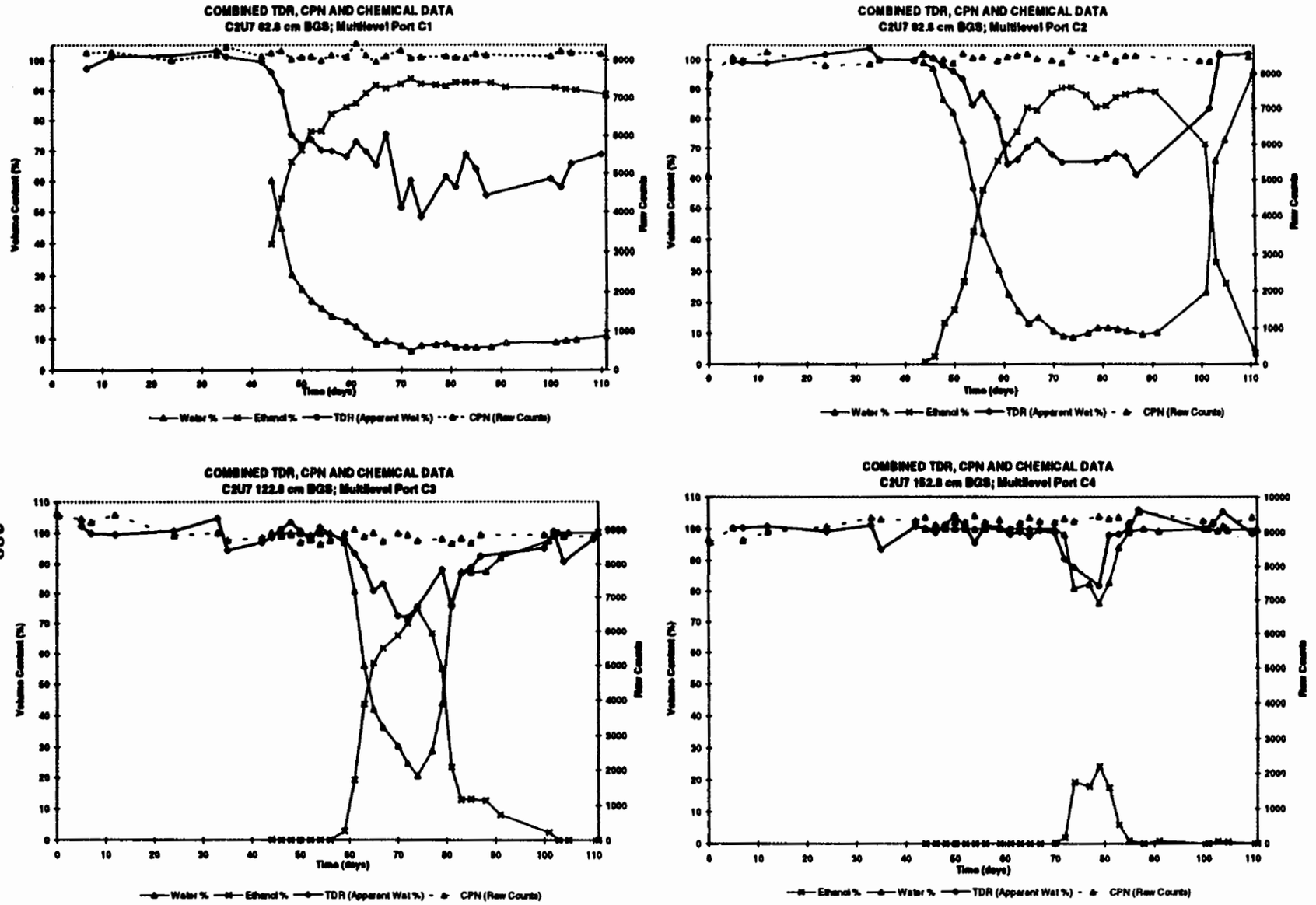

Figure X-2 - Combined measurements of ethanol and water saturation from TDR, CPN and fluid samples analyses for the ports of multilevel C and correspondent depths for access tube C2U7.

Eth. %	Water % *apparent*	Best Fit	Diel. Perm. Liquid+Soil (Kliq+soil)
0	0.392	0.382927	24.14
2	0.357	0.378785	21
40	0.319	0.300096	18
60	0.260	0.258681	14
80	0.217	0.217266	11.5
100	0.168	0.175851	9

b= 0.383

m= -0.00207

Equation for Fitting Curve

Wap = - 0.00207 Eth% + 0.383

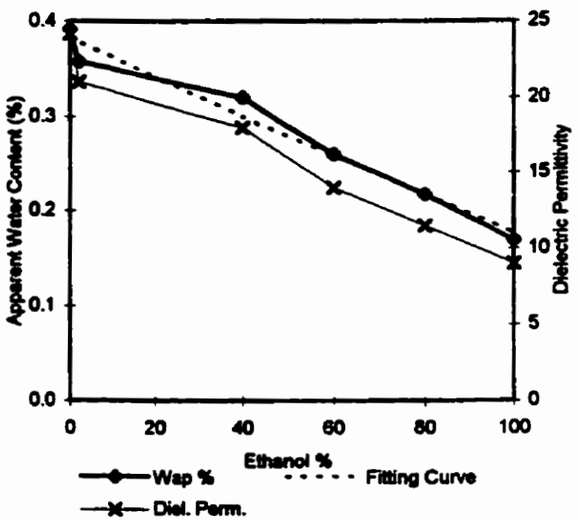

Figure X-3 - Diagram showing the relationship between the ethanol saturation in the dielectric permittivity values and the final determination of the water saturation.

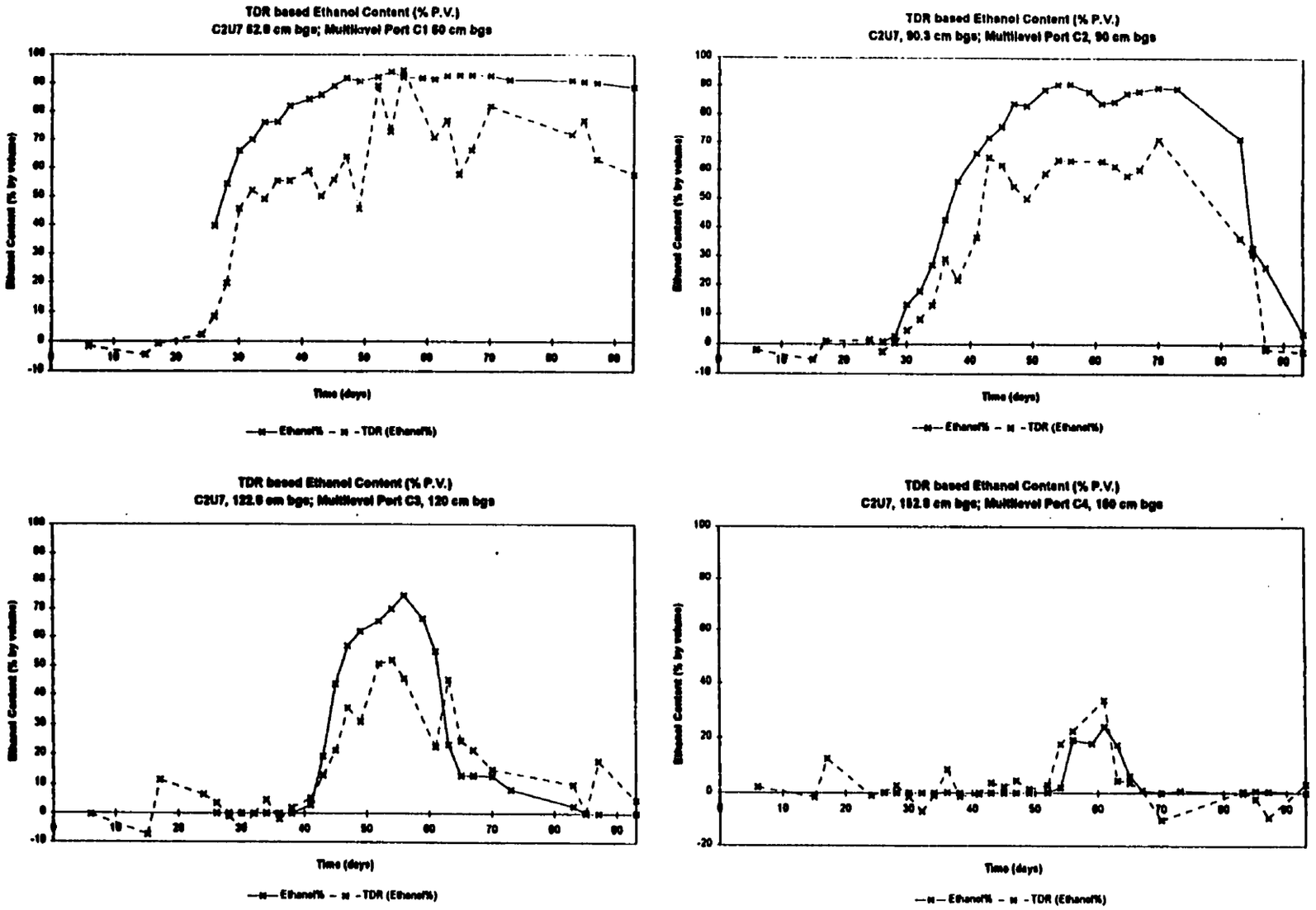

Figure X-4 - TDR-based ethanol saturation compared to ethanol saturation determined by UV analyses of fluid samples for the ports of multilevel C and correspondent depths for access tube C2U7